THE DEVELOPMENT AND USE OF CHEMICAL TOOLS TO IDENTIFY ACTIVE MYCOBACTERIAL ESTERASES

By

Katie Ree Tallman

A DISSERTATION

Presented to the Department of Physiology & Pharmacology

and the Oregon Health & Science University

School of Medicine

in partial fulfillment of the requirements for the degree of

Doctor of Philosophy

July 2016

School of Medicine

Oregon Health & Science University

CERTIFICATE OF APPROVAL

This is to certify that the PhD dissertation of

Katie Ree Tallman

has been approved

_____

Kimberly Beatty, PhD (Mentor)

_____

Thomas Scanlan, PhD (Committee Chair)

_____

Buddy Ullman, PhD (Member)

_____

Michael Cohen, PhD (Member)

_____

Summer Gibbs, PhD (Member)

_____

Fikadu Tafesse, PhD (Member)

TABLE OF CONTENTS

Acknowledgments

Graduate school is often described as an isolating experience. In reality, we do not—and cannot—go through this alone, and I have many people to thank for helping me along my journey. I am incredibly thankful to my advisor, Prof. Kimberly Beatty, for accepting me into her lab virtually untested. She has challenged me to become a creative, productive, and well-rounded scientist, and I am so grateful that she gave me the opportunity to be part of such an exciting project. I am also thankful for the friendship and support of my lab mates (past and present), especially Sam Levine, Hannah Zane, Julia Doh, and Jon White. In particular, it has been extremely rewarding to collaborate with Sam on this project.

I came to OHSU with interests in pharmacology and chemical biology, and I have gotten to pursue both to a certain extent. Before joining the Beatty lab, I studied methamphetamine pharmacology with Prof. David Grandy. I am very grateful to Prof. Grandy for accepting me into his group and believing in my abilities.

I would like to thank my dissertation advisory committee, Prof. Tom Scanlan, Prof. Buddy Ullman, Prof. Mike Cohen, and Prof. Summer Gibbs, for their mentorship and support. Additionally, I would like to thank Prof. Fikadu Tafesse for taking part in my defense. A great advisory committee goes a long way.

I am also incredibly grateful for my undergraduate education at Western Washington University. I received top-notch instruction from professors who were not only brilliant, but also devoted to teaching. I am grateful to Prof. Jim Vyvyan for mentoring me in organic synthesis. I would also like to thank Prof. Clint Spiegel (Biochemistry) and Prof. Millie Johnson (Mathematics) for their continued mentorship and encouragement.

Finally, I would like to thank my family and friends for all of their support. My parents, Dick and Laurie Tallman, have been a constant source of love and encouragement throughout my life. They truly go above and beyond, and I feel lucky to be their daughter. My sisters, Marci and Emily Tallman, are the best siblings I could ask for, and they helped me stay sane. To all of my friends, thank you for all of the laughs and adventures. You helped make graduate school a great experience.

List of Tables

List of Figures

List of Abbreviations

ABP	activity-based probe
ABPP	activity-based protein profiling
AME	acetoxymethyl ether
BCG	bacillus Calmette-Guérin
BME	butanoylmethyl ether
BSA	bovine serum albumin
Culp	cutinase-like protein
DAG	diacylglycerol
DCF	2',7'-dichlorofluorescein
DCM	4-(dicyanomethylene)-2-methyl-6-(4-dimethylaminostyryl)-4*H*-pyran
DDAO	7-hydroxy-9*H*-(1,3-dichloro-9,9-dimethylacridin-2-one)
DMEM	Dulbecco's modified Eagle's medium
DMSO	dimethyl sulfoxide
DTT	dithiothreitol
E-600	diethyl-*p*-nitrophenyl phosphate
ESI	electrospray ionization
FBS	fetal bovine serum
FDA	fluorescein diacetate
FP	fluorophosphonate

HEPES	4-(2-hydroxyethyl)-1-piperazineethanesulfonic acid
HMBC	heteronuclear multiple bond correlation
HSL	hormone-sensitive lipase
HSQC	heteronuclear single quantum correlation
LC-MS/MS	liquid chromatography-tandem mass spectrometry
MAFP	methyl arachidonyl fluorophosphonate
MAG	monoacylglycerol
Mtb	*Mycobacterium tuberculosis*
MTBC	*Mycobacterium tuberculosis* complex
NIR	near-infrared
NMR	nuclear magnetic resonance
NOESY	nuclear Overhauser effect spectroscopy
OADC	oleic acid, albumin, dextrose, catalase
OME	octanoylmethyl ether
p-NPA	*p*-nitrophenyl acetate
PAGE	polyacrylamide gel electrophoresis
PBS	phosphate buffered saline
PE	proline-glutamic acid
PEG	poly(ethylene glycol)
PLE	porcine liver esterase
PMSF	phenylmethyl sulfonyl fluoride

PPE	proline-proline-glutamic acid
RD	region of deletion
Res	resorufin
SDS	sodium dodecyl sulfate
TAG	triacylglycerol
TB	tuberculosis
TCEP	*tris*(2-carboxyethyl)phosphine
TFA	trifluoroacetic acid
THL	tetrahydrolipstatin
TLC	thin-layer chromatography
TMS	tetramethylsilane
UV	ultraviolet

Abstract

Tuberculosis (TB) is a pulmonary disease caused by *Mycobacterium tuberculosis* (*Mtb*). Approximately one-third of the global population is infected with latent TB, an asymptomatic form of the disease that is phenotypically drug-tolerant. Dormant *Mtb* reactivates when the immune system weakens, contributing to the nearly 10 million new cases of active TB that occur each year. In order to better diagnose, treat, and ultimately eradicate TB, there is an urgent need to understand the enzymes associated with dormancy and reactivation.

In my dissertation research, I used chemical tools to identify *Mtb* enzymatic activity associated with dormant, reactivating, and active *Mtb*. My research focused on esterases, including the lipase subclass, which influence *Mtb* pathogenicity and reactivation from dormancy. Prior studies used transcriptomics and shotgun proteomics to identify proteins that are differentially regulated in dormancy and reactivation, while my research focused on determining how esterase activity changes under these conditions. First, I developed a set of fluorogenic esterase probes that become fluorescent following esterase-mediated hydrolysis and used them to screen mycobacterial esterase activity in a native protein gel assay (Chapter 2). Next, I expanded this probe set to include more favorable lipase substrates (Chapter 3). Lastly, I used both fluorogenic probes and activity-based probes to profile changes in *Mtb* esterase activity in dormancy, during reactivation, and in active *Mtb* (Chapter 4). Although

most esterase activity decreased in dormant and reactivating *Mtb*, I identified several esterases that retain activity in dormancy. These esterases may be valuable diagnostic and therapeutic targets.

Chapter 1: Introduction

Tuberculosis

Tuberculosis (TB) is a deadly airborne disease caused by several closely related species and strains of mycobacteria, collectively called the *Mycobacterium tuberculosis* complex (MTBC). Primarily a pulmonary disease, characteristic TB symptoms include chronic cough with blood-tinged sputum, fever, fatigue, and weight loss. Early MTBC strains emerged in Africa around 70,000 years ago and co-evolved with humans.[1] MTBC members include *M. tuberculosis* (*Mtb*), *M. bovis*, *M. microti*, *M. africanum*, *M. pinnipedii*, and *M. caprae*. These species share 99% of their DNA sequence identity—an extreme example of genetic conservation.[2] While human infections from other species can occur, *Mtb* and *M. africanum* are the only MTBC members that have sustained and efficient human-to-human transmission.[3] *M. africanum* strains are restricted to West Africa and are less virulent than *Mtb*, in part due to mutations in genes encoding a virulence regulator.[3]

Mtb is arguably the most successful pathogen in human history. TB has caused more deaths than any other infectious disease, with over one billion deaths in the past two hundred years alone.[4] For example, in 17th to 19th century Europe, 20–30% of all deaths were due to TB.[5] During this time, society's understanding of TB—including whether or not it was infectious in nature—was

limited,[6] and factors like crowded living conditions and poor nutrition contributed to its high mortality rate.[5]

A turning point for TB research came in 1882. Robert Koch, a physician and bacteriologist, presented his discovery of the "tubercle bacillus," proving that TB was caused by a bacterium.[7] In 1921, Albert Calmette and Camille Guérin introduced a TB vaccine derived from attenuated *M. bovis*. Even though the bacillus Calmette-Guérin (BCG) vaccine has variable efficacy and primarily only protects against childhood TB, it remains the only approved TB vaccine.[8] In 1944, streptomycin, the first antibiotic effective against *Mtb*, was isolated, and TB became a drug-treatable disease.[9]

Despite advances in medicine and our understanding of *Mtb* pathogenesis, TB remains the most lethal single-agent infectious disease today.[10] In particular, TB continues to devastate developing countries.[4,10] TB incidence rates support this; in 2014, 58% of new infections occurred in South-East Asia and the Western Pacific. Africa had 28% of new cases and the most severe burden relative to population.[10] Ultimately, there were an estimated 9.6 million new cases and 1.5 million deaths from TB worldwide in 2014.[10] Global efforts to control TB are complicated by the emergence of drug-resistant bacteria as well as a vast reservoir of latent infection (*vide infra*).[11]

Disease Pathogenesis

TB is transmitted through pathogen-containing aerosols, which are expelled into the air by an individual with pulmonary TB. *Mtb* then infects a new host through the respiratory tract. Upon inhalation, *Mtb* is phagocytosed by resident alveolar macrophages and dendritic cells. These cells are designed to kill pathogens and initiate the adaptive immune response, but *Mtb* has developed countermeasures. *Mtb* evades killing by macrophages and instead replicates within them until the host develops acquired immunity.[12] The acquired immune response ultimately results in granuloma formation.[12,13]

Initially, the granuloma consists of a core of infected macrophages surrounded by "foamy" macrophages rich in lipid bodies, other mononuclear phagocytes, and lymphocytes.[12-14] Over time, the macrophage core is encased in a fibrous capsule.[12] In most people, the granuloma contains the infection in a "stalemate," not only keeping the bacteria from spreading but also preventing further immune responses.[12,13] Some granulomas even resolve on their own.[12,13] However, in progressive infection, the granuloma center undergoes caseous necrosis, liquefies, and cavitates, releasing infectious *Mtb* into the airways, which can be transmitted to others.[12]

Latent TB

Approximately one-third of the global population is infected with latent TB.[15] Latent TB infection is defined as the presence of an immune response to

Mtb antigens in the absence of TB symptoms.[10,16,17] About 5–15% of latently-infected individuals will develop active TB within their lifetimes, usually within the first several years post-infection.[10] The probability of reactivation is higher for the immunocompromised. Thus, TB and HIV/AIDS comorbidity significantly contributes to the global TB burden.[18] Other factors, such as aging, malnutrition, pregnancy, and diabetes, can also trigger reactivation.[19] Currently, there is no method to distinguish the 90% of latently-infected individuals who will never develop TB from the 10% who will. Furthermore, the most common TB screening methods, the tuberculin skin test and the interferon-γ release assay, do not distinguish between individuals with active disease, those with latent infections, and those who have completely cleared the infection and do not require treatment.[16,17]

In latent TB, *Mtb* slows its metabolism and exists primarily in a dormant, non- or slowly-replicating state.[16,17] The conversion to this phenotype is triggered by stresses exerted on *Mtb* by the immune system. These include acidic, oxidative, nitrosative, hypoxic, and nutritional stresses.[20,21] *Mtb* adapts to these stresses through a variety of mechanisms, many of which are poorly understood. Overall, researchers hypothesize that dormant *Mtb* utilizes distinct metabolic pathways for survival, which is supported by the fact that very few compounds kill both dormant and actively replicating *Mtb*.[20] Dormant *Mtb* is phenotypically drug-tolerant, which contributes to the prolonged (i.e., 6–9 months), multi-drug treatment required to cure drug-sensitive TB.[20] Patient non-compliance during

this long treatment course has contributed to the rise of drug-resistant TB,[11,22] which now comprises more than 3% of new cases.[10] Therefore, a central goal in TB research is to identify enzymes that are indispensable to *Mtb* during dormancy or reactivation so that they can be targeted with new therapeutics.

Dormancy Models

In order to investigate latent TB biology, researchers have developed *in vitro* dormancy models that subject *Mtb* to stresses encountered in the human host and drive the pathogen into a non- or slowly-replicating state.[23-30] However, there is no one generally accepted model, and no single model fully encompasses physiological conditions. Despite their limitations, *in vitro* dormancy models provide insights into *Mtb*'s strategies for persistence during latent infection. It is likely that each model induces a unique stress response, with common players essential for non-replicating persistence induced across all models.[20,31]

There are several nutrient deprivation models. The Loebel model uses phosphate-buffered saline in oxygen-rich conditions for complete starvation, which forces *Mtb* to utilize stores of trehalose, glycogen, fatty acids from lipids, and glutamate.[20,29] Although developed in the 1930s, this model is still used today.[24,32,33] However, *Mtb* is unlikely to be completely starved of nutrients in the human host.[20] A less extreme nutrient starvation model, the carbon starvation model, cultures *Mtb* in a base broth without additional carbon sources.[25] This

medium contains essential cofactors and trace elements but does not contain enough carbon to support replication.[25]

As many TB granulomas are severely hypoxic,[34] the well-studied hypoxia model exposes *Mtb* to a low oxygen environment in nutrient-rich medium.[23] This model has become the gold standard for inducing dormancy due to its ease of use.[35] However, even within this model, there are variations on hypoxia induction (e.g., slow versus rapid withdrawal of oxygen) that influence the long-term viability of the bacteria.[35]

Multi-stress models combine microenvironmental components that *Mtb* encounters in the human host. Deb *et al.* used acidic pH, hypoxia, high CO_2, and low nutrients to induce dormancy.[27] A model developed by the Nathan laboratory includes acidic pH, hypoxia, reactive nitrogen intermediates, and a fatty acid as the sole carbon source.[26,28]

In my work, I have employed the carbon starvation model and the hypoxia model to identify mycobacterial esterases and lipases that are active across *Mtb* metabolic states (Chapter 4).

Esterases and Lipases in *Mycobacterium tuberculosis*

Lipids comprise 40–60% of the dry weight of *Mtb*, suggesting that lipids and lipid metabolism play a central role throughout the *Mtb* life cycle.[36] Furthermore, *Mtb* triggers macrophages—both infected and uninfected—to

accumulate lipids, resulting in so-called "foamy macrophages."[12,14] Electron micrographs of *Mtb*-infected foamy macrophages showed bacilli-containing phagosomes positioned near host lipid bodies and lipid accumulation within the bacilli.[14] *Mtb* utilizes these lipids as a carbon source in an otherwise nutrient-deprived environment during dormancy and reactivation, making lipid-metabolizing enzymes attractive targets for new diagnostic biomarkers and therapeutics.[37-40] The importance of lipid metabolism for *Mtb* growth, persistence, and pathogenicity is also reflected in the 250 *Mtb* genes linked to lipid processing—about five times as many as found in *E. coli*, which has a similarly-sized genome.[41]

A subset of the 250 genes associated with lipid metabolism encodes esterases. Esterases are widely expressed across all kingdoms of life and use water and a catalytic serine to cleave an ester into an alcohol and an acid (Figure 1.1). These enzymes are classified based on the type of ester bond they hydrolyze (e.g., carboxylesterases, thioesterases, phosphodiesterases). Carboxylesterases cleave carboxylic esters and are often simply called "esterases." Lipases, which are maximally active with long-chain esters (i.e., lipids; Figure 1.2), constitute a sub-class of carboxylesterase.[42] Unlike esterases, lipases can hydrolyze emulsions of water-insoluble medium- and long-chain esters, such as eight-carbon (C8) and longer esters.[43,44] Esterases and lipases can be further distinguished by kinetic studies, with esterases displaying significantly lower apparent K_M values with short-chain esters than lipases.[44]

There were 21 genes initially annotated as encoding esterases or lipases in the *Mtb* H37Rv genome—the so-called "Lip" family.[41] The cutinase-like proteins (Culps) comprise another set of *Mtb* esterases. However, approximately one-third of the *Mtb* protein-coding genes encode conserved hypothetical proteins or proteins of unknown function,[45] and many misannotated esterases have already been identified.[46-51] Therefore, the list of *Mtb* esterases continues to grow (Table 1.1). Although we only have a partial understanding of which esterases are most utilized during different stages of infection, certain esterases, discussed in the following sections, are implicated in *Mtb* pathogenicity. A clearer picture of the esterases pivotal for dormancy and reactivation will further aid TB diagnostic and drug development efforts.

The Lip Family

LipC through LipW were annotated in 1998 when the *Mtb* H37Rv genome was first sequenced.[41] LipX (Rv1169c), LipY (Rv3097c), and LipZ (Rv1843) were identified using a homology screen and added to the Lip family in 2006.[37] Some of the Lip family members have been characterized and their esterase activity confirmed (Table 1.2). Others, including LipK (Rv2385) and LipS (Rv3176c), were re-annotated.[52] LipJ (Rv1900c) has both an N-terminal α/β hydrolase domain and a C-terminal cyclase homology domain.[53] Thus far, only the adenylyl cyclase activity of LipJ has been characterized.[53]

Despite being called the “Lip” family, most of the characterized Lip esterases are non-lipolytic—that is, unable to hydrolyze water-insoluble esters. Cao *et al.* expressed 10 Lip family members (LipI, LipL, LipM, LipN, LipQ, LipT, LipU, LipY, and LipZ).[54] Of the enzymes screened, LipL (Rv1497) had the greatest activity with long-chain esters. However, LipL still had higher activity with C2 and C4 esters than long-chain esters, highlighting the fact that many of these enzymes can accommodate a variety of substrate chain lengths. LipL also has β-lactamase activity—the first example of a mycobacterial enzyme with both activities.[55] As β-lactamases render treatment with β-lactam antibiotics ineffective, these findings suggest a dual role for LipL in lipid metabolism and intrinsic antibiotic resistance.[56]

The gene encoding LipF (Rv3487c) lies within a gene cluster related to virulence.[57] In support of its potential role in virulence, a *lipF* mutant had attenuated growth in mouse bone marrow-derived macrophages.[57] In addition to hydrolyzing short-chain esters,[58] LipF has phospholipase C activity, hydrolyzing phosphatidylcholine to generate diacylglycerol (DAG), a signaling molecule that can activate macrophages.[59] This suggests that LipF could contribute to the host immune response to *Mtb* infection.

Twelve of the Lip family members (LipC, LipF, LipH, LipI, LipM, LipN, LipO, LipQ, LipR, LipU, LipW, and LipY) are also hormone-sensitive lipase (HSL) family members.[60] These enzymes are homologous to human HSL, which mobilizes free fatty acids from stored triacylglycerol (TAG) in adipocytes in

response to hormone stimulation.[61,62] That makes these *Mtb* esterases of particular interest for their potential roles in utilizing host-derived TAG in dormancy and reactivation.

Delorme *et al.* successfully expressed nine of these family members (LipC, LipF, LipH, LipI, LipN, LipR, LipU, LipW, and LipY) and examined their substrate preferences.[60] LipY (Rv3097c) was the only true lipase of the set, able to hydrolyze long-chain, insoluble TAG. This confirmed previous studies that characterized LipY as a lipase involved in TAG utilization.[37,60] Furthermore, *lipY* is under the control of the DosR regulon, which controls the initial transcriptional response to hypoxia.[63-69] Quantitative PCR studies confirmed *lipY*'s transcriptional upregulation.[63] Together, these findings strongly implicated a role for LipY in *Mtb* dormancy and reactivation, and LipY emerged as a promising new candidate for latent TB-targeted therapeutics.[70-72]

Despite its transcriptional upregulation, LipY has not been identified in shotgun proteomic studies of lysates from normoxic or hypoxic cultures.[73-75] This suggests that transcript level does not correlate with LipY abundance. LipY has only been found in a proteomic study of *Mtb*-infected guinea pig lungs 90 days post-infection,[76] providing evidence that it is expressed at appreciable levels during infection.

LipY is also a PE protein. Nearly 10% of all *Mtb* proteins belong to the PE/PPE family, so-named for the proline-glutamic acid (PE) or proline-proline-glutamic acid (PPE) motifs in their N-terminal domains.[41] Although their functions

are largely unknown, PE/PPE proteins are implicated in mycobacterial virulence.[77-81] LipX, PE16 (Rv1430), and LipY are the only known esterases in the PE/PPE family. PE/PPE proteins are secreted via ESX-5, a type VII secretion system, and the PE/PPE domains are then cleaved at the cell surface.[82] The PE domain of LipY contributes to its aggregation and decreases its enzymatic activity compared with LipY lacking the domain,[83,84] suggesting that it not only marks LipY for secretion but has a functional role in modulating its activity. However, LipY has not been detected in proteomic studies of culture filtrate,[85-87] showing that its secretion does not account for its absence in proteomic profiling experiments of *in vitro* cultures.

Several *Mtb* Lip family members have been explored as potential immunodiagnostic markers for TB. Recombinant LipC and LipY both elicited a strong immune response in patients with active TB but not in individuals with latent TB.[40,88] Recombinant LipL also induced an immune response in sera from TB patients that was significantly higher than that from healthy controls.[54] Overall, these results indicate that *Mtb* esterases may be useful biomarkers for distinguishing patients with active TB infections from those with latent infections. However, there is still a pressing need for latent TB-specific biomarkers.[10,89,90]

Cutinase-Like Proteins

Cutinases are a specialized class of esterase that cleave cutin, a hydroxy and epoxy fatty acid polyester found in plant cuticles.[91,92] The seven cutinase-

like proteins (Culps) of *Mtb* have a similar predicted active site to a well-characterized fungal cutinase from *Fusarium solani*.[93] However, these *Mtb* enzymes do not cleave cutin.[47]

Culp6 (Rv3802c) has the most similarity to CulpL of *Mycobacterium leprae*, an organism that has undergone reductive evolution, suggesting that the other *Mtb* Culps are products of gene duplication.[47] Two secreted Culps, Culp1 (Rv1984c) and Culp4 (Rv3452), share 52% identity and 66% homology, suggesting that they are structurally related.[94] However, biochemical characterization revealed different enzyme activities (Table 1.3). Culp1 showed a preference for C8 monoester substrates.[95] Culp4 has phospholipase A_2 activity[95,96] and moderate activity with short-chain esters.[47] Both of these enzymes may contribute to mycobacterial dissemination; Culp1 induces alveolar epithelial cell apoptosis,[97] and Culp4 induces macrophage lysis *in vitro*.[95] The gene encoding Culp1 lies within the region of deletion 2 (RD2), a genomic region that is missing from *M. bovis* (BCG) substrains but retained in *Mtb*.[41,98,99] Immunization with recombinant Culp1 provided partial protection against TB,[100] and supplementing the BCG vaccine with Culp1 and other RD antigens enhanced the vaccine's efficacy in mice.[101] Furthermore, both Culp1 and Culp4 have been explored as potential TB diagnostic biomarkers, with Culp4 having greater sensitivity and specificity.[40]

Of the remaining Culps, only Culp6 has appreciable esterase activity. It displayed lipase, phospholipase, and thioesterase activities.[102] Notably, this

enzyme is essential for *in vitro* growth.[103,104] Like Culp1, Culp6 has been explored as a vaccine candidate due to its ability to protect against TB in mice.[105]

Other Identified Esterases and Lipases

Rv0183 was the second *Mtb* lipase to be purified and biochemically characterized.[106,107] Rv0183 is a monoacylglycerol (MAG) lipase active against MAGs of varying chain lengths (C4–C18) (Table 1.4).[106] Although Rv0183 also hydrolyzes DAGs and vinyl esters to a lesser extent, it does not hydrolyze TAGs.[106,107] This suggests that Rv0183 completes the TAG lipolysis process started by TAG lipases such as LipY.

The Rv0183 *Mycobacterium smegmatis* ortholog, MSMEG_0220, has similar biochemical properties to Rv0183.[107] *M. smegmatis* is a non-pathogenic species of mycobacteria frequently used as a model organism to investigate mycobacterial physiology. Dhouib and colleagues disrupted *MSMEG_0220*, reasoning that this would also inform on the physiological role of Rv0183 in *Mtb*.[107] The mutant strain was unable to grow with monoolein as the sole carbon source, indicating that MSMEG_0220 is essential for the metabolism of this lipid. These findings suggest a role for Rv0183 in *Mtb* exogenous lipid metabolism and have prompted researchers to identify selective Rv0183 inhibitors.[70,71,108]

Whereas Rv0183 is lipolytic, carboxylesterase A (CaeA, Rv2224c) is a non-lipolytic cell wall-associated esterase.[46] Originally annotated as a proteinase, the gene encoding CaeA was identified as a putative virulence

gene.[109-111] Interestingly, only esterase activity was observed when CaeA was first characterized. However, subsequent studies also detected proteolytic activity, and CaeA is therefore also known as Hip1 (hydrolase important for pathogenesis 1).[112] In a mouse model of TB, mutant *Mtb* strains lacking CaeA had a smaller bacterial burden and were less lethal than wild type *Mtb*,[46,113] indicating that CaeA is required for full *Mtb* virulence. Further studies showed that CaeA dampens macrophage proinflammatory responses[112,114] and impairs dendritic cell functions,[115] suggesting that CaeA accelerates disease progression.

Rv0045c was originally annotated as a hydrolase of unknown function, sharing little sequence similarity to other mycobacterial esterases and lipases.[116] However, biochemical characterization defined Rv0045c as an esterase, hydrolyzing C2–C14, but not longer-chain *p*-nitrophenyl esters.[48] The structure of Rv0045c was determined using X-ray crystallography and showed similarity to two very different bacterial hydrolases: ybfF hydrolase from *E. coli* and (*E*)-2-(acetamindomethylene) succinate hydrolase from *Mesorhizobium loti.*[116-119] The ybfF hydrolases catalyze the hydrolysis of 1,2-*O*-isopropylideneglycerol esters[120] as well as the thioester of malonyl-CoA[118] whereas (*E*)-2-(acetamindomethylene) succinate hydrolase catalyzes the final step in the degradation of vitamin B_6.[119] Thus, structural homology did not inform on the natural substrate specificity of Rv0045c.

In an effort to better define the reactivity of this unique *Mtb* esterase, Lukowski *et al.* characterized Rv0045c with a diverse library of fluorogenic

hydrolase substrates.[121] They found that although Rv0045c had a broad, open binding pocket, two residues bordering the binding pocket, Gly90 and His187, narrowed its substrate selectivity to short, straight chain alkyl substrates.

Recently, Kumar and colleagues performed an *in silico* analysis to identify additional uncharacterized esterases and lipases.[122] Rv0421c, Rv0519c, Rv0774c, Rv1191, Rv1592c, and Rv3591c all contained the characteristic serine hydrolase α/β hydrolase fold and the G-X-S-X-G esterase active site motif. Biochemical characterization of these hypothetical proteins confirmed esterase activity. Rv0421c, Rv0519c, Rv0774c, and Rv1191 favored short to medium-chain (C2–12) esters, while Rv1592c and Rv3591c could also hydrolyze longer chain esters (C18).

Chemical Tools for Detecting Esterase Activity

Despite difficulties expressing and isolating active *Mtb* esterases,[37,47,60] researchers have made substantial progress in characterizing these enzymes *in vitro*. However, such characterizations usually only hint at an esterase's biological role. *Mtb* gene and protein expression data provide further information for identifying esterases that may be utilized in dormancy and reactivation (Tables 1.5 and 1.6). Yet, serine hydrolases, including esterases, can be post-translationally regulated,[123] so protein abundance is not an indication of functional enzyme.

Unlike transcriptomics and whole-cell proteomics, chemical tools provide a means of determining changes in enzyme *activity*. These versatile probes can target specific enzyme classes in complex mixtures or living organisms.[124-126] A handful of enzyme-targeted probes have been used to better understand *Mtb*. Substrate analogs have been employed to annotate the genome,[127] identify therapeutic targets,[128,129] and to characterize enzymatic activity.[130] My dissertation research utilized two classes of chemical tools for *Mtb* esterase detection and characterization: fluorogenic probes and activity-based probes (Figure 1.3).

Fluorogenic Probes

Enzyme-targeted fluorogenic probes become fluorescent upon enzyme turnover, providing a sensitive and direct readout of enzyme activity.[131] These probes are not specific for *Mtb* enzymes but are targeted to a particular enzyme class. Fluorogenic probes can be used in a variety of applications, including enzyme characterization assays (e.g., kinetics, inhibitor screens, substrate screens), *in vivo* enzyme detection,[132] and fluorescence microscopy.[133,134]

The simplest fluorogenic esterase probes are fluorophores masked by acetate esters (e.g., fluorescein diacetate, FDA), but these suffer from high background fluorescence due to significant levels of spontaneous hydrolysis.[135-137] Thus, researchers have developed a variety of masking strategies to create more stable substrates.[135-141] A foremost example of this is the acyloxymethyl

ether masking moiety.[135,137,139] Ester cleavage yields a hydroxymethyl ether, which rapidly decomposes to generate the parent fluorophore.

Activity-Based Probes

Activity-based probes (ABPs) form a covalent bond with an enzyme's catalytic residue, resulting in stoichiometric labeling.[124,142] ABPs have three main parts: a reactive group that binds to the catalytic residue of a particular enzyme class based on its reaction mechanism; a linker region, which can also include a specificity element to narrow the reactivity of the probe; and a tag for detection. The tag can be a fluorophore for in-gel fluorescence visualization or an affinity handle for targeted enrichment and protein identification by mass spectrometry. This makes ABPs particularly powerful for identifying enzymes of a specific class based on their activity, with no prior knowledge of the enzyme needed.

APBs can be designed to be narrowly or broadly reactive. For example, an ABP analogue of a selective covalent inhibitor can be used to determine the inhibitor's targets.[128] Broadly reactive ABPs are useful for global profiling and genome annotation.[123,127,143] Fluorophosphonates (FPs) specifically react with the active site serine of serine hydrolases.[123,144] Therefore, FP ABPs can be employed to globally profile serine hydrolases, including esterases, in *Mtb*.[123]

Dissertation Overview

The overarching goal of my dissertation research was to develop and use chemical tools to study *Mtb*. I hypothesized that *Mtb* esterases are utilized across pathogen metabolic states, and a better understanding of the active esterases would aid TB diagnostic and drug development efforts. First, I developed broadly reactive fluorogenic esterase substrates and showed that they could be used to examine *Mtb* esterases in cellular lysates (Chapter 2). Next, I collaborated with Dr. Samantha Levine, a post-doctoral researcher in the Beatty lab, to develop an expanded probe set with longer-chain moieties that are superior lipase substrates. I used these probes to reveal active *Mtb* esterases in lysates from *Mtb*-infected macrophages (Chapter 3). Then, I used both fluorogenic probes and ABPs to identify active *Mtb* esterases in replicating, dormant, and reactivating bacteria (Chapter 4). Overall, I developed an assay for screening mycobacterial esterase activity across stages of infection, which could be applied to other infection models or enzyme targets. Furthermore, I identified esterases that remain active in dormant bacteria, which can be exploited as diagnostic biomarkers or drug targets.

Tables

Table 1.1. Essentiality, size, and cellular location of known *Mtb* esterases.

	Name	Rv	Essential	Mass (kDa)	Localization[a]	Ref
Lip Family	LipC	Rv0220	N	44.3	cell surface	88,103,104
	LipD	Rv1923	N	47.2	cell membrane, whole-cell lysate	103,104,145,146
	LipE	Rv3775	N	45.3	cell membrane, whole-cell lysate	103,104,146-148
	LipF	Rv3487c	N	29.4	ND	58,59,103,104
	LipG	Rv0646c	N/Y[b]	32.9	cell membrane	103,104,148,149
	LipH (NlhH)	Rv1399c	N	33.9	whole-cell lysate	44,103,104,147,150
	LipI	Rv1400c	Y	34.1	whole-cell lysate	104,147
	LipJ	Rv1900c	N	49.7	whole-cell lysate	103,104,147
	LipL	Rv1497	N	45.8	cell surface	54,55,103,104
	LipM	Rv2284	N	46.7	cell membrane, whole-cell lysate	103,104,146-148,151
	LipN	Rv2970c	N	40.1	cell membrane, whole-cell lysate	103,104,146-148,152
	LipO	Rv1426c	N	46.1	cell membrane	103,104,151
	LipP	Rv2463	N/Y[b]	42.8	cell membrane	103,104,149,151
	LipQ	Rv2485c	N	45.2	cytosol	103,104,151
	LipR	Rv3084	N	32.6	cell membrane	103,104,151
	LipT	Rv2045c	N	56.1	ND	103,104
	LipU	Rv1076	Y	31.6	ND	104
	LipV	Rv3203	N	23.6	whole-cell lysate	103,104,147,153
	LipW	Rv0217c	N	32.2	ND	103,104
	LipX (PE11)	Rv1169c	Y	10.8	cell membrane	103,146,147,154
	LipY	Rv3097c	N	45.0	cell surface, cytosol	37,60,103,104
	LipZ	Rv1834	N	31.6	ND	103,104
Cutinase-Like Proteins	Culp1 (Cfp21)	Rv1984c	N	21.8	culture filtrate, cell membrane, whole cell	47,86,87,95,104,146,147
	Culp2 (Cut2, Cfp25)	Rv2301	N	23.9	culture filtrate, cell membrane, whole cell	47,86,87,103,104,146,147
	Culp3 (Cut3)	Rv3451	N	26.5	culture filtrate, cell membrane	47,87,103,104,146,147
	Culp4 (Cut4)	Rv3452	N	23.1	secreted	47,95,103,104
	Culp5 (Cut1)	Rv1758	N	17.9	ND	47,103,104
	Culp6	Rv3802c	Y	35.4	culture filtrate, cell membrane	47,103,104,146,147,155
	Culp7 (Cut5b)	Rv3724B	ND	18.8	ND	47
Other Esterases	—	Rv0045c	N	32	whole-cell lysate	103,104,147
	—	Rv0183	N	30.3	cell wall and membrane	103,104,146-148,151
	—	Rv0421c	N	21.7	cytosol	103,122,151
	—	Rv0519c	N	31.3	culture filtrate only	103,104,122,147
	—	Rv0774c	N	30.1	culture filtrate, whole-cell lysate	87,103,104,122,147
	—	Rv1191	N	32.6	membrane	103,104,122,146-148
	—	Rv1592c	N	48.0	ND	103,104,122
	—	Rv1683	Y	107.4	cell membrane, whole-cell lysate	103,104,146-148,151
	—	Rv2525c	N	25.4	culture filtrate only	103,104,147
	CaeA (Hip1)	Rv2224c	N/Y[b]	55.9	cytosol, cell membrane, culture filtrate	46,87,103,104,109,146-149,151,155
	PE16	Rv1430	N	54.6	ND	103,104,110
	TB22.2	Rv3036c	N	24.4	cell membrane, culture filtrate	87,103,104,147

Data curated from TubercuList: http://www.tuberculist.epfl.ch. "ND" denotes "no data."

[a]Enzyme localization determined by proteomic studies or Western blot. See references for more information.

[b]Non-essential for *in vitro* growth but essential for *Mtb* survival in macrophages.

Table 1.2. Ester substrate preferences of characterized Lip family members.

	Maximal Activity				
Esterase	**Ester Chain**	**Temp (°C)**	**pH**	**Inhibitors**	**Ref**
LipC	C4				*60,88*
LipD	C16	40	8	THL	*60,128,145*
LipF	C2	35	7.5		*58,60*
LipH	C3	45	7	E-600, THL	*60,128,150*
LipI	C4				*60*
LipL	C2–C4	37	8		*54,55*
LipN	C2	45	8	THL	*60,152*
LipR	C8				*60*
LipU	C8				*60*
LipV	C14	50	8	THL	*128,153*
LipW	C4				*60*
LipY	C4			THL	*60*

Table 1.3. Ester substrate preferences of characterized *Mtb* Culps.

	Maximal Activity				
Esterase	**Ester Chain**	**Temp (°C)**	**pH**	**Inhibitors**	**Ref**
Culp1	C8	37	7.5	E-600, THL	*47,95*
Culp4	C4		7.5	E-600, THL	*47,95*
Culp6	C12			E.600, THL	*47,102*

Table 1.4. Ester substrate preferences of other characterized *Mtb* esterases.

	Maximal Activity				
Esterase	**Ester Chain**	**Temp (°C)**	**pH**	**Inhibitors**	**Ref**
CaeA	C4	39	7	E-600	*46*
PE16	C6	37	7–8	PMSF	*49*
Rv0045c	C4	39	8		*48,121*
Rv0183	C8 (MAG)	50	7.4	PMSF, E-600, THL	*106,107*
Rv0421c	C4				*122*
Rv0519c	C4				*122*
Rv0774c	C8				*122*
Rv1191	C12				*122*
Rv1592c	C12				*122*
Rv2525c	C4	38	8		*51*
Rv3036c	C2	38	8		*50*
Rv3591c	C12				*122*

Table 1.5. *Mtb* esterase genes that are differentially regulated in various growth conditions.

	Condition			
Esterase	**Starvation[24]**	**Hypoxia[63,156]**	**Murine Adipocyte[157]**	**Other**
caeA	↑			↑ macrophage infection[111]
culp2	↑			
culp3	↑			
lipC	↑		↓	
lipD			↓	↑ oxidative stress[145]
lipE			↓	
lipF	↓		↑	↑ acid stress[58,158,159]
lipG			↓	
lipH			↑	
lipI			↑	
lipJ			↑	
lipL				↑ acid stress[55]
lipM			↓	
lipN			↑	↑ acid stress[152]
lipP			↓	
lipQ			↑	
lipR				↑ acid stress[159]
lipT	↑			
lipU	↑			
lipV			↑	↑ acid stress[153]
lipW			↓	
lipX	↑	↑	↑	↑ acid stress,[159] high temp[160]
lipY		↑	↑	
lipZ			↓	
Rv1592c	↓	↑		

The up arrow denotes transcriptional upregulation, and the down arrow denotes transcriptional downregulation. The absence of an arrow means the transcript level was not significantly changed in the indicated studies.

Table 1.6. *Mtb* esterase identification in proteomic profiling experiments.

			Guinea Pig Lungs		
Esterase	**Normoxia**	**Hypoxia**	**30 days**	**90 days**	**Ref**
CaeA	X	X			*73-75,161*
Culp1	X	X			*74,75,161*
Culp2	X	X		X	*75,76,161,162*
Culp3	X				*73,161*
Culp5				X	*76*
Culp6	X	X			*73,75,161*
LipC	X	X			*73,161,162*
LipD	X	X			*73-75,161,162*
LipE	X	X			*73-75,161,162*
LipF	X	X			*73,75,161,162*
LipG	X	X			*73,75,161,162*
LipH	X	X			*74,75,161,162*
LipI	X	X			*73-75,161,162*
LipJ	X	X			*75,161*
LipL	X				*161,162*
LipM	X	X			*73-75,161,162*
LipN	X	X			*73-75,161,162*
LipO	X	X			*73,75,161,162*
LipP	X				*73,161,162*
LipQ	X				*74,161,162*
LipR	X	X		X	*74-76,161,162*
LipT	X				*73,161,162*
LipV	X	X			*73-75,161,162*
LipW	X	X			*73,75,161,162*
LipY				X	*76*
LipZ	X				*73,161*
Rv0045c	X	X			*73,75,161*
Rv0183	X	X		X	*73-75,161*
Rv0421c	X	X	X		*75,76,161*
Rv0774c	X	X			*75,161*
Rv1191	X	X			*74,75,161*
Rv1592c	X	X			*75,161*
Rv1683	X	X			*73-75*
Rv2525c	X				*161*
Rv3036c	X	X			*73-75,161*
Rv3591c	X	X			*74,75,161*

An “X” indicates that the protein was identified in the corresponding condition.

Figures

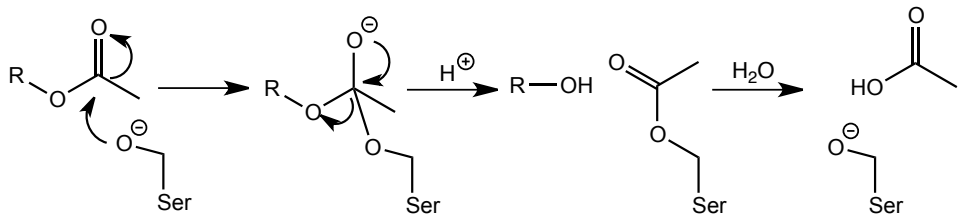

Figure 1.1. Esterases hydrolyze an ester into an alcohol and an acid.

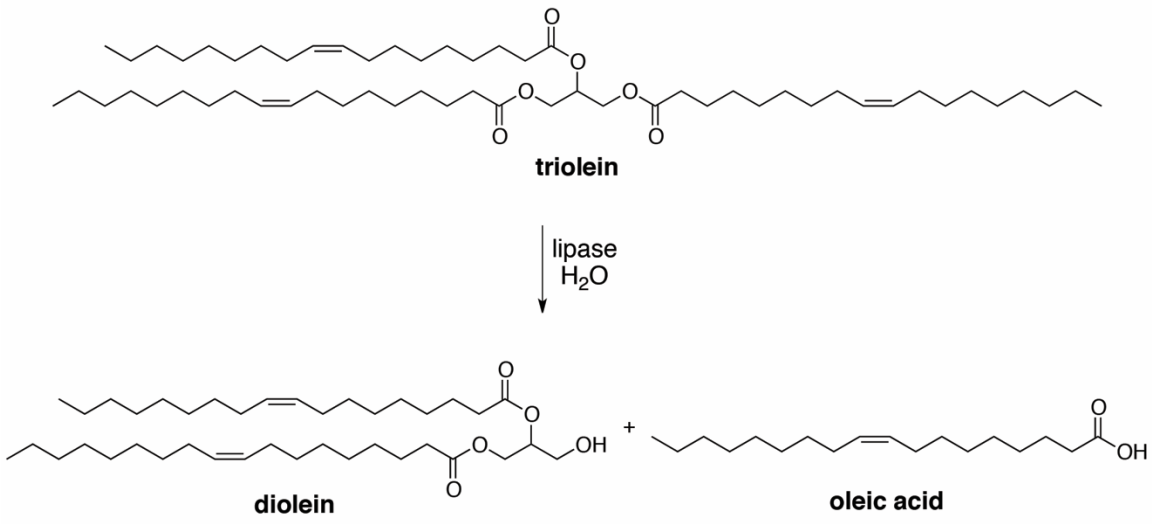

Figure 1.2. Lipases cleave water-insoluble esters.

In this example, a TAG lipase hydrolyzes triolein to release diolein and oleic acid.

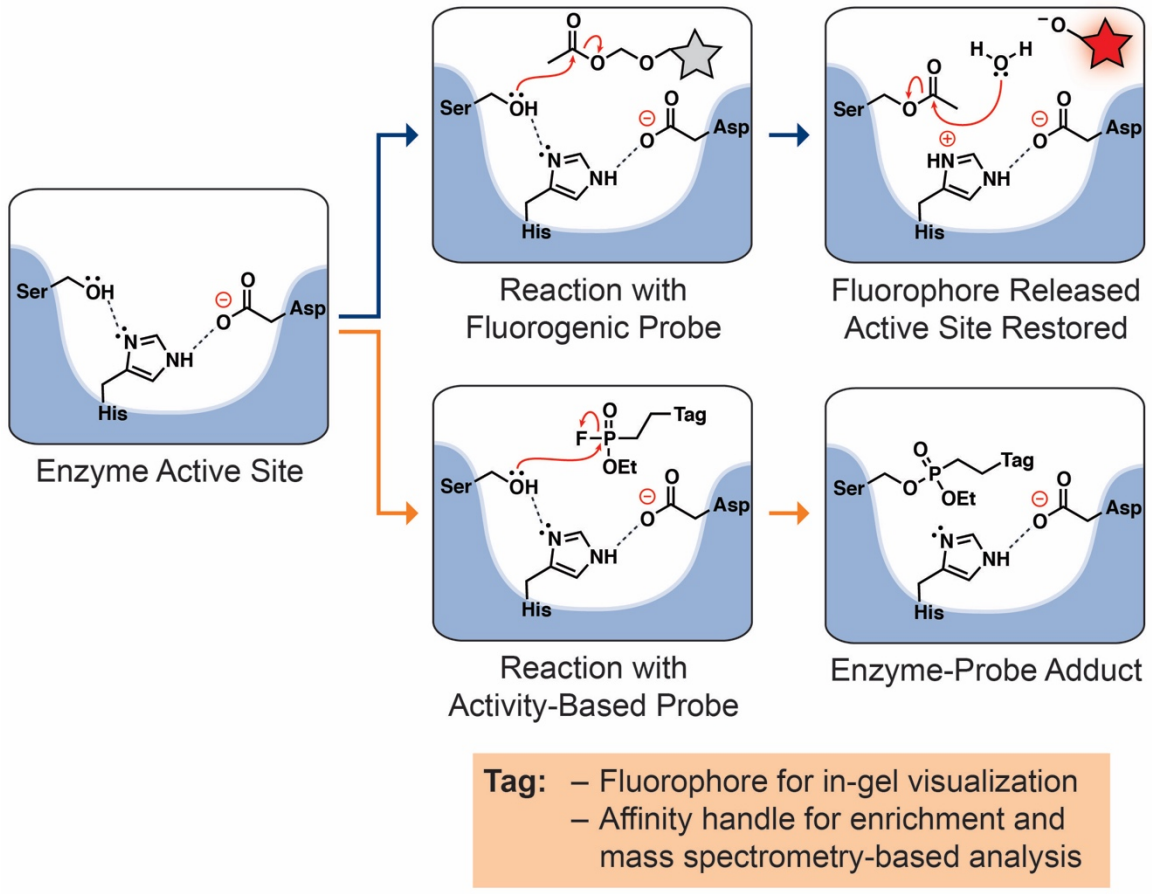

Figure 1.3. Chemical tools for esterase characterization.

Fluorogenic probes and ABPs both react with the catalytic serine of active esterases. Whereas fluorogenic probes produce an amplifiable signal, ABPs covalently label the active site residue for stoichiometric (1:1) labeling. Fluorogenic probes become fluorescent upon enzyme turnover, but ABPs must include a reporter tag for detection.

Chapter 2: Far-Red Fluorogenic Probes for Esterase and Lipase Detection

Katie R. Tallman and Kimberly E. Beatty

This work was originally published by *ChemBioChem* on January 2, 2015 in volume 16, issue 1, pages 70–75 (Copyright 2014 John Wiley and Sons).[163] It has been adapted for this dissertation and reprinted with permission.

Abstract

Fluorogenic enzyme probes go from a dark to a bright state following hydrolysis and can provide a sensitive, real-time readout of enzyme activity. They are useful for examining enzymatic activity in bacteria, including the human pathogen *Mycobacterium tuberculosis*. Herein, we describe two fluorogenic esterase probes derived from the far-red fluorophore 7-hydroxy-9*H*-(1,3-dichloro-9,9-dimethylacridin-2-one) (DDAO). These probes offer enhanced optical properties compared to existing esterase probes because the hydrolysis product, DDAO, excites above 600 nm while retaining a good quantum yield (ϕ = 0.40). We validated both probes with a panel of commercially available enzymes alongside known resorufin- and fluorescein-derived esterase substrates. Furthermore, we used these probes to reveal esterase activity in protein gel-

resolved mycobacterial lysates. These probes represent new tools for esterase detection and characterization and should find use in a variety of applications.

Introduction

Tuberculosis (TB) is a serious human disease caused by several mycobacterial species, including *Mycobacterium tuberculosis* (*Mtb*). Small molecule probes are versatile tools for studying bacterial pathogens because they can target specific enzyme classes in complex mixtures or living organisms.[124-126] A variety of enzyme-targeted probes have been used to better understand *Mtb*. Substrate analogs have been employed to annotate the genome,[127] identify therapeutic targets,[128,129] and to characterize enzymatic activity.[92] A small but powerful subset of mycobacterially-targeted probes are fluorogenic, which enables a sensitive and direct read-out of enzyme activities.[131] For example, a fluorogenic probe specific for the *Mtb* β-lactamase BlaC has been used to detect infections in mouse models[132] and sputum samples.[164] Furthermore, we recently used fluorogenic probes to examine mycobacterial sulfatases in a protein gel-based assay.[165,166] We found that while most mycobacterial species, including *Mtb*, could hydrolyze sulfated fluorophores, the pattern of sulfatase activity varied from one species to another.

Fluorogenic probes could be ideal tools to detect, classify, and characterize mycobacterial esterases, of which there are more than 30 predicted

in the *Mtb* genome.[167,168] This enzyme class includes lipases, which are most active with long-chain, water insoluble esters.[42] Although few *Mtb* esterases or lipases have been biochemically characterized,[37,88] it is likely that they have roles in cell wall remodeling, cell division, nutrient acquisition, and pathogenesis.[168] Detecting and characterizing these esterases has been difficult because most form inclusion bodies in heterologous hosts (i.e., *E. coli*).[37,58,88,145,150,153,169] Fluorogenic enzyme probes could directly detect enzyme activities in intact organisms[132,164] or in protein gel-resolved lysates without the need for isolated enzyme.[165,166,170]

The simplest fluorogenic esterase probes are fluorophores masked by acetate esters (e.g., fluorescein diacetate, FDA), but these suffer from high background fluorescence due to significant levels of spontaneous hydrolysis.[135-137] Thus, researchers have developed a variety of masking strategies to create more stable substrates.[135-141] A foremost example of this is the acetoxymethyl ether (AME) masking moiety,[135,137,139] which we have used to mask substrates in this work. Ester cleavage yields a hydroxymethyl ether, which spontaneously decomposes to generate the free fluorophore (Scheme 2.1).

Among the existing scaffolds, there is a shortage of esterase probes that excite above 600 nm, where cellular autofluorescence and light scattering are diminished.[171] Most existing fluorogenic esterase substrates are based on coumarin,[135,138,141] fluorescein,[137,172] rhodamine,[140,141,173] and resorufin[137,174] scaffolds. The Nagano group reported a ratiometric esterase probe with

fluorescence emission at 760 nm,[175] but most standard laboratory equipment lacks sensitive detection in the near-infrared (NIR). Probes derived from far-red fluorophores, which excite above 600 nm but do not require NIR detection, could prove quite useful. In this category, the far-red fluorophore 7-hydroxy-9*H*-(1,3-dichloro-9,9-dimethylacridin-2-one) (DDAO, $\lambda_{abs/em}$ = 646/660 nm) was successfully developed into a sulfatase[165] and a β-galactosidase probe.[176,177] Additionally, DDAO's high fluorescence above its pK_a of 5.7 makes DDAO-derived probes usable across a broad pH range. Despite these favorable properties, DDAO had not been previously converted into an esterase substrate.

In this work, we report two new fluorogenic probes that are versatile tools for detecting esterase and lipase activity. We synthesized DDAO-7-AME and DDAO-2-AME, two distinct AME-masked fluorogenic probes derived from DDAO. We also synthesized the known compound resorufin acetoxymethyl ether (Res-AME)[137] to enable comparative analyses. We validated each substrate using a commercial panel of esterases and lipases. Ultimately, we used each probe to examine esterase activity in gel-resolved lysates derived from a set of mycobacterial pathogens.

Results and Discussion

DDAO was converted into fluorogenic esterase substrates through a silver-mediated *O*-alkylation. The reaction yielded two regioisomers, DDAO-7-

AME and DDAO-2-AME (Scheme 2.2), which were separable by column chromatography. The site of *O*-alkylation was determined using Nuclear Overhauser Effect Spectroscopy (NOESY; see Figures 2.1–2.2). Res-AME was synthesized as previously described.[137]

A critical feature of any fluorogenic probe is its spectral distinction from the parent fluorophore. We determined the spectral characteristics of DDAO-7-AME, DDAO-2-AME, and Res-AME (Scheme 2.2 and Table 2.1). Although they are regioisomers, DDAO-7-AME and DDAO-2-AME have different absorbance and emission spectra (Figure 2.3). DDAO-7-AME ($\lambda_{abs/em}$ = 465/625 nm) is blue-shifted compared with DDAO ($\lambda_{abs/em}$ = 646/660 nm, ϕ = 0.40[114]) and has a six-fold decrease in quantum yield (ϕ = 0.07). DDAO-2-AME is further blue-shifted (λ_{abs} = 395) and has no detectable fluorescence, making this an exceptional "turn-on" probe. Resorufin ($\lambda_{abs/em}$ = 571/588 nm) and Res-AME ($\lambda_{abs/em}$ = 475/605 nm) have some overlap in their absorbance and emission spectra (Figure 2.3), but Res-AME has a substantial decrease in quantum yield (ϕ = 0.01) compared with resorufin (ϕ = 0.74[178]). Both DDAO and resorufin have favorable pK_a values of 5.7 and 5.8, respectively, and are fluorescent above pH 6 (Figure 2.4, Table 2.1).

Since it is imperative that probes remain masked in the absence of enzyme, we assessed the hydrolytic stability of DDAO-7-AME, DDAO-2-AME, and Res-AME alongside the commercially available substrate FDA. The

fluorescence generated through spontaneous unmasking was monitored at 37 °C in PBS (pH 7.4) or in Dulbecco's Modified Eagle's Medium supplemented with 10% fetal bovine serum (DMEM-FBS) (Figure 2.5). All three AME probes were more stable in PBS than in DMEM-FBS (Table 2.2). FDA was less stable than any of the AME-masked probes, with a calculated half-life ($t_{1/2}$) of 8 h in PBS. Res-AME underwent limited hydrolysis in PBS, with a calculated half-life of 13 h. DDAO-7-AME and DDAO-2-AME both offered improved stability, with half-lives of 27 and 41 h, respectively. In DMEM-FBS, all probes were more susceptible to spontaneous hydrolysis, with calculated half-lives of approximately 0.3 h. The enhanced stability of the two DDAO-AME probes in PBS compared with Res-AME and FDA allows high signal-to-noise to be maintained over longer time course experiments.

We confirmed that DDAO-7-AME and DDAO-2-AME were broadly useful esterase substrates using a panel of commercially available fungal, bacterial, and mammalian esterases and lipases (Figure 2.6). We evaluated three esterases, from porcine liver (PLE), *Saccharomyces cerevisiae*, and *Bacillus subtilis*. The enzyme panel also included nine lipases, from *Aspergillus* sp., *Candida antarctica, Candida rugosa, Mucor miehei, Pseudomonas cepacia, Pseudomonas fluorescens, Rhizopus arrhizus, Rhizopus niveus,* and porcine pancreas. All enzymes rapidly hydrolyzed DDAO-7-AME and DDAO-2-AME to produce a statistically significant ($P < 0.01$) fluorescent signal within 10 min. Res-AME and FDA were cleaved by many of the enzymes, but showed little or

no activation in the presence of *M. miehei* lipase, porcine pancreas lipase, and *S. cerevisiae* esterase. The DDAO-based probes were excellent substrates for *P. fluorescens* lipase, an enzyme that was only modestly active with Res-AME and FDA. Since PLE gave a high signal-to-noise ratio for all probes, we used it to confirm that active enzyme was required for probe cleavage. We reduced PLE's catalytic activity using the esterase inhibitor diethyl-*p*-nitrophenyl phosphate (E-600) or heat inactivation; both methods resulted in an attenuated signal. Overall, the DDAO-AME probes were hydrolyzed rapidly by all of the esterases and lipases examined, demonstrating that these probes offer enhanced speed and versatility for characterizing a diverse set of enzymes, including enzymes that prefer lipid-containing substrates.

Highly sensitive fluorogenic probes are well-suited for verifying the presence of scarce esterases inside cells or in complex lysates.[142] In order to examine the sensitivity of our probes, we determined the PLE detection limit of the DDAO-AME probes alongside Res-AME, FDA, and the chromogenic substrate *p*-nitrophenyl acetate (*p*-NPA; Table 2.3 and Figure 2.7). Each probe was incubated in 10 mM HEPES (pH 7.3) at 37 °C with varying amounts of PLE (0.55 to 2750 pg). After 10 min, the signal from each hydrolyzed probe was measured. FDA was the most sensitive for PLE detection and could detect the lowest amount of PLE evaluated (0.55 pg), while *p*-NPA was the least sensitive (2750 pg). Res-AME detected 27.5 pg PLE, while DDAO-7-AME (11 pg) and DDAO-2-AME (2.75 pg) were able to detect 2.5- to 10-fold less PLE,

respectively. These results demonstrate the high sensitivity of fluorogenic probes for detecting extremely small amounts of esterase.

Next, we characterized the kinetics of a subset of esterases (PLE and *B. subtilis* esterase; Figures 2.8–2.9) and lipases (*C. antarctica* and *M. miehei*; Figures 2.10–2.11) with DDAO-7-AME and Res-AME. Unfortunately, DDAO-2-AME's limited aqueous solubility above 30 μM prevented us from accurately determining the Michaelis constant, K_M, or the maximal velocity, V_{max}. The enzymes evaluated represent a range of hydrolytic activities observed in our enzyme screen (see Figure 2.6). As summarized in Table 2.4, DDAO-7-AME and Res-AME both gave K_M values in the low micromolar range with each enzyme evaluated. DDAO-7-AME was a favorable substrate for PLE (K_M = 7.5 ± 0.8 μM, V_{max} = 1.2 pmol/s). Res-AME was also efficiently cleaved by PLE, with a calculated K_M of 4.9 ± 0.7 μM and a maximal velocity of 0.69 pmol/s. This is close to the reported K_M value for this compound (K_M = 21 μM[137]), and the discrepancy may be due to differences in the concentration range of substrate evaluated or the amount of enzyme used. PLE is a well-defined enzyme, which enabled us to determine the catalytic constant (k_{cat}) and the specificity constant (k_{cat}/K_M) of PLE with DDAO-7-AME (k_{cat} = 1.8 s^{-1}, k_{cat}/K_M = 2.4 x 10^5 M^{-1} s^{-1}) and Res-AME (k_{cat} = 10 s^{-1}, k_{cat}/K_M = 2.0 x 10^6 M^{-1} s^{-1}). Of the enzymes examined, *M. miehei* lipase had the slowest rate of hydrolysis with each probe, consistent with the low activity observed in the enzyme screen (Figure 2.6). Furthermore, a larger amount of enzyme was required to obtain accurate kinetics data for the

lipases than the esterases, suggesting that the probes are better esterase substrates. This is expected, as the AME masking moiety has a short chain ester. Based on our results, we predict that DDAO-7-AME will be useful for the kinetic characterization of a variety of esterases and a subset of lipases, including enzymes isolated from *Mtb*.

We hypothesized that the DDAO-derived esterase probes could be used to detect mycobacterial esterase activity without requiring purified enzyme. We were most interested in the enzymes found in the mycobacterial species that cause TB in humans, which are all classified as members of the *Mtb* complex (MTBC). We therefore evaluated MTBC lysates prepared from three strains of *Mtb* (Erdman, H37Rv, and CDC1551), *Mycobacterium africanum*, and *Mycobacterium bovis* (bacillus Calmette-Guérin, BCG). We included *Mycobacterium kansasii*, *Mycobacterium avium*, and *Mycobacterium intracellulare* in our analysis because these three species also cause pulmonary disease.[179] For comparison, we evaluated lysates from four other species (i.e., *Mycobacterium smegmatis*, *Mycobacterium marinum*, *Mycobacterium flavescens*, and *Mycobacterium nonchromogenicum*). We prepared lysates from each species as previously described[165] and confirmed that DDAO-7-AME, DDAO-2-AME, and Res-AME could each detect mycobacterial esterase activity in a 96-well plate format. All species hydrolyzed the AME to produce a detectable fluorescent signal within 10 min (Figure 2.12).

We previously described a native protein gel-based assay for profiling sulfatase activity in mycobacterial lysates.[165,166] For the current work, we reasoned that we could use AME-masked probes to examine esterase activity in an analogous format. The lysates from twelve mycobacterial species and strains (*vide supra*) were resolved by native polyacrylamide gel electrophoresis (PAGE) on three identical gels. Each gel was soaked in a solution of DDAO-7-AME (1 μM), DDAO-2-AME (1 μM), or Res-AME (5 μM). After 5 min, fluorescence imaging revealed bands of hydrolyzed probe corresponding to discrete mycobacterial esterases in every species examined (Figure 2.13).

This assay format enabled us to identify probe-specific and species-specific patterns of activity. Res-AME had lower signal-to-noise and produced faint banding patterns with the MTBC members (lanes 8–12), despite using 5-fold more probe. In contrast, DDAO-7-AME and DDAO-2-AME each produced strong, clear banding patterns with the MTBC members. These banding patterns were similar for each of the five MTBC samples, but dissimilar from those produced by other mycobacterial species. Notably, DDAO-7-AME revealed an enzyme band that is missing in *M. africanum* (lane 9) but present in the other MTBC members. This subtle difference in banding patterns was not so apparent using DDAO-2-AME or Res-AME.

All three probes revealed distinctive banding patterns with *M. kansasii* (lane 5), *M. avium* (lane 6), and *M. intracellulare* (lane 7), three “atypical” mycobacterial species that cause pulmonary disease. These patterns were

different from those observed for members of the MTBC and could hint at a way to distinguish mycobacterial pathogens in the clinic. Res-AME produced many discrete fluorescent bands with *M. kansasii*, indicating that this probe could be particularly useful for evaluating esterase activity in this species. Importantly, these fluorogenic probes quickly revealed mycobacterial esterases in gel-resolved crude lysates, bypassing the need for technically challenging enzyme expression or lengthy refolding procedures.

Although there is overlap in the activity patterns revealed by each probe, the bands are not identical. This is consistent with the differential activity observed in the enzyme screen (Figure 2.6). Together, these results confirm that esterases have substrate preferences. Additionally, our results imply that the fluorophore scaffold, not just the masking group, can substantially influence reactivity. In the future, the reactivity and selectivity of fluorogenic probes could be fine-tuned for specific enzymes by utilizing alternative fluorophores or altering the acyl group.[172,180]

In conclusion, we synthesized and characterized AME-masked esterase probes starting from the far-red fluorophore DDAO. The attachment of the AME group caused a significant change in spectral properties, making these activatable probes trivial to distinguish from DDAO. The DDAO-AME probes provide a longer wavelength option compared to previously described substrates. These probes were highly sensitive, able to detect low picogram amounts of PLE after a short incubation. DDAO-7-AME displayed K_M values in the low

micromolar range for every enzyme evaluated. Additionally, we used these fluorogenic probes in a new application. We revealed distinct esterase activity patterns in gel-resolved mycobacterial lysates using DDAO-7-AME, DDAO-2-AME, and Res-AME. With these fluorogenic probes in hand, we look forward to developing assays that can stratify mycobacterial strains, annotate enzyme function, and track specific esterase activities during different stages of TB infection.

Materials and Methods

Unless otherwise stated, reactions were magnetically stirred in oven-dried glassware under argon atmosphere. Anhydrous solvents were purchased in sure-seal bottles and kept under argon atmosphere. All chemicals were purchased from Sigma-Aldrich or Fisher Scientific unless otherwise noted and used as received. Reactions were monitored by thin-layer chromatography (TLC) using glass-backed silica gel plates. Flash column chromatography was performed with the indicated solvents using Silicycle SiliaFlash P60 as the stationary phase. Mass spectra were acquired on an electrospray ionization (ESI) spectrometer and obtained by peak matching.

^{1}H-NMR data were obtained at ambient temperature at 400 MHz in $CDCl_3$. ^{13}C-NMR data were obtained at 101 MHz in $CDCl_3$. Chemical shifts are reported as δ values in ppm and were calibrated with tetramethylsilane (TMS). Coupling

constants (*J*) are reported in Hertz (Hz) and are rounded to the nearest 0.1 Hz. Multiplicities are defined as: s = singlet, d = doublet, m = multiplet, dd = doublet of doublets.

Synthesis of DDAO-7-AME and DDAO-2-AME

DDAO (Synchem OHG, 20 mg, 0.065 mmol), powdered 4-Å molecular sieves (60 mg), and silver(I) oxide (38 mg, 0.16 mmol, 2.5 equiv) were suspended in anhydrous acetonitrile (1.5 mL). Bromomethyl acetate (8 μL, 0.08 mmol, 1.2 equiv) was added, and the mixture was stirred for 24 h at room temperature. The reaction mixture was diluted with dichloromethane (CH_2Cl_2), filtered through a plug of Celite® S, and concentrated by rotary evaporation to give an orange solid. Purification by silica gel flash chromatography (5% ethyl acetate/40% CH_2Cl_2/55% hexanes) yielded two products: one bright orange and fluorescent under ultraviolet (UV) light (DDAO-7-AME, R_f = 0.26; 14 mg, 57% yield), and the other yellow and not fluorescent under UV light (DDAO-2-AME, R_f = 0.14; 6.4 mg, 26% yield). NOESY was used to assign the two regioisomers (Figures 2.1–2.2).

DDAO-7-AME (Figures 2.14–2.15)

^{1}H NMR (400 MHz, $CDCl_3$) δ (ppm): 7.65 (s, 1H), 7.65 (d, J = 8.7 Hz, 1H), 7.14 (d, J = 2.7 Hz, 1H), 7.08 (dd, J = 8.7, 2.7 Hz, 1H), 5.86 (s, 2H), 2.17 (s, 3H), 1.89 (s, 6H).

^{13}C NMR (101 MHz, $CDCl_3$) δ (ppm): 173.2, 169.7, 159.6, 148.5, 140.5, 139.4, 137.0, 136.8, 135.0, 133.9, 114.7, 114.6, 84.5, 39.1, 26.7, 20.9.

ESI-MS $[M+H]^+$ m/z calculated for $C_{18}H_{16}Cl_2NO_4$: 380.0456; found: 380.0459.

DDAO-2-AME (Figures 2.16–2.17)

^{1}H NMR (400 MHz, $CDCl_3$) δ (ppm): 7.78 (s, 1H), 7.37 (d, J = 10.1 Hz, 1H), 6.70 (m, 2H), 5.80 (s, 2H), 2.16 (s, 3H), 1.81 (s, 6H).

^{13}C NMR (101 MHz, $CDCl_3$) δ (ppm): 187.3, 170.0, 153.0, 151.7, 148.2, 140.9, 140.5, 133.3, 132.6, 132.3, 129.5, 128.8, 127.9, 88.0, 38.1, 28.8, 20.9.

ESI-MS $[M+H]^+$ m/z calculated for $C_{18}H_{16}Cl_2NO_4$: 380.0456; found: 380.0458.

Synthesis of Res-AME

Res-AME was synthesized on a 100 mg scale according to the published protocol.[137] Following extraction, Res-AME was purified by silica gel flash chromatography (0 to 10% MeOH in CH_2Cl_2). The product was isolated as a dark yellow solid (53 mg, 40% yield).

Res-AME (Figures 2.18–2.19)

^{1}H NMR (400 MHz, $CDCl_3$) δ (ppm): 7.75 (d, J = 8.8 Hz, 1H), 7.43 (d, J = 9.8 Hz, 1H), 7.05 (dd, J = 8.9, 2.6 Hz, 1H), 7.00 (d, J = 2.6 Hz, 1H), 6.85 (dd, J = 9.8, 2.1 Hz, 1H), 6.34 (d, J = 2.0 Hz, 1H), 5.84 (s, 2H), 2.16 (s, 3H).

^{13}C NMR (101 MHz, $CDCl_3$) δ (ppm): 186.3, 169.6, 160.1, 149.6, 146.7, 145.3, 134.8, 134.6, 131.7, 129.3, 114.3, 107.0, 102.6, 84.6, 20.9.

ESI-MS $[M+H]^+$ m/z calculated for $C_{15}H_{12}NO_5$: 286.0715; found: 286.0714.

pK_a Determination

The pK_a's of DDAO and resorufin were determined by measuring their fluorescence over a pH range. The following buffers were prepared at room temperature at the indicated pH: citric acid-disodium phosphate (pH 2.8, 2.9, 3.1, 3.4, 3.8, 4.4, 4.9, 5.3, 5.9, 6.1, 6.4); potassium phosphate (pH 4.7, 5.6, 6.6, 7.2, 7.6); Tris (pH 7.8, 8.0, 8.1, 8.6, 8.8); and sodium carbonate-sodium bicarbonate (pH 9.2, 9.6, 10.3). DDAO (5 mM in DMSO) and resorufin (20 mM in 0.1 N NaOH) were diluted to 10 μM in H_2O. Fluorophores were then further diluted to 1 μM in buffer at each pH (n = 3 for each pH). Fluorescence was assessed on a Tecan Infinite M200 Pro microplate reader (DDAO: λ_{ex} 635 nm, λ_{em} 670 nm; resorufin: λ_{ex} 550 nm, λ_{em} 600 nm). Data were plotted and fit to a sigmoidal curve in GraphPad Prism 6. The pK_a was determined as the inflection point of the curve (Figure 2.4).

Spectral characterization

The spectral properties of DDAO-7-AME, DDAO-2-AME, and Res-AME are summarized in Table 2.1. Absorbance and emission spectra were acquired

on a Tecan Infinite M200 Pro microplate reader in fluorescence-grade quartz cuvettes for absorbance reads (2 nm step size) and in black 96-well plates for fluorescence reads (10 reads per well; 2 nm step size). Compounds were diluted to 1 μM in 10 mM HEPES (pH 7.3).

The extinction coefficient was determined for DDAO, resorufin, DDAO-7-AME, DDAO-2-AME, and Res-AME. Three to four separate stock solutions were prepared in DMSO (5 mM for DDAO, DDAO-7-AME, DDAO-2-AME, and Res-AME) or 0.1 N NaOH (20 mM resorufin). Experiments were performed in a 96-well plate format using a pathlength correction based on the absorbance of water: sample pathlength (cm) = ($Abs977_{water}$ – $Abs900_{water}$)/0.182, where 0.182 = ($Abs977_{water}$ – $Abs900_{water}$) in a 1 cm cuvette. The absorbance at λ_{max} was then divided by the sample pathlength for the pathlength-corrected absorbance (i.e., the absorbance for a 1 cm pathlength). Molar extinction coefficients were calculated as the slope of the absorbance vs. probe concentration using Beer's Law ($A=\varepsilon cl$; A = absorbance, ε = extinction coefficient, c = concentration, l = pathlength). Only pathlength-corrected absorbance values between 0.1 and 1 were used for these calculations.

The relative quantum yields[181] of DDAO-7-AME and Res-AME were determined using 4-(dicyanomethylene)-2-methyl-6-(4-dimethylaminostyryl)-4*H*-pyran (DCM, Exciton; ϕ = 0.44 in EtOH) as the reference standard. Each sample was excited at 450 nm, and the full fluorescence emission curve was obtained on a Tecan Infinite M200Pro microplate reader. DDAO-7-AME and Res-AME were

evaluated in both DMSO and in 10 mM HEPES (pH 7.3) buffer. DDAO-2-AME was not evaluated, as it displayed no detectable fluorescence.

Aqueous stability

DDAO-7-AME, DDAO-2-AME, Res-AME, and FDA were diluted to 1 μM in PBS (pH 7.4), DMEM-FBS [Dulbecco's Modified Eagle Medium (Gibco®) supplemented with 10% fetal bovine serum (HyClone™)], or DMEM-FBS (h.i.) (heat-inactivated serum; heated at 56 °C for 40 min). Samples, prepared in triplicate, were incubated at 37 °C, and fluorescence was measured every 5 min for 15 h on a Molecular Devices SpectraMax M5 microplate reader (DDAO: λ_{ex} 635 nm, λ_{em} 670 nm; resorufin: λ_{ex} 550 nm, λ_{em} 600 nm; fluorescein: λ_{ex} 490 nm, λ_{em} 525 nm). Stability curves are shown in Figure 2.5. Because samples were completely hydrolyzed within the 15 h time course in DMEM-FBS and DMEM-FBS (h.i.), curves were fit to a one phase decay equation ($Y = [Y_0 - Plateau]*exp(-K*X) + Plateau$, where Y = fluorescence, K = the rate constant, X = time, and the half-life is calculated as ln(2)/K in GraphPad Prism 6. Because the probes did not completely hydrolyze in PBS, each probe was also diluted into PBS containing 1 μg PLE and allowed to react for the duration of the experiment to obtain the fluorescence value (plateau) of fully hydrolyzed probe. The one phase decay equation was constrained with this value in order to calculate the probe half-life in PBS. Calculated half-lives are reported in Table 2.2.

Esterase screen

Esterases and lipases were purchased from Sigma-Aldrich. Lipases were purchased as Lipase Basic Kit (product number 62327). Enzymes were prepared as 10 mg/mL stocks and diluted to 5 μg/mL in 10 mM HEPES buffer (pH 7.3). Heat-inactivated PLE was prepared by incubating PLE at 90 °C for 15 min. Alternatively, PLE activity was inhibited by incubation with 50 μM E-600 (Sigma-Aldrich, 36186) at 37 °C for 60 min prior to probe addition. The reactions were initiated with 5 μM DDAO-7-AME, DDAO-2-AME, Res-AME, or FDA. The reactions were incubated at 37 °C before reading on a Tecan Infinite M200Pro microplate reader (fluorescein: λ_{ex} 485 nm, λ_{em} 530 nm; resorufin: λ_{ex} 550 nm, λ_{em} 600 nm; DDAO: λ_{ex} 635 nm, λ_{em} 670 nm) at 10 min (Figure 2.6).

PLE detection limit

PLE was diluted in 10 mM HEPES (pH 7.3) so that the final amount in each reaction mixture ranged from 0.275 pg to 550 pg for DDAO-7-AME, DDAO-2-AME, Res-AME, and FDA. A larger range, from 1.1 pg to 2750 pg, was used for *p*-NPA owing to the lower sensitivity for detecting *p*-NP absorbance. The reactions were initiated by the addition of substrate at a final concentration of 25 μM for DDAO-7-AME, DDAO-2-AME, Res-AME, and FDA, or 1700 μM for *p*-NPA and incubated at 37 °C (Figure 2.7). Fluorescence (DDAO, resorufin, and fluorescein) or absorbance (*p*-NP) was measured on a Tecan Infinite M200Pro

microplate reader (DDAO: λ_{ex} 635 nm, λ_{em} 670 nm; resorufin: λ_{ex} 550 nm, λ_{em} 600 nm; fluorescein: λ_{ex} 490 nm, λ_{em} 525 nm; *p*-NP: λ_{abs} 348 nm).

Kinetics

All kinetic assays were performed in triplicate or sextuplicate in 10 mM HEPES buffer (pH 7.3) at 37 °C. Probe solutions were pre-incubated at 37 °C for 15 min prior to enzyme addition. For each enzyme and probe pair, the amount of enzyme used was optimized to allow an accurate measurement of the initial rate. After enzyme addition, fluorescence was measured every 20 or 30 s on a Molecular Devices SpectraMax M5 microplate reader. Kinetic parameters were calculated using GraphPad Prism 6 software with the method of initial rates.[182] Data were fit to a Michaelis-Menten enzyme kinetics curve, $V = V_{max}[S]/(K_M + [S])$, where V is the reaction rate and S is the substrate concentration.

Porcine liver esterase was evaluated with DDAO-7-AME and Res-AME at a final concentration of 500 ng/mL enzyme with DDAO-7-AME and a final concentration of 50 ng/mL enzyme for Res-AME (Figure 2.8). DDAO-7-AME was used at a concentration range of 3 to 80 μM, and enzyme-catalyzed hydrolysis was measured by detecting DDAO formation (λ_{ex} 635 nm, λ_{em} 670 nm). Res-AME was used at a concentration range of 0.4 and 40 μM, and hydrolysis was measured by detecting resorufin formation (λ_{ex} 550 nm, λ_{em} 600 nm).

B. subtilis esterase was evaluated with DDAO-7-AME and Res-AME at a final concentration of 500 ng/mL enzyme (Figure 2.9). DDAO-7-AME was used

at a concentration range of 0.6 to 80 μM, and hydrolysis was measured by detecting DDAO formation (λ_{ex} 635 nm, λ_{em} 670 nm). Res-AME was used at a concentration range of 0.4 to 40 μM, and hydrolysis was measured by detecting resorufin formation (λ_{ex} 550 nm, λ_{em} 600 nm).

C. antarctica lipase was evaluated with DDAO-7-AME and Res-AME at a final concentration of 10 μg/mL enzyme (Figure 2.10). DDAO-7-AME was used at a concentration range of 0.6 to 80 μM, and hydrolysis was measured by detecting DDAO formation (λ_{ex} 635 nm, λ_{em} 670 nm). Res-AME was used at a concentration range of 0.6 to 80 μM, and hydrolysis was measured by detecting resorufin formation (λ_{ex} 550 nm, λ_{em} 600 nm).

M. miehei lipase was evaluated with DDAO-7-AME and Res-AME at a final concentration of 10 μg/mL enzyme for DDAO-7-AME and 20 μg/mL enzyme for Res-AME (Figure 2.11). DDAO-7-AME was used at a concentration range of 0.6 to 80 μM, and hydrolysis was measured by detecting DDAO formation (λ_{ex} 635 nm, λ_{em} 670 nm). Res-AME was used at a concentration range of 0.6 to 80 μM, and hydrolysis was measured by detecting resorufin formation (λ_{ex} 550 nm, λ_{em} 600 nm).

Mycobacterial lysate screen

Mycobacteria were cultured, harvested, and lysed as previously described.[165] Each species was handled using appropriate biosafety level 2 or 3 precautions. The species analyzed included *M. smegmatis*, *M. marinum*, *M.*

flavescens, *M. nonchromogenicum*, *M. kansasii*, *M. avium*, *M. intracellulare*, *M. bovis* (BCG), *M. africanum*, and three strains of *Mtb* (Erdman, H37Rv, and CDC1551). Lysates (1 μg of total protein) were evaluated with 5 μM of DDAO-7-AME, DDAO-2-AME, or Res-AME in triplicate in 10 mM HEPES (pH 7.3). Reactions were incubated at 37 °C for 10 min, and hydrolyzed probe fluorescence was measured on a Tecan Infinite M200Pro microplate reader (DDAO: λ_{ex} 635 nm, λ_{em} 670 nm; resorufin: λ_{ex} 550 nm, λ_{em} 600 nm). After 10 min, each species displayed significant esterase activity (Figure 2.12).

In-gel activity assay

Lysates (1 to 8 μg of total protein per lane, adjusted to approximately normalize band brightness) were resolved by native gel electrophoresis (10–20% Tris-HCl Criterion gel, Bio-Rad). Gels were run on ice for 95 min at 200 V in 1X Tris-Glycine buffer (Bio-Rad) prepared in deionized water without methanol. NativeMark Unstained Protein Standard (Life Technologies) was included, although it is difficult to accurately estimate molecular weight on a native protein gel. Gels were incubated in 10 mM HEPES (pH 7.3) containing 1–5 μM fluorogenic probe for 5 min before imaging on a fluorescence scanner (Typhoon 9410 Variable Mode Imager, GE Healthcare). DDAO-7-AME and DDAO-2-AME were evaluated at 1 μM instead of 5 μM due to optimal signal-to-noise at this concentration. DDAO was detected using 633 nm excitation and a 670 nm (bp

30) emission filter. Resorufin was detected using 532 nm excitation and a 580 nm (bp 30) emission filter. The resulting images were analyzed in ImageJ.[183]

Acknowledgments

We are grateful to Nicholas Lopez, Ben Doron, and Geoffrey Melly for their assistance with this project and to Dr. Luke Lavis (Janelia Farm Research Campus, HHMI) for valuable discussions. We thank Prof. Summer Gibbs, Dr. Samantha Levine, Dr. Meredith Hartley, and Dr. Hannah Zane for their critical reading of the manuscript. We are grateful to Prof. Gibbs for the use of her plate reader and LC-MS and Prof. Brian Druker for the use of his Typhoon fluorescence imager. Funding for K.R.T. was generously provided by the OHSU Department of Physiology and Pharmacology's Steinberg Fund. K.E.B. is grateful for generous support and funding from the OHSU Center for Spatial Systems Biomedicine, the Knight Cancer Institute, and the Collins Medical Trust.

Tables

Table 2.1. Spectral characteristics of fluorogenic probes and parent fluorophores.

Compound	$\lambda_{abs/em}$ (nm)[a]	pK_a	ε ($M^{-1}cm^{-1}$)	ϕ (Solvent)
DDAO	646/660	5.7	33,000[b]	0.40 (PBS pH 7.4)[165]
DDAO-7-AME	465/625	—	1,400[a,c]	0.07 (10 mM HEPES pH 7.3) 0.02 (DMSO)
DDAO-2-AME	395/—	—	2,300[a,c]	—
Resorufin	571/588	5.8	57,000[d]	0.74 (pH 9.5 buffer)[178]
Res-AME	475/605	—	4,100[a]	0.01 (10 mM HEPES pH 7.3) 0.001 (DMSO)

[a]in 10 mM HEPES, pH 7.3

[b]in PBS, pH 7.4

[c]These values were subsequently re-measured using another method, which we believe to be more accurate (see Table 3.1 and Chapter 3 Materials and Methods).

[d]in 0.1 N NaOH

Table 2.2. Half-life (h) for the hydrolysis of each probe in different buffer conditions.

Probe	PBS (pH 7.4)	DMEM-FBS	DMEM-FBS (heat-inactivated)
DDAO-7-AME	27	0.3	2.6
DDAO-2-AME	41	0.4	3.1
Res-AME	13	0.3	2.0
FDA	8	0.3	0.3

Table 2.3. PLE detection limit of DDAO-7-AME, DDAO-2-AME, Res-AME, FDA, and *p*-NPA.

Probe (*μ*M)	**Detection Limit (pg PLE)**
DDAO-7-AME (25)	11
DDAO-2-AME (25)	2.75
Res-AME (25)	27.5
FDA (25)	0.55
p-NPA (1700)	2750

Table 2.4. Kinetic parameters of DDAO-7-AME and Res-AME with esterases and lipases.

Probe	Enzyme (Amount)	V_{max} (pmol/s)	K_M (μM)
DDAO-7-AME	PLE (0.5 μg/mL)	1.19	7.5 $\pm$ 0.8
	B. subtilis esterase (0.5 μg/mL)	0.45	6.7 $\pm$ 0.5
	C. antarctica lipase (10 μg/mL)	0.24	9.5 $\pm$ 1.1
	M. miehei lipase (10 μg/mL)	0.06	4.4 $\pm$ 0.7
Res-AME	PLE (0.050 μg/mL)	0.69	4.9 $\pm$ 0.7
	B. subtilis esterase (0.5 μg/mL)	0.30	19 $\pm$ 2
	C. antarctica lipase (10 μg/mL)	0.30	6.8 $\pm$ 0.4
	M. miehei lipase (20 μg/mL)	0.16	19 $\pm$ 3

Figures

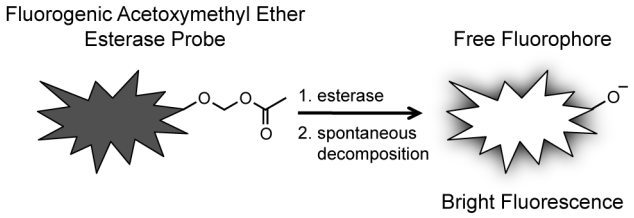

Scheme 2.1. Esterases activate, or "turn-on," AME-masked fluorogenic probes. The hydroxymethyl ether intermediate (not shown) spontaneously decomposes following ester hydrolysis, which releases free fluorophore. Fluorogenic probes of this design are useful for examining enzymes in complex mixtures (e.g., cell lysates or living cells).

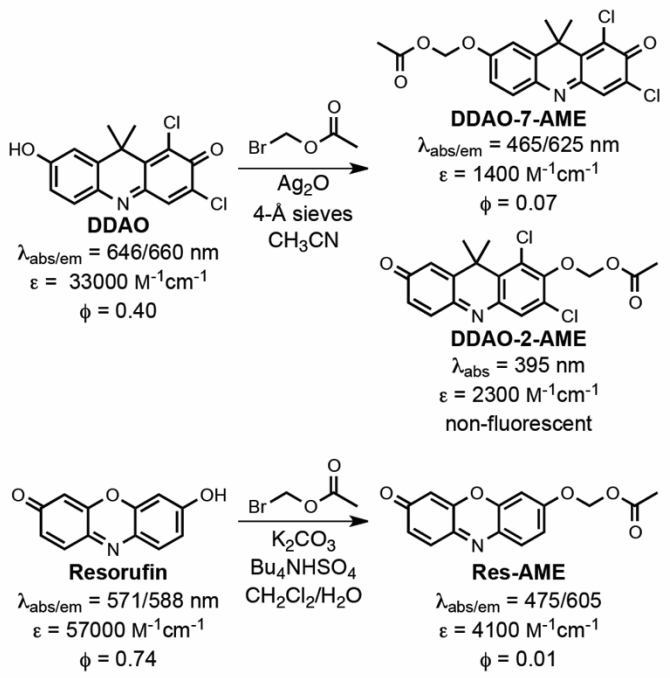

Scheme 2.2. The synthesis of AME-masked fluorogenic probes and their spectral properties.

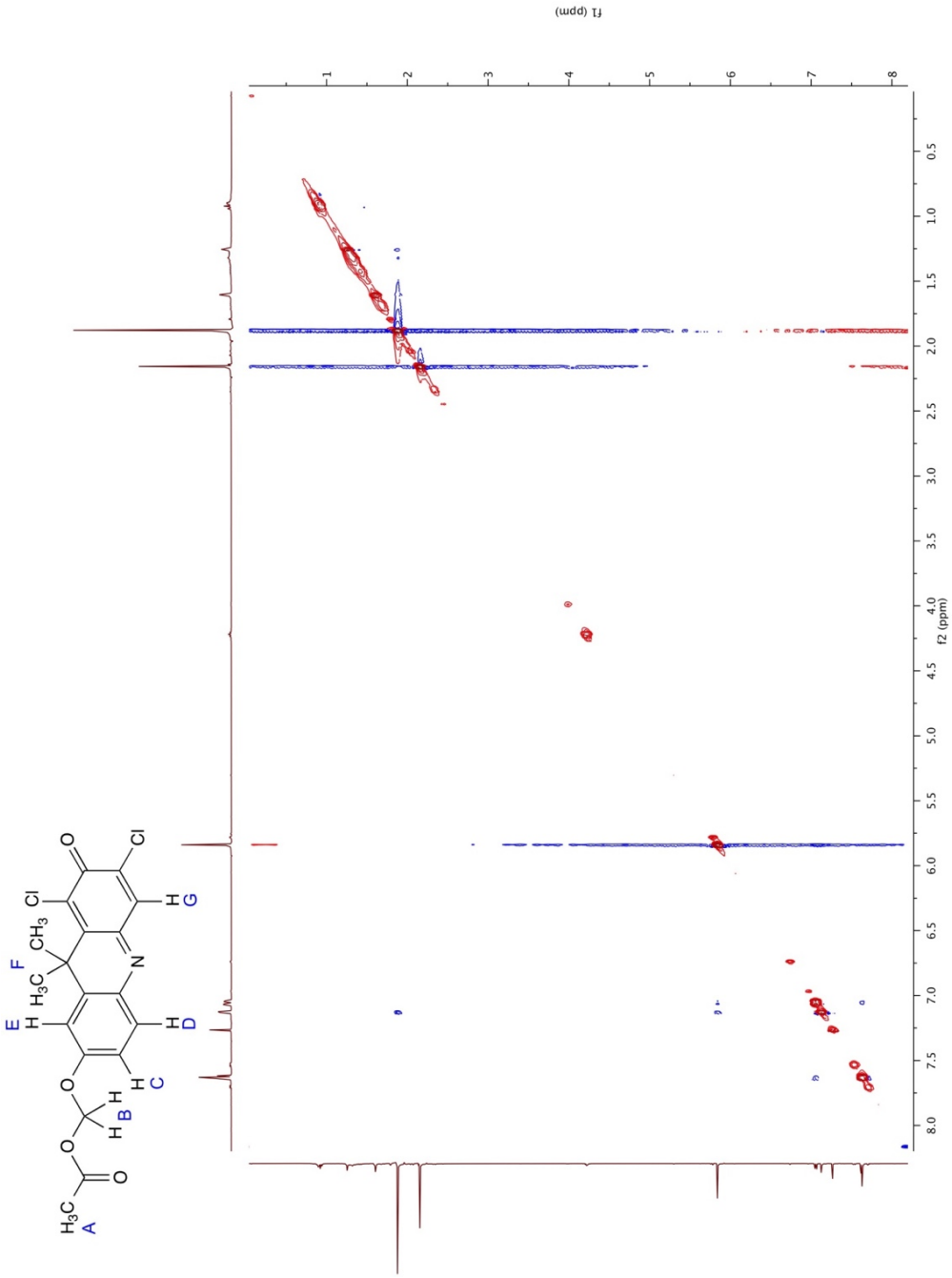

Figure 2.1. NOESY spectrum of DDAO-7-AME.

The methylene protons (H_B) of the AME moiety (s, 2H, 5.86 ppm) exhibit Nuclear Overhauser effects (NOEs) with aromatic protons H_E (d, 1H, 7.14 pm) and H_C (dd, 1H, 7.08 ppm), showing that *O*-alkylation occurred on the side of the molecule opposite the chlorides.

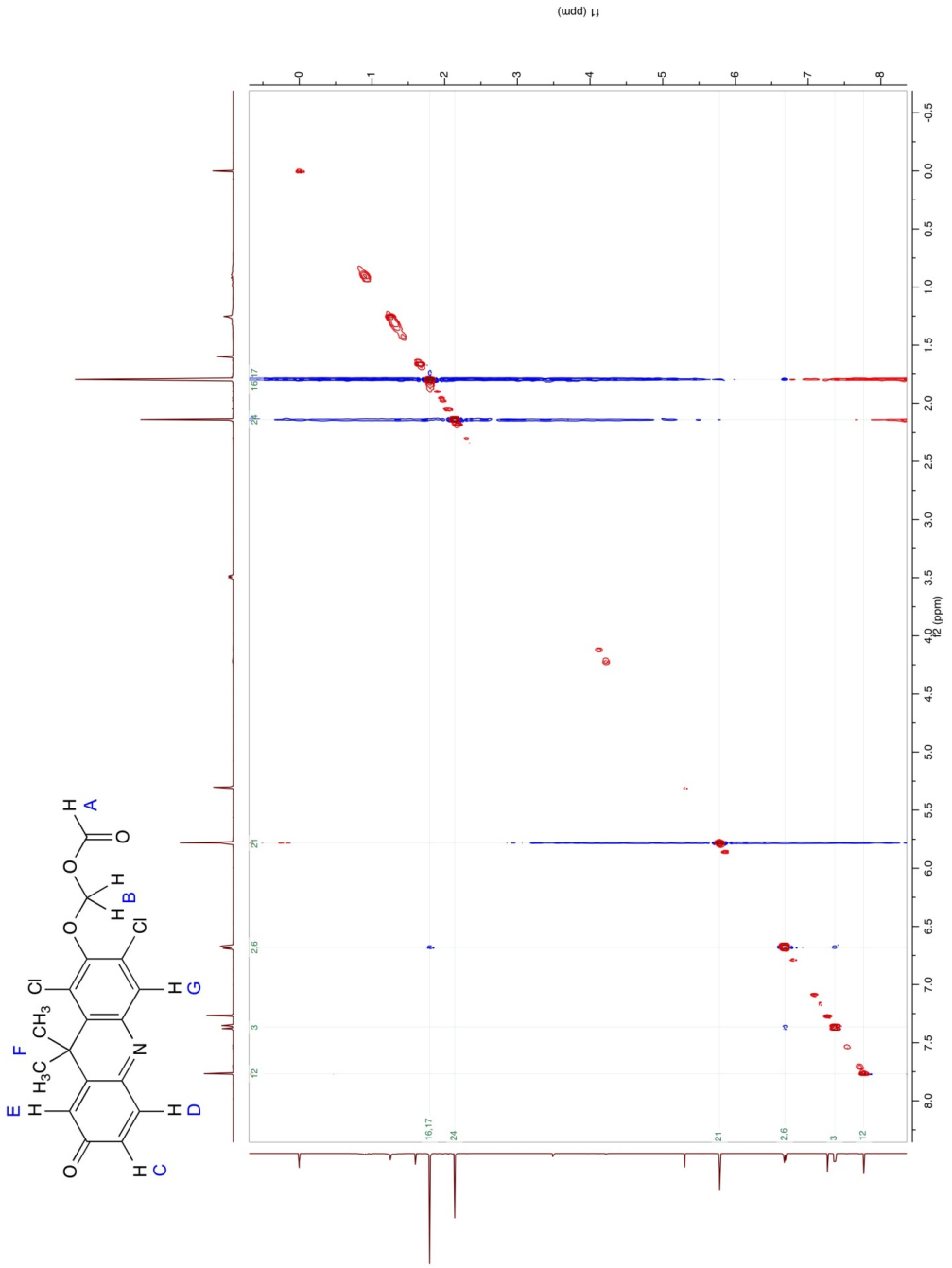

Figure 2.2. NOESY spectrum of DDAO-2-AME.

The methylene protons (H_B) of the AME moiety (s, 2H, 5.80 ppm) exhibit no NOEs, indicating that the AM ether group is between the two chlorides.

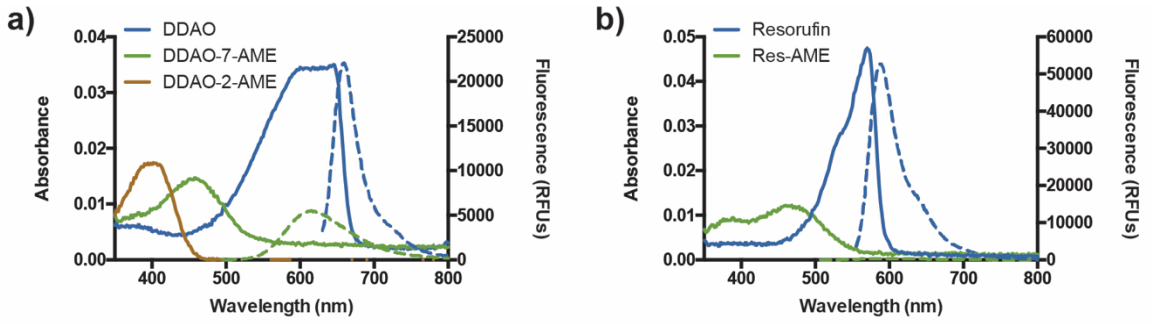

Figure 2.3. The absorbance and emission spectra of AME fluorogenic probes.

The absorbance curves are shown as solid lines, while the emission curves are dashed lines. (a) Spectra for DDAO (λ_{ex} 600 nm), DDAO-7-AME (λ_{ex} 465 nm), and DDAO-2-AME (non-fluorescent). (b) Spectra for resorufin (λ_{ex} 525 nm) and Res-AME (λ_{ex} 475 nm). Each sample was prepared as 1 μM probe in 10 mM HEPES buffer (pH 7.3).

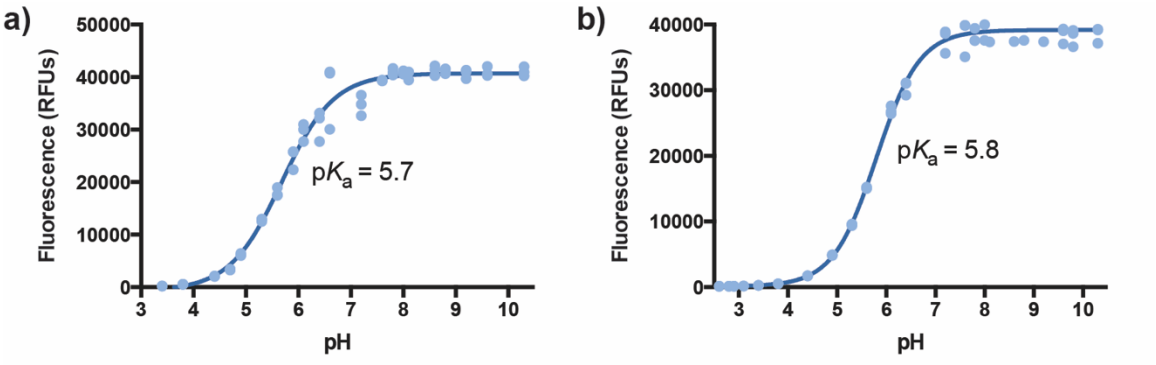

Figure 2.4. Determination of the pK_a of DDAO and resorufin.

The fluorescence of (a) DDAO (λ_{ex} 635 nm, λ_{em} 670 nm) and (b) resorufin (λ_{ex} 550 nm, λ_{em} 600 nm) was measured in triplicate in buffers at various pH's (ranging from 2.8 to 10.3) and is reported in relative fluorescence units (RFUs). Data were fit to a sigmoidal curve, and the pK_a of each fluorophore was determined as the inflection point of the curve.

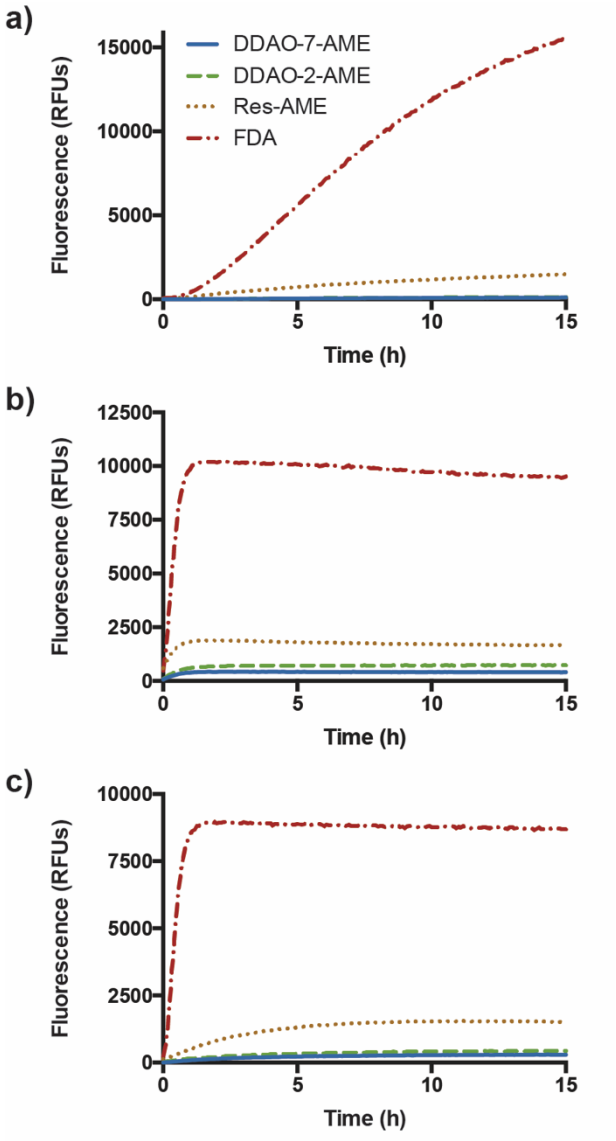

Figure 2.5. The stability of esterase probes in various buffers.

Each probe (DDAO-7-AME, DDAO-2-AME, Res-AME, and FDA) was diluted to 25 μM in (a) PBS, (b) DMEM-FBS, or (c) DMEM-FBS with heat-inactivated serum. Parent fluorophore fluorescence (in relative fluorescence units, RFUs) was measured every 15 min for 15 h (DDAO: λ_{ex} 635 nm, λ_{em} 670 nm; resorufin: λ_{ex} 550 nm, λ_{em} 600 nm; fluorescein: λ_{ex} 490 nm, λ_{em} 525 nm). Each line represents the average of three replicates.

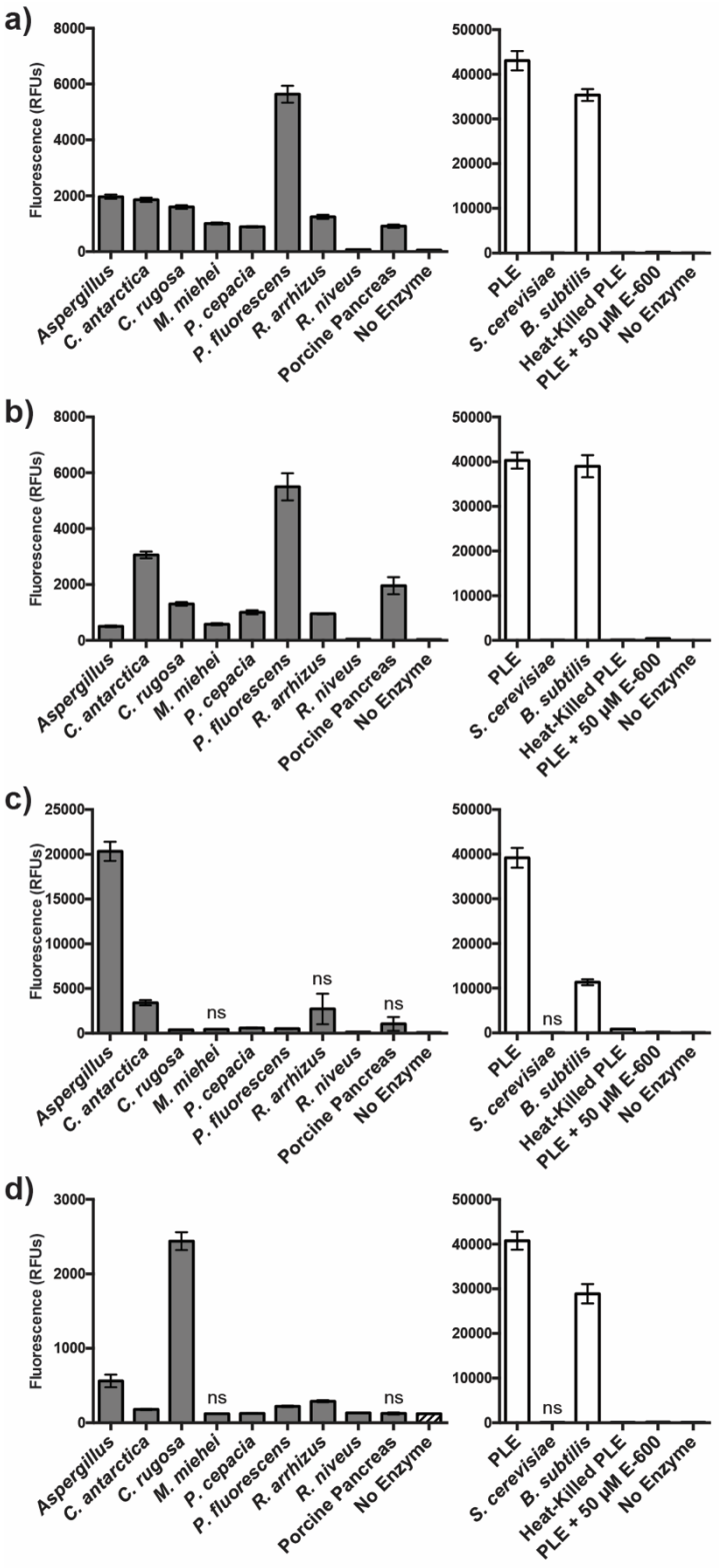

Figure 2.6. Fluorogenic esterase probes can be hydrolyzed by a variety of enzymes.

(a) 5 μM DDAO-7-AME. (b) 5 μM DDAO-2-AME. (c) 5 μM Res-AME. (d) 5 μM FDA. Enzymes (5 μg/mL) were incubated with 5 μM probe in 10 mM HEPES (pH 7.3) for 10 min at 37 °C. Probe cleavage was detected by an increase in fluorescence (in relative fluorescence units, RFUs) compared to the no enzyme control (DDAO: λ_{ex} 635 nm, λ_{em} 670 nm; resorufin: λ_{ex} 550 nm, λ_{em} 600 nm; fluorescein: λ_{ex} 485 nm, λ_{em} 530 nm). Lipases are indicated by gray bars, and esterases are indicated by white bars. Heat-killed PLE was prepared by heating the sample at 90 °C for 15 min. Inhibited enzyme was pre-incubated with 50 μM E-600 for 1 h at 37 °C prior to probe addition. The no enzyme control is the same data set for both lipases and esterases. All unlabeled responses are statistically significant ($P < 0.01$). Reponses labeled “ns” are not significant compared to the no enzyme control. Error bars represent one standard deviation (n = 6).

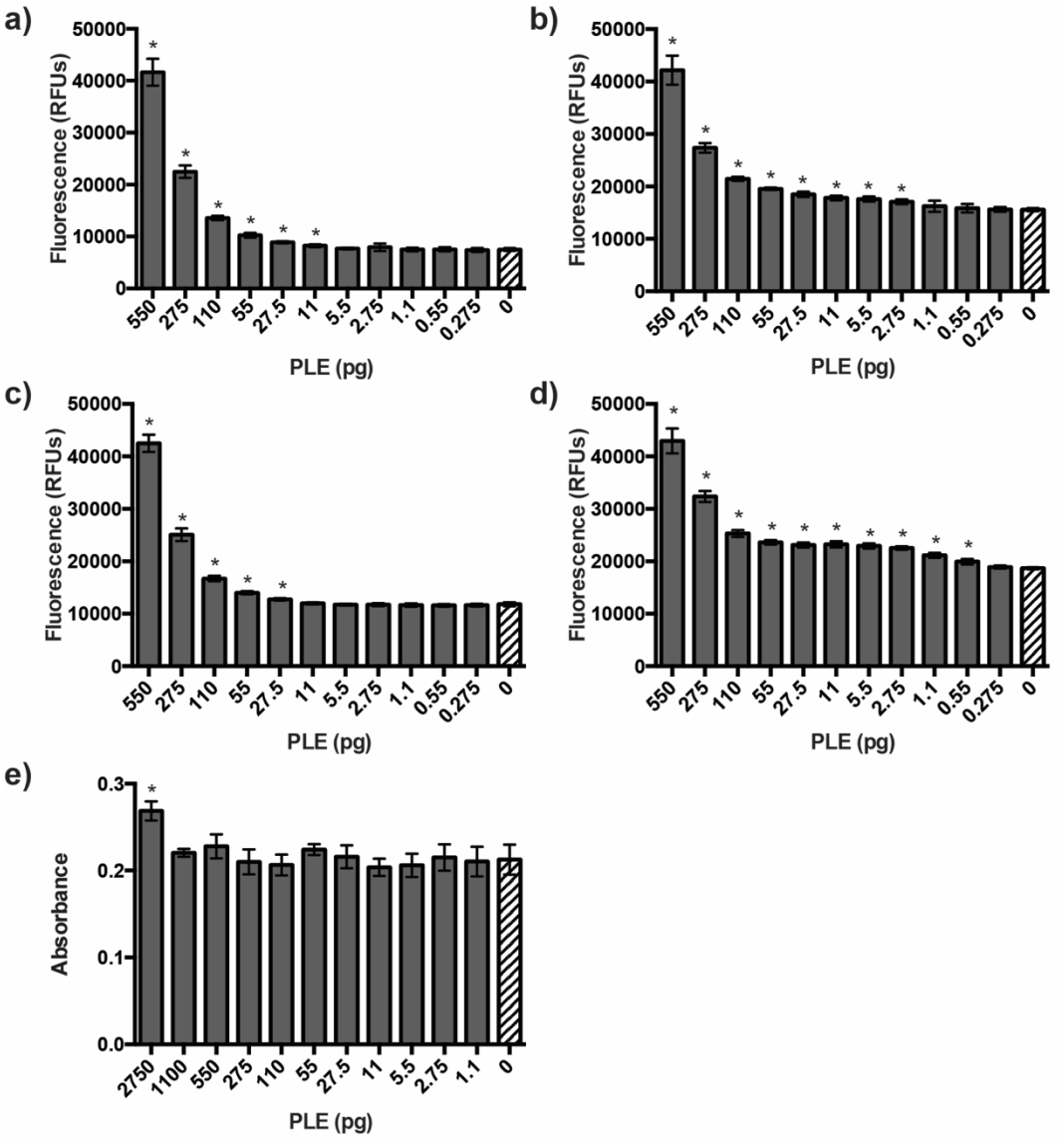

Figure 2.7. The PLE detection limit after a 10 min incubation with fluorogenic or chromogenic probes.

(a) DDAO-7-AME (25 μM). (b) DDAO-2-AME (25 μM). (c) Res-AME (25 μM). (d) FDA (25 μM). (e) *p*-NPA (1700 μM). Enzyme was diluted in 10 mM HEPES (pH 7.3) and incubated with probe for 10 min at 37 °C. The formation of hydrolyzed product was detected by measuring the fluorescence of DDAO (λ_{ex} 635 nm, λ_{em} 670 nm), resorufin (λ_{ex} 550 nm, λ_{em} 600 nm), or fluorescein (λ_{ex} 490 nm, λ_{em} 525 nm). Fluorescence is shown in relative fluorescence units (RFUs). Alternatively, *p*-NPA hydrolysis was detected by measuring the absorbance of *p*-nitrophenol at 348 nm. The detection limit was determined as the lowest statistically significant detectable amount compared to the no enzyme control ($^*P < 0.01$). Error bars represent one standard deviation ($n = 6$).

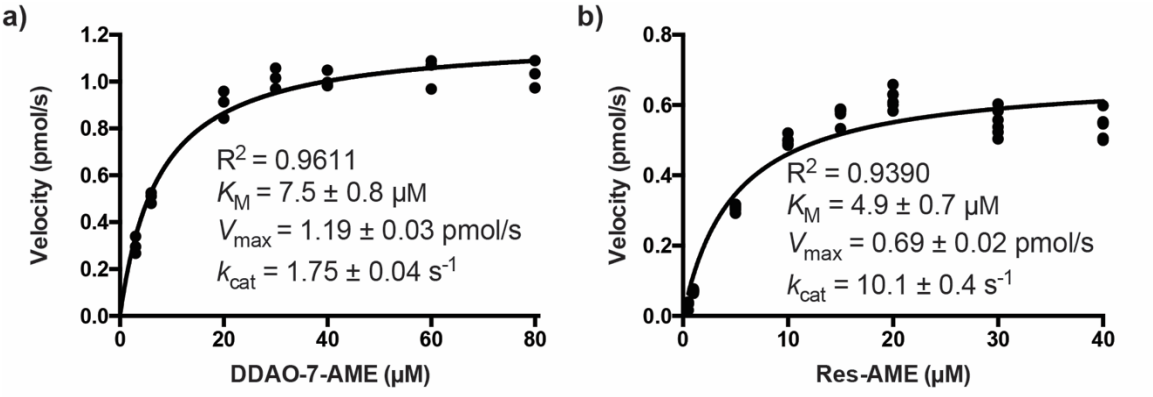

Figure 2.8. Kinetic evaluation of DDAO-7-AME and Res-AME with PLE.

(a) DDAO-7-AME (ranging from 3–80 μM) was evaluated with 500 ng/mL PLE in triplicate. DDAO: λ_{ex} 635 nm, λ_{em} 670 nm. (b) Res-AME (ranging from 0.5–40 μM) was evaluated with 50 ng/mL PLE in sextuplicate. Resorufin: λ_{ex} 550 nm, λ_{em} 600 nm. Experiments were performed in 10 mM HEPES buffer (pH 7.3) at 37 °C. Fluorescence generation was measured every 20 or 30 s. All data were fit to a Michaelis-Menten enzyme kinetics curve, and did not fit a substrate inhibition curve.

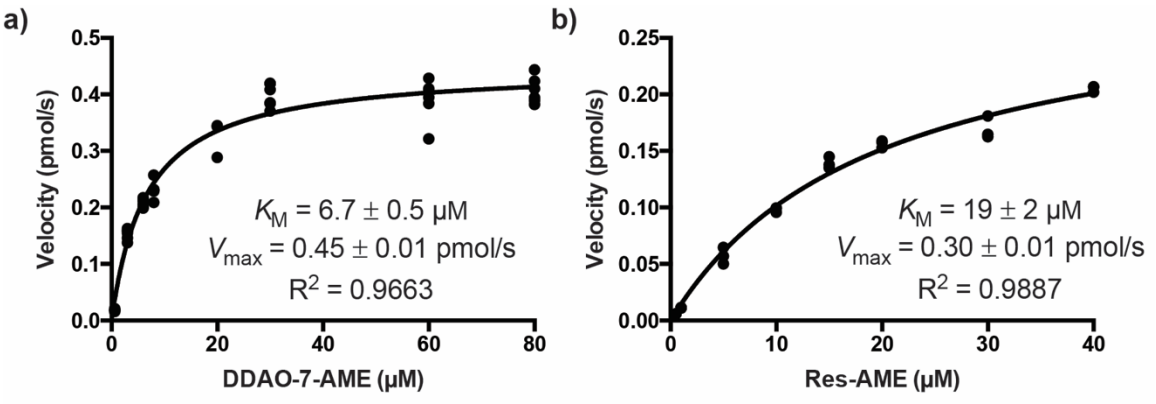

Figure 2.9. Kinetic evaluation of DDAO-7-AME and Res-AME with *Bacillus subtilis* esterase. (a) DDAO-7-AME (ranging from 0.6–80 μM) was evaluated with 500 ng/mL *B. subtilis* esterase in sextuplicate. DDAO: λ_{ex} 635 nm, λ_{em} 670 nm. (b) Res-AME (ranging from 0.4–40 μM) was evaluated with 500 ng/mL *B. subtilis* esterase in triplicate. Resorufin: λ_{ex} 550 nm, λ_{em} 600 nm. Experiments were performed in 10 mM HEPES buffer (pH 7.3) at 37 °C. Fluorescence generation was measured every 20 s. Data were fit to a Michaelis-Menten enzyme kinetics curve.

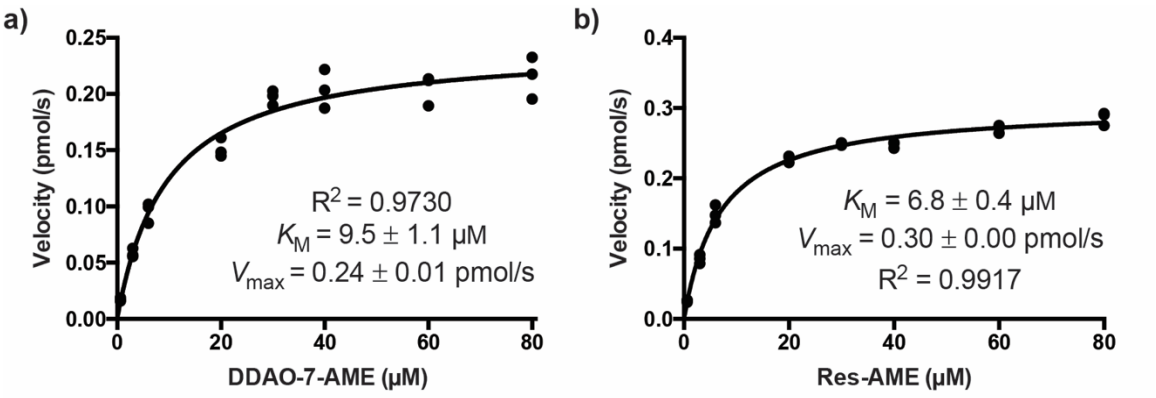

Figure 2.10. Kinetic evaluation of DDAO-7-AME and Res-AME with *Candida antarctica* lipase. (a) DDAO-7-AME (ranging from 0.6–80 μM) was evaluated with 10 μg/mL *C. antarctica* lipase. DDAO: λ_{ex} 635 nm, λ_{em} 670 nm. (b) Res-AME (ranging from 0.6–80 μM) was evaluated with 10 μg/mL *C. antarctica* lipase. Resorufin: λ_{ex} 550 nm, λ_{em} 600 nm. Experiments were performed in triplicate in 10 mM HEPES buffer (pH 7.3) at 37 °C. Fluorescence generation was measured every 20 s. Data were fit to a Michaelis-Menten enzyme kinetics curve.

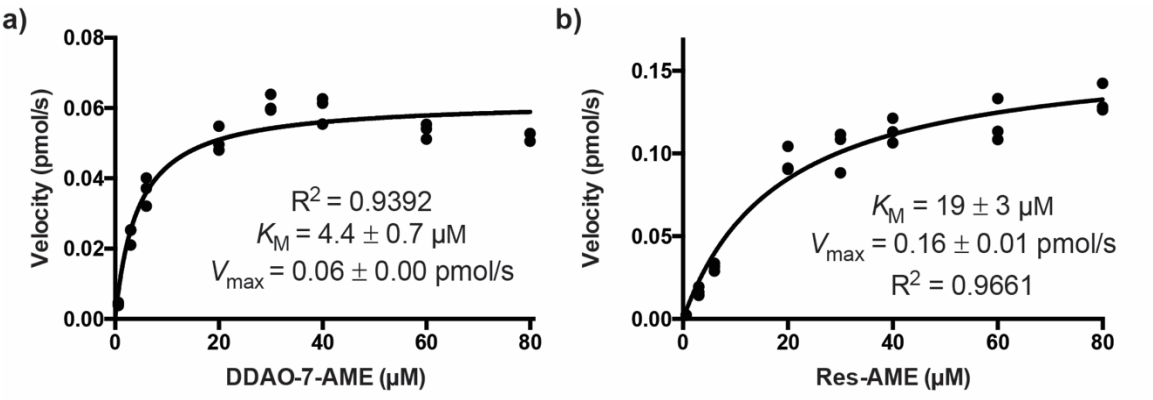

Figure 2.11. Kinetic evaluation of DDAO-7-AME and Res-AME with *Mucor miehei* lipase. (a) DDAO-7-AME (ranging from 0.6–80 μM) was evaluated with 10 μg/mL *M. miehei* lipase. DDAO: λ_{ex} 635 nm, λ_{em} 670 nm. (b) Res-AME (ranging from 0.6–80 μM) was evaluated with 20 μg/mL *M. miehei* lipase. Resorufin: λ_{ex} 550 nm, λ_{em} 600 nm. Experiments were performed in triplicate in 10 mM HEPES buffer (pH 7.3) at 37 °C. Fluorescence generation was measured every 20 s. Data were fit to a Michaelis-Menten enzyme kinetics curve. Data did not fit a substrate inhibition curve.

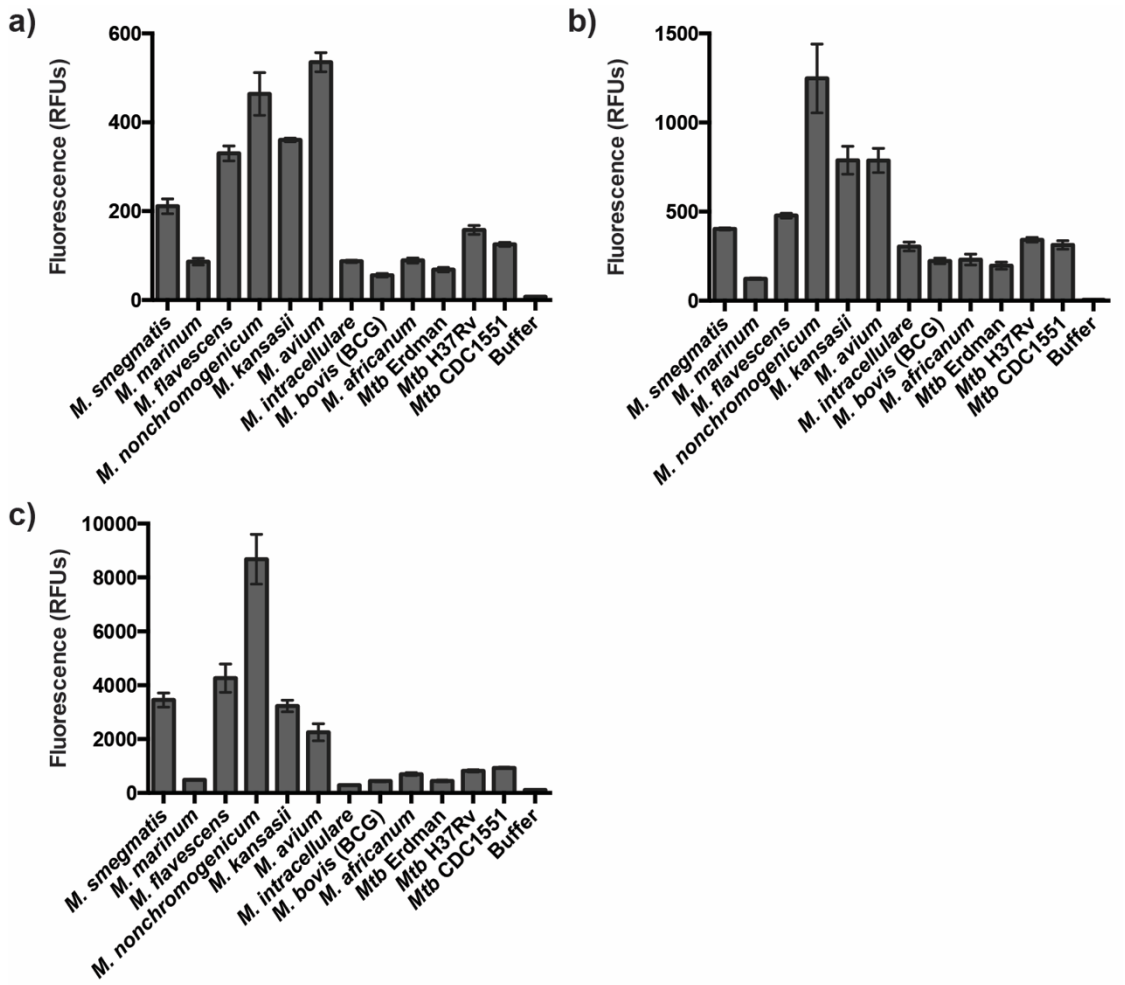

Figure 2.12. Mycobacterial lysates have esterase activity.

Lysates (1 μg) were incubated with 5 μM fluorogenic probe in 10 mM HEPES (pH 7.3) for 10 min at 37 °C. Probe cleavage was detected by an increase in fluorescence (in relative fluorescence units, RFUs) compared to the buffer control. (a) DDAO-7-AME (DDAO: λ_{ex} 635 nm, λ_{em} 670 nm). (b) DDAO-2-AME (DDAO: λ_{ex} 635 nm, λ_{em} 670 nm). (c) Res-AME (resorufin: λ_{ex} 550 nm, λ_{em} 600 nm). All responses are statistically significant ($P < 0.01$) compared to the no enzyme control. Error bars represent one standard deviation ($n = 3$).

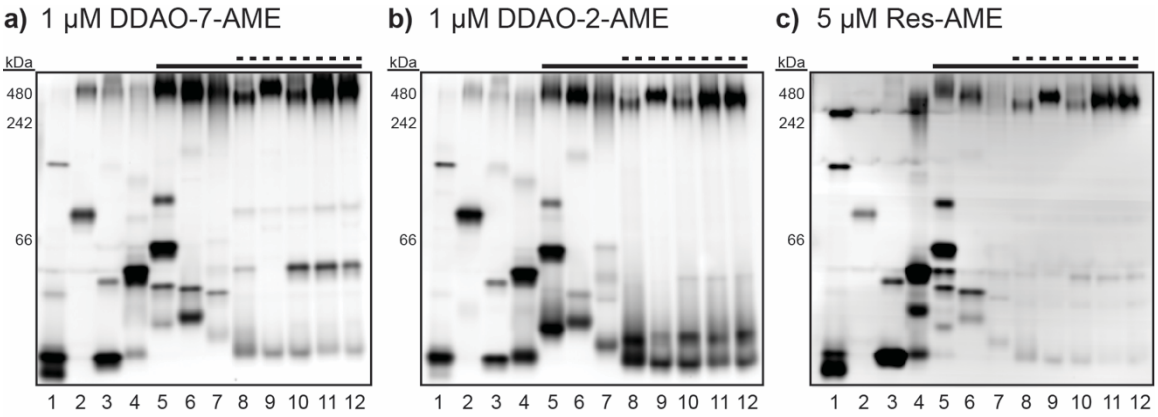

Figure 2.13. Fluorogenic esterase probes reveal distinct mycobacterial esterase activities. Mycobacterial lysates (1–8 μg of total protein per lane) were resolved using native polyacrylamide gel electrophoresis (10–20% Tris-HCl gradient gel). NativeMark molecular weight ladder was run on each gel (not shown), and the apparent molecular weights are provided. The dashed line indicates species that cause pulmonary disease and the solid line indicates members of the MTBC. Each gel was incubated for 5 min in 10 mM HEPES (pH 7.3) with (a) 1 μM DDAO-7-AME, (b) 1 μM DDAO-2-AME, or (c) 5 μM Res-AME. The gels were imaged to reveal fluorescent bands corresponding to hydrolyzed probe. Lane assignments: 1, *M. smegmatis*; 2, *M. marinum*; 3, *M. flavescens*; 4, *M. nonchromogenicum*; 5, *M. kansasii;* 6, *M. avium*; 7, *M. intracellulare*; 8, *M. bovis* (BCG); 9, *M. africanum;* 10, *Mtb* Erdman; 11, *Mtb* H37Rv; 12, *Mtb* CDC1551.

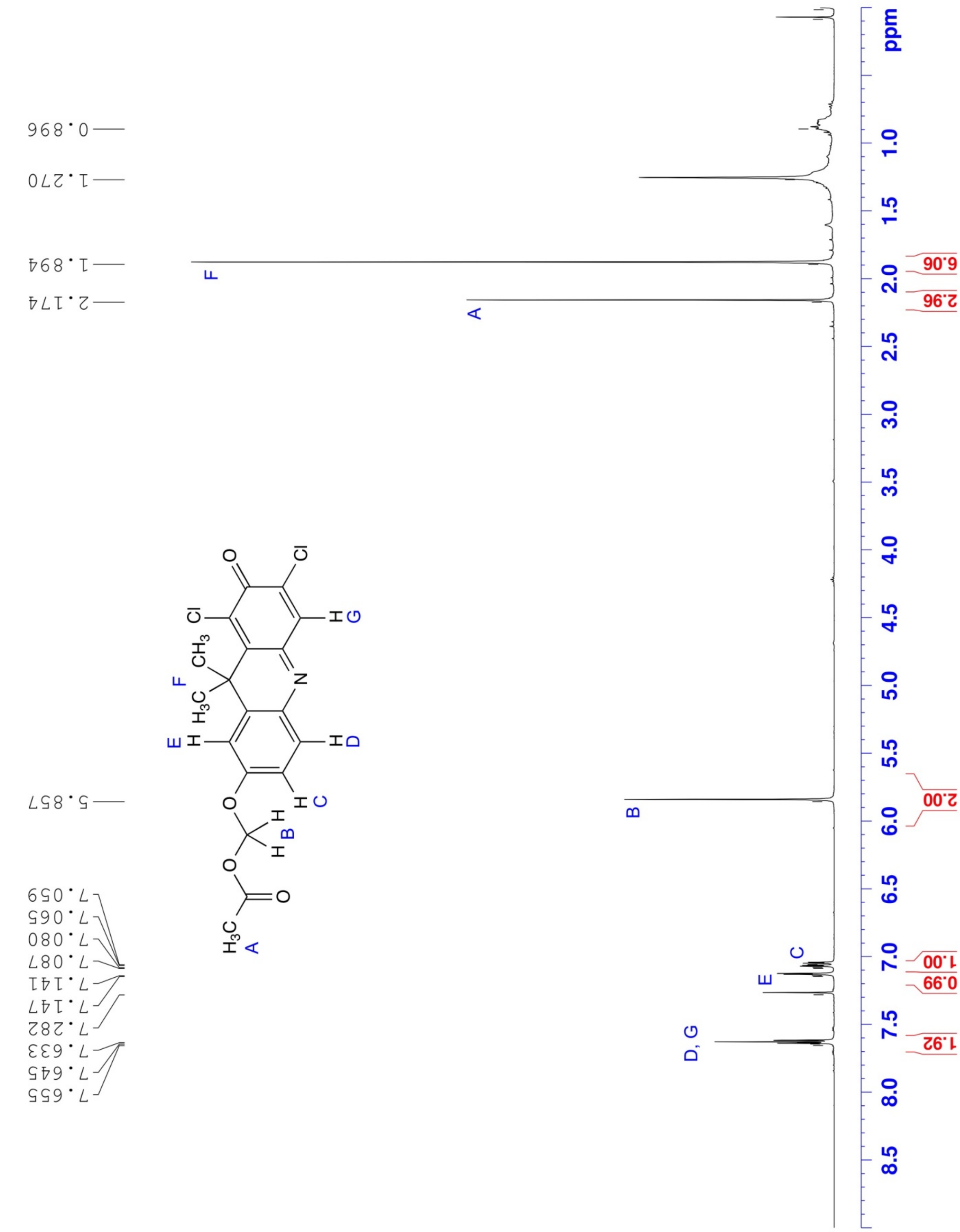

Figure 2.14. ^{1}H-NMR spectrum of DDAO-7-AME (400 MHz; $CDCl_3$).

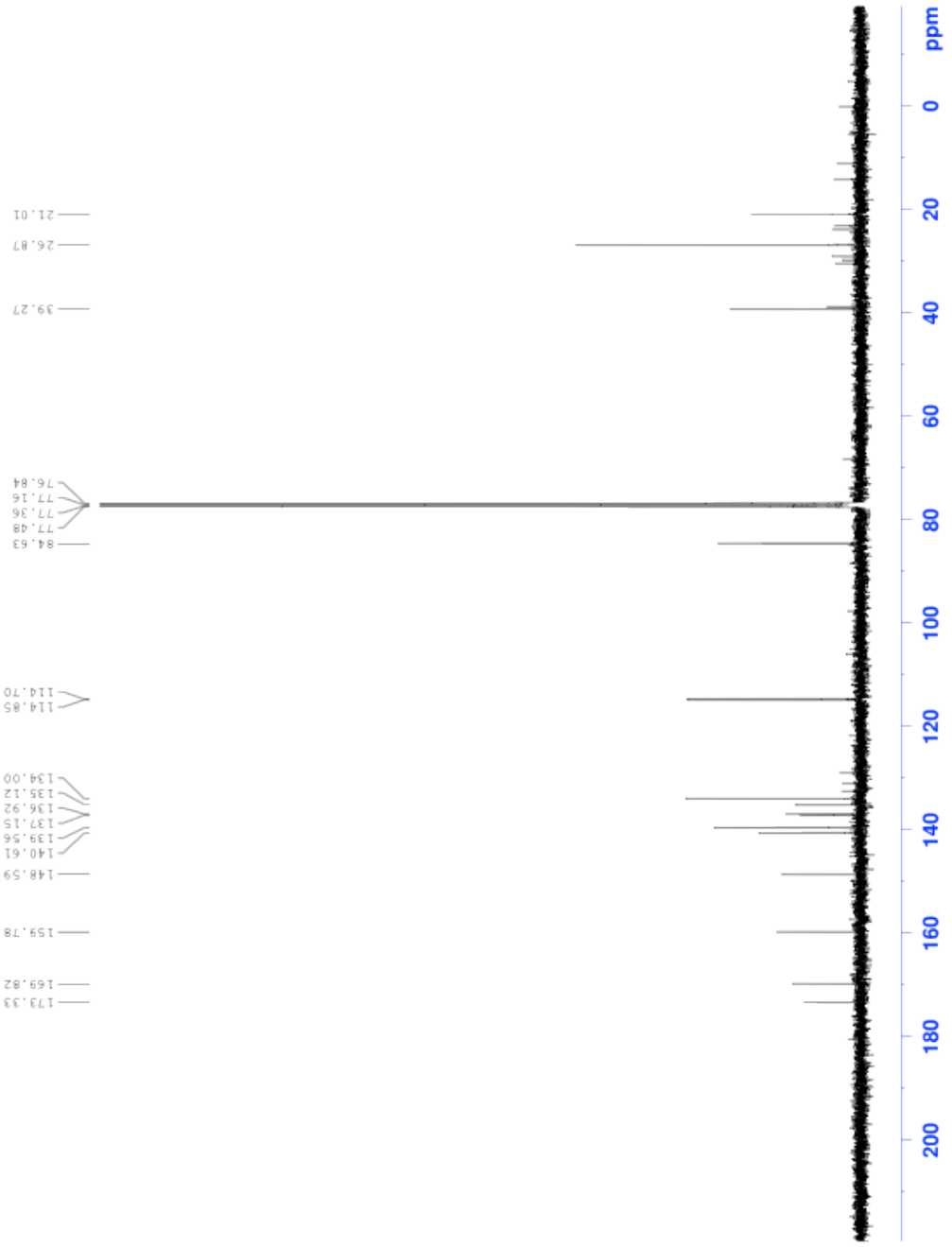

Figure 2.15. ^{13}C-NMR spectrum of DDAO-7-AME (101 MHz; $CDCl_3$).

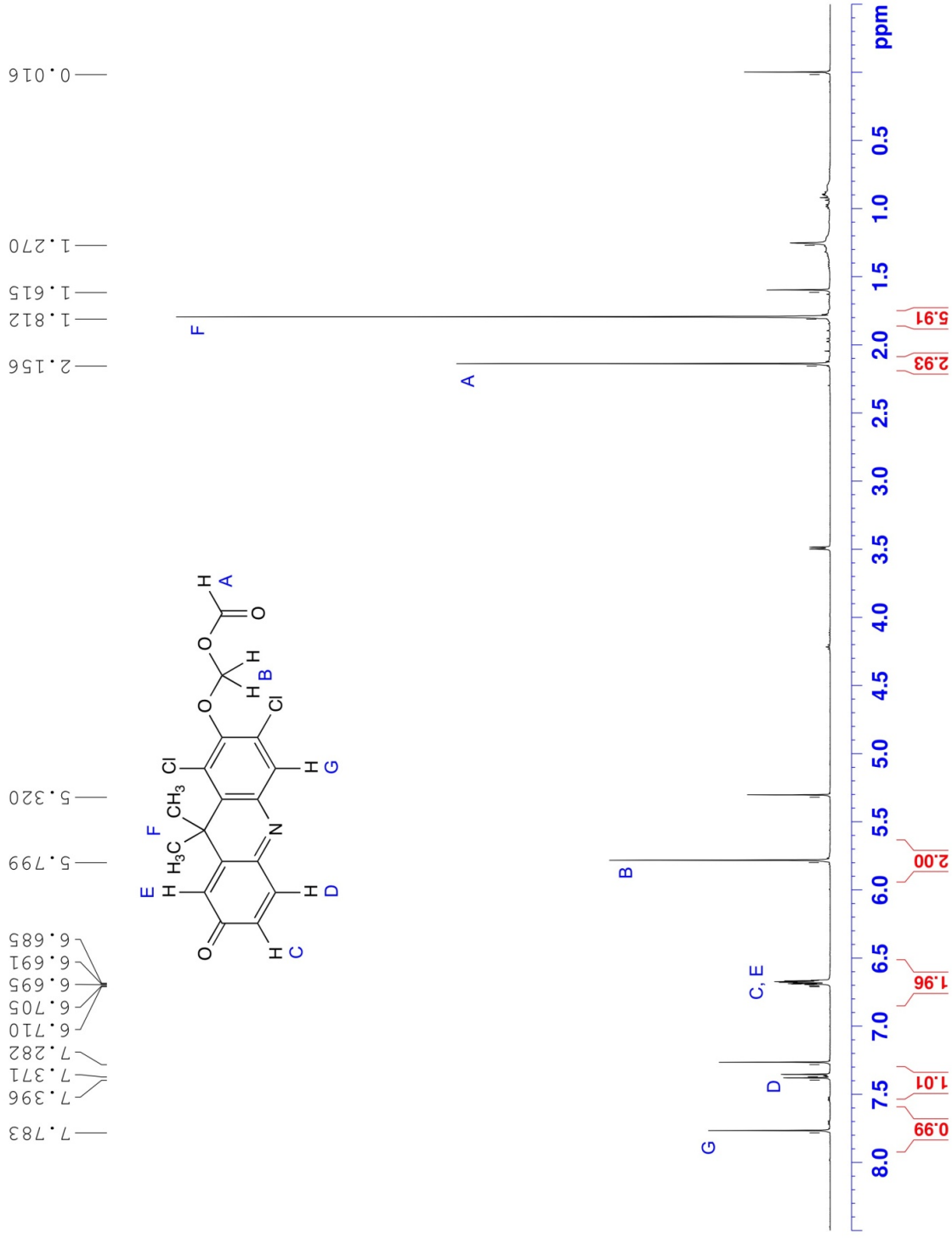

Figure 2.16. ^{1}H-NMR spectrum of DDAO-2-AME (400 MHz; $CDCl_3$).

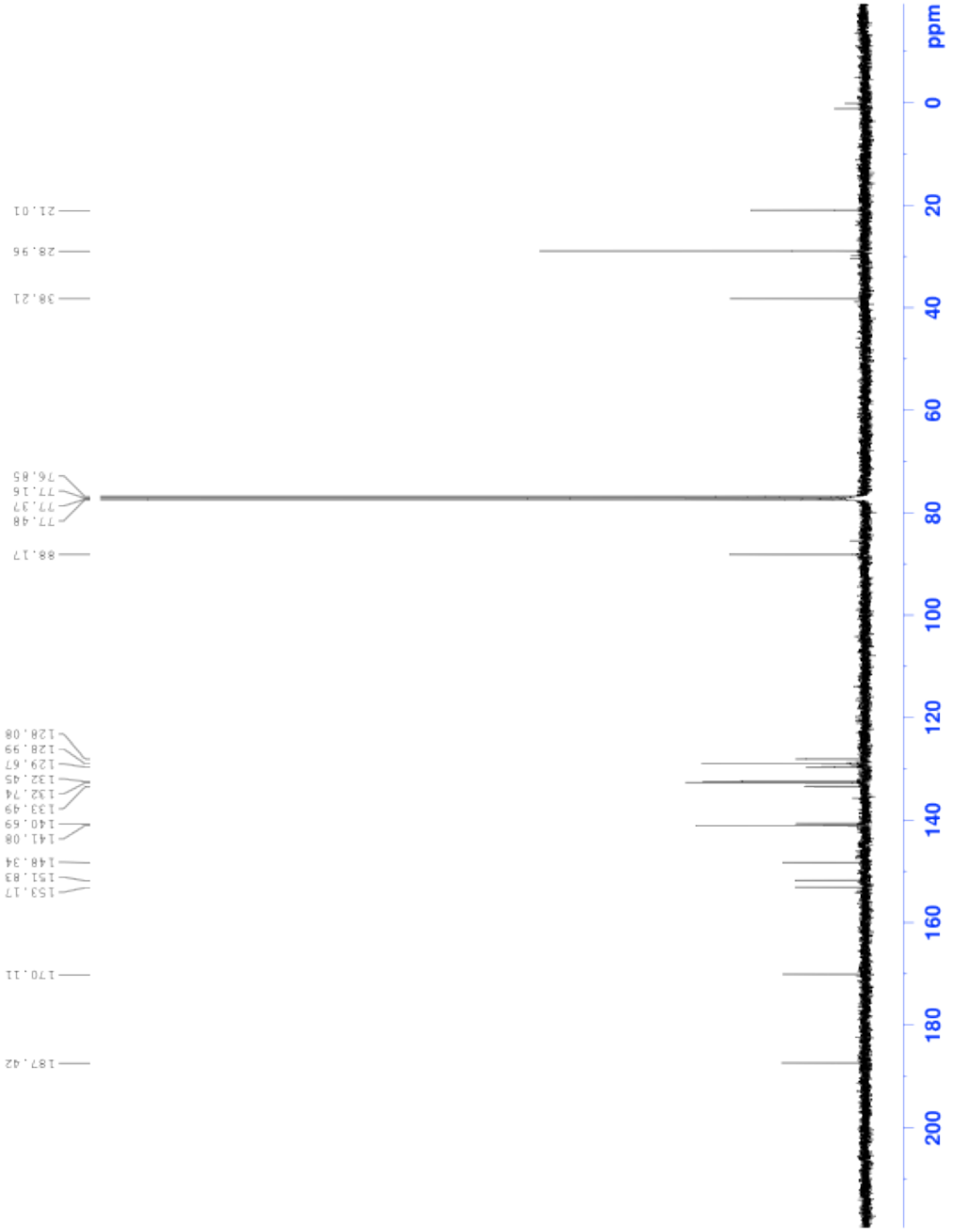

Figure 2.17. ^{13}C-NMR spectrum of DDAO-2-AME (101 MHz; $CDCl_3$).

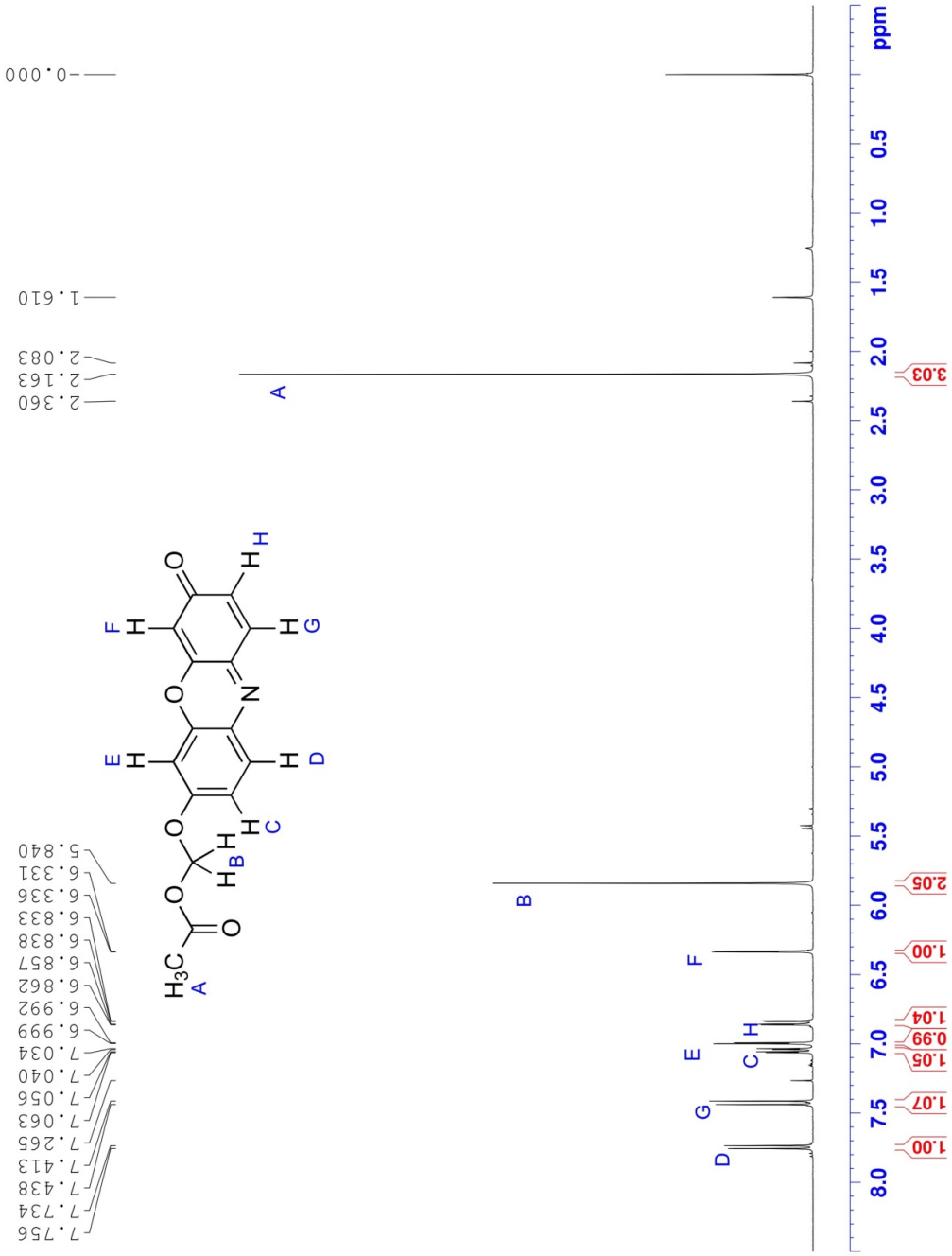

Figure 2.18. ^{1}H-NMR spectrum of Res-AME (400 MHz; $CDCl_3$).

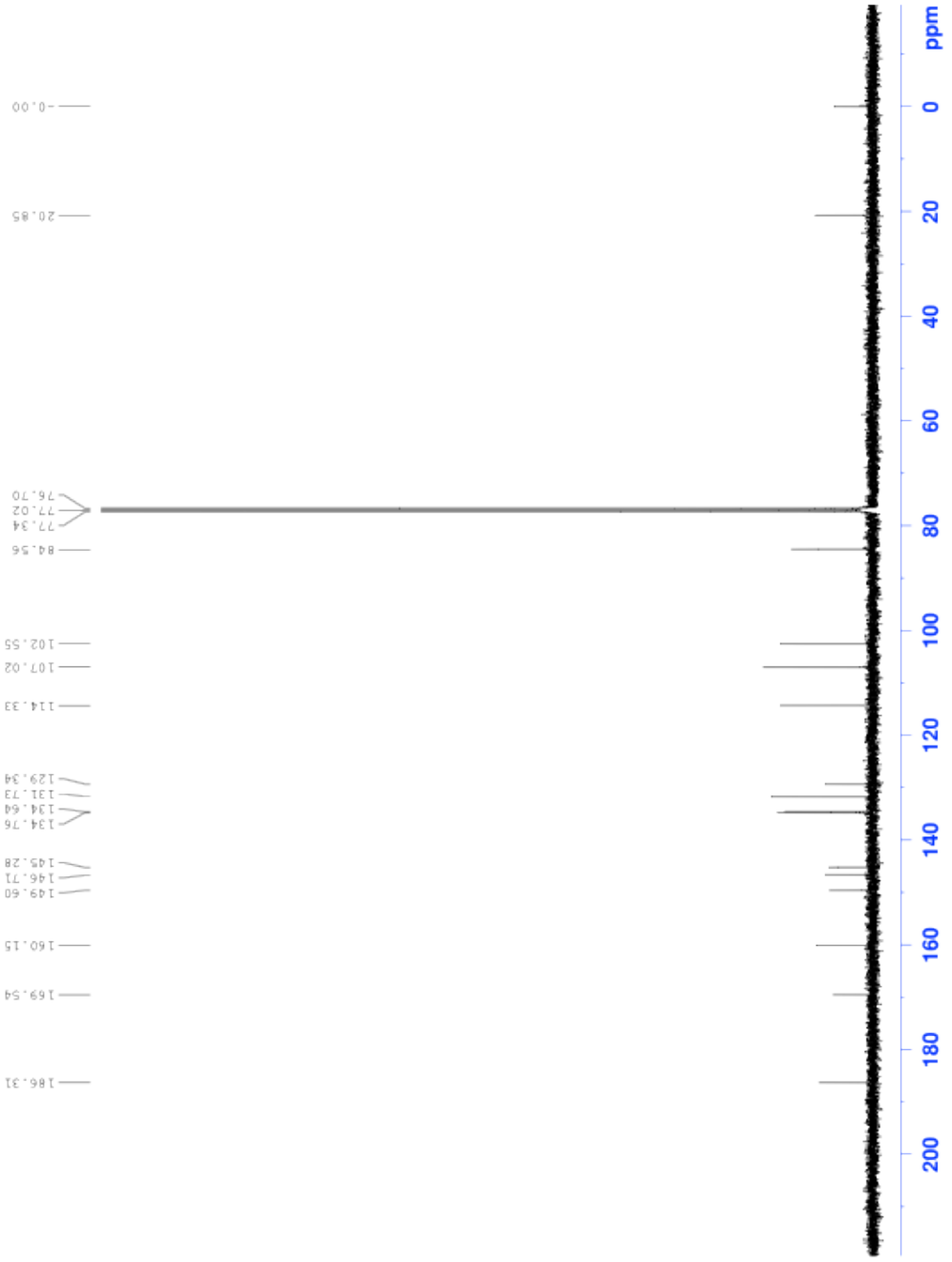

Figure 2.19. ^{13}C-NMR spectrum of Res-AME (101 MHz; $CDCl_3$).

Chapter 3: Profiling Esterases in *Mycobacterium tuberculosis* Using Far-Red Fluorogenic Substrates

Katie R. Tallman, Samantha R. Levine, and Kimberly E. Beatty

This work was originally published by *ACS Chem. Biol.* on July 15, 2016 in volume 11, issue 17, pages 1810–1815 (Copyright 2016 American Chemical Society).[184] It has been adapted for this dissertation and reprinted with permission. This project was a close collaboration with Dr. Samantha Levine, who synthesized and characterized the C4 and C8 DDAO substrates.

Abstract

Enzyme-activated, fluorogenic probes are powerful tools for studying bacterial pathogens, including *Mycobacterium tuberculosis* (*Mtb*). In prior work, we reported two 7-hydroxy-9*H*-(1,3-dichloro-9,9-dimethylacridin-2-one) (DDAO)-derived acetoxymethyl ether probes for esterase and lipase detection. Here, we report four-carbon (C4) and eight-carbon (C8) acyloxymethyl ether derivatives, which are longer-chain fluorogenic substrates. These new probes demonstrate greater stability and lipase reactivity than the two-carbon (C2) acetoxymethyl ether-masked substrates. We used these new C4 and C8 probes to profile

esterases and lipases from *Mtb*. The C8-masked probes revealed a new esterase band in gel-resolved *Mtb* lysates that was not present in lysates from non-pathogenic *M. bovis* (bacillus Calmette-Guérin), a close genetic relative. We identified this *Mtb*-specific enzyme as the secreted esterase Culp1 (Rv1984c). Our C4- and C8-masked probes also produced distinct *Mtb* banding patterns in lysates from *Mtb*-infected macrophages, demonstrating the potential of these probes for detecting *Mtb* esterases that are active during infections.

Introduction

Mycobacterium tuberculosis (*Mtb*) is the causative agent of tuberculosis (TB), a major global health threat. In 2014, there were an estimated 9.6 million new cases and 1.5 million deaths from TB, making it the most lethal single-agent infectious disease.[10] After initial infection, *Mtb* can persist for decades as a latent, asymptomatic infection, with reactivation from dormancy occurring in approximately 10% of individuals.[19] In both latent and active TB, *Mtb* adapts to its environment by regulating enzyme activity, but hydrolase regulation in latency and the roles of these enzymes during reactivation are poorly understood. This is due, in part, to the scarcity of tools available to monitor and track hydrolase activities in complex samples (e.g., lysates and tissues).

Mtb utilizes host-derived lipids as an energy source during dormancy and reactivation, making lipid metabolizing enzymes attractive targets for new

diagnostic biomarkers or therapeutics.[37-40] The importance of lipid metabolism for *Mtb* growth, persistence, and pathogenicity is reflected in the 250 *Mtb* genes linked to lipid processing—about five times as many as found in *E. coli*, which has a similarly-sized genome.[41] Of these 250 genes, 21 were initially annotated as encoding esterases or lipases, a lipid-preferring subclass, but the actual number is likely at least two-fold higher. Ninety-four gene products are predicted to contain the α/β hydrolase fold characteristic of these enzymes,[185] and misannotated esterases and lipases continue to be identified.[46,47,49-51] However, difficulties expressing and isolating active *Mtb* esterases and lipases have hindered *in vitro* characterization of these enzymes.[37,47,60]

To circumvent this challenge, we directly assessed *Mtb* hydrolase activities using an assay that combined fluorogenic probes with native polyacrylamide gel electrophoresis (PAGE)-resolved cellular lysates. Distinct hydrolases were detected in-gel by selecting an appropriate fluorogenic probe, such as fluorogenic arylsulfates to reveal sulfatases[165,166] or acetoxymethyl ether (AME)-masked probes to detect esterases.[163] Originally, we reported that this assay could distinguish mycobacterial species and strains based on sulfatase activity.[165] More recently, we observed highly conserved esterase activity for *Mtb* complex (MTBC) members—organisms that cause TB.[163] However, we saw far fewer fluorescent bands in this assay than we anticipated based on the *Mtb* genome, and we suspected that our two-carbon (C2) AME probes were hydrolyzed by only a subset of the *Mtb* esterases. Many *Mtb* esterases and

lipases, including Culp1, LipC, LipH, LipI, and LipY, prefer longer four-carbon (C4) and eight-carbon (C8) substrates.[47,60,95,121] Therefore, we report herein an expanded probe set with C4 and C8 acyloxymethyl ether derivatives of DDAO, a far-red fluorophore. We validated these probes with a panel of esterases and lipases. We then used these new substrates to reveal esterase activity in lysates from mycobacteria and *Mtb*-infected macrophages.

Results and Discussion

In our work, much of our probe development has focused on far-red fluorophores that excite above 600 nm (i.e., DDAO[163,165] or DSACO[186]). Cellular autofluorescence and light scattering is minimal in this region of the spectrum, giving far-red fluorophores superior fluorescent properties for imaging in living systems.[171] Therefore, we modified DDAO to create a set of fluorogenic esterase probes (Scheme 3.1a). The archetypical fluorogenic esterase probe is green-fluorescent fluorescein diacetate, but acetate-masked probes are hydrolytically unstable. Chemists have used acyloxymethyl ethers to create esterase probes with improved stability.[135-137] We synthesized AME-masked DDAO substrates through a silver-mediated *O*-alkylation, as previously described.[163] The C4 butanoylmethyl ether (BME)- and C8 octanoylmethyl ether (OME)-masked substrates were synthesized in good yields under biphasic conditions from DDAO and the corresponding iodomethyl esters (Scheme 3.1b).

Both reactions produced a mixture of 2- and 7-substituted regioisomers, which were separated by column chromatography. The lower calculated pK_a[187] of the 2-position phenol tautomer favored formation of the 2-substituted product under these reaction conditions. We assigned substrate regiochemistry though heteronuclear single quantum correlation (HSQC) and heteronuclear multiple bond correlation (HMBC) 2D-NMR spectroscopy, as described in the Materials and Methods.

We determined the spectral properties of each compound (Table 3.1 and Figure 3.1), including absorbance (λ_{abs}) and emission (λ_{em}) maxima, extinction coefficients (ε), and quantum yields (ϕ). Consistent with the DDAO-AME probes,[116] the absorbance maxima of the BME- and OME-masked DDAO compounds were significantly blue-shifted from DDAO. The extinction coefficients of these compounds were also 2- to 3-fold lower compared with the parent compound. All of the 2-substituted regioisomers were non-fluorescent, and the 7-substituted regioisomers were minimally fluorescent. DDAO-7-BME and DDAO-7-OME had over a 50-fold reduction in quantum yield compared with DDAO. These were also an order of magnitude lower than DDAO-7-AME. We measured the relative fluorescence of the masked compounds using DDAO's excitation and emission settings (λ_{ex} 635 nm, λ_{em} 670 nm); all six exhibited a 650-fold to 1420-fold reduction in fluorescence compared with DDAO. Because the 2-masked substrates are non-fluorescent, the fluorescence detected with

these settings is likely due to trace amounts of DDAO. These data show that the acyloxymethyl ether-masked DDAO probes are excellent “turn on” substrates.

We assessed probe reactivity with a diverse panel of commercially available esterases and lipases (Figure 3.2). Heat-killed porcine liver esterase (PLE) did not hydrolyze our substrates, demonstrating that an active enzyme is required for probe cleavage. After 30 minutes, all of the probes were hydrolyzed by every enzyme, but to varying degrees. As expected, the longer-chain BME- and OME-masked probes were improved lipase substrates compared with the AME-masked probes, but they also retained high esterase reactivity. DDAO-7-BME was a moderately less favorable substrate for this enzyme panel compared with DDAO-2-BME and the two OME-masked probes. Despite their different chain lengths, DDAO-2-BME and DDAO-2-OME displayed nearly identical reactivity profiles. Overall, the longer-chain DDAO-derived probes had improved reactivity compared to the AME-masked probes, highlighting the versatility of these new probes as esterase and lipase substrates.

We further characterized the probes with PLE, determining their kinetic parameters (Figure 3.3) and detection limits (Figure 3.4). All six fluorogenic probes were good PLE substrates with Michaelis constants (K_M) ranging from 3 to 9 μM. The catalytic efficiency (k_{cat}/K_M) ranged from 0.2 μM^{-1} s^{-1} (DDAO-2-AME) to 0.7 μM^{-1} s^{-1} (DDAO-2-OME). The AME-masked probes were the least sensitive for PLE detection (25 pg/mL), while DDAO-2-BME, DDAO-7-OME, and DDAO-2-OME were 10-fold more sensitive (2.5 pg/mL). DDAO-7-BME had

intermediate sensitivity (5 pg/mL). Additionally, the new probes had improved hydrolytic stability, with ≥90% of each probe remaining after 60 h (Table 3.2, Figure 3.5).

Fluorogenic esterase probes are common reagents for live-cell imaging.[134] We evaluated our new probes with a human osteosarcoma cell line using confocal fluorescence microscopy. All of our DDAO-derived probes were rapidly internalized and hydrolyzed by intracellular esterases to generate DDAO-stained cells (Figure 3.6). The AME- and BME-masked probes produced more DDAO fluorescence than the OME-masked probes at the same probe concentration. Therefore, DDAO acyloxymethyl ethers are a far-red alternative to fluorescein derivatives for live-cell imaging.

Next, we used these six probes to profile *Mtb* esterase and lipase activities. Many of these enzymes are secreted[47,50] or cell wall-associated,[46,88] making them good targets for assessing whole-cell esterase activity. We found that all six probes were hydrolyzed by live *Mtb* mc^{2}6020, an auxotrophic strain derived from the virulent H37Rv lab strain (Figure 3.7).[188] However, this whole-cell assay did not indicate whether the new probes could reveal esterases missed by our AME-masked probes. We used a native PAGE-based assay to profile esterase and lipase activity patterns, as previously described.[163,165,166] We evaluated lysates from *M. smegmatis*, *M. marinum*, *Mtb* mc^{2}6020, and *M. bovis* (BCG), an attenuated vaccine strain (Figure 3.8a). Overall, the four species displayed different esterase activity patterns, but with high similarity between *Mtb*

mc^{2}6020 and *M. bovis* (BCG), two members of the MTBC. Despite biochemical evidence that many *Mtb* esterases prefer longer-chain substrates,[47,60,95,121] DDAO-7-AME revealed the greatest number of *Mtb* esterases. A subset of these enzymes were revealed by the BME-masked probes, with the absent bands likely attributable to esterases specific for C2 esters. The OME-masked probes were activated by the same *Mtb* enzymes as the BME probes but revealed an additional band not detected with the shorter-chain probes. Interestingly, this band was present in the *Mtb* lysate and not in the BCG lysate. The differences revealed by these probes highlight the benefits of using probes of varying chain lengths in order to track different enzyme sub-classes. These results also demonstrate the power of fluorogenic probes coupled with the in-gel activity-based assay for observing enzyme differences in closely related species.

Because we had previously observed highly conserved esterase activity patterns for MTBC members,[163] we were intrigued by the *Mtb*-specific esterase band revealed by the OME probes. We excised this band and subjected it to in-gel tryptic digestion and protein identification by mass spectrometry. The gel slice contained peptides corresponding to Culp1 (Rv1984c), a secreted cutinase-like protein with esterase activity (Table 3.3).[86,100] The gene encoding Culp1 lies within the region of deletion 2 (RD2), a genomic region that is deleted in *M. bovis* (BCG) substrains but retained in *Mtb*.[41,98,99] This genomic difference accounts for the band's absence in *M. bovis* (BCG) lysate.

We used an *Mtb* CDC1551 transposon mutant to confirm that the fluorescent signal was produced through Culp1-mediated hydrolysis. The OME-specific band was present in lysates from the wild type *Mtb* CDC1551, but absent in the Culp1 transposon mutant (Figure 3.8b). We also examined conditioned medium from *Mtb* $mc^2$6020. We observed two strongly fluorescent bands at a lower apparent molecular weight than the Culp1 whole-cell lysate band (Figure 3.8c). Culp1 contains a signal sequence that is cleaved upon export,[87] and we reasoned that this post-translational modification could result in greater protein mobility in-gel. To test this hypothesis, we excised these bands and identified Culp1 peptides in both. Sequence coverage for both bands began at the *N*-terminus of the cleaved, secreted protein (Table 3.3).[87] Therefore, Culp1 is active both within bacilli and upon secretion. This result highlights the utility of fluorogenic probes for detecting *Mtb* esterases in both lysates and conditioned medium.

Culp1 is one of the best-studied *Mtb* esterases. Recombinant Culp1 was characterized as maximally active with a C4 substrate by West and co-workers,[47] but Schué *et al.* found that it was 86-times more active with a C8 substrate over a C4 substrate.[95] Our results indicate that Culp1 prefers C8 substrates, which agrees with the findings of Schué *et al*. Culp1 induces alveolar epithelial cell apoptosis,[97] suggesting that it may contribute to *Mtb* pathogenesis by facilitating mycobacterial dissemination. Because it is an immunodominant RD antigen, Culp1 has been explored as a potential candidate for an improved TB

vaccine.[100,101] Immunization with recombinant Culp1 provided partial protection against TB,[100] and supplementing the BCG vaccine with Culp1 and other RD antigens enhanced the vaccine's efficacy in mice.[101] The ability to track Culp1 activity using OME-masked fluorogenic substrates could benefit future investigations of this clinically-relevant esterase.

Next, we evaluated lysates from *Mtb* mc^{2}6020-infected murine macrophages (Figure 3.8d). Mock-infected macrophages were prepared in tandem to compare host cell esterase activity. In mock-infected macrophage lysates, DDAO-7-BME revealed the greatest number of esterases, while DDAO-7-OME revealed the fewest. *Mtb*-infected samples displayed esterase bands originating from both the host and the pathogen. Notably, a subset of the *Mtb* esterase bands could be distinguished from those originating from host cells based on their migration patterns. For example, macrophage-associated esterases generally appeared in the top portion of the gel, while *Mtb* esterases were more prominent in the lower quadrant. DDAO-7-OME provided the clearest *Mtb* banding patterns in these complex lysates and revealed Culp1 activity in *Mtb*-infected macrophages. These results demonstrate that our assay platform can track esterase activity in mixed cell populations without interference from host enzymes. We anticipate that this type of assay will be useful for analyzing esterase activity in other host-pathogen models, including *Mtb*-infected animal tissues or patient-derived samples.

In conclusion, we synthesized and characterized C4 and C8 acyloxymethyl ether-masked fluorogenic probes from the far-red fluorophore DDAO. These probes were "turn-on" substrates with superior stability and esterase reactivity compared with our previously reported C2-masked probes. This expanded set is a powerful toolbox for uncovering substrate preferences, quantifying esterase activities, and live-cell microscopy. We used our DDAO-derived probes to examine *Mtb* esterases and lipases in whole cells and in native PAGE-resolved lysates. The OME-masked probes revealed a key difference in esterase activity between *Mtb* and *M. bovis* (BCG), two closely related species. The *Mtb*-specific band was identified as Culp1, a clinically-relevant secreted esterase. The OME-masked probes were also better for distinguishing mycobacterial esterases from host cell esterases in *Mtb*-infected macrophage lysates. Overall, our probes are long-chain, far-red fluorogenic substrates that can be used for detecting and tracking esterase and lipase activities in a wide range of assay formats.

Materials and Methods

ACS grade solvents were used as received. DDAO was purchased from Shanghai Medicilon Inc. All other chemicals were purchased from Sigma-Aldrich, Fisher Scientific, or VWR Scientific and used as received. Unless otherwise stated, reactions were magnetically stirred. Reactions were monitored

by thin-layer chromatography (TLC) on glass-backed silica gel plates (Silicycle 60 Å, 250 μM). Flash column chromatography was performed with the indicated solvents on Silicycle SiliaFlash P60.

Mass spectra were acquired at Portland State University's BioAnalytical Mass Spectrometry Facility on a ThermoElectron LTQ-Orbitrap Discovery high-resolution mass spectrometer with electrospray ionization (ESI).

NMR spectra were acquired at ambient temperature at Portland State University's NMR facility. ^{1}H-NMR data were obtained in the specified solvent on a Bruker Avance II at 400 MHz. ^{13}C-NMR data were obtained on the same instrument in the specified solvent at 101 MHz. Spectra were calibrated to the residual solvent peak. Chemical shifts are reported in ppm. Coupling constants (*J*) are reported in Hertz (Hz) and rounded to the nearest 0.1 Hz. Multiplicities are defined as: s = singlet, d = doublet, dd = doublet of doublets, t = triplet, m = multiplet, br s = broad singlet.

Synthesis of iodomethyl butyrate

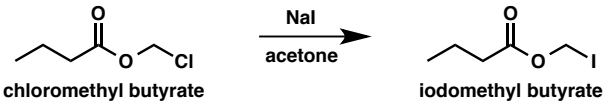

Sodium iodide (0.28 g, 1.97 mmol, 6 equiv) was combined with acetone (2 mL) in a 20 mL scintillation vial. Chloromethyl butyrate (0.25 mL, 1.97 mmol, 6 equiv) was dissolved in acetone (0.5 mL), and the solution was added to the vial dropwise via syringe. The syringe was rinsed with 0.5 mL acetone, and the vial

was sealed and protected from light. After stirring overnight, 3 mL of CH_2Cl_2 was added to the vial, and the resulting mixture was filtered through fiberglass filter paper (Whatman GF/A). Concentration *in vacuo* and resuspension in CH_2Cl_2 was followed by a second filtration. Concentration of the resulting clear solution produced 0.277 g of iodomethyl butyrate as a brown oil (62% yield), which was used without further purification.

Synthesis of DDAO-2-butanoylmethyl ether (DDAO-2-BME) and DDAO-7-butanoylmethyl ether (DDAO-7-BME)

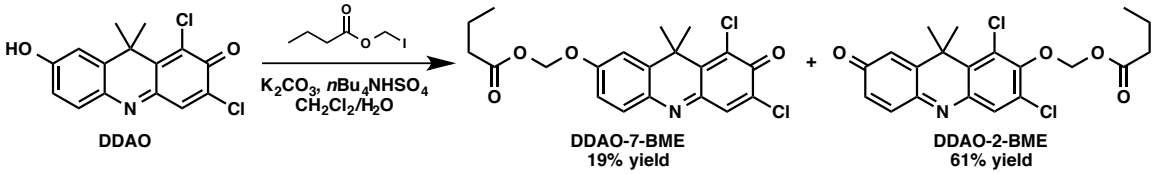

A 20 mL scintillation vial was charged with DDAO (0.1002 g, 0.325 mmol, 1 equiv) and tetrabutylammonium hydrogen sulfate (0.0112 g, 0.033 mmol, 0.1 equiv). Then CH_2Cl_2 (3.3 mL) was added, resulting in a deep red suspension. A solution of K_2CO_3 (0.1348 g, 0.975 mmol, 3 equiv) in H_2O (1 mL) was added via pipet, followed by an additional 0.625 mL H_2O (0.2 M total). The reaction mixture became dark blue upon vigorous stirring. Iodomethyl butyrate was added via pipet, followed by additional CH_2Cl_2 (1 mL, 0.08 M total), and the vial was sealed and protected from light. Additional H_2O (2 mL, 0.13 M) was added after 21 h, and the reaction mixture was stirred for another 3 days. The reaction mixture was transferred to a separatory funnel with additional CH_2Cl_2 and H_2O. The layers were separated, and the organic layer was washed with H_2O (1 x 15 mL).

The combined aqueous layers were extracted with CH_2Cl_2 (3 x 15 mL). The combined organic layers were washed with brine (1 x 20 mL), dried over $MgSO_4$, filtered, and concentrated *in vacuo* to a yellow-brown oil. Purification by column chromatography (SiO_2, loaded in toluene, 1.5 to 5% EtOAc in hexanes with 40% CH_2Cl_2 as a co-solvent) yielded two major products: an orange solid identified as DDAO-7-BME (R_f = 0.66, 10% EtOAc/45% hexanes/45% CH_2Cl_2) (0.0248 g, 19% yield) and a yellow-orange solid identified as DDAO-2-BME (R_f = 0.48, 10% EtOAc/45% hexanes/45% CH_2Cl_2) (0.0806 g, 61% yield).

DDAO-2-BME (Figures 3.9–3.12):

^{1}H-NMR (400 MHz; $CDCl_3$): δ 7.74 (s, 1H), 7.35 (d, J = 10.1 Hz, 1H), 6.66 (d, J = 1.8 Hz, 1H), 6.66 (dd, J = 10.0, 2.0 Hz, 1H), 5.79 (s, 2H), 2.36 (t, J = 7.4 Hz, 2H), 1.78 (s, 6H), 1.65 (sextet, J = 7.4 Hz, 2H), 0.94 (t, J = 7.4 Hz, 3H).

^{13}C-NMR (101 MHz, $CDCl_3$): δ 187.36, 172.66, 153.08, 151.87, 148.30, 141.03, 140.59, 133.40, 132.68, 132.38, 129.62, 128.92, 127.97, 88.12, 38.17, 35.97, 28.91, 18.02, 13.77.

ESI-HRMS $[M+H]^+$ m/z calculated for $C_{20}H_{20}Cl_2NO_4$: 408.0764; found: 408.0774.

DDAO-7-BME (Figures 3.13–3.16):

^{1}H-NMR (400 MHz; $CDCl_3$): δ 7.62 (s, 1H), 7.62 (d, J = 8.7 Hz, 1H), 7.13 (d, J = 2.6 Hz, 1H), 7.05 (dd, J = 8.7, 2.7 Hz, 1H), 5.85 (s, 2H), 2.37 (t, J = 7.4 Hz, 2H), 1.87 (s, 6H), 1.67 (sextet, J = 7.4 Hz, 2H), 0.94 (t, J = 7.4 Hz, 3H).

^{13}C-NMR (101 MHz, $CDCl_3$): δ 173.30, 172.43, 159.84, 148.54, 140.59, 140.57, 139.55, 137.12, 136.88, 135.08, 133.98, 114.86, 114.76, 84.52, 39.27, 36.10, 26.85, 18.30, 13.69.

ESI-HRMS $[M+H]^+$ m/z calculated for $C_{20}H_{20}Cl_2NO_4$: 408.0764; found: 408.0771.

Synthesis of chloromethyl octanoate

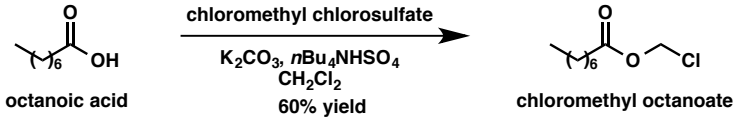

Octanoic acid (0.5 mL, 3.16 mmol, 1 equiv) and tetrabutylammonium hydrogen sulfate (0.0536 g, 0.16 mmol, 0.05 equiv) were dissolved in CH_2Cl_2 (3 mL) in a 20 mL scintillation vial. A solution of K_2CO_3 (1.75 g, 12.6 mmol, 4 equiv) in H_2O (3 mL, 1 M final concentration) was then added, and the reaction mixture was stirred for 3 min. Chloromethyl chlorosulfate (0.4 mL, 3.94 mmol, 1.25 equiv) was dissolved in 3 mL CH_2Cl_2 (0.5 M total) and added to the reaction mixture portion-wise over 50 min. The reaction mixture was then stirred for an additional 70 min. The reaction mixture was transferred to a separatory funnel with additional CH_2Cl_2 and H_2O. The layers were separated, and the organic layer was washed with H_2O (1 x 15 mL). The combined aqueous layers were then extracted with CH_2Cl_2 (2 x 15 mL). The combined organic layers were washed with brine and dried over Mg_2SO_4. Filtration and concentration *in vacuo* gave the crude product. Purification by SiO_2 plug (loaded in hexanes, 1 to 2.5%

EtOAc in hexanes) and concentration *in vacuo* gave 0.36 g (60% yield) of the product as a clear, pale yellow oil. Spectral data matched that reported in the literature.[189]

Synthesis of iodomethyl octanoate

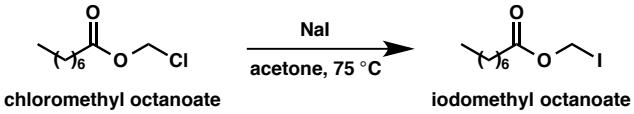

Sodium iodide (0.2548 g, 1.7 mmol, 1.01 equiv) was combined with acetone (2 mL) in a 2-dram vial. Chloromethyl octanoate (0.3221 g, 1.68 mmol, 1 equiv) in acetone (1 mL) was added dropwise, followed by 1 mL acetone (0.42 M total). The vial was sealed and protected from light, and the reaction mixture was stirred for 7 h. CH_2Cl_2 (1 mL) was added, followed by filtration through fiberglass filter paper, concentration *in vacuo*, refiltration, and concentration under a stream of air to give an orange oil, which was used without further purification.

Synthesis of DDAO-2-octanoylmethyl ether (DDAO-2-OME) and DDAO-7-octanoylmethyl ether (DDAO-7-OME)

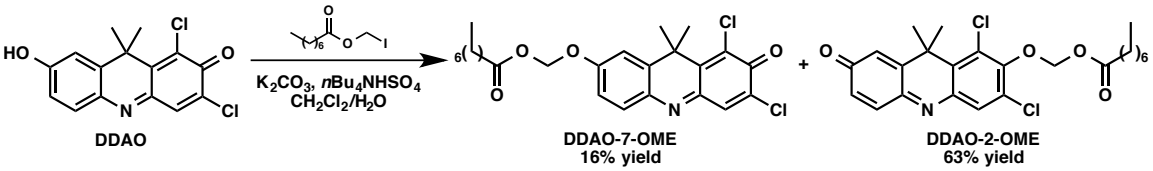

In a 20 mL scintillation vial, DDAO (0.1022 g, 0.332 mmol, 1 equiv) and tetrabutylammonium hydrogen sulfate (0.0113 g, 0.032 mmol, 0.1 equiv) were

combined in CH_2Cl_2 (3 mL) to give a deep red suspension. A solution of K_2CO_3 (0.1376 g, 1 mmol, 3 equiv) in H_2O (1 mL) was added to the reaction mixture, followed by an additional 2 mL H_2O (0.1 M total). Iodomethyl octanoate (0.48 g, 1.7 mmol, 5 equiv) was then added via pipet, followed by an additional 3 mL CH_2Cl_2 (0.05 M total). The reaction mixture was stirred vigorously for 40 h and then transferred to a separatory funnel with additional CH_2Cl_2 and H_2O. The layers were separated, and the organic layer was washed with H_2O (1 x 15 mL). The combined aqueous layers were extracted with CH_2Cl_2 (3 x 15 mL). The combined organic layers were washed with brine (1 x 20 mL), dried over $MgSO_4$, filtered, and concentrated *in vacuo* to a brown oil. Purification by column chromatography (SiO_2, loaded in toluene, 1.5 to 5% EtOAc in hexanes with 40% CH_2Cl_2 as a co-solvent) gave two major products: an orange solid identified as DDAO-7-OME (R_f = 0.71, 10% EtOAc/45% hexanes/45% CH_2Cl_2) (0.0239 g, 16% yield) and a yellow-orange solid identified as DDAO-2-OME (R_f = 0.60, 10% EtOAc/45% hexanes/45% CH_2Cl_2) (0.0842 g, 63% yield).

DDAO-2-OME (Figures 3.17–3.20):

^{1}H-NMR (400 MHz; $CDCl_3$): δ 7.75 (s, 1H), 7.35 (d, J = 10.2 Hz, 1H), 6.66 (d, J = 1.8 Hz, 1H), 6.66 (dd, J = 10.2, 1.8 Hz, 1H), 5.79 (s, 2H), 2.37 (t, J = 7.5 Hz, 2H), 1.78 (s, 6H), 1.61 (quintet, J = 7.4 Hz, 2H), 1.30-1.24 (m, 8H), 0.86 (t, J = 6.9 Hz, 3H).

^{13}C-NMR (101 MHz, $CDCl_3$): δ 187.37, 172.87, 153.08, 151.88, 148.31, 141.05, 140.60, 133.40, 132.70, 132.40, 129.64, 128.94, 127.99, 88.14, 38.18, 34.13, 31.74, 29.14, 29.02, 28.93, 24.54, 22.70, 14.19.

ESI-HRMS $[M+H]^+$ m/z calculated for $C_{24}H_{28}Cl_2NO_4$: 464.1390; found: 464.1398.

DDAO-7-OME (Figures 3.21–3.24):

^{1}H-NMR (400 MHz; $CDCl_3$): δ 7.62 (s, 1H), 7.62 (d, J = 8.7 Hz, 1H), 7.13 (d, J = 2.6 Hz, 1H), 7.05 (dd, J = 8.7, 2.7 Hz, 1H), 5.84 (s, 2H), 2.38 (t, J = 7.5 Hz, 2H), 1.87 (s, 6H), 1.62 (dd, J = 14.8, 7.4 Hz, 3H), 1.28-1.22 (m, 10H), 0.84 (t, J = 7.0 Hz, 3H).

^{13}C-NMR (101 MHz, $CDCl_3$): δ 173.30, 172.62, 159.83, 148.53, 140.59, 140.57, 139.55, 137.12, 136.88, 135.08, 133.98, 114.84, 114.75, 84.48, 39.27, 34.28, 31.72, 29.08, 28.98, 26.86, 24.81, 22.68, 14.18.

ESI-HRMS $[M+H]^+$ m/z calculated for $C_{24}H_{28}Cl_2NO_4$: 464.1390; found: 464.1396.

Regioisomer determination for the C4 and C8 probes

^{1}H-NMR data were used to identify the protons on the methylether unit. We confirmed the identity of the methylether carbon by combining ^{13}C-NMR with a heteronuclear single quantum correlation (HSQC) experiment. A heteronuclear multiple bond correlation (HMBC) experiment was used to identify the aromatic

carbon in the phenolic ether by its relationship to the protons on the methylether, which were three bonds away. Further examination of the HMBC data then allowed us to determine the aromatic proton(s) that were three bonds away from that carbon. The regioisomers were assigned based on whether or not the phenolic ether carbon was correlated with an aromatic proton that exhibited coupling in the ^{1}H-NMR spectrum. Coupling indicated a regioisomer substituted at the 7-position, whereas no coupling indicated a regioisomer substituted at the 2-position.

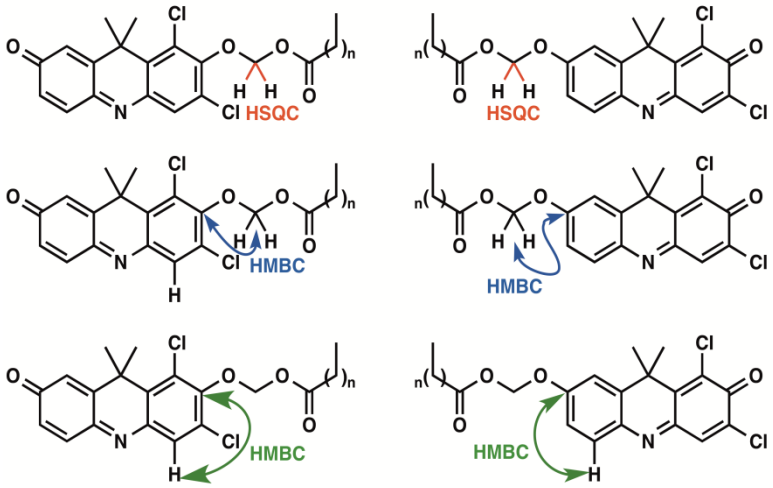

With our data, along with that available from previously reported DDAO-derived compounds,[163,190,191] we verified a method for determining the regioisomers based on the ^{1}H-NMR chemical shifts of the protons at the 6 and 8 positions. Substitution at the 2-position is characterized by those protons having a chemical shift between 6.5 and 7 ppm. Substitution at the 7-position is characterized by a chemical shift of 7–7.5 ppm. This assignment strategy was

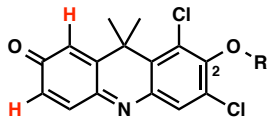

H = 6.5 – 7 ppm

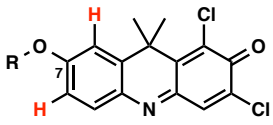

H = 7 – 7.5 ppm

previously proposed by Warther *et al.*, who synthesized the 2 and 7 allyl ether-substituted regioisomers of DDAO and assigned their structures by HSQC and HMBC.[190]

Spectral characterization of fluorogenic probes

Spectra were acquired on a Tecan Infinite M200 Pro microplate reader in clear 96-well microplates for absorbance reads or black 96-well microplates for fluorescence reads (10 reads per well, 1 nm step size). All measurements were performed in 10 mM HEPES buffer (pH 7.3). In order to remain within the linear range of the instrument, compounds were diluted to 5 μM for absorbance reads and 2.5 μM for fluorescence reads. Compound fluorescence was excited at 602 nm (DDAO), 453 nm (DDAO-7-BME), or 451 nm (DDAO-7-OME). DDAO-2-BME and DDAO-2-OME were non-fluorescent.

The fluorescence of each probe (1 μM) was directly compared to the fluorescence of DDAO (1 μM) by measuring each compound's emission at 670 nm following excitation at 635 nm. The fluorescence decrease, as provided in Table 3.1, was calculated as the ratio of DDAO fluorescence and fluorogenic probe fluorescence and reported as a fold decrease in fluorescence compared to DDAO.

Extinction coefficients were measured in 10 mM HEPES (pH 7.3). Four independent 5 mM stocks were prepared in DMSO for each compound. Two independent 10 μM solutions were prepared from each stock in 10 mM HEPES (pH 7.3). Absorbance was measured with a Tecan Infinite M200 Pro microplate reader in a Starna Cell 18F-Q-10 quartz cuvette at the wavelength of maximum absorption. The molar extinction coefficients were calculated using Beer's law ($A = \varepsilon cl$; A = absorbance, ε = extinction coefficient, c = concentration, l = path length). The reported extinction coefficients are the average of eight reads per compound.

The relative quantum yield of DDAO was determined using oxazine 1 (Anaspec, $\phi = 0.15$ in EtOH) as the reference. The relative quantum yields of DDAO-7-BME and DDAO-7-OME were determined using fluorescein (Sigma-Aldrich, $\phi = 0.89$ in 0.1 N NaOH) as the reference. A 10 μM solution of each compound was diluted into the appropriate solvent [DDAO, DDAO-7-BME, and DDAO-7-OME: 10 mM HEPES (pH 7.3); oxazine 1: EtOH; fluorescein: 0.1 N NaOH]. The absorbance of each solution was measured on a Tecan Infinite M200 Pro microplate reader in a Starna Cell 18F-Q-10 quartz cuvette. DDAO and oxazine 1 were measured at 520 nm. DDAO-7-BME, DDAO-7-OME, and fluorescein were measured at 400 nm. For each compound, three independent dilutions at a calculated absorbance of 0.01 were prepared from the 10 μM solution. Three samples from each dilution (for a total of $n = 9$) were excited at 520 nm (DDAO and oxazine 1) or 400 nm (DDAO-7-BME, DDAO-7-OME, and

fluorescein) in a 96-well black plate, and the fluorescence emission curves were obtained on a Tecan Infinite M200 Pro microplate reader. The total fluorescence was calculated by integrating the area under the curve using GraphPad Prism 6 software. The quantum yields were calculated as: $\phi_x = \left(\frac{A_s}{A_x}\right)\left(\frac{F_x}{F_s}\right)\left(\frac{n_x}{n_s}\right)^2 \phi_s$. In this formula, ϕ = quantum yield, A = absorbance, F = total fluorescence, n = refractive index of the solvent, s = standard, and x = unknown.

Enzyme panel screen

Esterases and lipases were purchased from Sigma-Aldrich. Enzymes were prepared as 10 mg/mL stocks and diluted to 1 μg/mL in 10 mM HEPES (pH 7.3). Heat-killed porcine liver esterase (PLE) was prepared by heating PLE at 90 °C for 20 min. The reactions were initiated with 5 μM substrate and incubated for 30 min at 37 °C (n = 4). Probe cleavage was detected by measuring DDAO fluorescence on a Tecan Infinite M200Pro microplate reader (λ_{ex} 635 nm, λ_{em} 670 nm).

Esterase	**Product #**
porcine liver esterase	E2884
Bacillus subtilis esterase	96667
Aspergillus sp. lipase	84205
Candida antarctica lipase	65986
Candida rugosa lipase	62316
Mucor miehei lipase	62298
Pseudomonas cepacia lipase	62309
Pseudomonas fluorescens lipase	95608
Rhizopus arrhizus lipase	62305

PLE kinetics

Probes were evaluated with 50 ng/mL PLE. Kinetic assays were performed in triplicate at 37 °C in 10 mM HEPES buffer (pH 7.3) with 20% (v/v) DMSO as a co-solvent. Probe solutions were pre-incubated at 37 °C for 10 min

prior to enzyme addition. After enzyme addition, DDAO fluorescence was measured every 30 s on a Tecan Infinite M200Pro microplate reader (λ_{ex} 635 nm, λ_{em} 670 nm). Kinetic parameters were calculated using GraphPad Prism 6 software with the method of initial rates.[182] Data were fit to a Michaelis-Menten enzyme kinetics curve, $V = V_{max}[S]/(K_M + [S])$, where V is the reaction rate, S is the substrate concentration, and K_M is the Michaelis constant. Relative fluorescence units were converted to pmol of DDAO using a DDAO standard curve.

PLE detection limit

PLE (1 pg/mL to 2500 pg/mL) was serially diluted in 10 mM HEPES (pH 7.3) + 20% (v/v) acetonitrile. Reactions were initiated with 25 μM esterase probe and incubated at 37 °C for 10 min ($n = 4$). Fluorescence was measured on a Tecan Infinite M200Pro microplate reader (λ_{ex} 635 nm, λ_{em} 670 nm). The detection limit was defined as the lowest statistically significant ($P < 0.01$) detectable amount of enzyme compared to the no-enzyme control using an unpaired, two-tailed t test with Welch's correction.

Probe hydrolytic stability

DDAO-7-BME, DDAO-2-BME, DDAO-7-OME, and DDAO-2-OME were diluted to 1 μM in PBS. Samples ($n = 6$ for each probe) were incubated at 37 °C, and DDAO fluorescence (λ_{ex} 635 nm, λ_{em} 670 nm) was measured every 10 min

for 60 h on a Tecan Infinite M200Pro microplate reader. Since the probes did not completely hydrolyze in PBS within 60 h, each probe was also diluted into PBS containing PLE (10 µg/mL) to determine the fluorescence value of fully-hydrolyzed probe. We used the fluorescence value of PLE-hydrolyzed probe to calculate the percent of each probe hydrolyzed after 60 h (Table S1).

Fluorescence microscopy of mammalian cells

U2OS epithelial cells were generously provided by Prof. Xiaolin Nan (OHSU). Cells were maintained in Dulbecco's Modified Eagle's Medium (DMEM, Gibco®) supplemented with 10% (v/v) FBS (VWR), 100 U/mL penicillin, and 100 μg/mL streptomycin (Invitrogen) in a humidified incubator at 37 °C and 5% CO_2. Cells were seeded in an 8-well chambered cover glass (Cellvis) at a density of 5 $\times$ 10^4 cells per well and allowed to adhere overnight. Cells were counterstained with 1 μg/mL Hoechst 33342 (Invitrogen) before esterase probe treatment. Cells were incubated with 10 μM fluorogenic probe for 10 min at room temperature in Live Cell Imaging Solution (Molecular Probes; 140 mM NaCl, 2.5 mM KCl, 1.8 mM $CaCl_2$, 1 mM $MgCl_2$, 20 mM HEPES). The cells were washed once with additional Live Cell Imaging Solution and imaged in the same medium. Images were collected using a Zeiss 40X/0.95 NA objective on a Yokogawa CSU-X1 spinning disk confocal mounted on a Zeiss Axio Observer microscope at OHSU's Advanced Light Microscopy Core. Hoechst 33342 fluorescence was obtained by excitation at 405 nm (450/50 nm emission filter), and DDAO fluorescence was

obtained by excitation at 638 nm (690/50 nm emission filter). Images were processed in ImageJ.[183] The brightness and contrast settings were optimized for the Hoechst nuclear stain, and the same settings were used for all images (Figure 3.6; false-colored green). Although all six probes produced DDAO fluorescence in live cells (false-colored magenta), the fluorescence varied from probe to probe. Therefore, the maximum brightness and contrast setting was determined separately for each probe. We used the same minimum value for all probes. To enable a direct comparison, the same DDAO settings were applied to a corresponding image of DMSO-treated cells; no far-red fluorescence was detected in DMSO-treated cells using any of our display settings.

Mycobacterial culture conditions

M. smegmatis mc^{2}155 (700084) and *M. marinum* (BAA-535) were obtained from ATCC. *M. bovis* (BCG) was obtained from G. Purdy (OHSU). *Mtb* mc^{2}6020 (Δ*lysA* Δ*panCD* mutant)[188] was obtained from W.R. Jacobs (Albert Einstein College of Medicine, HHMI). These strains were handled as BSL-2 pathogens with appropriate precautions. Cells were thawed from frozen stocks (stored at –80 °C in 6% glycerol). *M. bovis* (BCG), *M. smegmatis*, and *M. marinum* were cultured in 7H9 broth supplemented with 0.5% (v/v) glycerol, 0.05% (v/v) Tween 80, and 10% (v/v) ADC (albumin, dextrose, catalase). *Mtb* mc^{2}6020 was grown in the same 7H9 broth further supplemented with 80 μg/mL lysine, 24 μg/mL pantothenate, and 0.2% (w/v) casamino acids. Cultures were

grown at 37 °C (BCG, *M. smegmatis,* and *Mtb* mc^{2}6020) or 30 °C (*M. marinum*) with slow shaking (75–100 RPM).

Wild type *Mtb* CDC1551 (NR-13649) and a CDC1551 transposon mutant for MT2037/Rv1984c (NR-18745) were acquired from BEI Resources and handled as BSL-3 pathogens. Wild type CDC1551 was thawed from a frozen stock, and the transposon mutant was inoculated from an agar slant. Cultures were grown in 7H9 supplemented with 0.5% (v/v) glycerol, 0.05% (v/v) Tween 80, and 10% (v/v) ADC at 37 °C and 5% CO_2 with stirring.

To prepare conditioned medium (CM), *Mtb* mc^{2}6020 was grown to an OD between 0.5 and 1, pelleted, washed twice with Sauton's Minimal Medium, and resuspended in Sauton's Minimal Medium. Cultures were grown at 37 °C with slow shaking (75 RPM). Cells were grown to an OD ~1 and pelleted. The pellet was stored for subsequent lysis (–30 °C), and the clarified CM was sterile filtered through a 0.2 μm membrane (SteriFlip, Millipore) and stored (–30 °C). Thawed CM was subsequently concentrated with a 10 kDa MWCO filter (Amicon).

Mycobacterial whole-cell assay

Mtb mc^{2}6020 was cultured to an OD_{600} between 0.5 and 1.0 in rich growth medium and then diluted to an OD_{600} of 0.2 in PBS (pH 7.4) with 0.05% Tween 80. Varying numbers of bacilli (3,000,000 to 0) were incubated with 10 μM fluorogenic probe (DDAO-2-AME, DDAO-7-AME, DDAO-2-BME, DDAO-7-BME, DDAO-2-OME, or DDAO-7-OME) for 30 min at 37 °C (n = 4). Cells were treated

with phosphate-buffered formalin before DDAO fluorescence was measured on a Tecan Infinite M200Pro microplate reader (λ_{ex} 635 nm, λ_{em} 670 nm). We determined the significance ($P < 0.05$) of the fluorescence signal produced by each sample compared to a cell-free control using an unpaired, two-tailed *t* test with Welch's correction. The number of bacilli in each dilution was estimated by assuming that a culture with an OD_{600} of 1 contains 3 x 10^8 colony forming units (CFUs)/mL.[192]

RAW macrophage infection

RAW 264.7 macrophages were purchased from ATCC and maintained at 37 °C, 5% CO_2 in a humidified incubator. Cells were cultured in DMEM supplemented with 10% (v/v) FBS (HyClone™), 100 U/mL penicillin, and 100 μg/mL streptomycin. Near-confluent cells were dislodged with a cell scraper for sub-culturing.

Macrophages (4 x 10^7 cells/flask) in DMEM-FBS (no antibiotics) were infected with *Mtb* $mc^2$6020 (8 x 10^8 bacteria/flask; multiplicity of infection = 20). For mock infection, the same volume of vehicle (DPBS) was added. After a 4 h infection, the cells were washed twice with warm DPBS, and an initial time point was immediately harvested. The remaining flasks were changed to DMEM-FBS with 25 μg/mL amikacin. After 1 h, cells were washed twice with warm DPBS and placed in DMEM-FBS (no antibiotics). At each time point, cells were harvested by centrifugation (3000 RPM, 4 °C) and resuspended in lysis buffer [50

mM Tris (pH 7.5 at 4 °C), 200 mM NaCl, 0.5 mM $CaCl_2$, 0.5 mM $MgCl_2$, 0.2% (v/v) Triton X-100]. Samples were stored at –30 °C prior to lysis by mechanical disruption. The resulting lysates were sterile-filtered (0.2 μm membrane, PALL) and concentrated (10 kDa MWCO filters, Amicon). Protein concentration was determined by BCA assay (Pierce).

Native PAGE in-gel activity assay

Cell pellets were resuspended in lysis buffer [50 mM Tris (pH 7.5 at 4 °C), 200 mM NaCl, 0.5 mM $CaCl_2$, 0.5 mM $MgCl_2$, 0.2% (v/v) Triton X-100] and lysed by mechanical disruption. The resulting lysates were sterile-filtered (0.2 μm membrane, PALL), and protein concentration was determined by BCA assay (Pierce). Lysates were resolved by native polyacrylamide gel electrophoresis (10–20% Tris-HCl Criterion gel, Bio-Rad). For mycobacterial profiling, 1 to 8 µg of total protein was loaded per lane, approximately normalized by band brightness. For the macrophage infection samples, an equal amount of total protein (8 μg) was loaded per lane. Gels were run on ice for 2 h at 200 V in 1X Tris-Glycine buffer (Bio-Rad) prepared in deionized water without methanol. Gels were incubated in 10 mM HEPES (pH 7.3) (for DDAO-7-AME, DDAO-2-AME, DDAO-7-BME, and DDAO-2-BME) or 10 mM HEPES (pH 7.3) + 0.1% (v/v) Triton X-100 (for DDAO-7-OME and DDAO-2-OME) containing 5 μM probe. After 5–10 min, the gels were imaged on a fluorescence scanner (Typhoon 9410 Variable Mode Imager, GE Healthcare). DDAO was detected using a 633 nm

excitation laser with a 670 nm (bp 30) emission filter. The resulting images were analyzed in ImageJ.[183]

Identification of proteins by mass spectrometry

Esterase bands were excised from a protein gel based on DDAO fluorescence. Gel slices were submitted for protein tryptic digestion, peptide extraction, and LC-MS/MS analysis. For the band excised from whole cell lysate, analysis was performed by the OHSU Proteomics Shared Resource on a Thermo Scientific Orbitrap Fusion (NIH grant S10OD012246). This facility has partial support from NIH core grants P30EY010572 and P30CA069533. The resulting MS/MS spectra were analyzed using Sequest (Thermo Fisher Scientific). Sequest was set up to search the UniProt *M. tuberculosis* H37Rv database (8350 entries) assuming tryptic digestion. Sequest was searched with a fragment ion mass tolerance of 1.0 Da and a parent ion tolerance of 1.5 Da. Carbamidomethylation of cysteine was specified in Sequest as a fixed modification. Scaffold (Proteome Software Inc.) was used to validate MS/MS-based peptide and protein identifications. Peptide identifications were accepted if they could be established at greater than 50.0% probability by the Peptide Prophet algorithm[193,194] with Scaffold delta-mass correction. Protein identifications were accepted if they could be established at greater than 95.0% probability and contained at least 2 identified unique peptides (see Table S2 for a list of identified Culp1 peptides). Proteins that contained similar peptides and

could not be differentiated based on MS/MS analysis alone were grouped to satisfy the principles of parsimony.

For the CM bands, analysis was performed by the UC Davis Proteomics Core. The resulting MS/MS spectra were searched using X! Tandem (The GPM, thegpm.org; version CYCLONE 2013.02.01.1). X! Tandem was set up to search the uniprotM_20160127_ja6Dre database (8206 entries) assuming tryptic digestion. X! Tandem was searched with a fragment ion mass tolerance of 20 ppm and a parent ion tolerance of 20 ppm. Carbamidomethylation of cysteine was specified in X! Tandem as a fixed modification. Glu->pyro-Glu of the N-terminus, ammonia-loss of the N-terminus, Gln->pyro-Glu of the N-terminus, deamidation of Asp and Glu, oxidation of Met and Trp, dioxidation of Met and Trp, and acetylation of the N-terminus were specified in X! Tandem as variable modifications. Scaffold was used to validate MS/MS-based peptide and protein identifications. Peptide identifications were accepted if they exceeded specific database search engine thresholds. X! Tandem identifications required at least -Log(Expect Scores) scores greater than 1.5. Protein identifications were accepted if they contained at least 2 identified unique peptides. Proteins that contained similar peptides and could not be differentiated based on MS/MS analysis alone were grouped to satisfy the principles of parsimony.

Acknowledgements

We are grateful to our collaborators L. Lavis (Janelia Research Campus/HHMI) and J. Johnson (Butler University) for productive discussions. We thank M. Harriff and the D. Lewinsohn laboratory (OHSU) for assistance with our BSL-3 experiments. The W. Jacobs laboratory (Albert Einstein College of Medicine and HHMI) kindly shared their *Mtb* mc^{2}6020 auxotrophic strain. BEI Resources (NIAID, NIH) supplied the *Mtb* CDC1551 strains, both wild type and the transposon mutant 2944 (MT2037, Rv1984c; NR-18745). We thank J. Doh for her assistance with live-cell imaging. HRMS data were collected on Portland State University's ThermoElectron LTQ-Orbitrap Discovery (NSF instrument grant 0741993). Funding for this research was generously provided by the Knight Cancer Institute at OHSU, the Collins Medical Trust, and the Medical Research Foundation of Oregon. SRL was supported by an NIH T32 training grant (T32-AI07472).

Tables

Table 3.1. Spectral properties of DDAO and DDAO-derived fluorogenic probes in 10 mM HEPES (pH 7.3).

Compound	λ_{abs} (nm)	λ_{em} (nm)	ε ($M^{-1}cm^{-1}$)	ϕ^a	Fluorescence Decrease[b]
DDAO	646	659	36,000	0.39	–
DDAO-2-AME	395	–	11,000	–	1420-fold
DDAO-7-AME	465	625	4,900	0.07	890-fold
DDAO-2-BME	400	–	13,000	–	1015-fold
DDAO-7-BME	453	613	14,000	0.006	1180-fold
DDAO-2-OME	392	–	21,000	–	890-fold
DDAO-7-OME	451	614	23,000	0.007	650-fold

[a]The fluorescence quantum yields were measured at 25 °C using oxazine 1 (ϕ = 0.15 in EtOH) or fluorescein (ϕ = 0.89 in 0.1 M NaOH) as reference standards.

[b]The fluorescence decrease was calculated as the ratio of DDAO fluorescence and fluorogenic probe fluorescence at the same concentration (λ_{ex} 635 nm, λ_{em} 670 nm).

Table 3.2. Percentage of DDAO-derived probes hydrolyzed in PBS (pH 7.4) after 60 h.

Probe	% Hydrolyzed
DDAO-2-BME	8.0 ± 0.7
DDAO-7-BME	10.3 ± 0.6
DDAO-2-OME	2.0 ± 0.1
DDAO-7-OME	3.4 ± 0.3

Table 3.3. Identification of Culp1 by mass spectrometry.

Sample	Rv	Name	% Coverage	Peptide List[a]	Spectral Counts
Mtb lysate	Rv1984c	Culp1	14.7	R.SIGVYAVNYPASDDYR.A	3
				R.ASASNGSDDASAHIQR.T	2
Mtb CM (higher band)	Rv1984c	Culp1	36.4	R.ASASNGSDDASAHIQR.T	14
				Y.AVNYPASDDYR.A	1
				A.DPCSDIAVVFAR.G	6
				R.GTHQASGLGDVGEAFVDSLTSQVGGR.S	6
				R.SIGVYAVNYPASDDYR.A	5
				R.TVASCPNTR.I	1
Mtb CM (lower band)	Rv1984c	Culp1	32.3	R.ASASNGSDDASAHIQR.T	3
				A.DPCSDIAVVFAR.G	5
				R.GTHQASGLGDVGEAFVDSLTSQVGGR.S	3
				R.SIGVYAVNYPASDDYR.A	5

[a]Periods (.) separate found peptides from the previous and next residues in the protein sequence.

Figures

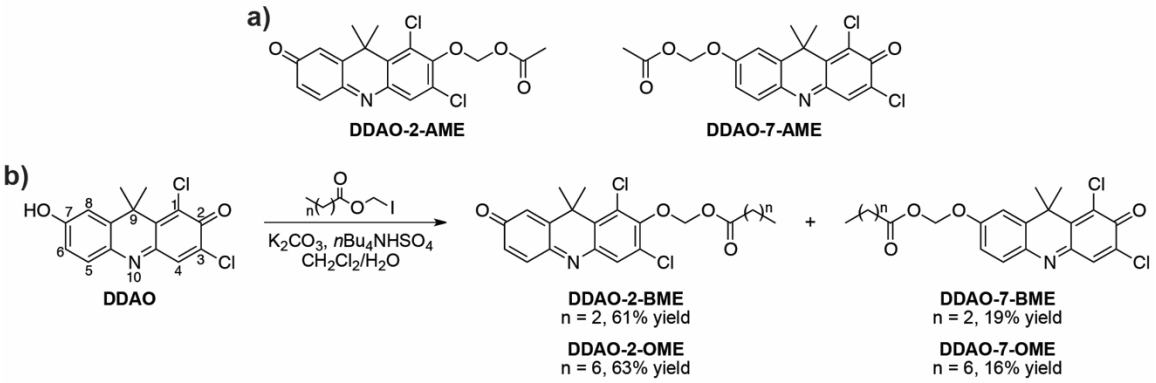

Scheme 3.1. The structures of DDAO-derived fluorogenic esterase probes.

(a) Previously reported DDAO-AME probes.[116] (b) Synthesis of longer-chain DDAO-acyloxymethyl ethers and illustration of the DDAO numbering scheme.

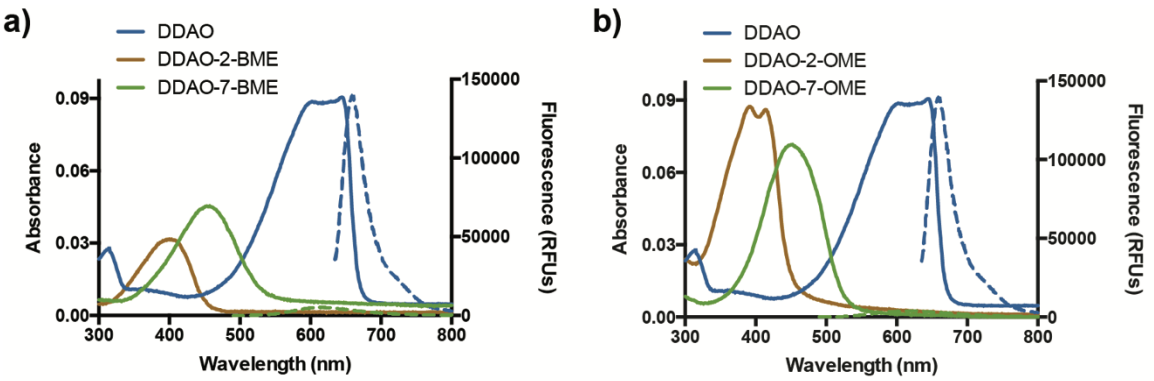

Figure 3.1. The absorbance and emission spectra of DDAO-derived fluorogenic probes. Solid lines indicate absorbance spectra for 5 μM compound and dashed lines indicate fluorescence emission spectra for 2.5 μM compound in HEPES (pH 7.3). (a) Spectra of DDAO (λ_{ex} = 602 nm), DDAO-2-BME (non-fluorescent), and DDAO-7-BME (λ_{ex} = 453 nm). (b) Spectra of DDAO (λ_{ex} = 602 nm), DDAO-2-OME (non-fluorescent), and DDAO-7-OME (λ_{ex} = 451 nm).

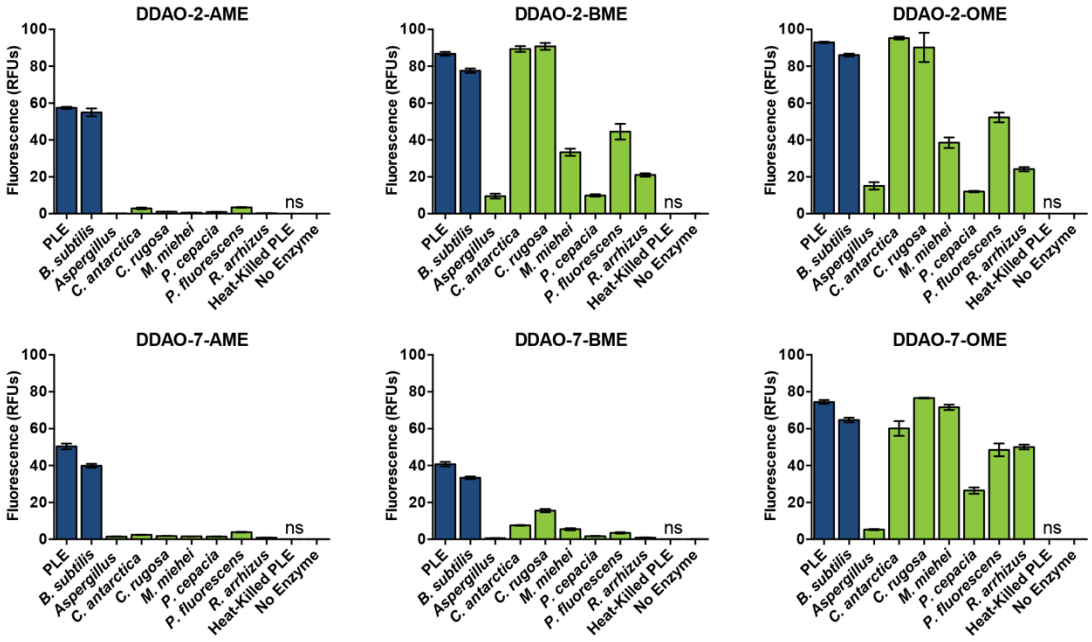

Figure 3.2. DDAO-based fluorogenic probes are versatile esterase and lipase substrates. Fluorescence generation by esterases (from PLE and *B. subtilis*, blue bars) and lipases (green bars) is given in relative fluorescence units (RFUs). All unlabeled responses are statistically significant ($P < 0.01$), and those labeled "ns" were not significant compared to the enzyme-free control. Error bars represent one standard deviation ($n = 4$).

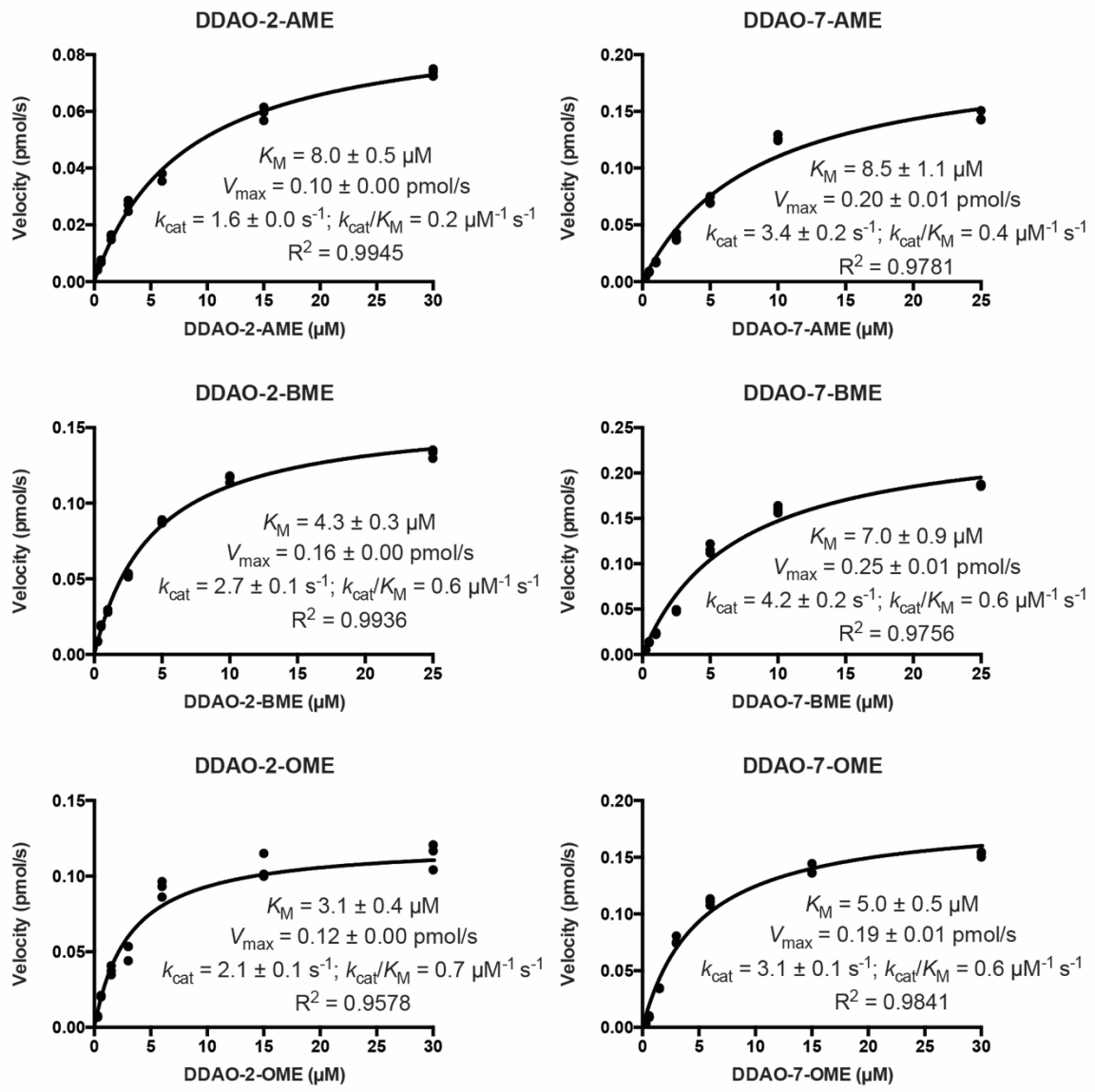

Figure 3.3. Kinetic evaluation of DDAO-derived fluorogenic probes with 500 ng/mL PLE. Reactions were performed in triplicate at 37 °C in 10 mM HEPES (pH 7.3) + 20% DMSO. Probe hydrolysis was detected by measuring DDAO fluorescence (λ_{ex} 635 nm, λ_{em} 670 nm).

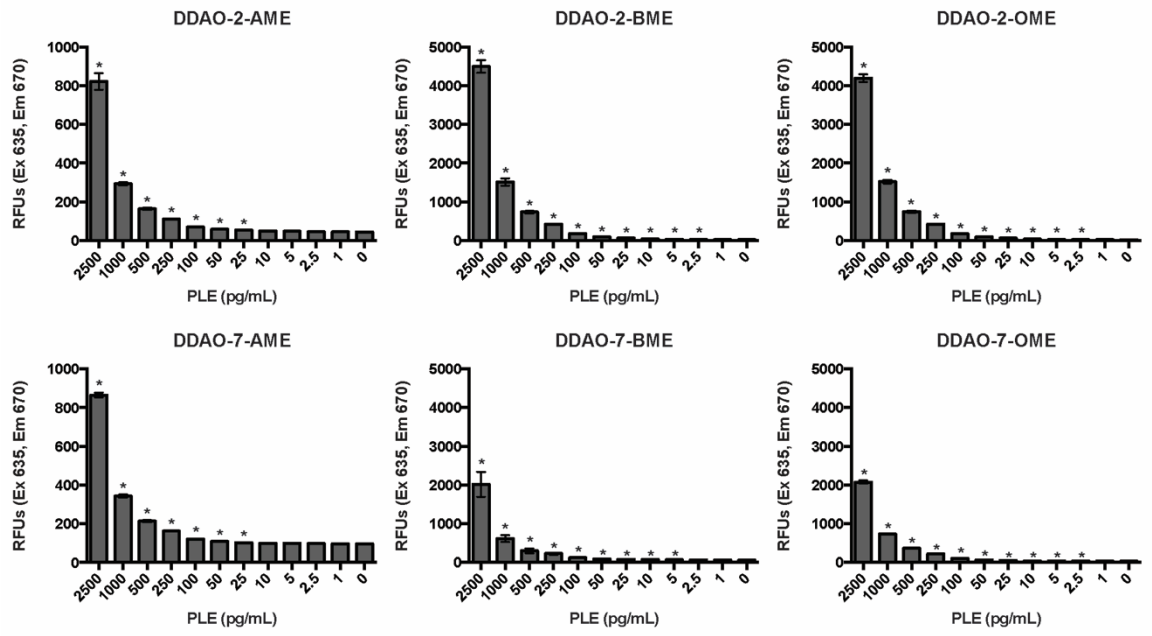

Figure 3.4. Threshold of PLE detection.

PLE was diluted in 10 mM HEPES (pH 7.3) + 20% acetonitrile and incubated with 25 μM probe for 10 min at 37 °C. Probe hydrolysis was detected by measuring DDAO fluorescence (λ_{ex} 635 nm, λ_{em} 670 nm), and the detection limit was determined as the lowest statistically significant signal compared to the enzyme-free control ($^*P < 0.01$). Error bars represent one standard deviation ($n = 4$).

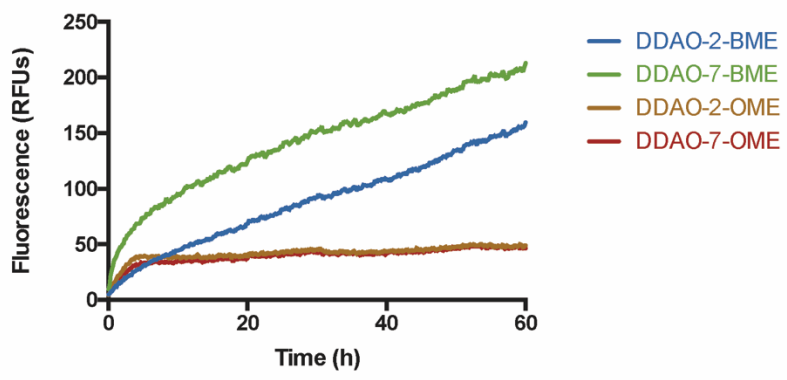

Figure 3.5. The stability of DDAO-derived acyloxymethyl ether probes in PBS (pH 7.4). Probes (1 μM) were incubated at 37 °C, and DDAO fluorescence (λ_{ex} 635 nm, λ_{em} 670 nm) was measured every 10 min for 60 h (n = 6). Graphs denote the average fluorescence value of all six replicates.

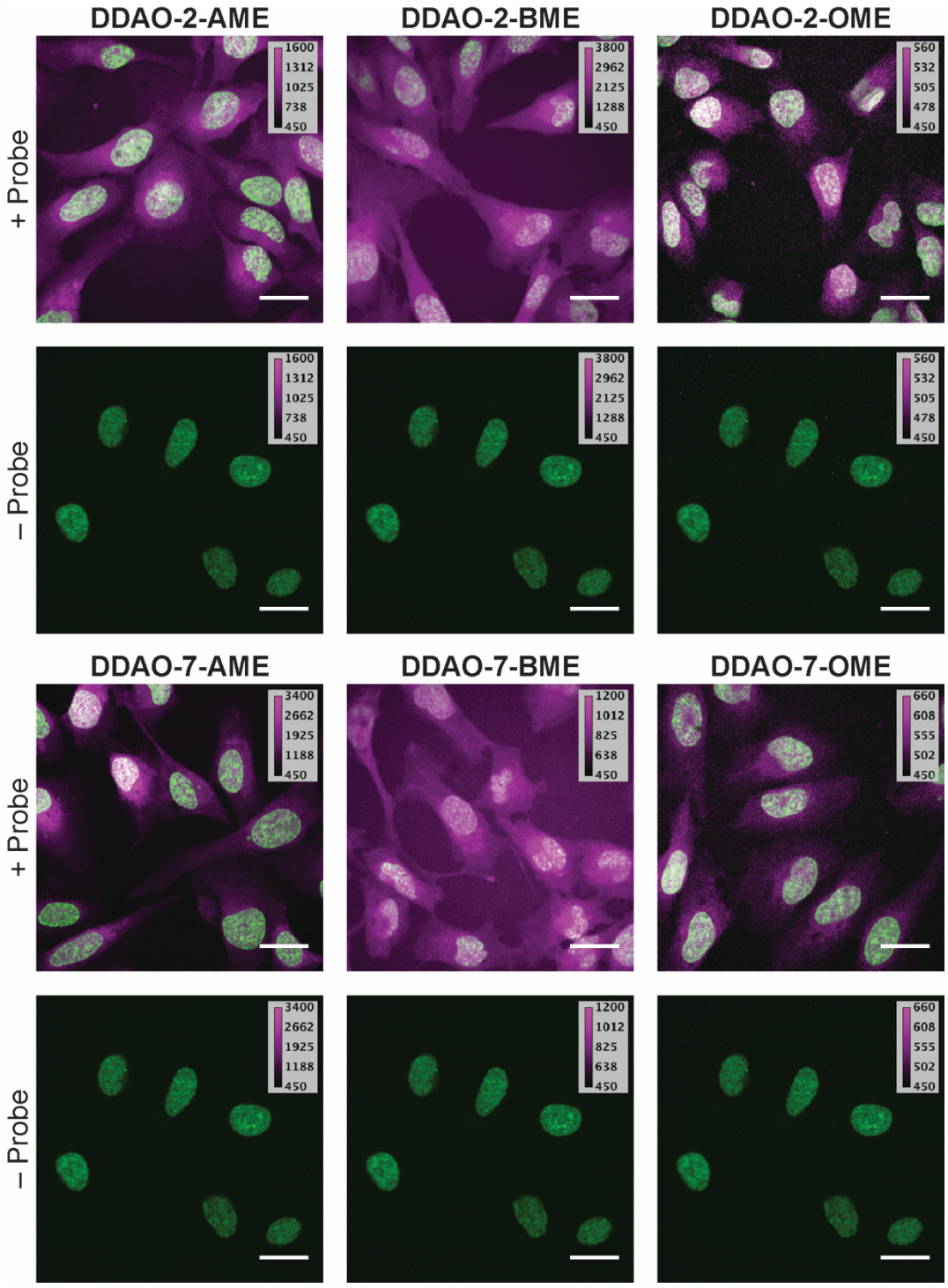

Figure 3.6. Live cell imaging of DDAO fluorescence (magenta) using DDAO-derived fluorogenic esterase probes.

Live U2OS cells were counterstained with Hoechst 33342 (green). The maximum DDAO display settings were optimized for each probe, with the minimum and maximum pixel values indicated. A DMSO control (– Probe) is provided to show background fluorescence in the far-red imaging channel, and has been adjusted to match each probe's image settings. Scale bars denote 20 μm.

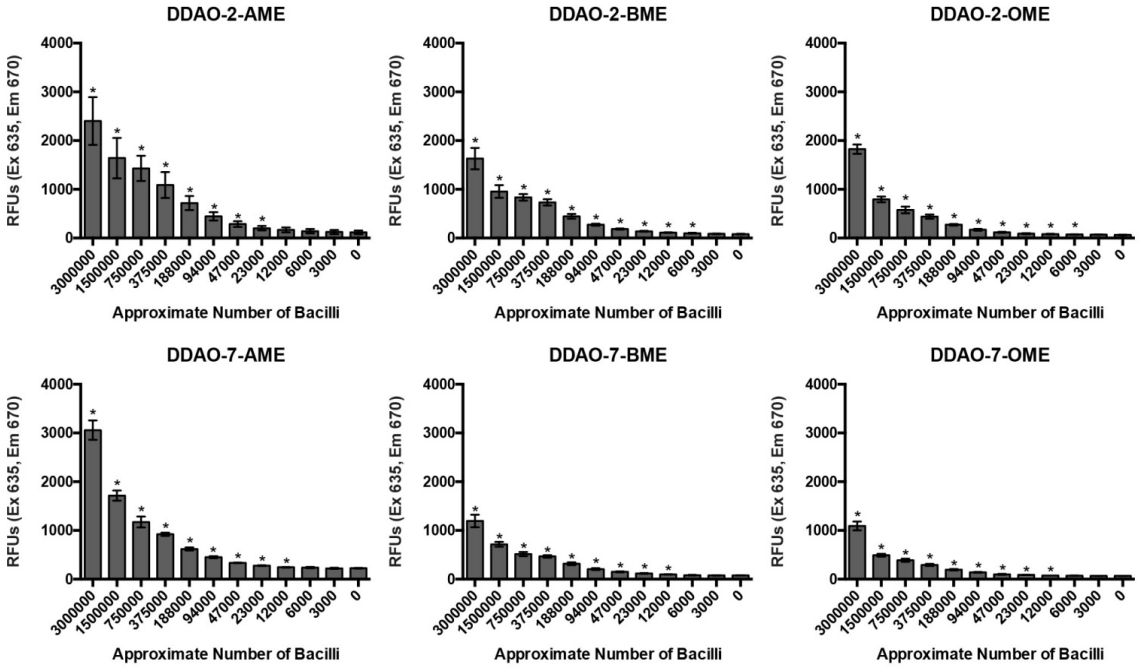

Figure 3.7. Live *Mtb* mc^{2}6020 hydrolyzes fluorogenic probes.

Bacilli were incubated with 10 μM probe for 30 min at 37 °C in PBS (pH 7.4) + 0.05% Tween 80. Cells were killed with phosphate buffered formalin before measuring DDAO formation (λ_{ex} 635 nm, λ_{em} 670 nm). Samples denoted with an asterisk (*) produced statistically significant fluorescence compared to the cell-free control ($P < 0.05$). Error bars represent one standard deviation ($n = 4$).

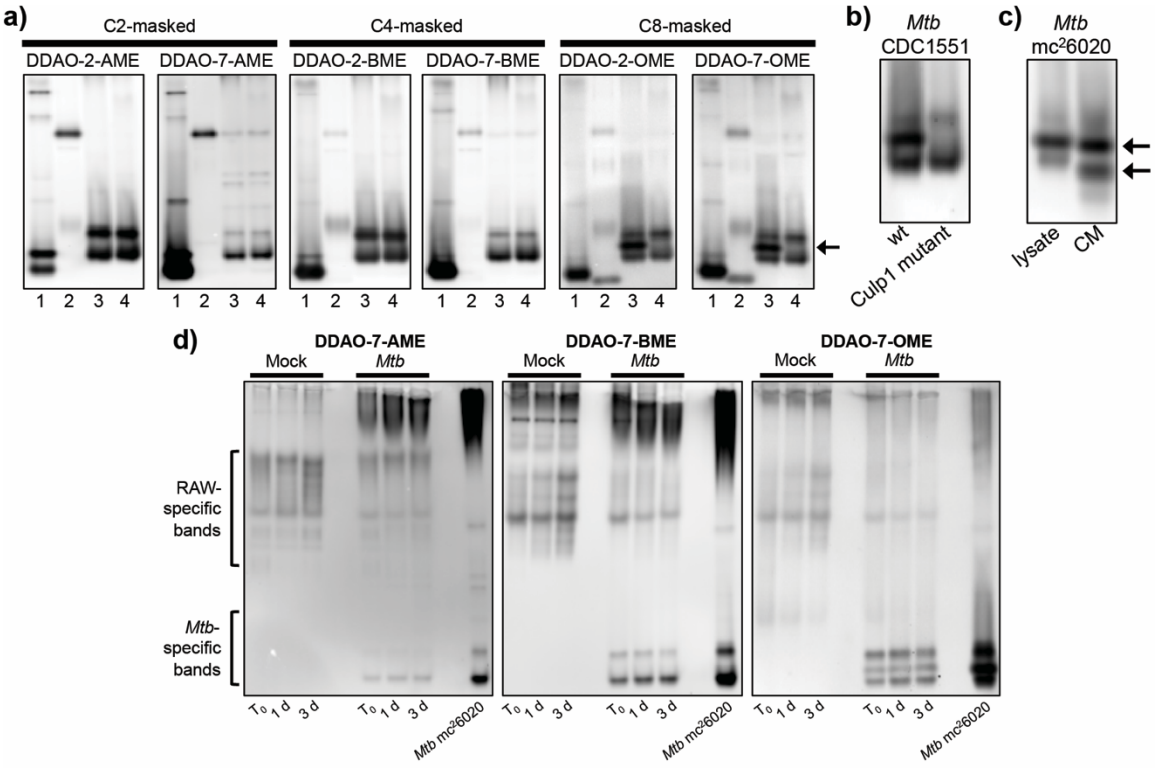

Figure 3.8. DDAO-derived fluorogenic probes reveal mycobacterial esterases and lipases in native PAGE-resolved lysates.

(a) Lysates from (1) *M. smegmatis*, (2) *M. marinum*, (3) *Mtb* mc^{2}6020, and (4) *M. bovis* (BCG) were examined. The arrow highlights an *Mtb*-specific band revealed by the OME probes. (b) Lysates from *Mtb* CDC1551 wild type (wt) and a Culp1 transposon mutant confirmed that the *Mtb*-specific band corresponds to Culp1 activity. (c) Whole-cell lysate and conditioned medium (CM) from *Mtb* mc^{2}6020 both displayed Culp1 activity. Arrows indicate bands in the CM identified as Culp1 by mass spectrometry-based proteomics. (d) *Mtb*-infected RAW macrophages were collected and lysed immediately after the 4 h infection (T_0), 1 d post-infection, or 3 d post-infection. Mock-infected macrophage lysates and *Mtb* mc^{2}6020 lysates were analyzed for comparison.

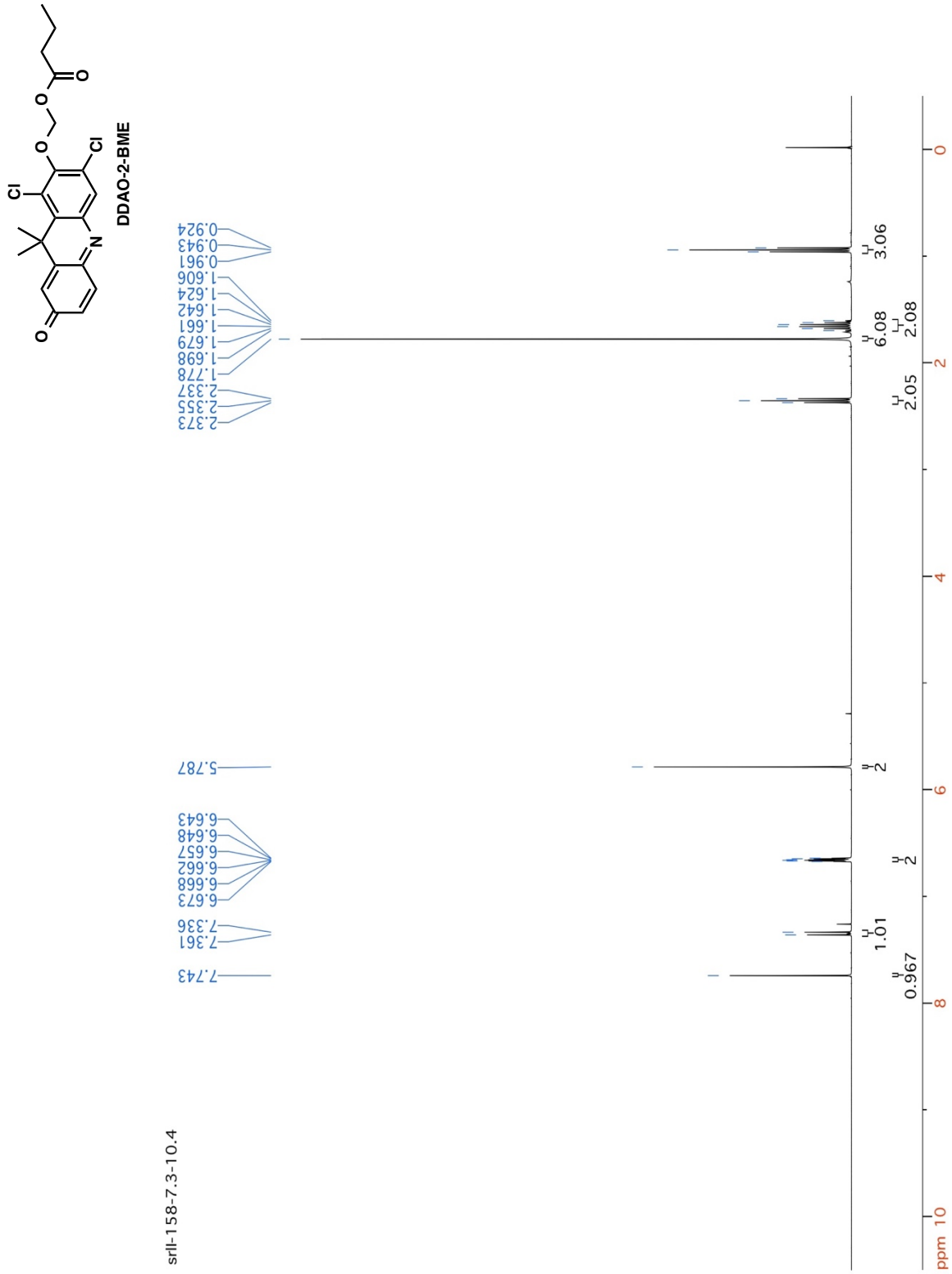

Figure 3.9. ^{1}H-NMR spectrum of DDAO-2-BME (400 MHz; $CDCl_3$).

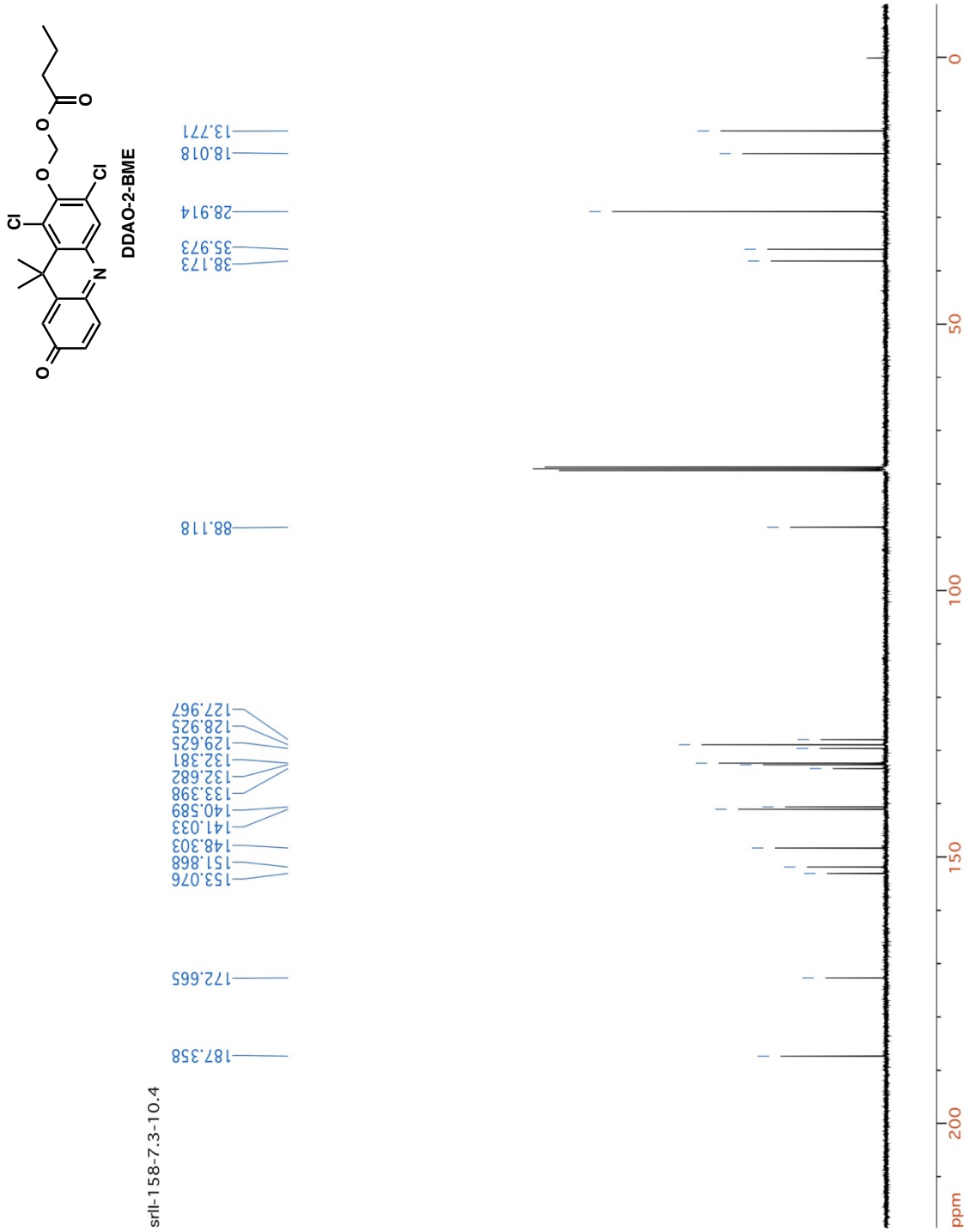

Figure 3.10. ^{13}C-NMR spectrum of DDAO-2-BME (101 MHz; $CDCl_3$).

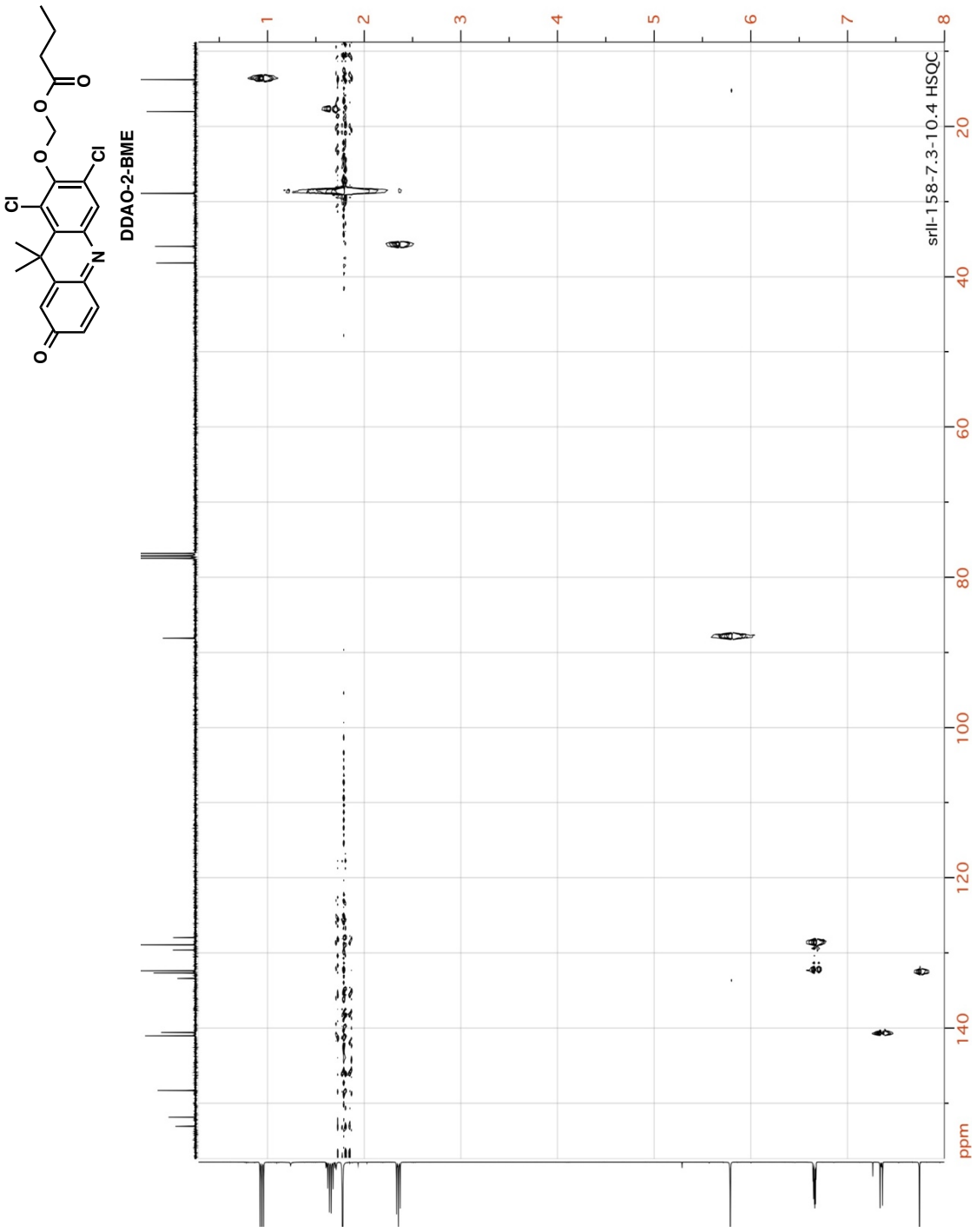

Figure 3.11. HSQC spectrum of DDAO-2-BME ($CDCl_3$).

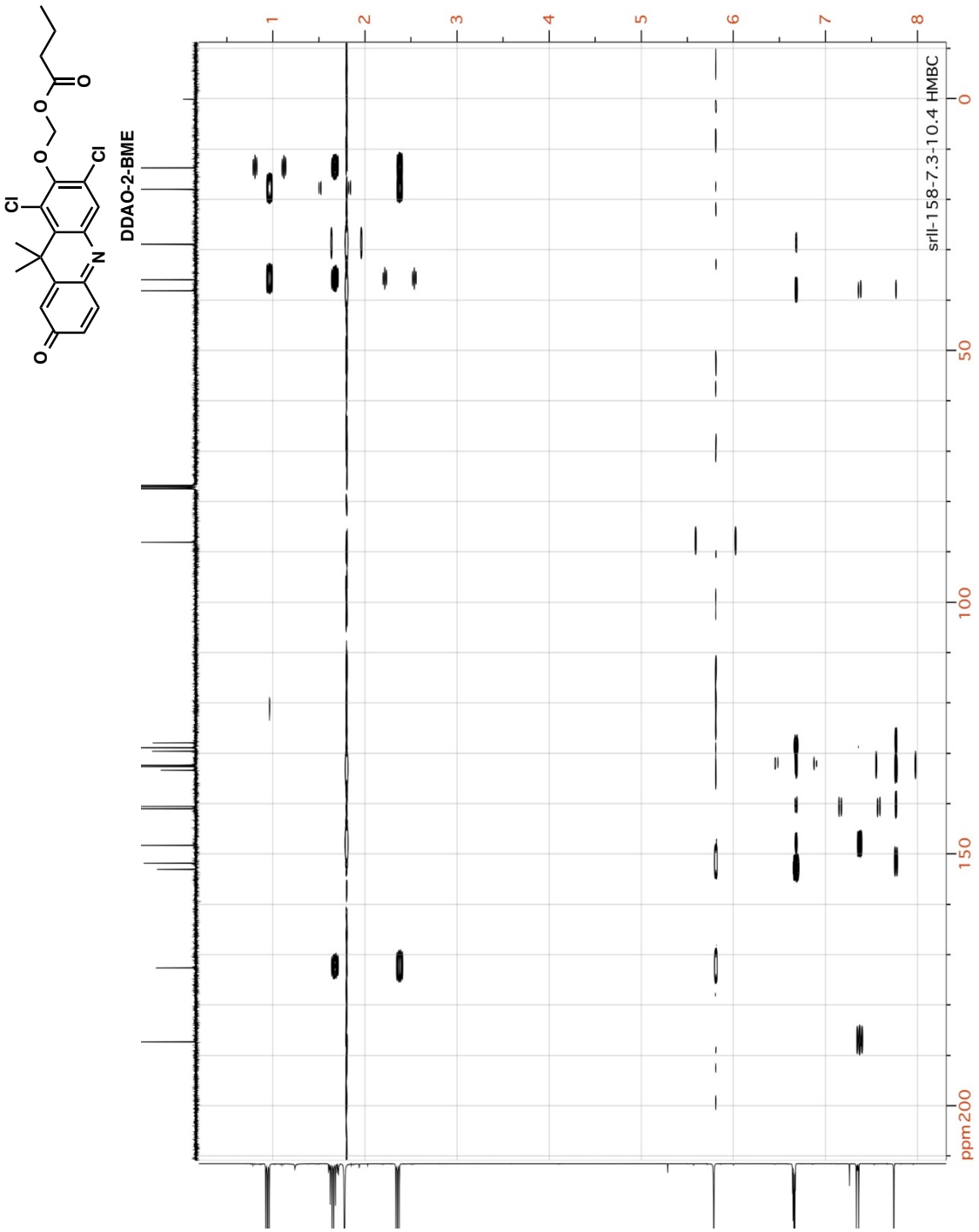

Figure 3.12. HMBC spectrum of DDAO-2-BME ($CDCl_3$).

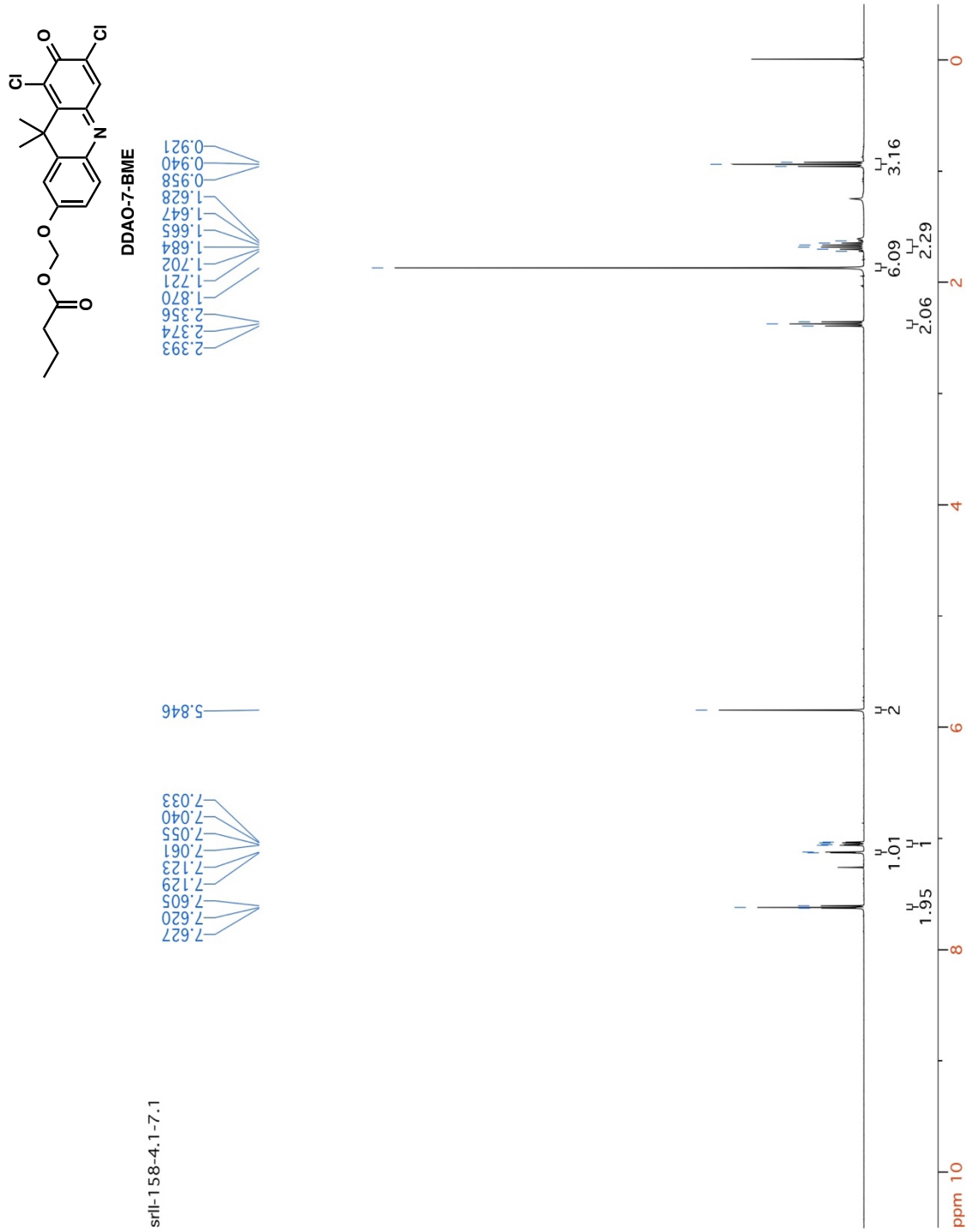

Figure 3.13. ^{1}H-NMR spectrum of DDAO-7-BME (400 MHz; $CDCl_3$).

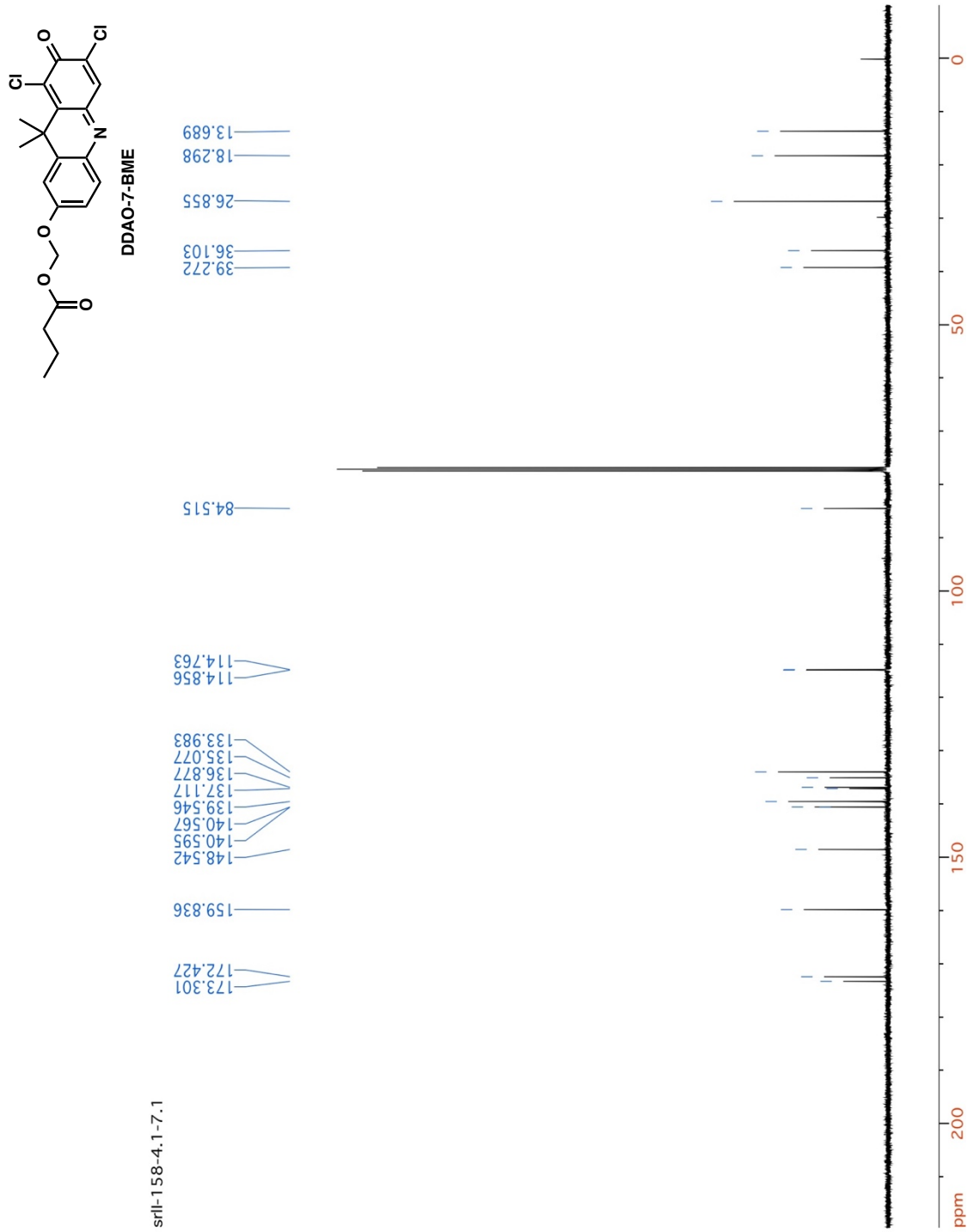

Figure 3.14. ^{13}C-NMR spectrum of DDAO-7-BME (101 MHz; $CDCl_3$).

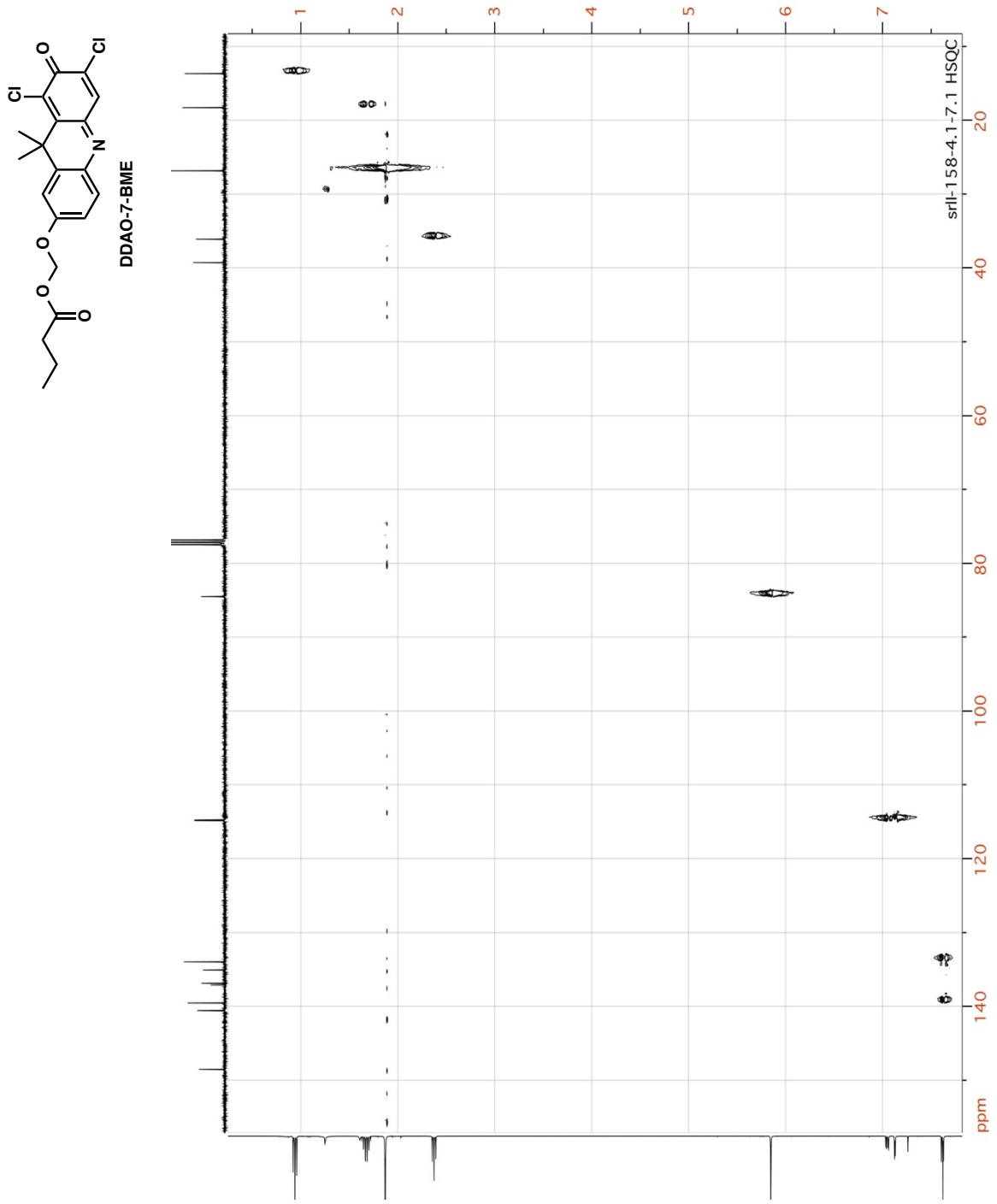

Figure 3.15. HSQC spectrum of DDAO-7-BME ($CDCl_3$).

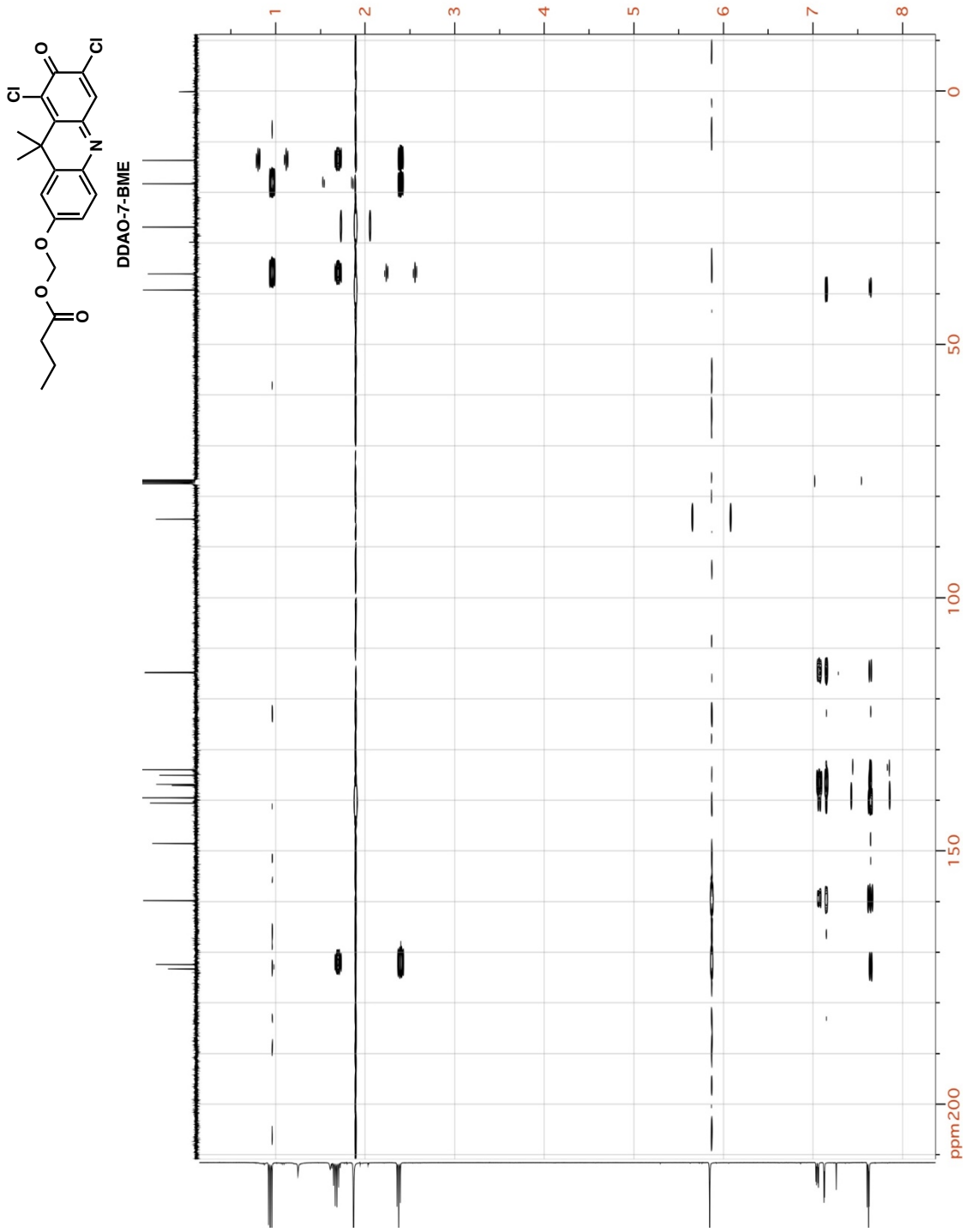

Figure 3.16. HMBC spectrum of DDAO-7-BME ($CDCl_3$).

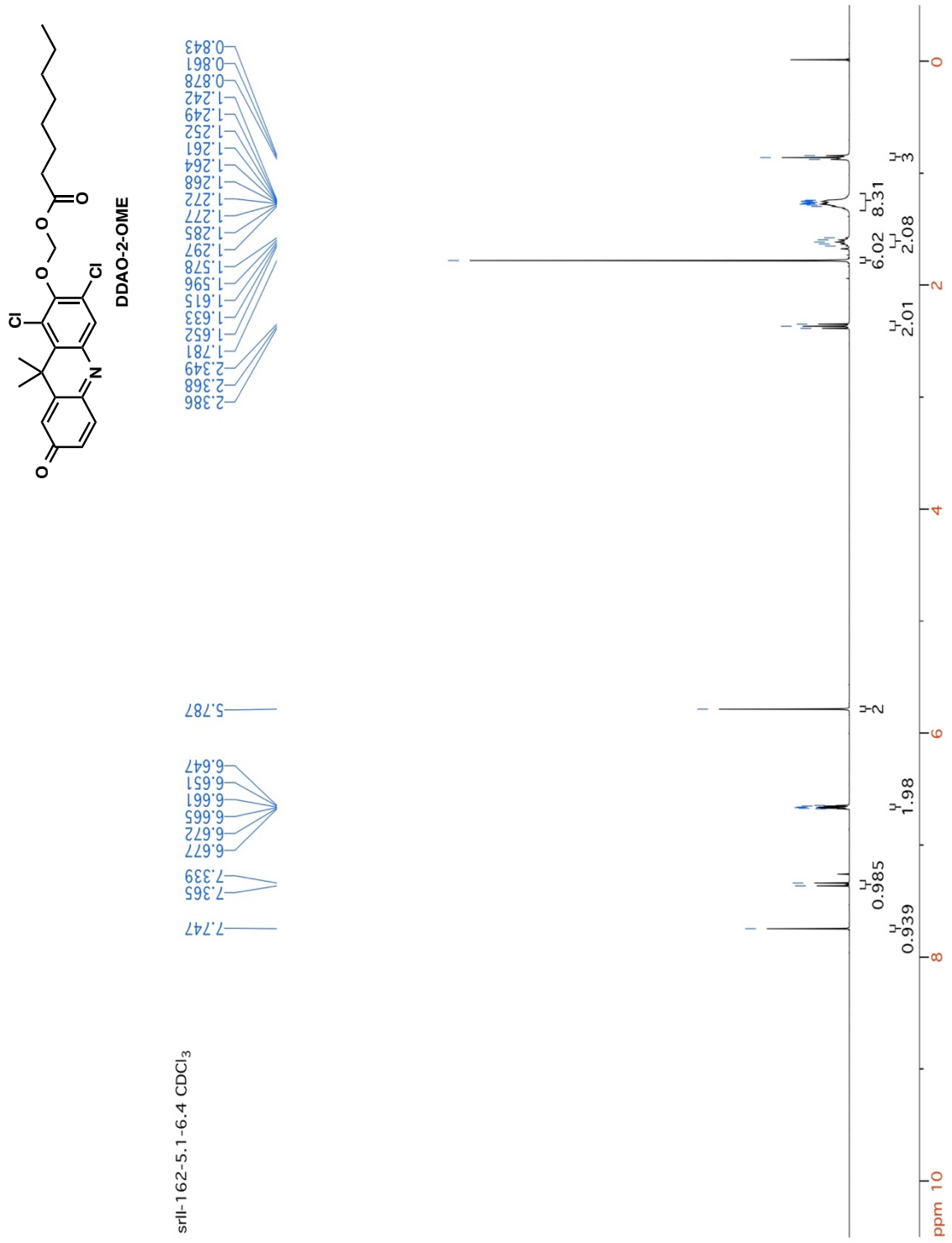

Figure 3.17. ^{1}H-NMR spectrum of DDAO-2-OME (400 MHz; $CDCl_3$).

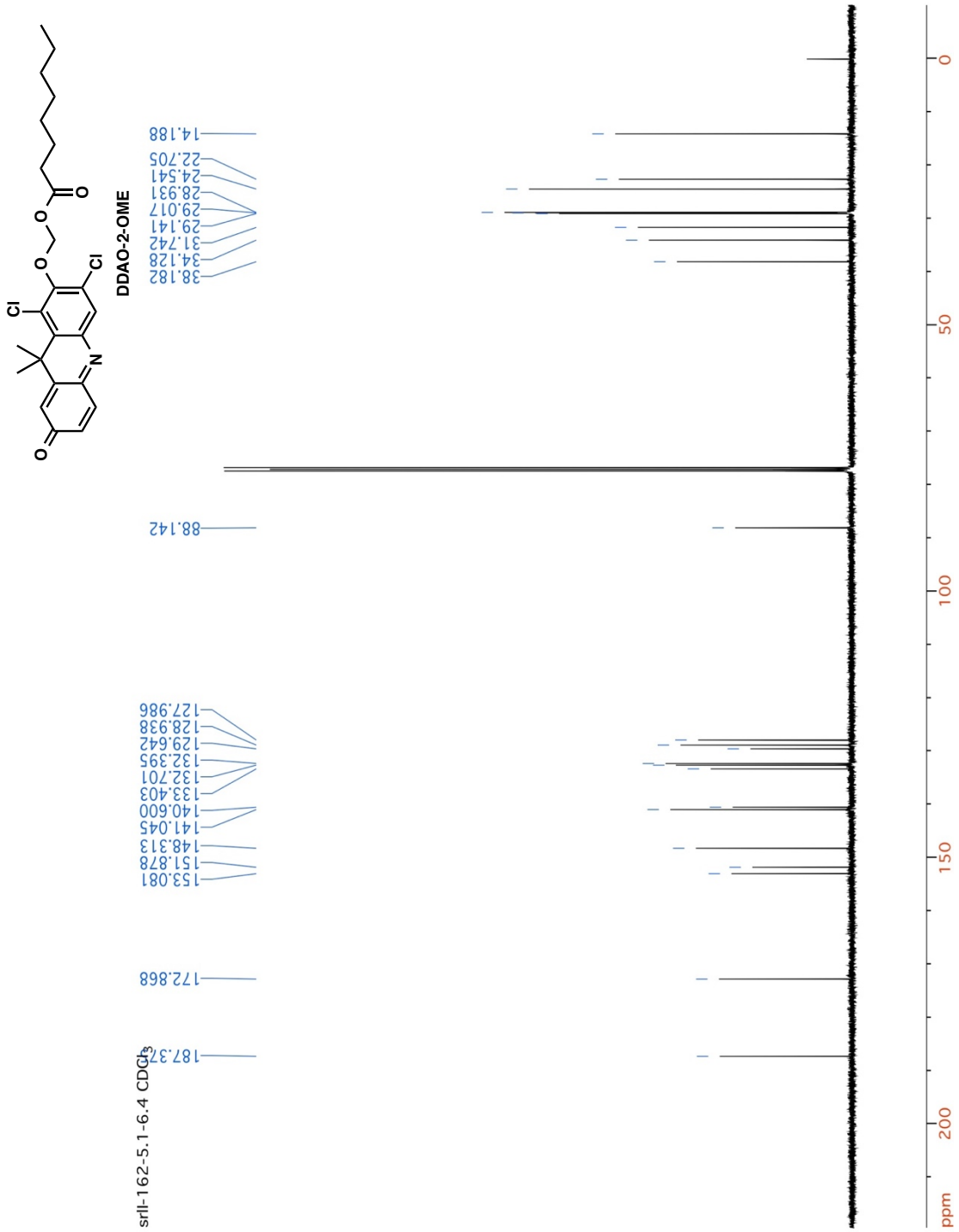

Figure 3.18. ^{13}C-NMR spectrum of DDAO-2-OME (101 MHz; $CDCl_3$).

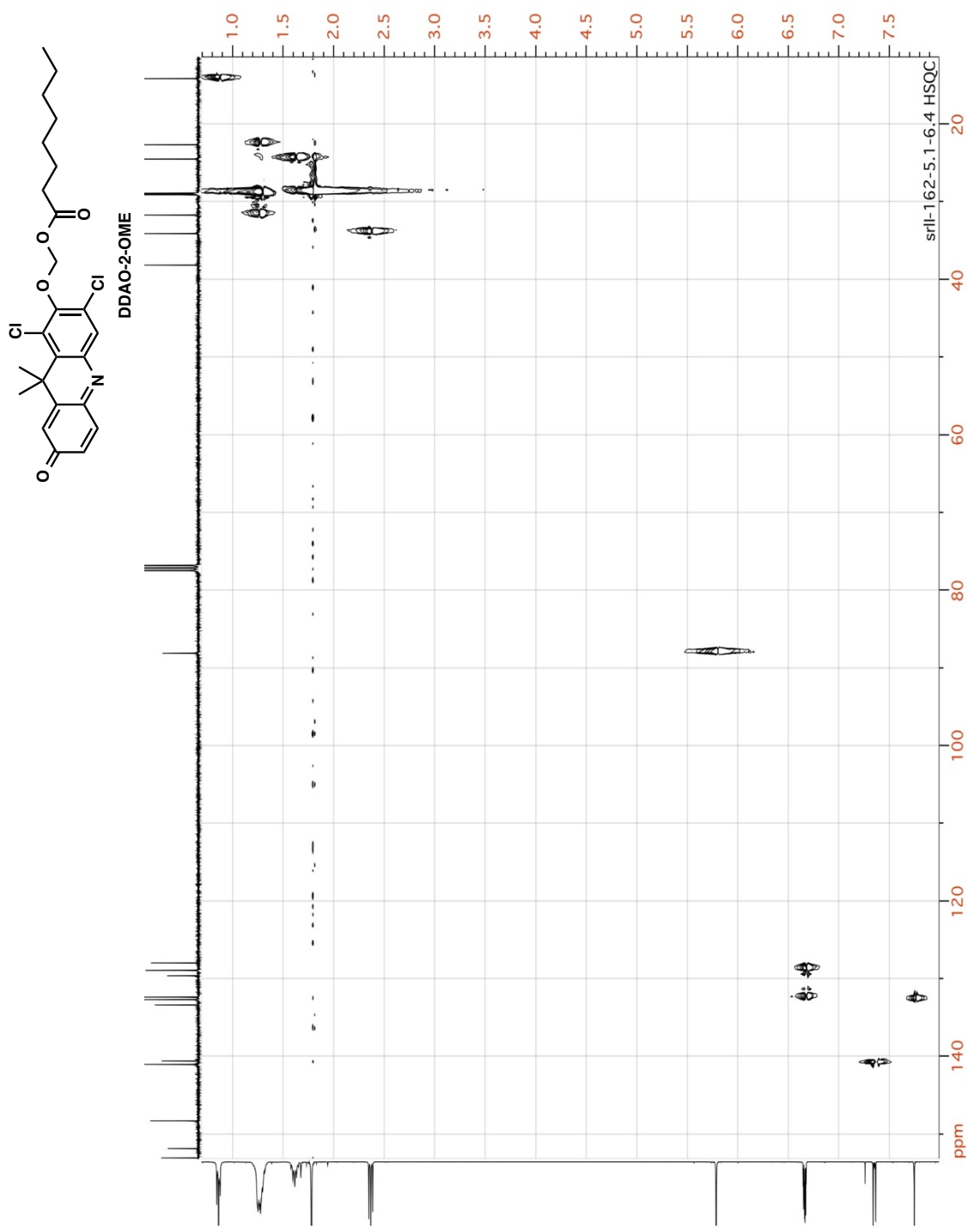

Figure 3.19. HSQC spectrum of DDAO-2-OME ($CDCl_3$).

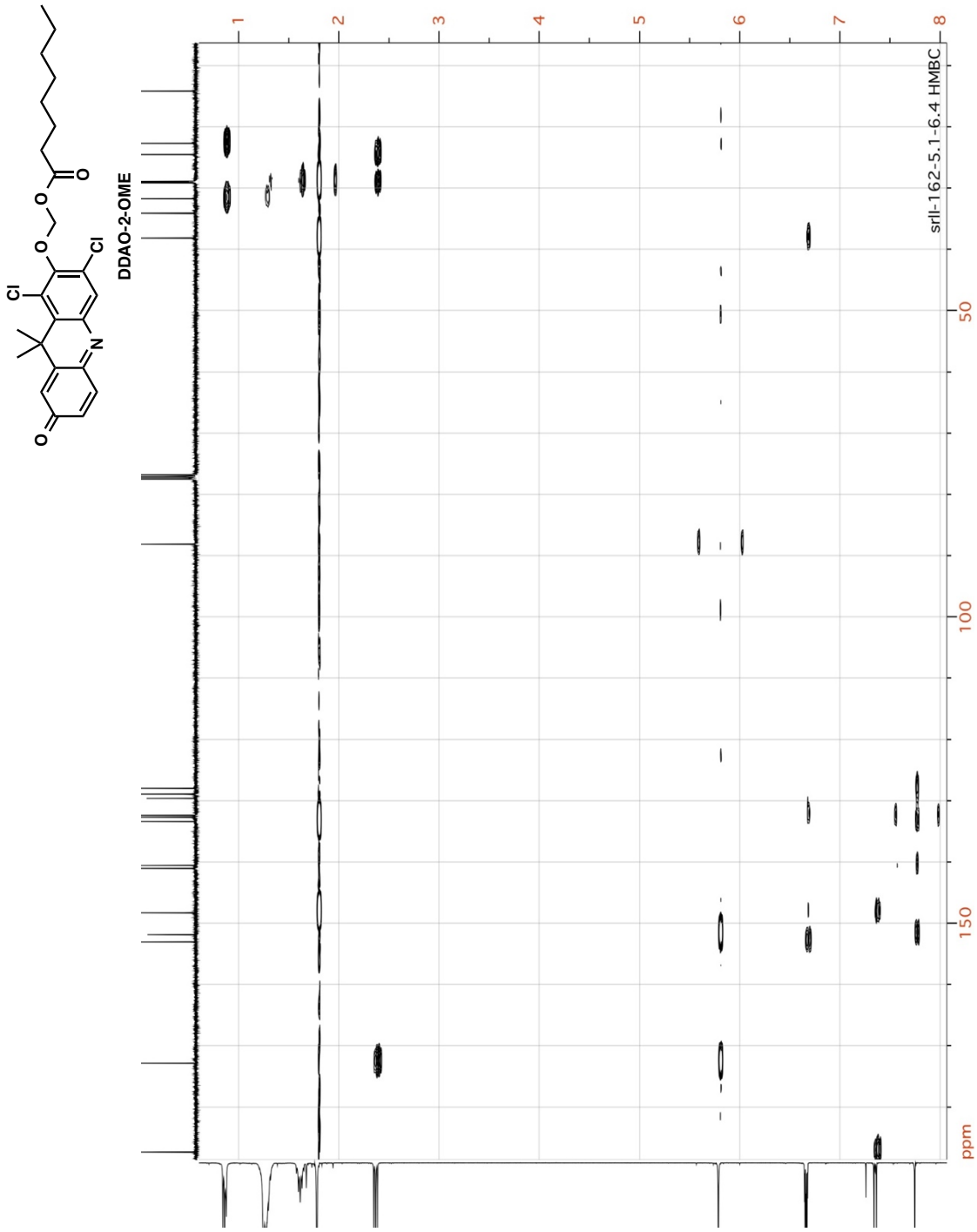

Figure 3.20. HMBC spectrum of DDAO-2-OME ($CDCl_3$).

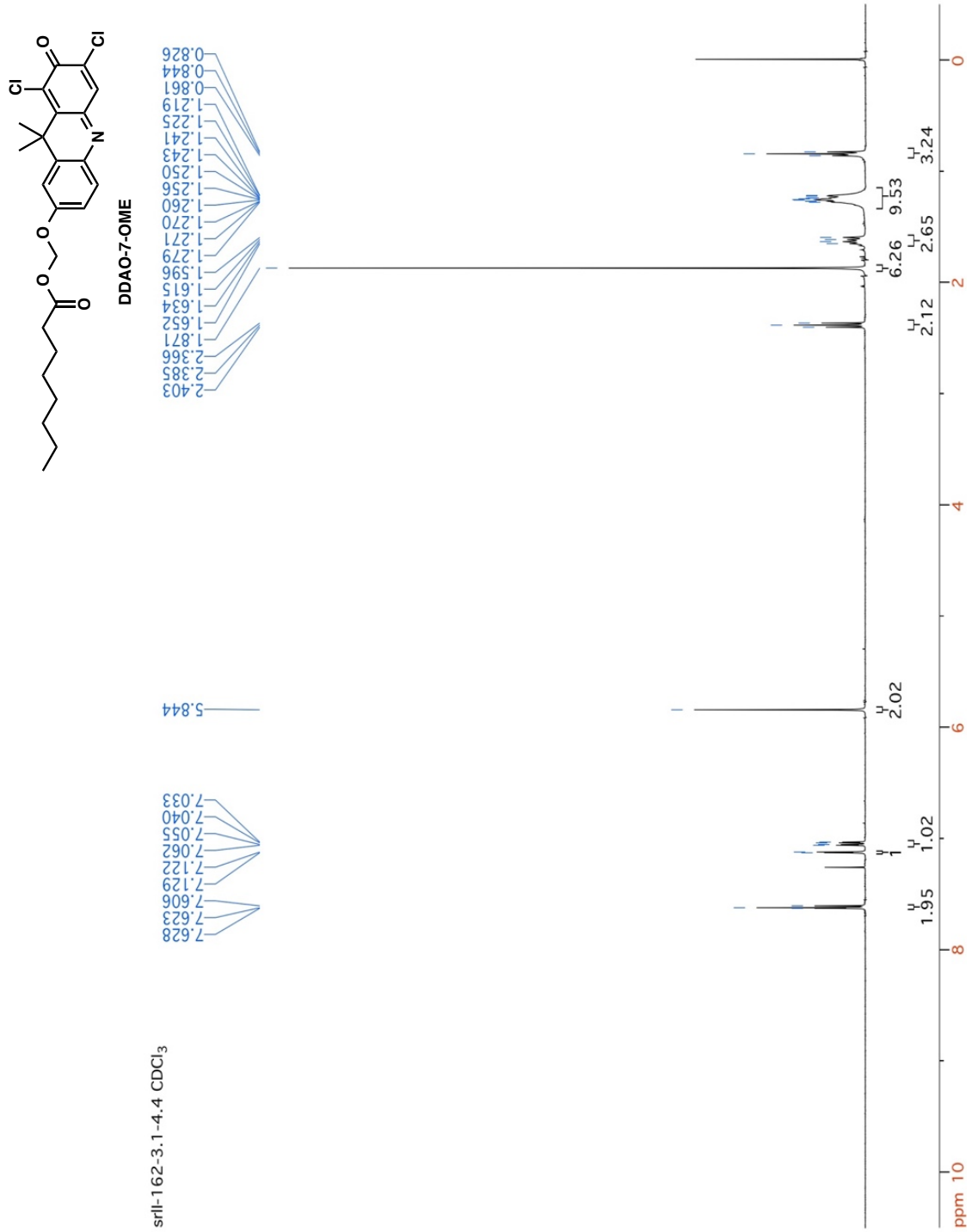

Figure 3.21. ^{1}H-NMR spectrum of DDAO-7-OME (400 MHz; $CDCl_3$).

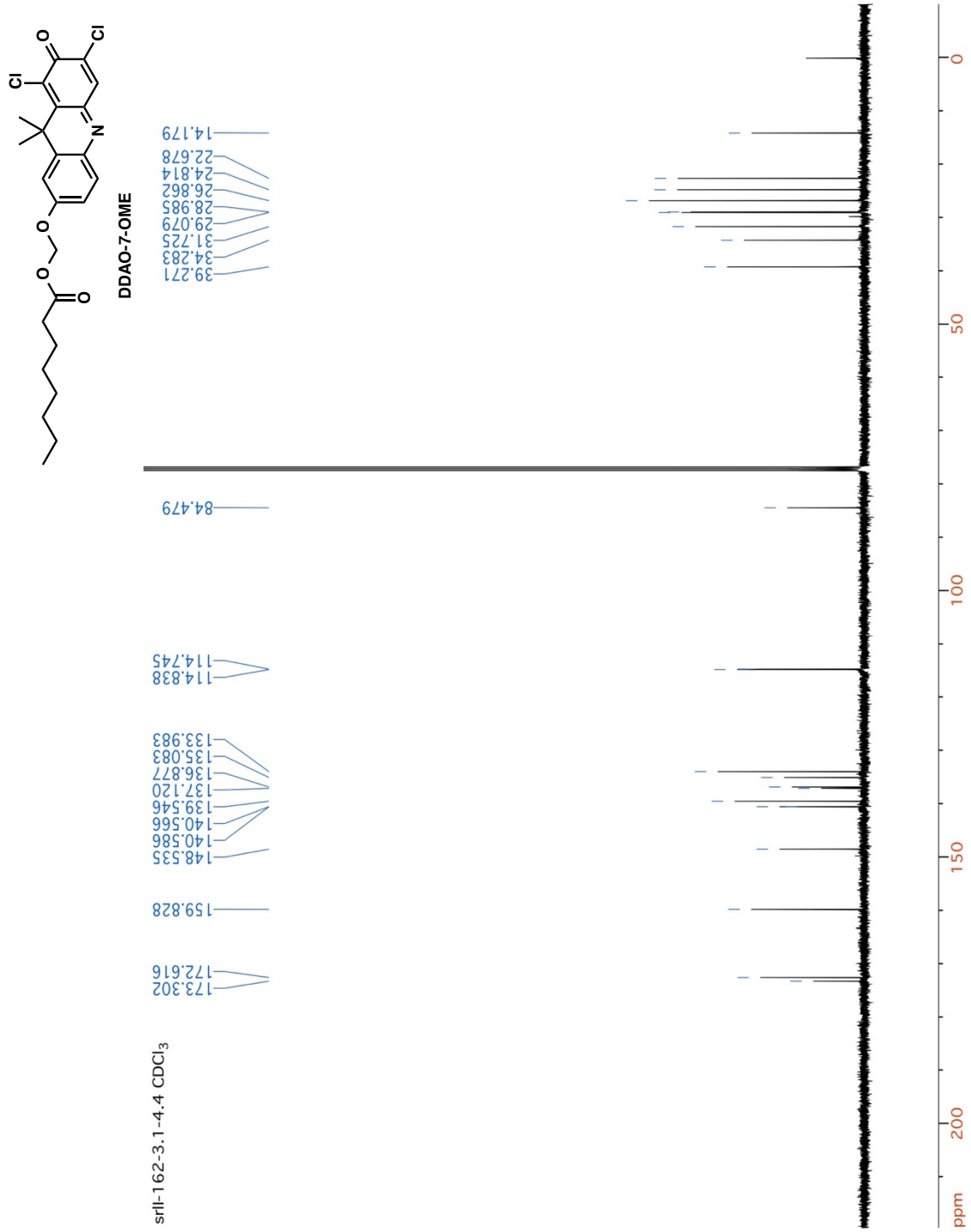

Figure 3.22. ^{13}C-NMR spectrum of DDAO-7-OME (101 MHz; $CDCl_3$).

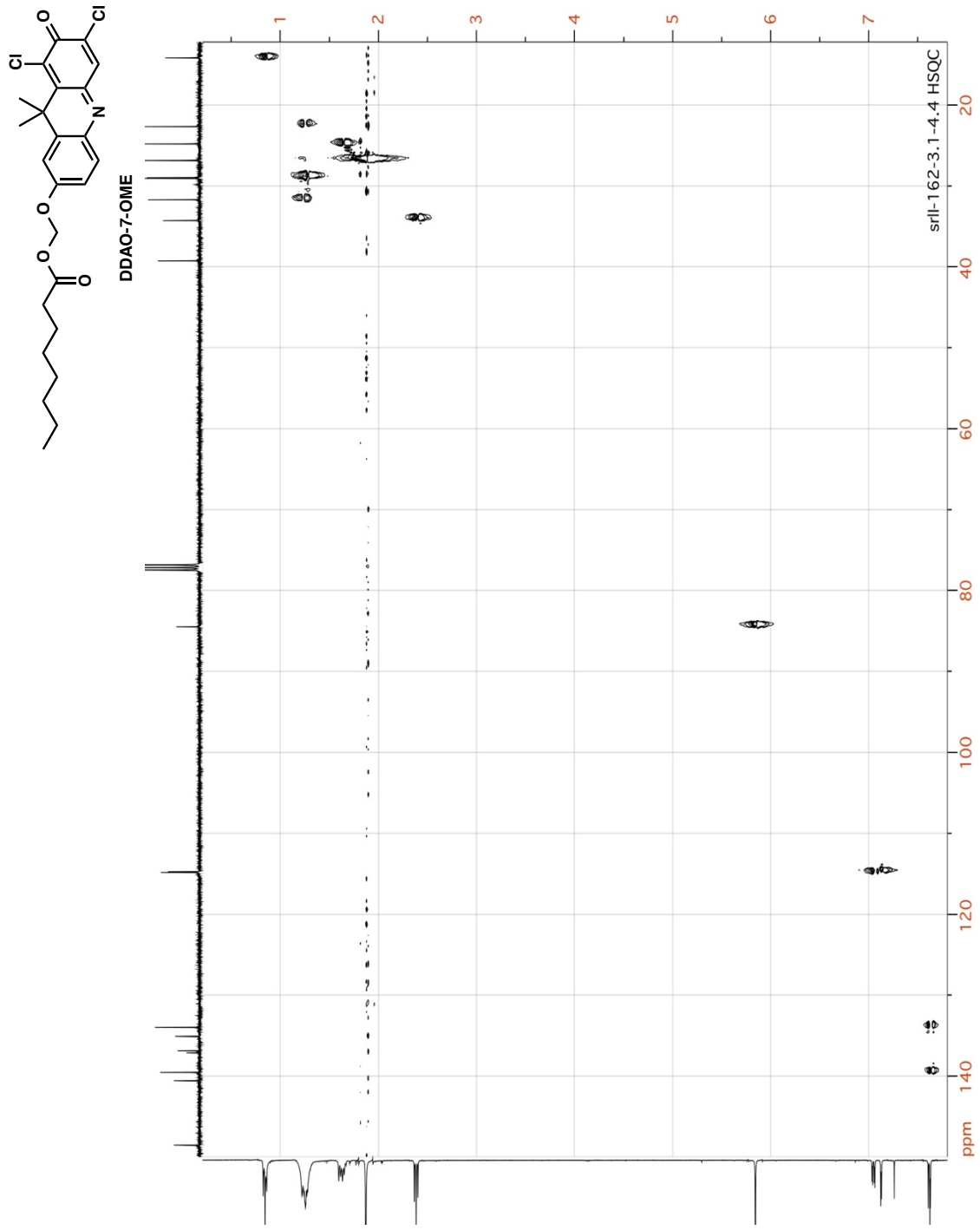

Figure 3.23. HSQC spectrum of DDAO-7-OME ($CDCl_3$).

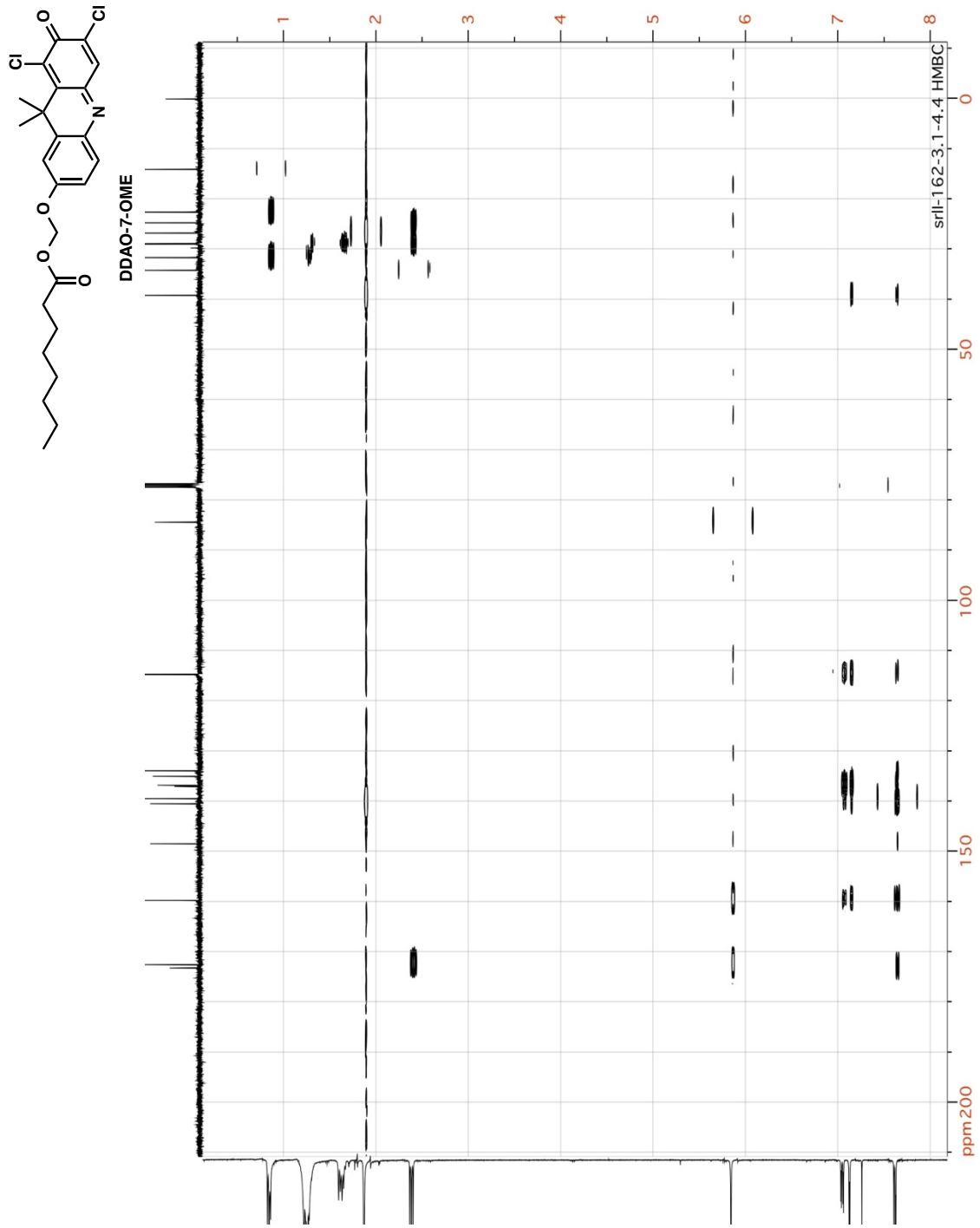

Figure 3.24. HMBC spectrum of DDAO-7-OME ($CDCl_3$).

Chapter 4: Small Molecule Probes Reveal Esterases with Persistent Activity in Dormant and Reactivating *Mycobacterium tuberculosis*

Katie R. Tallman, Samantha R. Levine, and Kimberly E. Beatty

This chapter details work from a manuscript in preparation. The project was a collaboration with Dr. Samantha Levine, who helped grow mycobacterial cultures for the activity-based protein profiling experiments and participated in the resulting data analysis.

Abstract

Mycobacterium tuberculosis (*Mtb*) is the deadliest bacterial pathogen in the world. An estimated one-third of humans harbor *Mtb* in a dormant state. These asymptomatic, latent infections impede tuberculosis eradication due to the long-term potential for reactivation. Dormant *Mtb* has reduced enzymatic activity, but hydrolases that remain active facilitate pathogen survival. We targeted *Mtb* esterases, a diverse set of enzymes in the serine hydrolase family, and studied their activities using both activity-based probes (ABPs) and fluorogenic esterase substrates. These small molecule probes revealed functional esterases in active, dormant, and reactivating cultures. We identified seven esterases that remained

active in dormant *Mtb* using ABPs, including Culp1 (Rv1984c), LipL (Rv1497), LipM (Rv2284), and LipN (Rv2970c). Three of the seven, CaeA (Rv2224c), Rv0183, and Rv1683, were catalytically active in all three culture conditions. Fluorogenic probes confirmed Culp1 activity and also revealed LipH (Rv1399c) and Rv3036c activity in dormant and active cultures. Esterases with persistent activity are potential diagnostic biomarkers or therapeutic targets for *Mtb*-infected individuals with latent or active tuberculosis.

Introduction

Mycobacterium tuberculosis (*Mtb*) is the causative agent of tuberculosis (TB), the world's most lethal single-agent infectious disease.[10] An estimated 2 billion people harbor latent TB, an asymptomatic form of the disease. In latent TB, *Mtb* slows its metabolism and converts to a dormant, non-replicating state.[16,17] Dormant *Mtb* is phenotypically drug-tolerant, which contributes to the prolonged, multi-drug treatment required to cure TB.[6] Furthermore, common TB screening methods do not distinguish between latent and active infections.[16,17] Approximately 5–15% of latently-infected individuals will transition to active TB.[10]

To investigate latent TB biology *in vitro*, researchers subject bacilli to stresses encountered in the human host, including hypoxia, nutrient deprivation, reactive nitrogen species, and acidic pH.[20] *Mtb* adapts to these stresses by converting to a non-replicating state that mimics latent infection. Dormant *Mtb*

has decreased metabolism,[195] phenotypic drug-resistance,[20,27] and a substantially altered transcriptome[24,63,195] and proteome.[74,75]

Survival during dormancy and reactivation relies on enzymes that process fatty acids as an energy source.[27,37,38,196] These enzymes—including esterases and the lipid-preferring lipase subclass—are ideal drug targets due to their roles in *Mtb* persistence.[70,71,108,167] Esterase regulation in dormancy has been inferred primarily from transcriptomic [24,37,63] and proteomic[74,75] data. However, those studies do not reveal whether or not an esterase is catalytically active. The activity of serine hydrolases, including esterases, can be post-translationally regulated.[123,197] Three *Mtb* esterases—LipE (Rv3775), LipN (Rv2970c), and Culp2 (Rv2301)—contain acetylated lysines, which could influence their activity.[198] LipI (Rv1400c) and LipN can be phosphorylated at their catalytic serine, which could be a mechanism for regulating catalytic activity.[199] Overall, it is unclear which of the approximately 40 *Mtb* esterases are active in dormant and reactivating *Mtb*.

Functional enzymes can be detected and identified in *Mtb* using activity-based probes (ABPs), which are irreversible, active-site targeted small molecules (Figure 4.1a).[124,142] Thus far, two studies have identified mycobacterial esterases through activity-based protein profiling (ABPP). Wenk and coworkers used an ABP to identify the targets of tetrahydrolipstatin (THL), a lipase and fatty acid synthase inhibitor with anti-*Mtb* activity.[200] They found 14 THL targets in normoxic (replicating) and hypoxic (dormant) cultures of *M. bovis* (BCG), a close

genetic relative of *Mtb*. Interestingly, they did not identify two validated *Mtb* targets of THL: Culp6 (Rv3802c)[102] or LipY (Rv3097c).[60]

In 2016, Grundner *et al.* used a serine-reactive fluorophosphonate (FP) ABP to identify serine hydrolases in dormant and replicating *Mtb* cultures.[123] Their analysis identified 78 proteins with serine hydrolase activity. They also demonstrated that *Mtb* serine hydrolase abundance and activity are poorly correlated. Unlike Wenk *et al*., they found Culp6 in both normoxic and hypoxic cultures. Similar to the prior study, they did not find LipY, a lipase that is transcriptionally upregulated in dormant *Mtb*.[37,63]

The *Mtb* esterases and lipases are members of a diverse group of serine hydrolases that cannot be identified using a single small molecule probe. With FP probes, even the linker can influence probe reactivity.[144] As a complement to ABPs, we previously developed fluorogenic probes for detecting *Mtb* hydrolases in a native polyacrylamide gel electrophoresis (PAGE) assay.[163,165,166,184] Unlike the stoichiometric (1:1) labeling of ABPs, fluorogenic probes are hydrolyzed to produce an amplifiable fluorescent signal that correlates with enzyme activity (Figure 4.1b).[142] We varied both the fluorescent reporter[163] and the masking group[184] to increase the diversity of the esterases we could detect. Most recently, we described a fluorogenic lipase substrate, DDAO-OME, that revealed Culp1 (Rv1984c) activity in *Mtb*—an esterase missing from the two prior ABPP studies.

In the present study, we used chemically diverse ABPs and fluorogenic probes to obtain a more comprehensive list of *Mtb* esterases that retain activity under replicating and non-replicating conditions. For the first time, we identified esterases that are functional during the early hours of reactivation from dormancy, a key pathophysiological transition. We used desthiobiotin-FP, an ABP, to identify 22 esterases in replicating, normoxic *Mtb*—the most comprehensive hit list to date. Of these esterases, seven retained activity in hypoxia, and three were active during reactivation. We used our fluorogenic probes to confirm esterase functionality and to detect esterases that were missed by ABPs (i.e., Rv3036c). We propose that esterases with persistent activity in dormancy and reactivation are valuable targets for new diagnostic assays or therapeutics.

Results and Discussion

We initiated our research using red-fluorescent TAMRA-FP (Figure 4.2) to detect serine hydrolases in replicating, normoxic cultures of *Mtb* mc^{2}6020 (an auxotrophic strain of H37Rv[33]). We observed fluorescent signal only in the ABP-treated protein gel-resolved lysates (Figure 4.3). TAMRA-FP labeling was reduced by pre-incubating the lysate with covalent serine hydrolase inhibitors, demonstrating that active enzyme is required for probe binding. Methyl arachidonyl FP (MAFP), a serine hydrolase inhibitor with an FP warhead,

blocked nearly all TAMRA-FP labeling. Diethyl-*p*-nitrophenyl phosphate (E-600, a carboxyl esterase inhibitor), phenylmethylsulfonyl fluoride (PMSF, a serine protease inhibitor), and THL each inhibited some of the serine hydrolases. No two inhibitors targeted the exact same set of enzymes, highlighting the diversity of the *Mtb* serine hydrolases.

Next, we induced *Mtb* dormancy using two different models: carbon starvation[25] and hypoxia.[23] Carbon starvation was induced by culturing *Mtb* in unsupplemented medium for 5 weeks, as described by Hung and coworkers.[25] Hypoxia was induced in standing flasks using a hypoxia chamber (1% O_2 and 5% CO_2) for 2 weeks. We allowed the hypoxic cultures of dormant *Mtb* to reactivate for 4.5 hours using two different reaeration conditions. In one, we reaerated in rich growth medium. In the other, we reaerated under carbon starvation to encourage the bacteria to utilize stored lipids (i.e., TAG).[37] We collected cells from each condition and treated the resulting lysates with TAMRA-FP (Figure 4.4). We resolved the lysates by SDS-PAGE and included recombinant, purified LipY (lane 6) as a positive control and molecular weight marker (45 kDa). TAMRA-FP labeling revealed substantial serine hydrolase activity downregulation in the dormant cultures compared with the replicating culture. Lysate from carbon-starved *Mtb* displayed a more pronounced decrease in serine hydrolase activity than the hypoxic culture. After reaeration in rich medium, some serine hydrolase activity was restored. By comparison, changes in activity were undetectable for reactivation under carbon starvation, which could

reflect a slower recovery from dormancy. Overall, the TAMRA-FP probe confirmed that serine hydrolase activities are modulated in response to environmental changes.

ABPs are powerful tools for enriching subsets of the proteome for mass spectrometry-based identification. We labeled lysates with desthiobiotin-FP to identify *Mtb* serine hydrolases active in replicating, dormant, and reactivating conditions. For these samples, we induced dormancy by hypoxia (2 weeks) and reactivated cultures by reaeration under carbon starvation (4.5 hours). We evaluated our labeling and enrichment by Western blot, probing with an anti-biotin antibody (Figure 4.5). Although we observed endogenously biotinylated proteins, as previously described,[201] there were additional biotinylated proteins in the desthiobiotin-FP-labeled samples. Biotinylated proteins were isolated by streptavidin affinity chromatography and digested with trypsin for liquid chromatography-tandem mass spectrometry (LC-MS/MS) analysis.

We identified 229 distinct proteins, including 48 proteins previously annotated as serine hydrolases (see Appendix A).[202] Positive hits were selected based on two or more distinct peptide hits per protein found in at least two of the three replicates. The identified serine hydrolases ranged in functional category annotation, including intermediary metabolism/respiration (24 proteins), lipid metabolism (11 proteins), cell wall/cell processes (7 proteins), conserved hypotheticals (4 proteins, including two putative esterases), and virulence/detoxification/adaptation (2 proteins). We identified fewer serine

hydrolases in dormancy and reactivation compared to normoxic lysates (Figure 4.6), consistent with prior studies.[123,128]

We narrowed our focus to known esterases and lipases (see Table 1.1). We then compared our findings with desthiobiotin-FP to prior studies with a THL-alkyne (Wenk)[128] and an alkyne-PEG-FP (Grundner)[123] (Table 4.1). Overall, Wenk identified fewer esterases because THL has a narrower reactivity profile. Many of the esterases we identified in our enrichment overlap with those found by Grundner *et al.*, although their alkyne-PEG-FP probe also revealed three esterases missed in our study (Culp6, Rv0421c, and Rv3591c). There were only two esterases identified by all three studies in both normoxic and hypoxic cultures: CaeA (Rv2224c) and LipM (Rv2284). This suggests that CaeA and LipM are potential therapeutic targets for both latent and active TB. In all three ABPP studies, LipD (Rv1923), LipI, and LipV (Rv3203) were associated only with replicating cultures. These esterases could be used to distinguish active TB from latent disease.

Esterases that remain active in dormant *Mtb* could facilitate survival during dormancy. In all three ABPP studies, no esterases were uniquely active during dormancy. We found seven esterases that remained catalytically active in dormancy: CaeA, Culp1, LipL (Rv1497), LipM, LipN, Rv0045c, and Rv1683. We identified only four esterases in *Mtb* undergoing reactivation from hypoxia: CaeA, LipR (Rv3084), Rv0183, and Rv1683. LipR was not identified in our

hypoxia samples, and it is possible that LipR activity is rapidly restored during reactivation.

Importantly, our ABPP with desthiobiotin-FP enabled us to identify five esterases that were missed by prior studies: Culp1 (Rv1984c), Culp4 (Rv3452), LipR, LipT (Rv2045c), and Rv1191. Culp1 and Culp4 are notable findings because they are both functionally linked to *Mtb* dissemination.[95,97] Immunization with recombinant Culp1 provides partial protection against TB,[100] and supplementing the BCG vaccine with Culp1 and other antigens enhances the vaccine's efficacy in mice.[101] Furthermore, both Culp1 and Culp4 are being explored as potential TB immunodiagnostic biomarkers, with Culp4 having the greatest sensitivity and specificity of the examined enzymes.[40]

Our identification of CaeA, Rv0183, and Rv1683 in dormant, reactivating, and active cultures suggests that these esterases are worth further investigation as diagnostic or therapeutic targets for all stages of TB disease. CaeA is a cell wall-associated dual-function esterase[46] and protease.[113] It is required for full virulence in a mouse model of TB[46] and is transcriptionally upregulated under nutrient starvation.[24] Rv0183 is a cell wall-associated monoacylglycerol (MAG) lipase that likely degrades host-cell lipids.[106,107] MAG lipase inhibitors—including ones specific for Rv0183—are being pursued as antimicrobials.[70,71,108] Rv1683 is annotated as a bifunctional long-chain acyl-CoA synthase and lipase, but has not yet been biochemically characterized. Rv1683 is essential for growth *in vitro*[103]

and is found in the cell membrane.[146] In addition to their persistent activities, CaeA, Rv0183, and Rv1683 are accessible targets due to their localization.

Desthiobiotin-FP and alkyne-PEG-FP have the same reactive warhead but react with different *Mtb* esterases (Table 4.1). This is consistent with our prior observation that fluorogenic esterase probes are not "one size fits all" substrates.[163,184] Thus, we further evaluated *Mtb* esterase activity in native protein gel-resolved lysates. Esterase activity patterns were revealed using a diverse set of fluorogenic esterase probes (Figure 4.7), including a new fluorogenic probe, 2',7'-dichlorofluorescein diacetyoxymethyl ether (DCF-AME), and our previously described probes (C2-masked DDAO-7-AME[163] and C8-masked DDAO-7-OME[184]).

DCF-AME and DDAO-7-AME revealed *Mtb* esterase activity patterns in normoxic lysates that were similar but not identical, with DCF-AME revealing a greater number of esterases (Figure 4.8). Esterase activity was inhibited by pre-incubating lysate with serine hydrolase inhibitors. As with the TAMRA-FP labeling, MAFP inhibited the greatest number of esterases, followed by E-600. PMSF and THL each inhibited only a few esterases. These results highlight the power of using fluorogenic probes with a native PAGE assay for fast inhibitor screens.

Because MAFP did not inhibit all of the active esterases in-gel, we analyzed samples treated with TAMRA-FP for residual activity with DCF-AME (Figure 4.9). TAMRA-FP abolished in-gel DCF fluorescence for all but one

enzyme, which we excised and identified as Rv3036c using MS-based proteomics (see Table 4.2 for peptide identifications). Rv3036c is cell wall-associated, secreted esterase that prefers two-carbon substrates.[50] It has a non-canonical S-X-X-K active site motif, which could affect its reactivity with FPs. Notably, this esterase retained activity under non-replicating conditions (see Figure 4.10).

Our ABPP experiments required large amounts of protein (~1 mg) for identification, whereas profiling with fluorogenic probes in a native PAGE assay uses substantially less (1–10 μg). The smaller sample amount enabled us to evaluate time-dependent changes in esterase activity for *Mtb* cultured in hypoxia and carbon starvation (Figure 4.10). We prepared lysates from cultures harvested after 2 h, 24 h, 4 d, or 2 weeks in hypoxia. We selected these time points because prior studies found that *Mtb* has an initial hypoxic response followed by an enduring hypoxic response, which is a more substantial and stable response that occurs by day 4.[66,203] For comparison, we harvested similar time points for *Mtb* subjected to carbon starvation.

In both models, the decrease in esterase activity was time-dependent. In the hypoxia model, esterase activity decreased by 2 h, with substantial downregulation by 24 h (Figure 4.10a). We observed further loss of activity by 4 days that remained absent through 2 weeks. Under carbon starvation, esterase activity was reduced by 2 h, with further downregulation by 24 h (Figure 4.10b). The 5-week carbon-starved culture showed minimal esterase activity.

We excised fluorescent esterase bands for identification by MS-based proteomics. We observed persistent activity in dormancy from an excised band containing LipH peptides. In our ABPP study, LipH was only identified in our replicating cultures (Table 4.1), highlighting an advantage of using amplifiable fluorogenic substrates to detect enzymes.

Other esterase activities correlated well between our ABPP and fluorogenic probe-based studies. For example, DDAO-7-OME revealed a fluorescent band that we previously identified as Culp1.[184] This band was present in lysates from both active and dormant cultures, which agreed with our ABPP findings. Our fluorogenic probes confirmed that LipV and Rv0045c were undetectable in dormant *Mtb*.

In conclusion, we used serine hydrolase ABPs and fluorogenic esterase probes to identify catalytically active esterases in replicating, dormant, and reactivating *Mtb*. These chemical tools revealed that many esterase activities were downregulated in dormancy. However, ABPs and fluorogenic probes together enabled us to identify nine esterases that retained activity in dormancy: CaeA, Culp1, LipH, LipL, LipM, LipN, Rv1683, Rv0183, and Rv3036c. We suggest that these esterases are worth investigating further as either diagnostic or therapeutic targets. Functional CaeA, Rv1683, Rv0183, and LipR were also present in recently reactivated *Mtb*. Our analysis enabled us to directly compare ABPP and fluorogenic probe-based profiling for evaluating *Mtb* esterase activity across metabolic states. Overall, ABPP worked well for enrichment and

identification of serine hydrolases, but fluorogenic probe-based profiling was more sensitive for detecting esterases with persistent activities and required 50–100-fold less protein.

Materials and Methods

Synthesis and characterization of DCF-AME

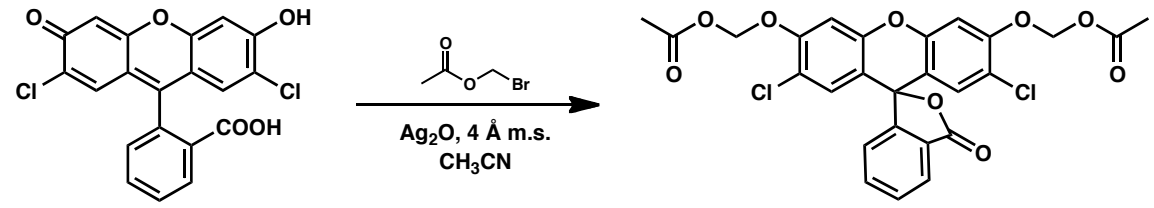

2',7'-dichlorofluorescein (DCF)
$\lambda_{abs/em}$ = 503/527
ϕ = 0.88

DCF-AME, 34% yield
colorless
nonfluorescent

All chemicals were purchased from Sigma-Aldrich and used as received. DCF-AME was synthesized according to a published protocol for masking a xanthene with an acetoxymethyl ether moiety.[137] DCF (2',7'-dichlorofluorescein, 134 mg, 0.36 mmol, 1 equiv) was combined with 4-Å molecular sieves (300 mg) and silver(I) oxide (Ag_2O, 210 mg, 0.91 mmol, 2.5 equiv) and put under argon atmosphere. The mixture was suspended in 6 mL anhydrous acetonitrile (CH_3CN), and bromomethyl acetate (0.15 mL, 1.4 mmol, 4 equiv) was added drop-wise via syringe. The mixture was stirred for 60 h at room temperature and monitored by TLC. The reaction mixture was diluted with dichloromethane (CH_2Cl_2) and filtered through a plug of Celite® S. The crude product was concentrated by rotary evaporation to give an orange oil and then purified by

silica gel chromatography (Biotage Isolera flash chromatography system, 0 to 40% ethyl acetate/hexanes with a constant 40% CH_2Cl_2). The product (DCF-AME, 62 mg, 34% yield), was isolated as a white crystalline solid (R_f = 0.67, 20% ethyl acetate/hexanes).

Mass spectra were acquired at Portland State University's BioAnalytical Mass Spectrometry Facility on a ThermoElectron LTQ-Orbitrap Discovery high-resolution mass spectrometer with electrospray ionization (ESI) (NSF instrument grant 0741993).

NMR spectra were acquired at ambient temperature in $CDCl_3$ at Portland State University's NMR facility on a Bruker Avance II. ^{1}H-NMR data were obtained at 400 MHz. ^{13}C-NMR data were at 101 MHz. Spectra were calibrated to the internal tetramethylsilane (TMS) peak. Chemical shifts are reported in ppm. Coupling constants (*J*) are reported in Hertz (Hz) and rounded to the nearest 0.1 Hz. Multiplicities are defined as: s = singlet, dt = doublet of triplets, td = triplet of doublets, m = multiplet, app = apparent.

^{1}H-NMR (400 MHz, $CDCl_3$) δ (ppm): 8.07 (app dt, *J* = 7.5, 0.9 Hz, 1H), 7.74 (app td, *J* = 7.4, 1.4 Hz, 1H), 7.70 (app td, *J* = 7.4, 1.2 Hz, 1H), 7.16 (app dt, *J* = 7.6, 0.8 Hz, 1H), 7.09 (s, 2H), 6.79 (s, 2H), 5.87–5.84 (m, 4H), 2.18 (s, 6H). (Figure 4.10)

^{13}C-NMR (101 MHz, $CDCl_3$) δ (ppm): 169.5, 168.6, 154.0, 151.9, 150.3, 135.6, 130.5, 129.2, 126.2, 125.6, 123.8, 119.6, 113.8, 104.1, 85.4, 81.1, 20.9. (Figure 4.11)

ESI-MS $[M+H]^+$ calculated for $C_{26}H_{18}Cl_2O_9$: 545.0406; found: 545.0415.

DCF-AME was spectrally characterized and validated as a fluorogenic esterase probe, using previously described methods.[163,184] We determined the kinetic parameters with 500 ng/mL porcine liver esterase and calculated an apparent Michaelis constant (K_M) of 3.9 ± 0.5 μM and a maximal velocity (V_{max}) of 0.11 pmol/s.

Mycobacterial culture conditions

Cells were thawed from frozen stocks (stored at –80 °C in 6% glycerol). *Mtb* mc^{2}6020 (*ΔlysA* and *ΔpanCD* mutant)[188] was cultured in 7H9 medium (7H9 broth, 0.5% glycerol, 0.05% Tween 80, 10% OADC) supplemented with 80 μg/mL lysine, 24 μg/mL pantothenate, and 0.2% casamino acids. Cultures were grown at 37 °C with 75 rpm shaking and handled as BSL-2 pathogens. Cells were collected by centrifugation, and the pellets were stored at –30 °C.

Culturing *Mtb* in hypoxic conditions

Cultures were grown to an OD_{600} between 0.5 and 1.0 and then diluted to an OD_{600} of 0.4 in 7H9 complete medium (see above). Cultures (200 mL) were grown at 37 °C in standing flasks with (0.2 μm filtered) vented caps in a Heracell 150i incubator (Thermo Scientific) at 1% O_2 and 5% CO_2. Cultures were harvested by centrifugation (5 min, 2800 x g, 4 °C) after 2 h, 24 h, 4 d, or 2

weeks. Methylene blue (1.5 μg/mL) decolorization in control cultures indicated oxygen depletion between 9 and 14 days, as previously reported.[24,26]

Culturing *Mtb* using a carbon starvation model

A modified version of the carbon starvation protocol developed by Grant *et al.* was used to induce dormancy.[25] Cultures were grown in 7H9 complete medium until an OD_{600} between 0.6 and 1.5 was reached. Cells were harvested by centrifugation (5 min, 2800 x g, 4 °C) and washed twice with PBS containing 0.05% tyloxapol. Cells were resuspended at an OD_{600} of 0.2 in carbon starvation medium (7H9 broth base with 0.05% tyloxapol) and grown as standing cultures in sealed 1 L bottles (200 mL culture per bottle) at 37 °C. Cultures were harvested by centrifugation (5 min, 2800 x g, 4 °C) after 2 h, 24 h, 4 d, or 5 weeks. Grant *et al.* reported that cultures become dormant by two weeks, but that the respiration rate of *Mtb* under starvation conditions continues to decline until a plateau is reached by five weeks.[25,29]

Preparation of reaeration samples

Cultures were grown under hypoxia as described above. After two weeks, cells were harvested by centrifugation (5 min, 2800 x g, 4 °C) and washed twice with PBS containing 0.05% tyloxapol. The pellets were resuspended in 50 mL of carbon starvation medium supplemented with 80 μg/mL lysine and 24 μg/mL

pantothenate or in 7H9 complete medium and then grown at 37 °C in atmospheric conditions.

Preparation of lysates for in-gel analysis with fluorogenic probes

Cell pellets were thawed and resuspended in lysis buffer [50 mM Tris (pH 7.5 at 4 °C), 200 mM NaCl, 0.5 mM $CaCl_2$, 0.5 mM $MgCl_2$, and 0.2% Triton X-100]. Cells were lysed by mechanical disruption on a BioSpec Beadbeater (3 x 1 min pulses with rests on ice) using 0.1 mm zirconia/silica beads (BioSpec Products) in screw cap tubes. Insoluble debris and beads were pelleted by centrifugation (13,000 x g, 4 °C, 10 min) and the clarified supernatant was transferred to a clean tube. Samples were further clarified by centrifugation (15,700 x g, 4 °C, 5 min) to remove residual insoluble material. Lysates were sterilized by filtration through a 0.2 μm PVDF membrane (Pall Acrodisc 13 mm syringe filter).

Preparation of lysates for ABPP

Pellets of normoxic and hypoxic samples were washed twice with PBS containing 0.05% Tween 80 in order to remove BSA. The pellets were then resuspended in lysis buffer [50 mM Tris (pH 7.5 at 4 °C), 50 mM NaCl, 0.5 mM $CaCl_2$, 0.5 mM $MgCl_2$, 0.2% Triton X-100] and lysed, as described above.

Pellets from hypoxic cultures reaerated in carbon starvation medium were resuspended in detergent-free lysis buffer [50 mM Tris (pH 7.5 at 4 °C), 50 mM

NaCl, 0.5 mM $CaCl_2$, 0.5 mM $MgCl_2$] and lysed by mechanical disruption. The supernatant was removed following centrifugation. Fresh detergent-free lysis buffer was added, and the pellet was mechanically disrupted once more in order to maximize protein yield. After centrifugation, this second supernatant was combined with the first. The remaining material was mixed with lysis buffer containing 0.2% Triton X-100 and mechanically disrupted for 60 s. After centrifugation, the supernatant was removed and combined with the other two fractions. All lysates were clarified by centrifugation and sterilized, as described above.

LipY expression and purification

LipY (Rv3097c) was cloned into pMyNT to attach an N-terminal His_6-tag (Addgene plasmid #42191) and expressed in *Mycobacterium smegmatis* mc^2155, as previously reported, with some modifications.[40] *M. smegmatis* carrying the LipY construct was used to inoculate 7H9/Hyg (7H9 medium supplemented with 10% ADC, 0.5% glycerol, 0.05% Tween 80, and 50 μg/mL hygromycin B). The culture was grown overnight to an OD_{600} of 4.9, then diluted 1:100 in expression medium (7H9, 0.2% glucose, 0.2% glycerol, 0.05% Tween 80, 50 μg/mL hygromycin B).[204] When an OD_{600} of 0.5 was reached, LipY expression was induced with 0.02% acetamide for 24 h. The culture was harvested by centrifugation (5 min, 2800 x g, 4 °C), and pellets were stored at –30 °C.

Pellets were thawed and washed twice with cold PBS containing 0.05% Tween 80. Cells were resuspended in lysis buffer [10 mM Tris (pH 8 at 4 °C), 150 mM NaCl, 1% N-lauroyl sarcosine] and lysed by mechanical disruption (see above).

The resulting lysate was loaded onto Ni-NTA resin (pre-equilibrated with lysis buffer) and bound for 1 h at 4 °C. The column was washed with 8 column volumes of wash buffer [10 mM Tris (pH 8 at 4 °C), 150 mM NaCl, 10 mM imidazole] and eluted with increasing concentrations of imidazole.

Impure LipY was buffer exchanged into 50 mM Tris (pH 8 at 4 °C), 0.5 mM $CaCl_2$, 0.5 mM $MgCl_2$, 0.2% Triton X-100 using a Zeba Spin Desalting Column (7K MWCO, Thermo Scientific). LipY was further purified by anion exchange chromatography (Pierce Q columns) in 50 mM Tris (pH 8 at 4 °C), 0.5 mM $CaCl_2$, 0.5 mM $MgCl_2$, 0.2% Triton X-100 with increasing NaCl concentration (LipY eluted around 100 mM NaCl). Finally, the His_6-tag was cleaved in-solution with ProTEV Plus (Promega) for 3 h at 30 °C, and the protease was removed using the His-Spin Protein Miniprep Kit (Zymo).

In-gel detection of active *Mtb* serine hydrolases using an activity-based probe

Lysates (15 μg total protein) or LipY (500 ng) were incubated with 10 μM ActivX TAMRA-FP (Fisher, PI88318) or DMSO (unlabeled control) for 1 h at room temperature. For inhibitor studies, lysates were pre-incubated with 100 μM

of inhibitor (MAFP, PMSF, E-600, or THL) for 1 h at room temperature prior to TAMRA-FP treatment. For 10% Bis-Tris PAGE, samples were boiled for 5 min in SDS-PAGE loading buffer, and insoluble material was removed by centrifugation. Proteins were resolved at 180 V for 1 h at 4 °C, and TAMRA fluorescence was detected (λ_{ex} 488 nm, λ_{em} 580 BP 30 nm) using a Typhoon 9400 Imager (GE Healthcare).

Identification of active *Mtb* serine hydrolases using desthiobiotin-FP

Mtb $mc^2$6020 lysates (n = 3 each condition) were concentrated to a volume of 45 μL using a 10 kDa MWCO centrifugal filter (Amicon). For normoxic and reactivation lysates, 750 μg of total protein was used. For hypoxic lysates, 500 μg was used due to the low protein content of those samples. The lysates were labeled with 100 μM ActivX desthiobiotin-FP (Fisher, PI88317) for 1 h at room temperature. Unreacted probe was removed using Zeba Spin Desalting Columns (7K MWCO, Thermo Scientific), and samples were exchanged into 500 μL of urea resuspension buffer (URB: 5 M urea, PBS pH 7.4, 0.1% Triton X-100). Lysates were enriched for labeled enzymes using 250 μL (bed volume) of pre-washed High Capacity Streptavidin Agarose Resin (Thermo Scientific). The lysate/resin suspensions were incubated overnight at 4 °C with constant rotation. Unbound proteins were removed from the resin using microcentrifuge spin columns (Pierce). Resin containing bound, biotinylated proteins was washed twice with urea wash buffer (UWB: PBS pH 7.4, 4 M urea), three times with

wash buffer A (WB-A: 1% Triton X-100, PBS pH 7.4), twice with wash buffer B (WB-B: 50 mM ammonium bicarbonate), twice with PBS pH 7.4, and twice with WB-B.[205] Aliquots (200 μL) of the unbound protein and all washes were concentrated by acetone precipitation and used for Western blot analysis.

The resin was resuspended in 435 μL of WB-B and incubated at 70 °C for 10 min. Urea was added to reach a concentration of 2 M, and the solution was cooled to room temperature. Samples were agitated for 30 min at room temperature with 3 mM TCEP followed by 11.3 mM iodoacetamide for 30 min at room temperature in the dark. $CaCl_2$ was added (0.1 mM final concentration), and the samples were treated with 1 μg sequencing grade trypsin (Promega) overnight at 37 °C with shaking. Digested peptides were separated from the resin using microcentrifuge spin columns (Pierce). Active site peptides were eluted from the resin using 0.1% TFA, 50% acetonitrile. Samples were stored at –30 °C prior to submission to the UC Davis Proteomics Core for analysis.

Proteomic identification of active serine hydrolases

The resulting MS/MS spectra were searched using X! Tandem (The GPM, thegpm.org; version X! Tandem Vengeance, 2015.12.15.3). X! Tandem was set up to search the uniprotM_20160127_ja6Dre database (8206 entries) assuming tryptic digestion with a maximum of one missed cleavage. X! Tandem was searched with a fragment ion mass tolerance of 20 ppm and a parent ion tolerance of 20 ppm. Carbamidomethylation of cysteine was specified in X!

Tandem as a fixed modification. Glu->pyro-Glu of the N-terminus, ammonia-loss of the N-terminus, Gln->pyro-Glu of the N-terminus, deamidation of Asp and Glu, oxidation of Met and Trp, dioxidation of Met and Trp, and acetylation of the N-terminus were specified in X! Tandem as variable modifications. Scaffold was used to validate MS/MS-based peptide and protein identifications. Peptide identifications were accepted if they could be established at greater than 14.0% probability for an FDR (false discovery rate) of less than 1.0% by the Scaffold Local FDR algorithm. Protein identifications were accepted if they could be established at greater than 98.0% probability for an FDR of less than 5.0% and contained at least 2 unique identified peptides. Protein probabilities were assigned by the Protein Prophet algorithm.[194] Proteins that contained similar peptides and could not be differentiated based on MS/MS analysis alone were grouped to satisfy the principles of parsimony.

Western blot analysis

Denatured protein samples were resolved on a 10% Bis-Tris polyacrylamide gel and transferred to a Immobilon-P PVDF membrane (Millipore; 90 V, 1 h). Membranes were blocked with 5% BSA in TBST for 1 h and incubated with 1:25,000 anti-biotin-HRP (Jackson ImmunoResearch) in 5% BSA/TBST for 1 h. Chemiluminescence was generated using Supersignal West Pico ECL substrate (Thermo Scientific) and detected on a MyECL imager (Thermo Scientific).

In-gel detection of active *Mtb* esterases using fluorogenic probes

For inhibitor competition experiments, lysates were pre-incubated with 100 μM inhibitor (MAFP, PMSF, E-600, or THL) for 1 h at room temperature. Lysates (8 μg total protein) were resolved by native PAGE as previously described.[184] Gels were equilibrated in 10 mM HEPES (pH 7.3), incubated with 5 μM probe for 5–10 min, and then imaged on a Typhoon 9400 Imager (DCF detection: λ_{ex} 488 nm, λ_{em} 520 BP 40 nm; DDAO detection: λ_{ex} 633 nm, λ_{em} 670 BP 30 nm).

Select bands were excised and submitted to the OHSU Proteomics Shared Resource for protein tryptic digestion, peptide extraction, and LC-MS/MS analysis, as previously described.[184] See Table S4 for peptide identifications.

Acknowledgements

Funding for this research was generously provided by the Knight Cancer Institute at OHSU, the Collins Medical Trust, and the Medical Research Foundation of Oregon. S.R.L. was supported by an NIH T32 training grant (T32-AI07472). We are grateful to I. Carter-O'Connell for helpful discussions. We thank the Sahay lab (OSU) for the use of their MyECL imager.

Tables

Table 4.1. Active *Mtb* esterases revealed by ABPP.

		THL-alkyne[a]		alkyne-PEG-FP[b]		desthiobiotin-FP	
Rv Number	**Esterase**	**N**	**H**	**N**	**H**	**N**	**H**
Rv2224c	CaeA	X	X	X	X	X	X
Rv1984c	Culp1					X	X
Rv2301	Culp2			X		X	
Rv3452	Culp4					X	
Rv3802c	Culp6			X	X		
Rv1923	LipD	X		X		X	
Rv3775	LipE			X		X	
Rv0646c	LipG	X				X	
Rv1399c	LipH	X		X		X	
Rv1400c	LipI	X		X		X	
Rv1497	LipL			X	X	X	X
Rv2284	LipM	X	X	X	X	X	X
Rv2970c	LipN	X		X	X	X	X
Rv1426c	LipO	X				X	
Rv3084	LipR					X	
Rv2045c	LipT					X	
Rv3203	LipV	X		X		X	
Rv0217c	LipW	X				X	
Rv0045c	Rv0045c			X		X	
Rv0183	Rv0183			X	X	X	X
Rv0421c	Rv0421c			X	X		
Rv0774c	Rv0774c			X		X	
Rv1191	Rv1191					X	
Rv1683	Rv1683			X	X	X	X
Rv3591c	Rv3591c			X	X		
	Total hits:	***10***	***2***	***17***	***9***	***22***	***7***

An "X" indicates that the esterase was identified in the corresponding condition for each study (N, normoxic; H, hypoxic). Esterases highlighted in green were found in all three studies in both N and H. Esterases highlighted in blue were uniquely identified in this study. [a]Wenk *et al.* performed ABPP in *M. bovis* (BCG) with a THL analog, and their proteins are listed as the *Mtb* (H37Rv) ortholog.[128] [b]Grundner *et al.* performed ABPP with an alkyne-PEG-FP.[123] For a compiled list of *Mtb* esterases, see Table 1.1.

Table 4.2. Identification of esterases within excised fluorescent bands by mass spectrometry.

Rv	Name	% Coverage	Peptide List[a]	Count	XCorr	DeltaCN
Rv3203	LipV	33.3	K.ATGAWADVDPPVLDAELDEHLVALPNGR.Y	2	3.7232	0.4450
			R.ISLPAMVCYWSELAR.D	1	3.3899	0.6121
			R.DIVLPPVGTATTLVR.A	1	2.9661	0.5791
			R.ASPAYVSDQLLAALDK.R	1	3.9791	0.6550
			R.ASPAYVSDQLLAALDKR.L	1	4.4774	0.6517
			R.ASPAYVSDQLLAALDKR.L	1	1.4800	0.3705
Rv3036c	TB22.2	12.3	R.DGFVNVAQGSPLR.D	2	2.6935	0.3894
			K.FFQDLGGAHPSTWYK.A	1	3.6171	0.6638
Rv0045c	–	18.4	R.VQAGAISALR.W	1	2.3210	0.3296
			R.EDGNYSPQLNSETLAPVLR.E	2	4.2688	0.7071
			R.LDNGNWVWR.Y	1	1.5701	0.2361
			R.GGSSGFVTDQDTAELHR.R	1	3.5035	0.6428
			R.GGSSGFVTDQDTAELHR.R	1	2.9242	0.5843
Rv1399c	LipH	33.8	K.TPPELLPELR.I	1	2.1334	0.4551
			R.DNLPVVVYYHGGGWSLGGLDTHDPVAR.A	1	3.4798	0.4964
			R.AHAVGAQAIVVSVDYR.L	1	4.4550	0.7224
			R.LAPEHPYPAGIDDSWAALR.W	1	1.7980	0.2240
			R.LAPEHPYPAGIDDSWAALR.W	1	2.3297	0.4376
			R.WVGENAAELGGDPSR.I	2	3.5699	0.6221
			R.IAVAGDSAGGNISAVMAQLAR.D	1	2.1501	0.4154

[a]Periods (.) separate found peptides from the previous and next residues in the protein sequence. The spectral count (Count) for each peptide is given.

Figures

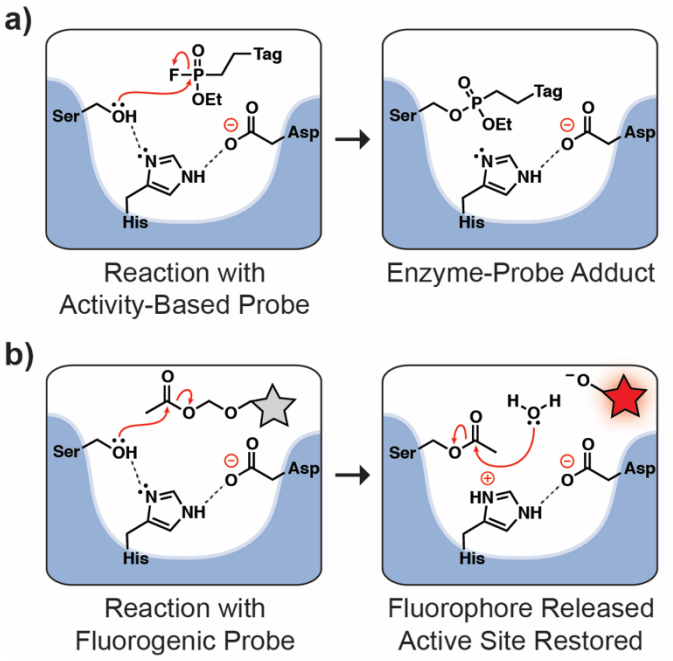

Figure 4.1. Small molecule probes for revealing active *Mtb* esterases.

(a) ABPs form a covalent bond with an active site serine for irreversible serine hydrolase labeling. ABPs contain a tag for direct detection or for affinity enrichment (i.e., for identification by mass spectrometry-based proteomics). (b) Fluorogenic esterase probes are substrates that produce fluorescence upon serine-mediated hydrolysis. Following probe cleavage, the active site is restored.

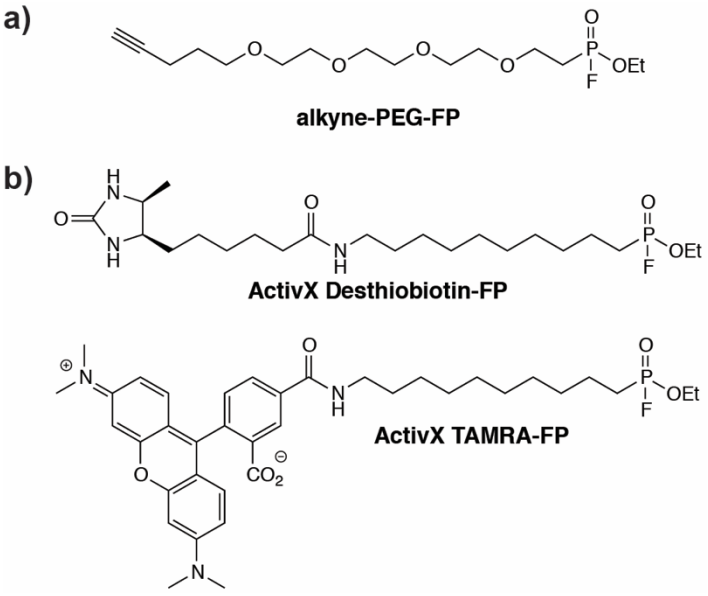

Figure 4.2. The structures of serine hydrolase-targeted ABPs.

(a) In their study of *Mtb* serine hydrolase regulation, Grundner *et al.* employed a "clickable" FP ABP, which was later reacted with an azide-derivatized Cy7.5 fluorescent reporter for in-gel detection or biotin-azide for enrichment.[123] (b) We used two FP ABPs in our study: desthiobiotin-FP for target enrichment and TAMRA-FP for in-gel fluorescence detection.

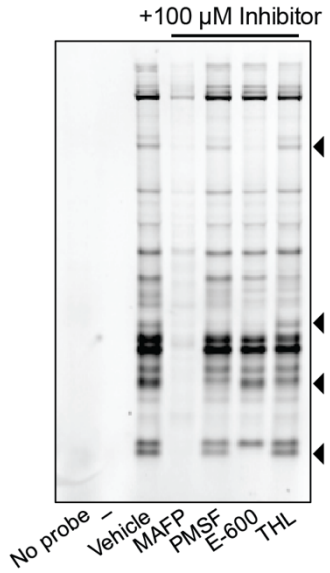

Figure 4.3. TAMRA-FP enables detection of active serine hydrolases in replicating *Mtb.* Lysates were treated with TAMRA-FP or vehicle (DMSO) for 1 h before SDS-PAGE analysis. Alternatively, lysates were pre-treated with 100 μM of the indicated inhibitor prior to TAMRA-FP labeling. Arrowheads highlight some of the differences in banding between PMSF, E-600, and THL inhibition.

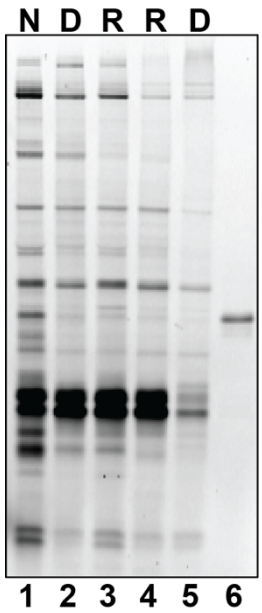

Figure 4.4. Serine hydrolase activity is reduced in dormancy.

Lysates from normoxic (N), dormant (D) and reaerated (R) cultures were treated with TAMRA-FP and then resolved by SDS-PAGE. Lane 1: normoxic lysates. Lane 2: hypoxic lysates. Lane 3: reaerated lysates, reactivated from hypoxia in rich growth medium. Lane 4: reaerated lysates, reactivated from hypoxia under carbon starvation. Lane 5: carbon-starved lysates. Lane 6: LipY.

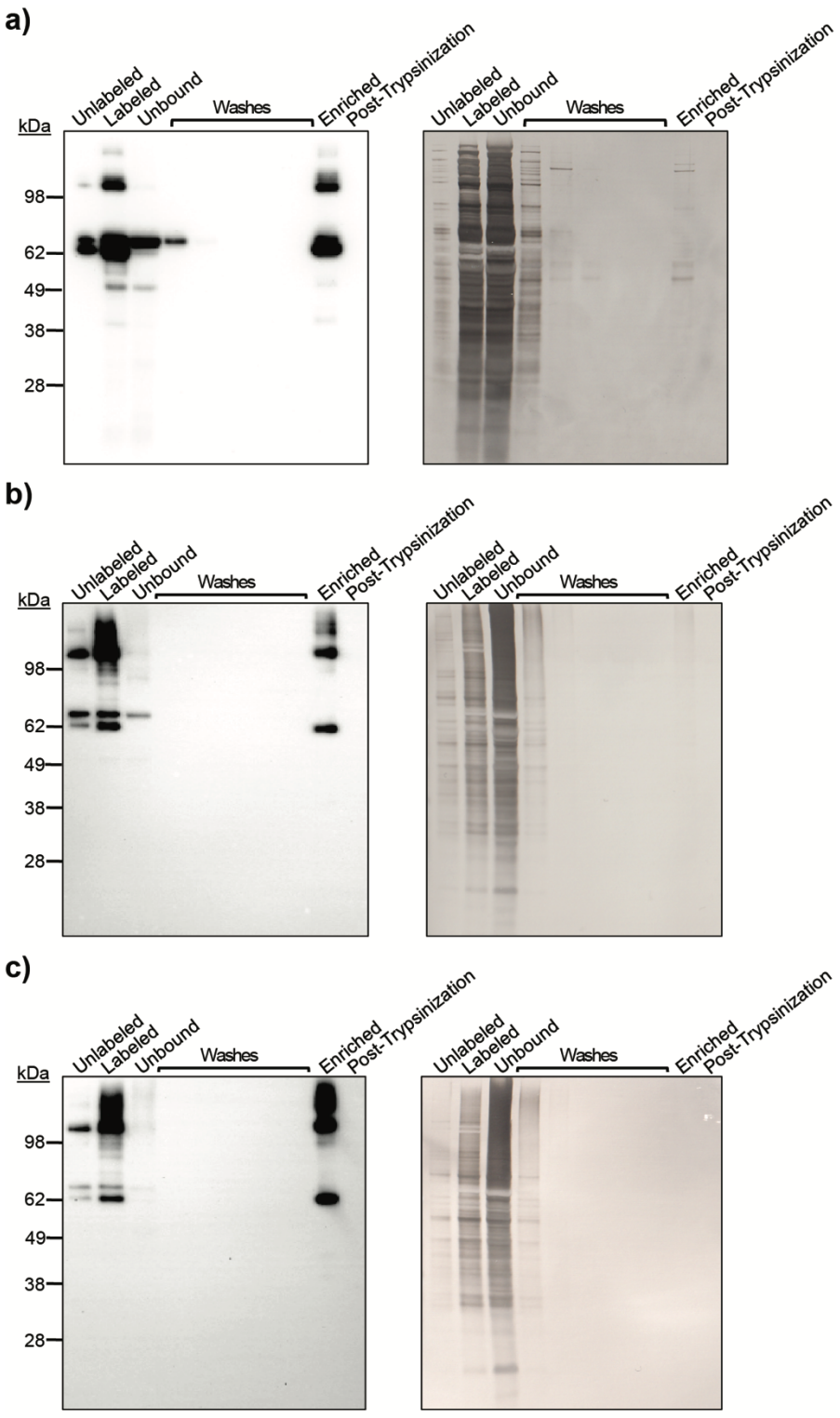
a)
b)
c)
kDa
98
62
49
38
28
Unlabeled
Labeled
Unbound
Washes
Enriched
Post-Trypsinization

Figure 4.5. ABP-based enrichment of *Mtb* serine hydrolases for LC-MS/MS analysis and target identification.

Mtb lysates from (a) normoxic, (b) hypoxic, or (c) reactivating cultures were treated with 100 μM desthiobiotin-FP for 1 h at room temperature. After incubation with streptavidin resin, the unbound proteins were separated from the resin by centrifugation. The resin was washed to remove proteins with non-specific binding before the bound proteins were digested with trypsin. Biotinylated proteins were detected using anti-biotin-HRP (left). The membranes were subsequently stained with India ink to reveal protein content (right).

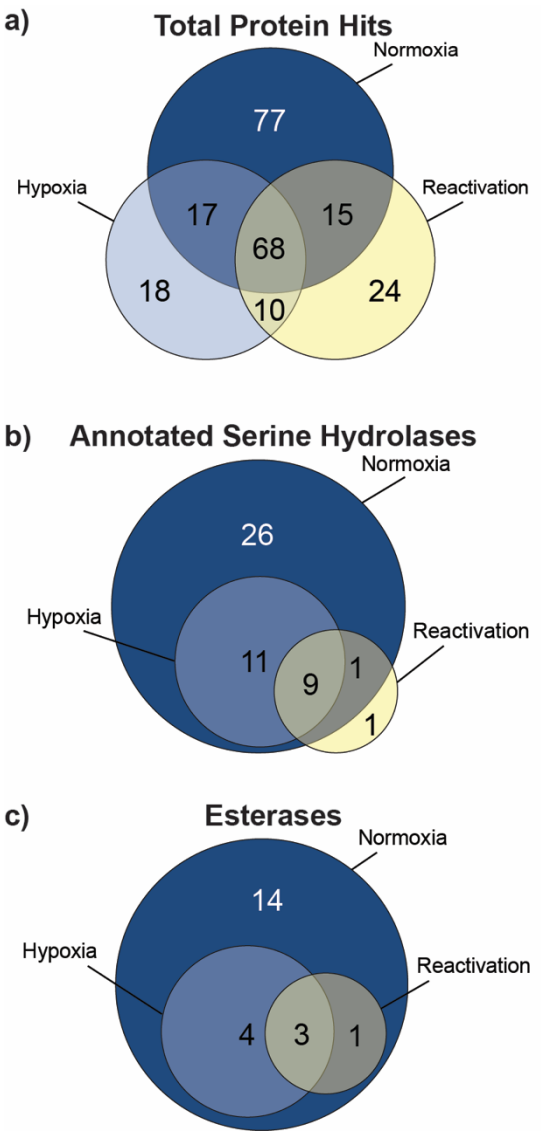

Figure 4.6. Diagrams of the number of ABPP hits found in each growth condition.

(a) Distribution of the 229 proteins identified in each condition. We used a cutoff of at least two unique peptides per protein in at least two replicates. (b) Distribution of the 48 enzymes bioinformatically annotated as serine hydrolases. (c) Distribution of the active esterases identified in each condition.

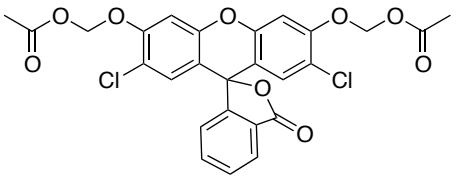

DCF-AME

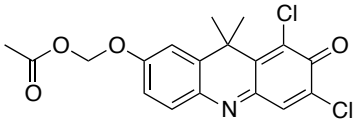

DDAO-7-AME

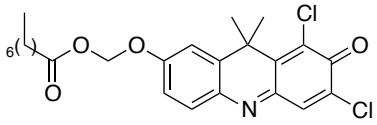

DDAO-7-OME

Figure 4.7. The chemical structures of the fluorogenic probes used in this study. DCF-AME is derived from the green fluorophore 2',7'-dichlorofluorescein. The DDAO probes are derived from the far-red fluorophore DDAO.

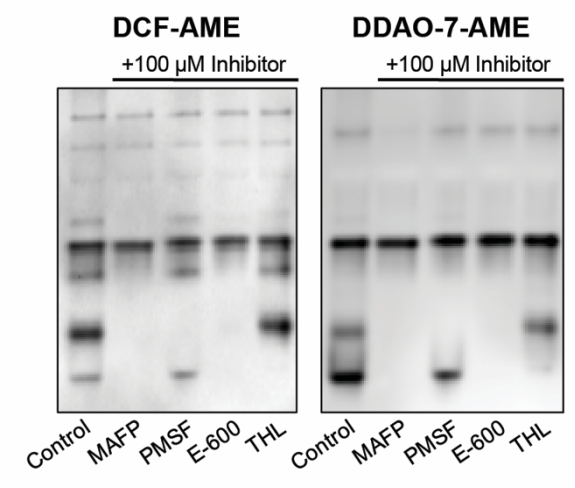

Figure 4.8. Fluorogenic probes detect active *Mtb* esterases.

Lysates were pre-incubated with 100 μM of the indicated inhibitor for 1 h at room temperature and then resolved by native PAGE. Gels were soaked in 5 μM probe (5–10 min) and imaged on a fluorescence scanner.

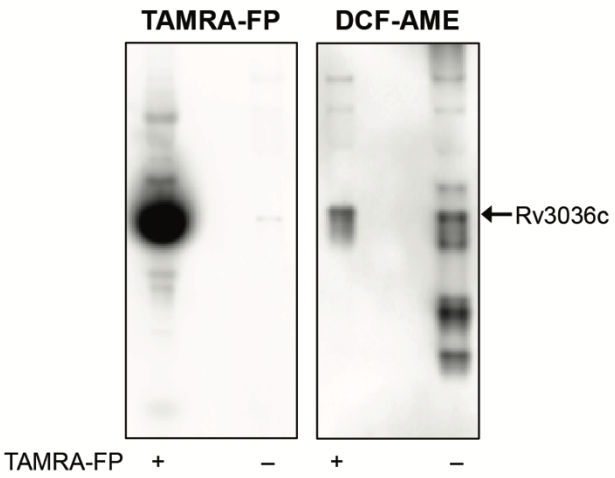

Figure 4.9. Fluorophosphonate ABPs and fluorogenic probes can reveal different active esterases in native gel-resolved lysates.

After TAMRA imaging, the gel was incubated with 5 μM DCF-AME and imaged again. A fluorescent band containing Rv3036c, a secreted esterase with a non-canonical active-site motif, was not labeled by TAMRA-FP or inhibited by MAFP but hydrolyzed DCF-AME.

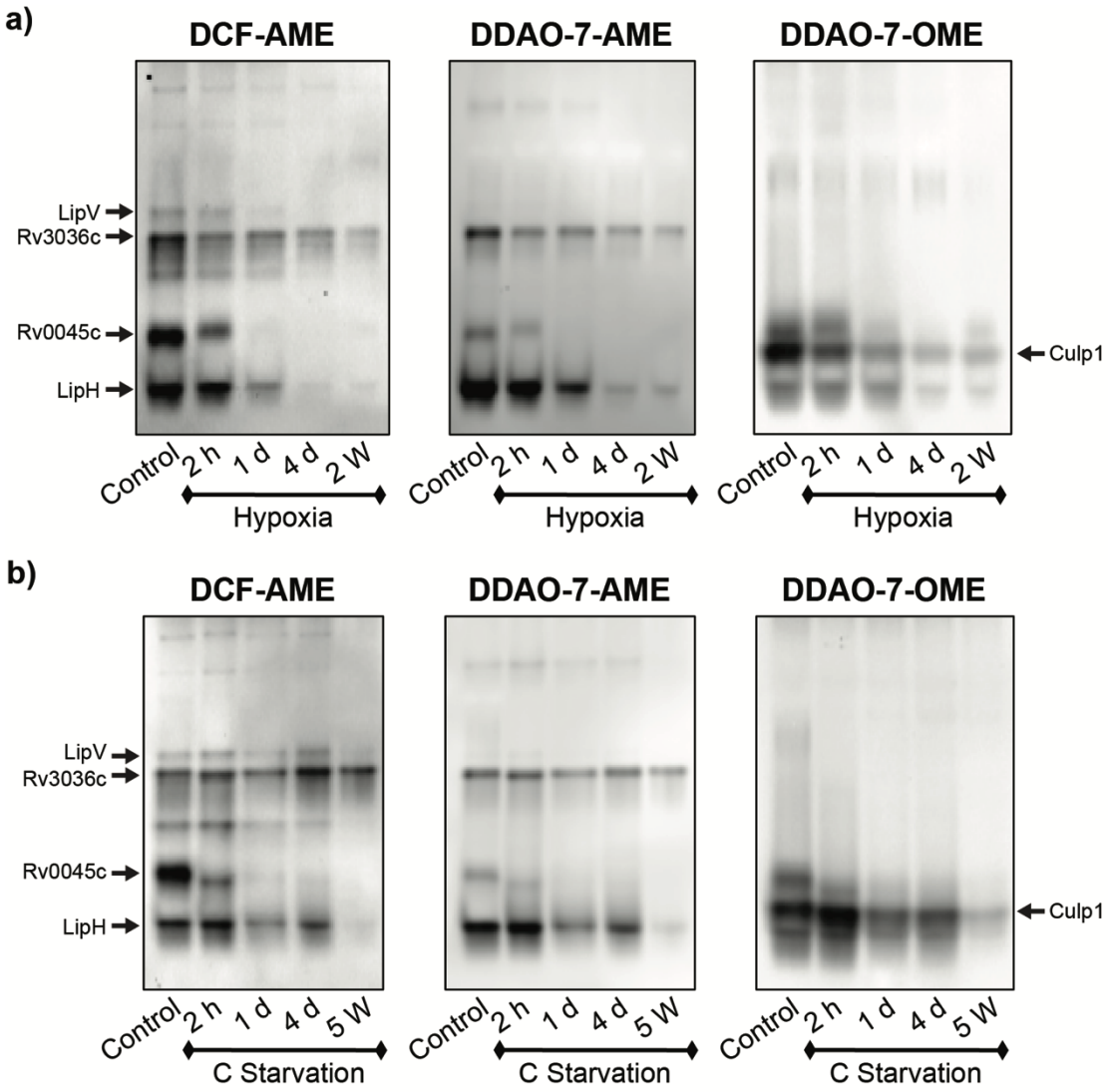

Figure 4.10. *Mtb* esterase activity is downregulated in dormancy in a time-dependent manner. Lysates were resolved by native PAGE, and the gels were incubated with 5 μM of the indicated probe (5–10 min) before imaging. Select fluorescent bands were excised, and esterases present within the bands were identified using mass spectrometry-based proteomics. (a) Cultures were harvested after 2 h, 1 d, 4 d, or 2 weeks in hypoxia. (b) Cultures were harvested after 2 h, 1 d, 4 d, or 5 weeks under carbon starvation.

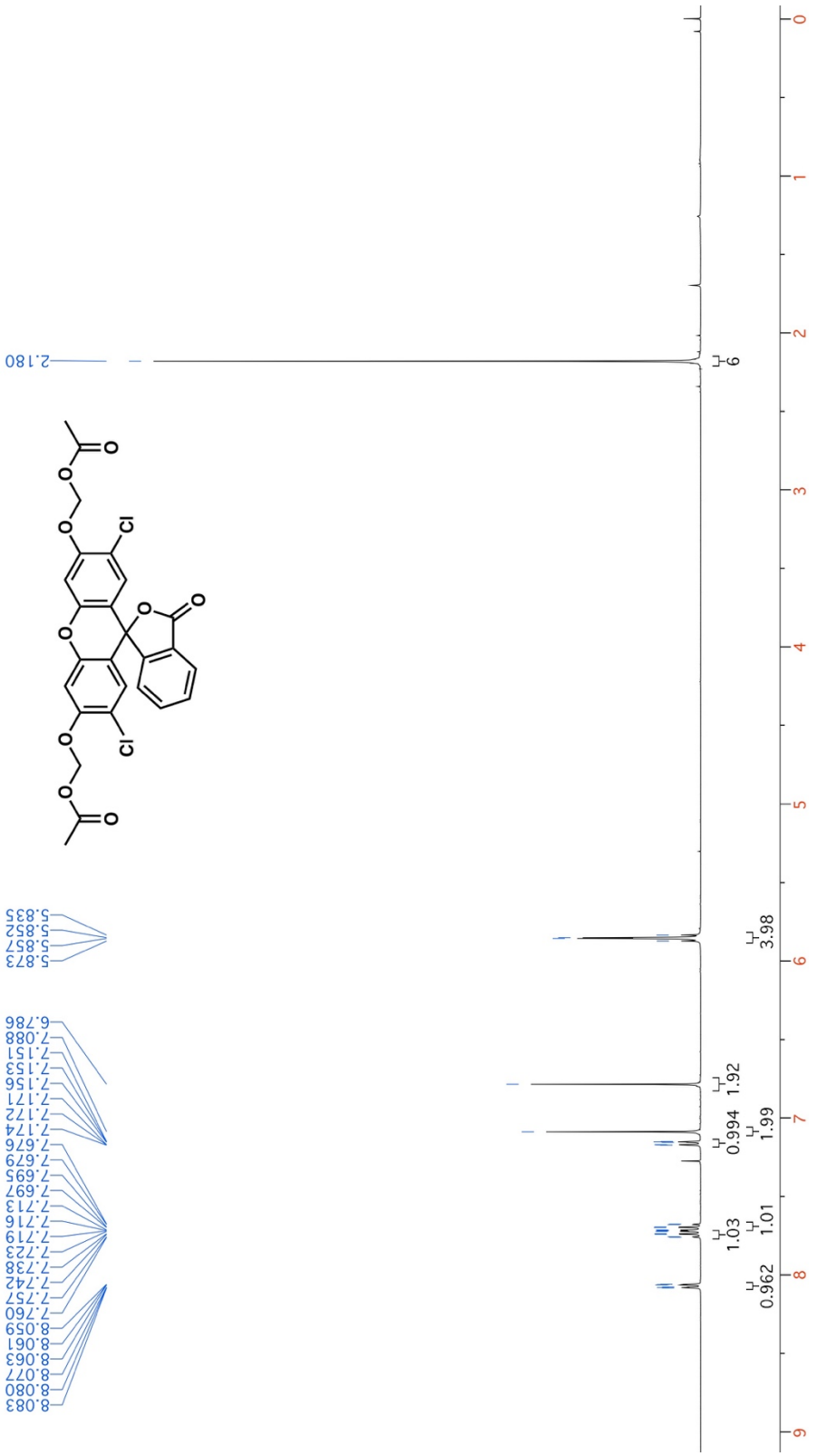

Figure 4.11. ^{1}H-NMR spectrum of DCF-AME (400 MHz; $CDCl_3$).

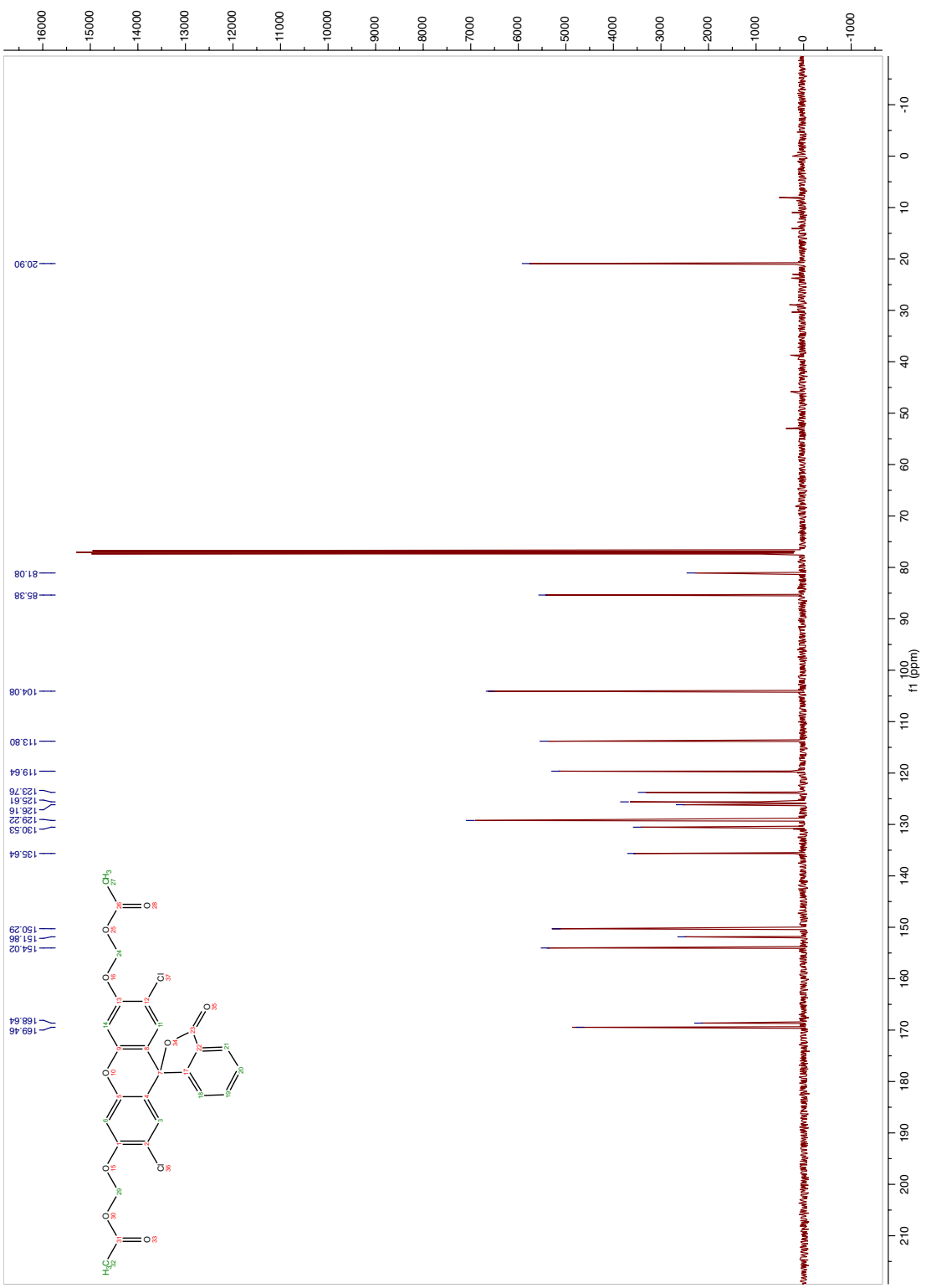

Figure 4.12. ^{13}C-NMR spectrum of DCF-AME (101 MHz; $CDCl_3$).

Chapter 5: Concluding Remarks

Mtb esterases have long been implicated in pathogen persistence and virulence but have been difficult to express and characterize using heterologous systems.[37,46,94,167] Furthermore, characterization studies of recombinant enzymes do not reveal changes in enzyme activities within the pathogen as it responds to its environment. In this work, I developed and used chemical tools to study the activity of *Mtb* esterases in active, dormant, and reactivating *Mtb*.

In Chapters 2 and 3, I described the development of generic fluorogenic esterase substrates from the far-red fluorophore DDAO. Although my dissertation research focused on using these probes to study *Mtb* esterases, I expect these tools to be broadly useful for biochemically characterizing esterases or for imaging applications requiring a far-red fluorescent read-out. Notably, we demonstrated that our DDAO-derived fluorogenic esterase probes can be used in live-cell imaging (Chapter 3).

Ultimately, I utilized fluorogenic probes in a native PAGE assay to rapidly screen mycobacterial esterase activity. Using this method, I determined that esterase activity is well-conserved across members of the MTBC (Chapter 2). Culp1, an enzyme that is genetically deleted in *M. bovis* (BCG), was a notable exception (Chapter 3). Furthermore, non-MTBC mycobacteria and mammalian cells produce distinct esterase activity patterns from *Mtb* (Chapters 2 and 3).

This enabled me to distinguish host-cell esterase activity from *Mtb* esterase activity in an *in vitro* macrophage infection model. In the future, these fluorogenic probes could be further optimized for tracking *Mtb* esterase activity in TB animal models or patient samples.

I observed that the substrate preferences of *Mtb* esterases can be revealed using fluorogenic probes and the native PAGE assay. For example, Culp1 was specifically detectable with C8 substrates. Other esterases, including one I putatively identified as Rv3036c, preferred C2 substrates. My data indicated that the *Mtb* esterases have substrate preferences despite their conserved catalytic mechanism. Even a change in regiochemistry, such as DDAO-2-AME and DDAO-7-AME, resulted in differing esterase reactivity.

Lastly, I used both fluorogenic probes and ABPs to identify esterases that were active in replicating, dormant, and reactivating *Mtb* (Chapter 4). By using a variety of esterase-targeted probes, I was able to generate a list of esterases that may be key to *Mtb* survival during dormancy and reactivation. Most notably, CaeA, Rv0183, Rv1683 retained activity across all three conditions. While CaeA[46,113] and Rv0183[106,107,206] have already been implicated in *Mtb* pathogenicity, Rv1683 is an exciting new target. Future work should focus on determining the natural substrates for Rv1683 and its role in dormancy and reactivation. Additionally, I directly compared ABPP and fluorogenic probe-based profiling. Our fluorogenic probes revealed that Rv3036c and LipH were active during both hypoxia- and carbon starvation-induced dormancy. Although

these enzymes have been biochemically characterized,[50,150] their roles in *Mtb* pathogenicity have not been explored. Overall, I anticipate that the results of my dissertation research will aid TB drug discovery and diagnostic development.

Appendix A: Serine Hydrolase Activity-Based Protein Profiling Hits

Table A.1. List of serine hydrolases identified by ABPP with desthiobiotin-FP and their functional annotations.

	Rv Number	Protein Name	Function	Category[a]
All Conditions	Rv0183	Rv0183	MAG lipase.	IMR
	Rv0457c	Rv0457c	Probable peptidase; likely hydrolyzes peptides and/or proteins.	IMR
	Rv1263	AmiB2	Amidase involved in cellular metabolism, active on 2- to 6- carbon aliphatic amides and on many aromatic amides.	IMR
	Rv1683	Rv1683	Possible bifunctional enzyme long-chain acyl-CoA synthase and lipase; supposed involvement in lipid biosynthesis and degradation.	LM
	Rv2224c	Carboxylesterase A (CaeA)	Converts unknown esters to corresponding free acid and alcohol.	CWP
	Rv2524c	Fas	Fatty acid synthetase; catalyzes the formation of long-chain fatty acids from acetyl-CoA, malonyl-CoA and NADPH.	LM
	Rv2940c	Mas	Mycocerosic acid synthase; catalyzes the elongation of N-fatty acyl-CoA with methylamalonyl-CoA (not malonyl-CoA) as the elongating agent to form mycocerosyl lipids.	LM
	Rv3671c	Rv3671c	Serine protease; hydrolyzes peptides and/or proteins.	IMR
	Rv3800c	Pks13	Polyketide synthase; involved in the final steps of mycolic acid biosynthesis. Catalyses the condensation of two fatty acyl chains.	LM
N Only	Rv0045c	Rv0045c	Converts unknown esters to corresponding free acid and alcohol.	LM
	Rv0125	PepA	Probable serine protease; possibly hydrolyzes peptides and/or proteins.	IMR
	Rv0217c	LipW	Probable esterase; lipolytic enzyme probably involved in cellular metabolism.	IMR
	Rv0405	Pks6	Polyketide synthase possibly involved in lipid synthesis.	LM
	Rv0646c	LipG	Probable esterase; lipolytic enzyme involved in cellular metabolism.	IMR
	Rv0774c	Rv0774c	Unknown; could possibly have lipolytic activity.	CWP
	Rv1062	Patatin (Uncharacterized protein)	Function unknown.	CH

	Rv Number	Protein Name	Function	Category[a]
	Rv1191	Rv1191	Converts unknown esters to corresponding free acid and alcohol.	CH
	Rv1399c	LipH (NlhH)	Converts unknown esters to corresponding free acid and alcohol.	IMR
	Rv1400c	LipI	Converts unknown esters to corresponding free acid and alcohol.	IMR
	Rv1426c	LipO	Converts unknown esters to corresponding free acid and alcohol.	IMR
	Rv1527c	Pks5	Polyketide synthase; involved in polyketide metabolism.	LM
	Rv1923	LipD	Converts unknown esters to corresponding free acid and alcohol.	IMR
	Rv2045c	LipT	Converts unknown esters to corresponding free acid and alcohol.	IMR
	Rv2214c	EphD	Probable oxidoreductase; thought to be involved in detoxification reactions following oxidative damage to lipids.	VDA
	Rv2223c	Carboxylesterase B (CaeB)	Function unknown; thought to hydrolyze peptides and/or proteins.	CWP
	Rv2301	Culp2	Function unknown; cutinase-like protein.	CWP
	Rv2385	MbtJ	Putative acetyl hydrolase; involved in the biogenesis of the hydroxyphenyloxazoline-containing siderophore mycobactins. Possibly required for N-hydroxylation of the two lysine residues at some stage during mycobactin assembly.	LM
	Rv2695	Rv2695	Conserved hypothetical alanine rich protein; function unknown.	CH
	Rv2888c	AmiC	Amidase; hydrolyzes a monocarboxylic acid amide and generates a monocarboxylate.	IMR
	Rv3203	LipV	Converts unknown esters to corresponding free acid and alcohol.	IMR
	Rv3341	Homoserine O-acetyltransferase	Catalyzes acylation of L-homoserine. Involved in biosynthesis of methionine; homoserine transacetylase variant; first step.	IMR
	Rv3375	AmiD	Putative amidase; involved in cellular metabolism.	IMR
	Rv3452	Culp4	Cutinase-like protein shown to have esterase and phospholipase activity.	CWP
	Rv3775	LipE	Converts unknown esters to corresponding free acid and alcohol.	IMR
	Rv3825c	Pks2	Phthioceranic/hydroxyphthioceranic acid synthase; supposedly involved in lipid metabolism.	LM
R Only	Rv0129c	Ag85c Fibronectin-binding protein C (Fbps C)	Diacylglycerol acyltransferase/mycolyltransferase. Proteins of the antigen 85 complex are responsible for the high affinity of mycobacteria to fibronectin. Possesses a mycolyltransferase activity required for the biogenesis of trehalose dimycolate (cord factor), a dominant structure necessary for maintaining cell wall integrity.	LM

	Rv Number	Protein Name	Function	Category[a]
N and H	Rv0554	BpoC	Putative non-heme bromoperoxidase; supposedly involved in detoxification reactions.	VDA
	Rv1192	Rv1192	Probable acetyl transferase.	CH
	Rv1223	HtrA	Probable serine protease; possibly hydrolyzes peptides and/or proteins (seems to cleave preferentially after serine residue).	IMR
	Rv1497	LipL	Converts unknown esters to corresponding free acid and alcohol.	IMR
	Rv1984c	Culp1	Cutinase-like protein shown to have esterase and lipase activity.	CWP
	Rv2037c	Rv2037c	Conserved transmembrane protein; function unknown.	CWP
	Rv2284	LipM	Converts unknown esters to corresponding free acid and alcohol.	IMR
	Rv2363	AmiA2	Generates monocarboxylate from monocarboxylic acid amide.	IMR
	Rv2715	Rv2715	Function unknown; probably involved in cellular metabolism.	IMR
	Rv2928	TesA	Thioesterase; probably involved in biosynthesis of phthiocerol dimycocerosate (PDIM).	LM
	Rv2970c	LipN	Converts unknown esters to corresponding free acid and alcohol.	IMR
N and R	Rv3084	LipR	Converts unknown esters to corresponding free acid and alcohol.	IMR

Entries are distinguished based on their identification in different growth conditions: all conditions, normoxia only (N Only), reactivation only (R Only), hypoxia and normoxia (H and N), and reactivation and normoxia (R and N).

[a]As annotated on TubercuList: http://www.tuberculist.epfl.ch (IMR, intermediary metabolism and respiration; LM, lipid metabolism; CWP, cell wall and cell processes; CH, conserved hypotheticals; VDA, virulence, detoxification, adaptation).

Table A.2. Total unique spectral counts of serine hydrolases identified by ABPP with desthiobiotin-FP.

				Spectral Counts Per Sample								
	Accession Number	Rv	Gene Name	N1	N2	N3	H1	H2	H3	R1	R2	R3
All Conditions	O07427	Rv0183	*Rv0183*	9	14	11	10	8	7	7	6	3
	O07178	Rv0457c	*Rv0457c*	22	25	24	20	12	10	16	11	19
	P9WQ97	Rv1263	*amiB2*	9	7	9	12	10	10	9	5	9
	O33185	Rv1683	*Rv1683*	31	39	37	19	16	25	7	7	7
	P9WHR3	Rv2224c	*caeA*	17	15	15	17	20	17	20	9	16
	P95029	Rv2524c	*fas*	49	58	55	32	3		29	3	
	I6Y231	Rv2940c	*mas*	53	50	41	33	37		28	25	21
	P9WHR9	Rv3671c	*Rv3671c*	6	6	5	8	8	9	4	5	5
	I6X8D2	Rv3800c	*pks13*	74	78	71	36	35	2	28	16	26
N Only	I6XU97	Rv0045c	*Rv0045c*	11	14	11						
	O07175	Rv0125	*pepA*	2	3	2						
	P96399	Rv0217c	*lipW*	6	7	6						
	O86335	Rv0405	*pks6*		13	10						
	P96935	Rv0646c	*lipG*	8	13	11						
	I6Y8R4	Rv0774c	*Rv0774c*	5	7	4						
	O53410	Rv1062	*Rv1062*	8	3	4						
	O05293	Rv1191	*Rv1191*	10	14	9						
	P9WK87	Rv1399c	*nlhH, lipH*	6	7	7						
	P71668	Rv1400c	*lipI*	9	12	12						
	O06832	Rv1426c	*lipO*	6	7	5						
	O53901	Rv1527c	*pks5*	12	10							
	P95290	Rv1923	*lipD*	13	16	19	3					
	O53488	Rv2045c	*lipT*	7	4	5						
	P9WGS3	Rv2214c	*ephD*	2	3	8						
	P9WHR5	Rv2223c	*caeB*	2	9	9						
	P9WP41	Rv2301	*cut2, culp2*	5	5	4						
	Q79FE8	Rv2385	*mbtJ*	4	6	3						
	I6Y1I1	Rv2695	*Rv2695*	6	5	7						
	P9WQ95	Rv2888c	*amiC*	3	6	3			4			
	L0TC47	Rv3203	*lipV*	7	8	8						
	P9WJY9	Rv3341	*metX, metA*	3	9	11						
	P9WQ93	Rv3375	*amiD*	9	10	8						
	O06319	Rv3452	*cut4, culp4*		2	4						
	P72041	Rv3775	*lipE*	13	11	14						
	P9WQE9	Rv3825c	*pks2 ,msl-2*	63	30	29						
R Only	P9WQN9	Rv0129c	*fbpC, mpt45*							3		4
N and H	P9WNH1	Rv0554	*bpoC*	14	14	14	6	4				
	O05294	Rv1192	*Rv1192*	7	11	9		2	5			
	O06291	Rv1223	*htrA*	10	11	12	12	14	10			
	P71778	Rv1497	*lipL*		3	3	5		3			
	P9WP43	Rv1984c	*Rv1984c*	6	6	8	4	6				
	L0TB61	Rv2037c	*Rv2037c*	6	4	5	4	6	6			4
	Q50681	Rv2284	*lipM*	17	19	15	13	5	2			
	P9WQ99	Rv2363	*amiA2*	5	11	7	10	6	5			5
	P9WNH3	Rv2715	*Rv2715*	14	16	15	7	6				
	P9WQD5	Rv2928	*tesA*	11	13	12	8	6				
	P95125	Rv2970c	*lipN*	9	11	10	2	3				
N and R	P9WK85	Rv3084	*lipR*	7	6	4				5	3	2

Entries are distinguished based on their identification in different growth conditions: all conditions, normoxia only (N Only), reactivation only (R Only), normoxia and hypoxia (N and H), and normoxia and reactivation (N and R).

Appendix B: Protocol for Activity-Based Protein Profiling with Desthiobiotin-FP

This protocol is modified from the Thermo Scientific/Pierce instructions for ActivX probes and combined with a proteomic profiling protocol.[205] I have included this detailed protocol because it has been optimized for the enrichment of *Mtb* serine hydrolases.

Reagents and Buffers

- **2X SDS-PAGE loading buffer (reducing):** 100 mM Tris-Cl (pH 7), 4% (w/v) SDS, 0.2% (w/v) bromophenol blue, 20% (v/v) glycerol, 200 mM dithiothreitol (DTT)
    - Store the SDS-PAGE loading buffer without DTT at room temperature.
    - Add DTT from a 1 M frozen stock just prior to use.
- **Lysis Buffer:** 50 mM Tris-Cl (pH 7.5 at 4 °C), 200 mM NaCl, 0.5 mM $CaCl_2$, 0.5 mM $MgCl_2$, 0.2% (v/v) Triton X-100
- **5 M Urea Resuspension Buffer (URB):** 5 M urea, 1X PBS, 0.1% (v/v) Triton X-100
- **Urea Wash Buffer (UWB):** 4 M urea, 1X PBS (pH 7.4).
- **Wash Buffer A (WB-A):** 1% (v/v) Triton X-100, 1X PBS (pH 7.4)
- **Wash Buffer B (WB-B):** 50 mM ammonium bicarbonate

- **Elution Buffer (EB):** 0.1% (v/v) trifluoroacetic acid (TFA), 50% (v/v) acetonitrile
- **0.5 M *tris*(2-carboxyethyl)phosphine (TCEP); make fresh**
- **0.5 M iodoacetamide; make fresh**
- **5 mM $CaCl_2$**
- **Blotting Buffer (4 L):** 400 mL 10X Tris/Glycine (Bio-Rad), 800 mL MeOH, 2800 mL H_2O
- **10X TBS (1 L):** 60.6 g Tris, 87.6 g NaCl
    - Dissolve Tris and NaCl in 800 mL H_2O.
    - Adjust to pH 7.5 with HCl.
    - Bring to 1 L with H_2O.
- **TBS (1 L):** 100 mL 10X TBS, 900 mL H_2O
- **TBST (1 L):** 100 mL 10X TBS, 10 mL 10% (v/v) Tween 20, 890 mL H_2O
- **Blocking Buffer:** 5% (w/v) BSA in TBST.
    - Heat-inactivate for 20 min at 56 °C.
    - Gravity-filter to remove particulates.
    - Store at 4 °C for up to 6 months.

A. Serine hydrolase labeling with ActivX Desthiobiotin-FP

1. Equilibrate the ActivX Desthiobiotin-FP (Fisher, PI88317) to room temperature in a desiccator.

2. Dissolve the probe in 10 μL DMSO (1 mM stock).
    a. Store unused probe at –80 °C for up to 6 months.
3. Concentrate lysate using a 10 kDa MWCO centrifugal filter.
    a. If possible, use 1 mg of total protein.
4. Bring lysate to 45 μL in Lysis Buffer.
5. Add 5 μL of 1 mM Desthiobiotin-FP (100 μM final concentration).
6. Incubate the samples for 1 h at room temperature.
7. Also prepare unlabeled sample for WB analysis: 2 μg lysate + appropriate volume of SDS-LD

B. Labeled protein enrichment

1. Use Zeba Spin Desalting Column (7K MWCO, Thermo Scientific, 89882) to remove unreacted probe.
    a. Exchange into 500 μL of URB.
    b. Save 25 μL of labeled sample for WB analysis.
    c. *Pause Point:* Samples can be stored at –20 °C overnight if necessary.
2. Pre-wash 250 μL (bed volume) of High Capacity Streptavidin Agarose resin (Pierce, 20357):
    a. Add 500 μL of 50% slurry to a clean microcentrifuge tube. Pellet resin.
    b. Wash with 250 μL of URB (x2).

3. Add labeled sample to pelleted streptavidin resin.
    a. *Pause Point:* Incubate overnight at 4 °C with constant rotation.
4. Load samples on Thermo spin columns (Fisher, PI69725).
5. Centrifuge at 1000 x g for 2 min and remove supernatant.
    a. *Note:* Save supernatant in case binding did not occur as expected
6. Add 500 µL of UWB to each column and vortex to mix. Repeat wash step.
    a. *Note:* Save all washes for Western blot analysis.
7. Wash each column thrice with 500 μL of WB-A.
8. Wash each column twice with 500 μL of WB-B.
9. Wash each column twice with 500 μL of 1X PBS (pH 7.4).
10. Wash each column twice with 500 μL of WB-B.
    a. Prior to pelleting second wash, remove 50 μL of suspension for “Enriched” sample.
        i. Spin down and remove supernatant.
        ii. Add 20 μL of SDS-PAGE loading buffer to resin and store at –20 °C until further use.
11. Perform acetone precipitation on 200 μL aliquots of supernatant and each wash step.

12. Resuspend pellets in 20 μL of WB-B. Add 20 μL of SDS-PAGE loading buffer and boil for 5 min.

C. On-bead trypsinization

1. Resuspend the resin from each column in 435 μL of NW-B.
    a. (Use 87 μL per 100 μL of 50% slurry used for enrichment.)
    b. This “reduced” volume is to compensate for a later volume gain caused by dissolving urea.
2. Transfer the resuspended resin to a clean microcentrifuge tube.
3. Heat the suspension for 10 min at 70 °C with periodic vortexing.
4. Immediately add 90 mg of urea (final concentration 2–3 M).
5. Allow the suspension to cool to room temperature.
6. Add 3.13 μL of 0.5 M TCEP (final concentration = 3.13 mM). Incubate at room temperature with constant agitation for 30 min.
7. Add 11.25 μL of 0.5 M iodoacetamide (final concentration = 11.25 mM). Incubate at room temperature with constant agitation (protected from light) for 30 min.
8. Add 10 μL of 5 mM $CaCl_2$ (final concentration = 0.1 mM).
9. Add 2.5 μL of 0.4 μg/μL trypsin (1 μg) to suspension.
10. Incubate overnight at 37 °C with constant agitation.
11. Remove the supernatant containing the tryptic peptides using a clean Thermo spin column.

12. Resuspend the resin in 250 μL of WB-B. Remove 50 μL. Pellet this aliquot and remove the supernatant.
    a. Add 25 μL of SDS-PAGE loading buffer to pelleted resin and store at –20 °C until further use as “Post-Trypsinization” sample.
13. Collect WB-B from the remaining resin and add this to the tryptic peptides.
14. Add 250 μL of EB to the resin. Incubate for 3 min and centrifuge to collect flow through containing active-site peptides. Add this to the tryptic peptides.
    a. Repeat with an additional 250 μL of EB (x2).
    b. *Pause Point:* Tryptic peptide samples can be stored at –20 °C prior to MS analysis.

D. Western blot detection

1. Boil all samples for 5 min. Centrifuge to pellet aggregates and insoluble material.
2. Load samples (5 μL/well) on a 26-well 10 or 12% Bis-Tris gel (Bio-Rad).
3. Run at 180 V, 55 min in 1X XT-MES at 4 °C.
    a. The low temperature keeps the protein from running in a “smile.”

4. Transfer proteins to Immobilon-P (PVDF) membrane.
    a. Pre-soak membrane in MeOH, and soak everything in Blotting Buffer.
    b. Transfer at 90 V for 1 h at 4 °C (with ice pack in rig).
5. Stain membrane with Ponceau S and image.
6. Wash membrane with TBS for ~10 min (x2).
7. Block for 1 h in 5% BSA/TBST (Blocking Buffer).
8. Dilute anti-biotin-HRP (Jackson ImmunoResearch, 200-032-211) 1:25,000 in Blocking Buffer.
9. Decant off blocking buffer and incubate membrane with anti-biotin-HRP for 1 h at rt.
    a. Can also use 1:50,000 anti-biotin-HRP overnight at 4 °C.
10. Decant and quickly rinse membrane with a small volume of TBST.
11. Wash membrane with TBST (x2) followed by TBS (~10 min each wash).
12. Image using chemiluminescent substrate.
    a. Mix SuperSignal West Pico (Fisher, PI34077) reagents 1:1.
        i. Make 0.1 mL of SuperSignal West Pico substrate per cm^2 of membrane.
    b. Incubate membrane in substrate for 3–5 min.
    c. Detect chemiluminescence on an appropriate imager (e.g., MyECL or FluorChemQ).

References

[1] Comas, I., Coscolla, M., Luo, T., Borrell, S., Holt, K. E., Kato-Maeda, M., Parkhill, J., Malla, B., Berg, S., Thwaites, G., Yeboah-Manu, D., Bothamley, G., Mei, J., Wei, L., Bentley, S., Harris, S. R., Niemann, S., Diel, R., Aseffa, A., Gao, Q., Young, D., and Gagneux, S. (2013) Out-of-Africa migration and Neolithic coexpansion of *Mycobacterium tuberculosis* with modern humans, *Nat. Genet. 45*, 1176-1182.

[2] Brites, D., and Gagneux, S. (2015) Co-evolution of *Mycobacterium tuberculosis* and *Homo sapiens*, *Immunol. Rev. 264*, 6-24.

[3] Gonzalo-Asensio, J., Malaga, W., Pawlik, A., Astarie-Dequeker, C., Passemar, C., Moreau, F., Laval, F., Daffé, M., Martin, C., Brosch, R., and Guilhot, C. (2014) Evolutionary history of tuberculosis shaped by conserved mutations in the PhoPR virulence regulator, *Proc. Natl. Acad. Sci. USA 111*, 11491-11496.

[4] Paulson, T. (2013) Epidemiology: A mortal foe, *Nature 502*, S2-3.

[5] Dye, C., and Williams, B. G. (2010) The Population Dynamics and Control of Tuberculosis, *Science 328*, 856-861.

[6] Daniel, T. M. (2006) The history of tuberculosis, *Respir. Med. 100*, 1862-1870.

[7] Sakula, A. (1979) Robert Koch (1843–1910): Founder of the science of bacteriology and discoverer of the tubercle bacillus, *Br. J. Dis. Chest 73*, 389-394.

[8] Moliva, J. I., Turner, J., and Torrelles, J. B. (2015) Prospects in *Mycobacterium bovis* Bacille Calmette et Guérin (BCG) vaccine diversity and delivery: Why does BCG fail to protect against tuberculosis?, *Vaccine 33*, 5035-5041.

[9] Schatz, A., Bugle, E., and Waksman, S. A. (1944) Streptomycin, a Substance Exhibiting Antibiotic Activity Against Gram-Positive and Gram-Negative Bacteria, *Exp. Biol. Med. 55*, 66-69.

[10] (2015) Global Tuberculosis Report 2015, World Health Organization.

[11] Marais, B. J. (2016) The global tuberculosis situation and the inexorable rise of drug-resistant disease, *Adv. Drug Deliv. Rev. 16*, 30050-30053.

[12] Russell, D. G., Cardona, P.-J., Kim, M.-J., Allain, S., and Altare, F. (2009) Foamy macrophages and the progression of the human tuberculosis granuloma, *Nat. Immunol. 10*, 943-948.

[13] Korb, V. C., Chuturgoon, A. A., and Moodley, D. (2016) *Mycobacterium tuberculosis*: Manipulator of Protective Immunity, *Int. J. Mol. Sci. 17*, 131.

[14] Peyron, P., Vaubourgeix, J., Poquet, Y., Levillain, F., Botanch, C., Bardou, F., Daffe, M., Emile, J. F., Marchou, B., Cardona, P. J., de Chastellier, C., and Altare, F. (2008) Foamy macrophages from tuberculous patients' granulomas constitute a nutrient-rich reservoir for *M. tuberculosis* persistence, *PLoS Pathog. 4*, e1000204.

[15] (2016) Tuberculosis Fact Sheet N°104, World Health Organization.

[16] Barry, C. E., 3rd, Boshoff, H. I., Dartois, V., Dick, T., Ehrt, S., Flynn, J., Schnappinger, D., Wilkinson, R. J., and Young, D. (2009) The spectrum of latent tuberculosis: rethinking the biology and intervention strategies, *Nat. Rev. Microbiol. 7*, 845-855.

[17] Esmail, H., Barry, C. E., 3rd, and Wilkinson, R. J. (2012) Understanding latent tuberculosis: the key to improved diagnostic and novel treatment strategies, *Drug Discov. Today*.

[18] Dye, C., Scheele, S., Dolin, P., Pathania, V., and Raviglione, M. C. (1999) Consensus statement. Global burden of tuberculosis: estimated incidence, prevalence, and mortality by country. WHO Global Surveillance and Monitoring Project, *JAMA 282*, 677-686.

[19] Tufariello, J. M., Chan, J., and Flynn, J. L. (2003) Latent tuberculosis: mechanisms of host and bacillus that contribute to persistent infection, *Lancet Infect. Dis. 3*, 578-590.

[20] Nathan, C., and Barry, C. E., 3rd. (2015) TB drug development: immunology at the table, *Immunol. Rev. 264*, 308-318.

[21] May, Y. L., and Ottenhoff, T. H. M. (2008) Not to wake a sleeping giant: new insights into host-pathogen interactions identify new targets for vaccination against latent *Mycobacterium tuberculosis* infection, *Biol. Chem. 389*, 497-511.

[22] Lutge, E. E., Wiysonge, C. S., Knight, S. E., Sinclair, D., and Volmink, J. (2015) Incentives and enablers to improve adherence in tuberculosis, *Cochrane Database Syst. Rev.*, CD007952.

[23] Wayne, L. G. (2001) In Vitro Model of Hypoxically Induced Nonreplicating Persistence of *Mycobacterium tuberculosis*, *Methods Mol. Med. 54*, 247-269.

[24] Betts, J. C., Lukey, P. T., Robb, L. C., McAdam, R. A., and Duncan, K. (2002) Evaluation of a nutrient starvation model of *Mycobacterium tuberculosis* persistence by gene and protein expression profiling, *Mol. Microbiol. 43*, 717-731.

[25] Grant, S. S., Kawate, T., Nag, P. P., Silvis, M. R., Gordon, K., Stanley, S. A., Kazyanskaya, E., Nietupski, R., Golas, A., Fitzgerald, M., Cho, S., Franzblau, S. G., and Hung, D. T. (2013) Identification of novel inhibitors of nonreplicating *Mycobacterium tuberculosis* using a carbon starvation model, *ACS Chem. Biol. 8*, 2224-2234.

[26] Bryk, R., Gold, B., Venugopal, A., Singh, J., Samy, R., Pupek, K., Cao, H., Popescu, C., Gurney, M., Hotha, S., Cherian, J., Rhee, K., Ly, L., Converse, P. J., Ehrt, S., Vandal, O., Jiang, X., Schneider, J., Lin, G., and Nathan, C. (2008) Selective killing of nonreplicating mycobacteria, *Cell Host Microbe 3*, 137-145.

[27] Deb, C., Lee, C. M., Dubey, V. S., Daniel, J., Abomoelak, B., Sirakova, T. D., Pawar, S., Rogers, L., and Kolattukudy, P. E. (2009) A novel in vitro multiple-stress dormancy model for *Mycobacterium tuberculosis* generates a lipid-loaded, drug-tolerant, dormant pathogen, *PLoS One 4*, e6077.

[28] Gold, B., Warrier, T., and Nathan, C. (2015) A multi-stress model for high throughput screening against non-replicating *Mycobacterium tuberculosis*, *Methods Mol. Biol. 1285*, 293-315.

[29] Loebel, R. O., Shorr, E., and Richardson, H. B. (1933) The Influence of Foodstuffs upon the Respiratory Metabolism and Growth of Human Tubercle Bacilli, *J. Bacteriol. 26*, 139-166.

[30] Loebel, R. O., Shorr, E., and Richardson, H. B. (1933) The Influence of Adverse Conditions upon the Respiratory Metabolism and Growth of Human Tubercle Bacilli, *J. Bacteriol. 26*, 167-200.

[31] Rodriguez, J. G., Hernandez, A. C., Helguera-Repetto, C., Aguilar Ayala, D., Guadarrama-Medina, R., Anzola, J. M., Bustos, J. R., Zambrano, M. M., Gonzalez, Y. M. J., Garcia, M. J., and Del Portillo, P. (2014) Global adaptation to a lipid environment triggers the dormancy-related phenotype of *Mycobacterium tuberculosis*, *mBio 5*, e01125-01114.

[32] Gengenbacher, M., Rao, S. P., Pethe, K., and Dick, T. (2010) Nutrient-starved, non-replicating *Mycobacterium tuberculosis* requires respiration, ATP synthase and isocitrate lyase for maintenance of ATP homeostasis and viability, *Microbiology 156*, 81-87.

[33] Wu, M. L., Tan, J., and Dick, T. (2015) Eagle Effect in Nonreplicating Persister Mycobacteria, *Antimicrob. Agents Chemother. 59*, 7786-7789.

[34] Via, L. E., Lin, P. L., Ray, S. M., Carrillo, J., Allen, S. S., Eum, S. Y., Taylor, K., Klein, E., Manjunatha, U., Gonzales, J., Lee, E. G., Park, S. K., Raleigh, J. A., Cho, S. N., McMurray, D. N., Flynn, J. L., and Barry, C. E., 3rd. (2008) Tuberculous granulomas are hypoxic in guinea pigs, rabbits, and nonhuman primates, *Infect. Immun. 76*, 2333-2340.

[35] Sohaskey, C. D., and Voskuil, M. I. (2015) In vitro models that utilize hypoxia to induce non-replicating persistence in Mycobacteria, *Methods Mol. Biol. 1285*, 201-213.

[36] Sartain, M. J., Dick, D. L., Rithner, C. D., Crick, D. C., and Belisle, J. T. (2011) Lipidomic analyses of *Mycobacterium tuberculosis* based on accurate mass measurements and the novel "Mtb LipidDB", *J. Lipid Res. 52*, 861-872.

[37] Deb, C., Daniel, J., Sirakova, T. D., Abomoelak, B., Dubey, V. S., and Kolattukudy, P. E. (2006) A novel lipase belonging to the hormone-sensitive lipase family induced under starvation to utilize stored triacylglycerol in *Mycobacterium tuberculosis*, *J. Biol. Chem. 281*, 3866-3875.

[38] Low, K. L., Rao, P. S., Shui, G., Bendt, A. K., Pethe, K., Dick, T., and Wenk, M. R. (2009) Triacylglycerol utilization is required for regrowth of in vitro hypoxic nonreplicating *Mycobacterium bovis* bacillus Calmette-Guerin, *J. Bacteriol. 191*, 5037-5043.

[39] Daniel, J., Maamar, H., Deb, C., Sirakova, T. D., and Kolattukudy, P. E. (2011) *Mycobacterium tuberculosis* uses host triacylglycerol to accumulate lipid droplets and acquires a dormancy-like phenotype in lipid-loaded macrophages, *PLoS Pathog. 7*, e1002093.

[40] Brust, B., Lecoufle, M., Tuaillon, E., Dedieu, L., Canaan, S., Valverde, V., and Kremer, L. (2011) *Mycobacterium tuberculosis* lipolytic enzymes as potential biomarkers for the diagnosis of active tuberculosis, *PLoS One 6*, e25078.

[41] Cole, S. T., Brosch, R., Parkhill, J., Garnier, T., Churcher, C., Harris, D., Gordon, S. V., Eiglmeier, K., Gas, S., Barry, C. E., Tekaia, F., Badcock, K.,

Basham, D., Brown, D., Chillingworth, T., Connor, R., Davies, R., Devlin, K., Feltwell, T., Gentles, S., Hamlin, N., Holroyd, S., Hornsby, T., Jagels, K., Krogh, A., McLean, J., Moule, S., Murphy, L., Oliver, K., Osborne, J., Quail, M. A., Rajandream, M. A., Rogers, J., Rutter, S., Seeger, K., Skelton, J., Squares, R., Squares, S., Sulston, J. E., Taylor, K., Whitehead, S., and Barrell, B. G. (1998) Deciphering the biology of *Mycobacterium tuberculosis* from the complete genome sequence, *Nature 393*, 537-544.

[42] Ali, Y. B., Verger, R., and Abousalham, A. (2012) Lipases or esterases: does it really matter? Toward a new bio-physico-chemical classification, *Methods Mol. Biol. 861*, 31-51.

[43] Chahinian, H., Nini, L., Boitard, E., Dubes, J. P., Comeau, L. C., and Sarda, L. (2002) Distinction between esterases and lipases: a kinetic study with vinyl esters and TAG, *Lipids 37*, 653-662.

[44] Chahinian, H., Ali, Y. B., Abousalham, A., Petry, S., Mandrich, L., Manco, G., Canaan, S., and Sarda, L. (2005) Substrate specificity and kinetic properties of enzymes belonging to the hormone-sensitive lipase family: Comparison with non-lipolytic and lipolytic carboxylesterases, *Biochim. Biophys. Acta 1738*, 29-36.

[45] Camus, J. C., Pryor, M. J., Medigue, C., and Cole, S. T. (2002) Re-annotation of the genome sequence of *Mycobacterium tuberculosis* H37Rv, *Microbiology 148*, 2967-2973.

[46] Lun, S., and Bishai, W. R. (2007) Characterization of a novel cell wall-anchored protein with carboxylesterase activity required for virulence in *Mycobacterium tuberculosis*, *J. Biol. Chem. 282*, 18348-18356.

[47] West, N. P., Chow, F. M., Randall, E. J., Wu, J., Chen, J., Ribeiro, J. M., and Britton, W. J. (2009) Cutinase-like proteins of *Mycobacterium tuberculosis*: characterization of their variable enzymatic functions and active site identification, *FASEB J. 23*, 1694-1704.

[48] Guo, J., Zheng, X., Xu, L., Liu, Z., Xu, K., Li, S., Wen, T., Liu, S., and Pang, H. (2010) Characterization of a novel esterase Rv0045c from *Mycobacterium tuberculosis*, *PLoS One 5*, 10.1371/journal.pone.0013143.

[49] Sultana, R., Vemula, M. H., Banerjee, S., and Guruprasad, L. (2013) The PE16 (Rv1430) of *Mycobacterium tuberculosis* is an esterase belonging to serine hydrolase superfamily of proteins, *PLoS One 8*, e55320.

[50] Chen, L., Dang, G., Deng, X., Cao, J., Yu, S., Wu, D., Pang, H., and Liu, S. (2014) Characterization of a novel exported esterase Rv3036c from *Mycobacterium tuberculosis*, *Protein Expr. Purif. 104C*, 50-56.

[51] Dang, G., Chen, L., Li, Z., Deng, X., Cui, Y., Cao, J., Yu, S., Pang, H., and Liu, S. (2015) Expression, Purification and Characterisation of Secreted Esterase Rv2525c from *Mycobacterium tuberculosis*, *Appl. Biochem. Biotechnol. 176*, 1-12.

[52] Quadri, L. E. N., Sello, J., Keating, T. A., Weinreb, P. H., and Walsh, C. T. (1998) Identification of a *Mycobacterium tuberculosis* gene cluster encoding the biosynthetic enzymes for assembly of the virulence-conferring siderophore mycobactin, *Chem. Biol. 5*, 631-645.

[53] Sinha, S. C., Wetterer, M., Sprang, S. R., Schultz, J. E., and Linder, J. U. (2005) Origin of asymmetry in adenylyl cyclases: structures of *Mycobacterium tuberculosis* Rv1900c, *EMBO J 24*, 663-673.

[54] Cao, J., Dang, G., Li, H., Li, T., Yue, Z., Li, N., Liu, Y., Liu, S., and Chen, L. (2015) Identification and Characterization of Lipase Activity and Immunogenicity of LipL from *Mycobacterium tuberculosis*, *PLoS One 10*, e0138151.

[55] Singh, G., Kumar, A., Arya, S., Gupta, U. D., Singh, K., and Kaur, J. (2016) Characterization of a novel esterase Rv1497 of *Mycobacterium tuberculosis* H37Rv demonstrating β-lactamase activity, *Enzyme Microb. Technol. 82*, 180-190.

[56] Voladri, R. K., Lakey, D. L., Hennigan, S. H., Menzies, B. E., Edwards, K. M., and Kernodle, D. S. (1998) Recombinant expression and characterization of the major beta-lactamase of *Mycobacterium tuberculosis*, *Antimicrob. Agents Chemother. 42*, 1375-1381.

[57] Camacho, L. R., Ensergueix, D., Perez, E., Gicquel, B., and Guilhot, C. (1999) Identification of a virulence gene cluster of *Mycobacterium tuberculosis* by signature-tagged transposon mutagenesis, *Mol. Microbiol. 34*, 257-267.

[58] Zhang, M., Wang, J. D., Li, Z. F., Xie, J., Yang, Y. P., Zhong, Y., and Wang, H. H. (2005) Expression and characterization of the carboxyl esterase Rv3487c from *Mycobacterium tuberculosis*, *Protein Expr. Purif. 42*, 59-66.

[59] Srinivas, M., Rajakumari, S., Narayana, Y., Joshi, B., Katoch, V. M., Rajasekharan, R., and Balaji, K. N. (2008) Functional characterization of the

phospholipase C activity of Rv3487c and its localization on the cell wall of *Mycobacterium tuberculosis*, *J. Biosci. 33*, 221-230.

[60] Delorme, V., Diomande, S. V., Dedieu, L., Cavalier, J. F., Carriere, F., Kremer, L., Leclaire, J., Fotiadu, F., and Canaan, S. (2012) MmPPOX inhibits *Mycobacterium tuberculosis* lipolytic enzymes belonging to the hormone-sensitive lipase family and alters mycobacterial growth, *PLoS One 7*, e46493.

[61] Lafontan, M., and Langin, D. (2009) Lipolysis and lipid mobilization in human adipose tissue, *Prog. Lipid Res. 48*, 275-297.

[62] Lampidonis, A. D., Rogdakis, E., Voutsinas, G. E., and Stravopodis, D. J. (2011) The resurgence of Hormone-Sensitive Lipase (HSL) in mammalian lipolysis, *Gene 477*, 1-11.

[63] Galagan, J. E., Minch, K., Peterson, M., Lyubetskaya, A., Azizi, E., Sweet, L., Gomes, A., Rustad, T., Dolganov, G., Glotova, I., Abeel, T., Mahwinney, C., Kennedy, A. D., Allard, R., Brabant, W., Krueger, A., Jaini, S., Honda, B., Yu, W. H., Hickey, M. J., Zucker, J., Garay, C., Weiner, B., Sisk, P., Stolte, C., Winkler, J. K., Van de Peer, Y., Iazzetti, P., Camacho, D., Dreyfuss, J., Liu, Y., Dorhoi, A., Mollenkopf, H. J., Drogaris, P., Lamontagne, J., Zhou, Y., Piquenot, J., Park, S. T., Raman, S., Kaufmann, S. H., Mohney, R. P., Chelsky, D., Moody, D. B., Sherman, D. R., and Schoolnik, G. K. (2013) The *Mycobacterium tuberculosis* regulatory network and hypoxia, *Nature 499*, 178-183.

[64] Leistikow, R. L., Morton, R. A., Bartek, I. L., Frimpong, I., Wagner, K., and Voskuil, M. I. (2010) The *Mycobacterium tuberculosis* DosR regulon assists in metabolic homeostasis and enables rapid recovery from nonrespiring dormancy, *J. Bacteriol. 192*, 1662-1670.

[65] Mehra, S., Foreman, T. W., Didier, P. J., Ahsan, M. H., Hudock, T. A., Kissee, R., Golden, N. A., Gautam, U. S., Johnson, A. M., Alvarez, X., Russell-Lodrigue, K. E., Doyle, L. A., Roy, C. J., Niu, T., Blanchard, J. L., Khader, S. A., Lackner, A. A., Sherman, D. R., and Kaushal, D. (2015) The DosR Regulon Modulates Adaptive Immunity and Is Essential for *Mycobacterium tuberculosis* Persistence, *Am. J. Respir. Crit. Care Med. 191*, 1185-1196.

[66] Park, H. D., Guinn, K. M., Harrell, M. I., Liao, R., Voskuil, M. I., Tompa, M., Schoolnik, G. K., and Sherman, D. R. (2003) Rv3133c/dosR is a transcription factor that mediates the hypoxic response of *Mycobacterium tuberculosis*, *Mol. Microbiol. 48*, 833-843.

[67] Minch, K. J., Rustad, T. R., Peterson, E. J., Winkler, J., Reiss, D. J., Ma, S., Hickey, M., Brabant, W., Morrison, B., Turkarslan, S., Mawhinney, C., Galagan, J. E., Price, N. D., Baliga, N. S., and Sherman, D. R. (2015) The DNA-binding network of *Mycobacterium tuberculosis*, *Nat. Commun. 6*, 5829.

[68] Rustad, T. R., Minch, K. J., Ma, S., Winkler, J. K., Hobbs, S., Hickey, M., Brabant, W., Turkarslan, S., Price, N. D., Baliga, N. S., and Sherman, D. R. (2014) Mapping and manipulating the *Mycobacterium tuberculosis* transcriptome using a transcription factor overexpression-derived regulatory network, *Genome Biol. 15*, 502.

[69] Turkarslan, S., Peterson, E. J., Rustad, T. R., Minch, K. J., Reiss, D. J., Morrison, R., Ma, S., Price, N. D., Sherman, D. R., and Baliga, N. S. (2015) A comprehensive map of genome-wide gene regulation in *Mycobacterium tuberculosis*, *Sci. Data 2*, 150010.

[70] Point, V., Malla, R. K., Diomande, S., Martin, B. P., Delorme, V., Carriere, F., Canaan, S., Rath, N. P., Spilling, C. D., and Cavalier, J. F. (2012) Synthesis and kinetic evaluation of cyclophostin and cyclipostins phosphonate analogs as selective and potent inhibitors of microbial lipases, *J. Med. Chem. 55*, 10204-10219.

[71] Point, V., Malla, R. K., Carriere, F., Canaan, S., Spilling, C. D., and Cavalier, J. F. (2013) Enantioselective inhibition of microbial lipolytic enzymes by nonracemic monocyclic enolphosphonate analogues of cyclophostin, *J. Med. Chem. 56*, 4393-4401.

[72] Saxena, A. K., Roy, K. K., Singh, S., Vishnoi, S. P., Kumar, A., Kashyap, V. K., Kremer, L., Srivastava, R., and Srivastava, B. S. (2013) Identification and characterisation of small-molecule inhibitors of Rv3097c-encoded lipase (LipY) of *Mycobacterium tuberculosis* that selectively inhibit growth of bacilli in hypoxia, *Int. J. Antimicrob. Agents 42*, 27-35.

[73] Schubert, Olga T., Mouritsen, J., Ludwig, C., Röst, Hannes L., Rosenberger, G., Arthur, Patrick K., Claassen, M., Campbell, David S., Sun, Z., Farrah, T., Gengenbacher, M., Maiolica, A., Kaufmann, Stefan H. E., Moritz, Robert L., and Aebersold, R. (2013) The Mtb Proteome Library: A Resource of Assays to Quantify the Complete Proteome of *Mycobacterium tuberculosis*, *Cell Host Microbe 13*, 602-612.

[74] Gopinath, V., Raghunandanan, S., Gomez, R. L., Jose, L., Surendran, A., Ramachandran, R., Pushparajan, A. R., Mundayoor, S., Jaleel, A., and Kumar, R. A. (2015) Profiling the Proteome of *Mycobacterium tuberculosis* during Dormancy and Reactivation, *Mol. Cell. Proteomics 14*, 2160-2176.

[75] Schubert, O. T., Ludwig, C., Kogadeeva, M., Zimmermann, M., Rosenberger, G., Gengenbacher, M., Gillet, L. C., Collins, B. C., Rost, H. L., Kaufmann, S. H., Sauer, U., and Aebersold, R. (2015) Absolute Proteome Composition and Dynamics during Dormancy and Resuscitation of *Mycobacterium tuberculosis*, *Cell Host Microbe 18*, 96-108.

[76] Kruh, N. A., Troudt, J., Izzo, A., Prenni, J., and Dobos, K. M. (2010) Portrait of a pathogen: the *Mycobacterium tuberculosis* proteome *in vivo*, *PLoS One 5*, e13938.

[77] Ramakrishnan, L., Federspiel, N. A., and Falkow, S. (2000) Granuloma-specific expression of *Mycobacterium* virulence proteins from the glycine-rich PE-PGRS family, *Science 288*, 1436-1439.

[78] Brennan, M. J., Delogu, G., Chen, Y., Bardarov, S., Kriakov, J., Alavi, M., and Jacobs, W. R., Jr. (2001) Evidence that mycobacterial PE_PGRS proteins are cell surface constituents that influence interactions with other cells, *Infect. Immun. 69*, 7326-7333.

[79] Li, Y., Miltner, E., Wu, M., Petrofsky, M., and Bermudez, L. E. (2005) A Mycobacterium avium PPE gene is associated with the ability of the bacterium to grow in macrophages and virulence in mice, *Cell. Microbiol. 7*, 539-548.

[80] Basu, S., Pathak, S. K., Banerjee, A., Pathak, S., Bhattacharyya, A., Yang, Z., Talarico, S., Kundu, M., and Basu, J. (2007) Execution of macrophage apoptosis by PE_PGRS33 of *Mycobacterium tuberculosis* is mediated by Toll-like receptor 2-dependent release of tumor necrosis factor-alpha, *J. Biol. Chem. 282*, 1039-1050.

[81] Nair, S., Ramaswamy, P. A., Ghosh, S., Joshi, D. C., Pathak, N., Siddiqui, I., Sharma, P., Hasnain, S. E., Mande, S. C., and Mukhopadhyay, S. (2009) The PPE18 of *Mycobacterium tuberculosis* interacts with TLR2 and activates IL-10 induction in macrophage, *J. Immunol. 183*, 6269-6281.

[82] Daleke, M. H., Cascioferro, A., de Punder, K., Ummels, R., Abdallah, A. M., van der Wel, N., Peters, P. J., Luirink, J., Manganelli, R., and Bitter, W. (2011) Conserved Pro-Glu (PE) and Pro-Pro-Glu (PPE) Protein Domains Target LipY Lipases of Pathogenic Mycobacteria to the Cell Surface via the ESX-5 Pathway, *J. Biol. Chem. 286*, 19024-19034.

[83] Garrett, C. K., Broadwell, L. J., Hayne, C. K., and Neher, S. B. (2015) Modulation of the Activity of *Mycobacterium tuberculosis* LipY by Its PE Domain, *PLoS One 10*, e0135447.

[84] Mishra, K. C., de Chastellier, C., Narayana, Y., Bifani, P., Brown, A. K., Besra, G. S., Katoch, V. M., Joshi, B., Balaji, K. N., and Kremer, L. (2008) Functional role of the PE domain and immunogenicity of the *Mycobacterium tuberculosis* triacylglycerol hydrolase LipY, *Infect. Immun. 76*, 127-140.

[85] Albrethsen, J., Agner, J., Piersma, S. R., Hojrup, P., Pham, T. V., Weldingh, K., Jimenez, C. R., Andersen, P., and Rosenkrands, I. (2013) Proteomic profiling of *Mycobacterium tuberculosis* identifies nutrient-starvation-responsive toxin-antitoxin systems, *Mol. Cell. Proteomics 12*, 1180-1191.

[86] Weldingh, K., Rosenkrands, I., Jacobsen, S., Rasmussen, P. B., Elhay, M. J., and Andersen, P. (1998) Two-dimensional electrophoresis for analysis of *Mycobacterium tuberculosis* culture filtrate and purification and characterization of six novel proteins, *Infect. Immun. 66*, 3492-3500.

[87] Malen, H., Berven, F. S., Fladmark, K. E., and Wiker, H. G. (2007) Comprehensive analysis of exported proteins from *Mycobacterium tuberculosis* H37Rv, *Proteomics 7*, 1702-1718.

[88] Shen, G., Singh, K., Chandra, D., Serveau-Avesque, C., Maurin, D., Canaan, S., Singla, R., Behera, D., and Laal, S. (2012) LipC (Rv0220) is an immunogenic cell surface esterase of *Mycobacterium tuberculosis*, *Infect. Immun. 80*, 243-253.

[89] (2011) The Global Plan to Stop TB 2011-2015: Transforming the Fight Towards Elimination of Tuberculosis, World Health Organization.

[90] Ruhwald, M., and Ravn, P. (2009) Biomarkers of latent TB infection, *Expert Rev. Respir. Med. 3*, 387-401.

[91] Ettinger, W. F., Thukral, S. K., and Kolattukudy, P. E. (1987) Structure of cutinase gene, cDNA, and the derived amino acid sequence from phytopathogenic fungi, *Biochemistry 26*, 7883-7892.

[92] Purdy, R. E., and Kolattukudy, P. E. (1975) Hydrolysis of plant cuticle by plant pathogens. Purification, amino acid composition, and molecular weight of two isozymes of cutinase and a nonspecific esterase from *Fusarium solani f. pisi*, *Biochemistry 14*, 2824-2831.

[93] Egmond, M. R., and de Vlieg, J. (2000) *Fusarium solani pisi* cutinase, *Biochimie 82*, 1015-1021.

[94] Dedieu, L., Serveau-Avesque, C., Kremer, L., and Canaan, S. (2013) Mycobacterial lipolytic enzymes: a gold mine for tuberculosis research, *Biochimie 95*, 66-73.

[95] Schué, M., Maurin, D., Dhouib, R., Bakala N'Goma, J. C., Delorme, V., Lambeau, G., Carriere, F., and Canaan, S. (2010) Two cutinase-like proteins secreted by *Mycobacterium tuberculosis* show very different lipolytic activities reflecting their physiological function, *FASEB J. 24*, 1893-1903.

[96] Parker, S. K., Curtin, K. M., and Vasil, M. L. (2007) Purification and characterization of mycobacterial phospholipase A: an activity associated with mycobacterial cutinase, *J. Bacteriol. 189*, 4153-4160.

[97] Vir, P., Gupta, D., Agarwal, R., and Verma, I. (2014) Interaction of alveolar epithelial cells with CFP21, a mycobacterial cutinase-like enzyme, *Mol. Cell. Biochem. 396*, 187-199.

[98] Mahairas, G. G., Sabo, P. J., Hickey, M. J., Singh, D. C., and Stover, C. K. (1996) Molecular analysis of genetic differences between *Mycobacterium bovis* BCG and virulent *M. bovis*, *J. Bacteriol. 178*, 1274-1282.

[99] Behr, M. A., Wilson, M. A., Gill, W. P., Salamon, H., Schoolnik, G. K., Rane, S., and Small, P. M. (1999) Comparative Genomics of BCG Vaccines by Whole-Genome DNA Microarray, *Science 284*, 1520-1523.

[100] Grover, A., Ahmed, M. F., Verma, I., Sharma, P., and Khuller, G. K. (2006) Expression and purification of the *Mycobacterium tuberculosis* complex-restricted antigen CFP21 to study its immunoprophylactic potential in mouse model, *Protein Expr. Purif. 48*, 274-280.

[101] Kalra, M., Grover, A., Mehta, N., Singh, J., Kaur, J., Sable, S. B., Behera, D., Sharma, P., Verma, I., and Khuller, G. K. (2007) Supplementation with RD antigens enhances the protective efficacy of BCG in tuberculous mice, *Clin. Immunol. 125*, 173-183.

[102] Parker, S. K., Barkley, R. M., Rino, J. G., and Vasil, M. L. (2009) *Mycobacterium tuberculosis* Rv3802c encodes a phospholipase/thioesterase and is inhibited by the antimycobacterial agent tetrahydrolipstatin, *PLoS One 4*, e4281.

[103] Sassetti, C. M., Boyd, D. H., and Rubin, E. J. (2003) Genes required for mycobacterial growth defined by high density mutagenesis, *Mol. Microbiol. 48*, 77-84.

[104] Griffin, J. E., Gawronski, J. D., Dejesus, M. A., Ioerger, T. R., Akerley, B. J., and Sassetti, C. M. (2011) High-resolution phenotypic profiling defines genes essential for mycobacterial growth and cholesterol catabolism, *PLoS Pathog. 7*, e1002251.

[105] Shanahan, E. R., Pinto, R., Triccas, J. A., Britton, W. J., and West, N. P. (2010) Cutinase-like protein-6 of *Mycobacterium tuberculosis* is recognised in tuberculosis patients and protects mice against pulmonary infection as a single and fusion protein vaccine, *Vaccine 28*, 1341-1346.

[106] Cotes, K., Dhouib, R., Douchet, I., Chahinian, H., de Caro, A., Carriere, F., and Canaan, S. (2007) Characterization of an exported monoglyceride lipase from *Mycobacterium tuberculosis* possibly involved in the metabolism of host cell membrane lipids, *Biochem. J. 408*, 417-427.

[107] Dhouib, R., Laval, F., Carriere, F., Daffe, M., and Canaan, S. (2010) A monoacylglycerol lipase from *Mycobacterium smegmatis* Involved in bacterial cell interaction, *J. Bacteriol. 192*, 4776-4785.

[108] Saravanan, P., Dubey, V. K., and Patra, S. (2012) Potential Selective Inhibitors against Rv0183 of *Mycobacterium tuberculosis* Targeting Host Lipid Metabolism, *Chem. Biol. Drug Des. 79*, 1056-1062.

[109] Sassetti, C. M., and Rubin, E. J. (2003) Genetic requirements for mycobacterial survival during infection, *Proc. Natl. Acad. Sci. USA 100*, 12989-12994.

[110] Lamichhane, G., Tyagi, S., and Bishai, W. R. (2005) Designer arrays for defined mutant analysis to detect genes essential for survival of *Mycobacterium tuberculosis* in mouse lungs, *Infect. Immun. 73*, 2533-2540.

[111] Dubnau, E., Fontan, P., Manganelli, R., Soares-Appel, S., and Smith, I. (2002) *Mycobacterium tuberculosis* genes induced during infection of human macrophages, *Infect. Immun. 70*, 2787-2795.

[112] Naffin-Olivos, J. L., Georgieva, M., Goldfarb, N., Madan-Lala, R., Dong, L., Bizzell, E., Valinetz, E., Brandt, G. S., Yu, S., Shabashvili, D. E., Ringe, D., Dunn, B. M., Petsko, G. A., and Rengarajan, J. (2014) *Mycobacterium tuberculosis* Hip1 modulates macrophage responses through proteolysis of GroEL2, *PLoS Pathog. 10*, e1004132.

[113] Rengarajan, J., Murphy, E., Park, A., Krone, C. L., Hett, E. C., Bloom, B. R., Glimcher, L. H., and Rubin, E. J. (2008) *Mycobacterium tuberculosis*

Rv2224c modulates innate immune responses, *Proc. Natl. Acad. Sci. USA 105*, 264-269.

[114] Madan-Lala, R., Peixoto, K. V., Re, F., and Rengarajan, J. (2011) *Mycobacterium tuberculosis* Hip1 dampens macrophage proinflammatory responses by limiting toll-like receptor 2 activation, *Infect. Immun. 79*, 4828-4838.

[115] Madan-Lala, R., Sia, J. K., King, R., Adekambi, T., Monin, L., Khader, S. A., Pulendran, B., and Rengarajan, J. (2014) *Mycobacterium tuberculosis* impairs dendritic cell functions through the serine hydrolase Hip1, *J. Immunol. 192*, 4263-4272.

[116] Xu, L., Guo, J., Zheng, X., Wen, T., Sun, F., Liu, S., and Pang, H. (2010) Crystallization and preliminary X-ray analysis of a novel esterase Rv0045c from *Mycobacterium tuberculosis*, *Acta Crystallogr. Sect. F Struct. Biol. Cryst. Commun. 66*, 1579-1582.

[117] Zheng, X., Guo, J., Xu, L., Li, H., Zhang, D., Zhang, K., Sun, F., Wen, T., Liu, S., and Pang, H. (2011) Crystal structure of a novel esterase Rv0045c from *Mycobacterium tuberculosis*, *PLoS One 6*, e20506.

[118] Park, S. Y., Lee, S. H., Lee, J., Nishi, K., Kim, Y. S., Jung, C. H., and Kim, J. S. (2008) High-resolution structure of ybfF from *Escherichia coli* K12: a unique substrate-binding crevice generated by domain arrangement, *J. Mol. Biol. 376*, 1426-1437.

[119] McCulloch, K. M., Mukherjee, T., Begley, T. P., and Ealick, S. E. (2010) Structure determination and characterization of the vitamin B6 degradative enzyme (E)-2-(acetamidomethylene)succinate hydrolase, *Biochemistry 49*, 1226-1235.

[120] Godinho, L. F., Reis, C. R., Tepper, P. G., Poelarends, G. J., and Quax, W. J. (2011) Discovery of an *Escherichia coli* esterase with high activity and enantioselectivity toward 1,2-*O*-isopropylideneglycerol esters, *Appl. Environ. Microbiol. 77*, 6094-6099.

[121] Lukowski, J. K., Savas, C. P., Gehring, A. M., McKary, M. G., Adkins, C. T., Lavis, L. D., Hoops, G. C., and Johnson, R. J. (2014) Distinct Substrate Selectivity of a Metabolic Hydrolase from *Mycobacterium tuberculosis*, *Biochemistry 53*, 7386-7395.

[122] Kumar, A., Sharma, A., Kaur, G., Makkar, P., and Kaur, J. (2016) Functional characterization of hypothetical proteins of *Mycobacterium*

tuberculosis with possible esterase/lipase signature: a cumulative in silico and in vitro approach, *J. Biomol. Struct. Dyn.*, 1-18.

[123] Ortega, C., Anderson, Lindsey N., Frando, A., Sadler, Natalie C., Brown, Robert W., Smith, Richard D., Wright, Aaron T., and Grundner, C. (2016) Systematic Survey of Serine Hydrolase Activity in *Mycobacterium tuberculosis* Defines Changes Associated with Persistence, *Cell Chem. Biol. 23*, 290-298.

[124] Cravatt, B. F., Wright, A. T., and Kozarich, J. W. (2008) Activity-Based Protein Profiling: From Enzyme Chemistry to Proteomic Chemistry, *Annu. Rev. Biochem. 77*, 383-414.

[125] Puri, A. W., and Bogyo, M. (2009) Using Small Molecules To Dissect Mechanisms of Microbial Pathogenesis, *ACS Chem. Biol. 4*, 603-616.

[126] Stanley, S. A., and Hung, D. T. (2009) Chemical tools for dissecting bacterial physiology and virulence, *Biochemistry 48*, 8776-8786.

[127] Ansong, C., Ortega, C., Payne, S. H., Haft, D. H., Chauvigne-Hines, L. M., Lewis, M. P., Ollodart, A. R., Purvine, S. O., Shukla, A. K., Fortuin, S., Smith, R. D., Adkins, J. N., Grundner, C., and Wright, A. T. (2013) Identification of widespread adenosine nucleotide binding in *Mycobacterium tuberculosis*, *Chem. Biol. 20*, 123-133.

[128] Ravindran, M. S., Rao, S. P., Cheng, X., Shukla, A., Cazenave-Gassiot, A., Yao, S. Q., and Wenk, M. R. (2014) Targeting lipid esterases in mycobacteria grown under different physiological conditions using activity-based profiling with tetrahydrolipstatin (THL), *Mol. Cell. Proteomics 13*, 435-448.

[129] Duckworth, B. P., Wilson, D. J., Nelson, K. M., Boshoff, H. I., Barry, C. E., 3rd, and Aldrich, C. C. (2012) Development of a selective activity-based probe for adenylating enzymes: profiling MbtA Involved in siderophore biosynthesis from *Mycobacterium tuberculosis*, *ACS Chem. Biol. 7*, 1653-1658.

[130] Cohen, S., Kushnick, J. B., and Purdy, C. V. (1953) Observations on mycobacterial esterases with a series of synthetic substrates, *J. Bacteriol. 66*, 266-273.

[131] Grimm, J. B., Heckman, L. M., and Lavis, L. D. (2013) Chapter One - The Chemistry of Small-Molecule Fluorogenic Probes, In *Progress in Molecular Biology and Translational Science*, pp 1-34, Academic Press.

[132] Kong, Y., Yao, H., Ren, H., Subbian, S., Cirillo, S. L. G., Sacchettini, J. C., Rao, J., and Cirillo, J. D. (2010) Imaging tuberculosis with endogenous β-lactamase reporter enzyme fluorescence in live mice, *Proc. Natl. Acad. Sci. USA 107*, 12239-12244.

[133] Razgulin, A., Ma, N., and Rao, J. (2011) Strategies for in vivo imaging of enzyme activity: an overview and recent advances, *Chem. Soc. Rev. 40*, 4186-4216.

[134] Johnson, I., and Spence, M. T. Z. (2010) *Molecular Probes Handbook: A Guide to Fluorescent Probes and Labeling Technologies*, Vol. 11, Life Technologies Corportation.

[135] Leroy, E., Bensel, N., and Reymond, J. L. (2003) A low background high-throughput screening (HTS) fluorescence assay for lipases and esterases using acyloxymethylethers of umbelliferone, *Bioorg. Med. Chem. Lett. 13*, 2105-2108.

[136] Sicart, R., Collin, M.-P., and Reymond, J.-L. (2007) Fluorogenic substrates for lipases, esterases, and acylases using a TIM-mechanism for signal release, *Biotechnol. J. 2*, 221-231.

[137] Lavis, L. D., Chao, T. Y., and Raines, R. T. (2011) Synthesis and utility of fluorogenic acetoxymethyl ethers, *Chem. Sci. 2*, 521-530.

[138] Klein, G., and Reymond, J. L. (1999) Enantioselective Fluorogenic Assay of Acetate Hydrolysis for Detecting Lipase Catalytic Antibodies, *Helvetica Chimica Acta 82*, 400.

[139] Babiak, P., and Reymond, J. L. (2005) A high-throughput, low-volume enzyme assay on solid support, *Anal. Chem. 77*, 373-377.

[140] Chandran, S. S., Dickson, K. A., and Raines, R. T. (2005) Latent fluorophore based on the trimethyl lock, *J. Am. Chem. Soc. 127*, 1652-1653.

[141] Lavis, L. D., Chao, T.-Y., and Raines, R. T. (2006) Latent Blue and Red Fluorophores Based on the Trimethyl Lock, *ChemBioChem 7*, 1151-1154.

[142] Baruch, A., Jeffery, D. A., and Bogyo, M. (2004) Enzyme activity—it's all about image, *Trends Cell Biol. 14*, 29-35.

[143] Bowyer, P. W., Simon, G. M., Cravatt, B. F., and Bogyo, M. (2010) Global Profiling of proteolysis during rupture of *P. falciparum* from the host erythrocyte, *Mol. Cell. Proteomics 10*, M110.001636.

[144] Kidd, D., Liu, Y., and Cravatt, B. F. (2001) Profiling Serine Hydrolase Activities in Complex Proteomes, *Biochemistry 40*, 4005-4015.

[145] Singh, G., Arya, S., Kumar, S., Narang, D., and Kaur, J. (2014) Molecular characterization of oxidative stress-inducible LipD of *Mycobacterium tuberculosis* H37Rv, *Curr. Microbiol. 68*, 387-396.

[146] Malen, H., Pathak, S., Softeland, T., de Souza, G. A., and Wiker, H. G. (2010) Definition of novel cell envelope associated proteins in Triton X-114 extracts of *Mycobacterium tuberculosis* H37Rv, *BMC Microbiol. 10*, 132-2180-2110-2132.

[147] de Souza, G. A., Leversen, N. A., Målen, H., and Wiker, H. G. (2011) Bacterial proteins with cleaved or uncleaved signal peptides of the general secretory pathway, *J. Proteomics 75*, 502-510.

[148] Gu, S., Chen, J., Dobos, K. M., Bradbury, E. M., Belisle, J. T., and Chen, X. (2003) Comprehensive proteomic profiling of the membrane constituents of a *Mycobacterium tuberculosis* strain, *Mol. Cell. Proteomics 2*, 1284-1296.

[149] Rengarajan, J., Bloom, B. R., and Rubin, E. J. (2005) Genome-wide requirements for *Mycobacterium tuberculosis* adaptation and survival in macrophages, *Proc. Natl. Acad. Sci. USA 102*, 8327-8332.

[150] Canaan, S., Maurin, D., Chahinian, H., Pouilly, B., Durousseau, C., Frassinetti, F., Scappuccini-Calvo, L., Cambillau, C., and Bourne, Y. (2004) Expression and characterization of the protein Rv1399c from *Mycobacterium tuberculosis*. A novel carboxyl esterase structurally related to the HSL family, *Eur. J. Biochem. 271*, 3953-3961.

[151] Mawuenyega, K. G., Forst, C. V., Dobos, K. M., Belisle, J. T., Chen, J., Bradbury, E. M., Bradbury, A. R., and Chen, X. (2005) *Mycobacterium tuberculosis* functional network analysis by global subcellular protein profiling, *Mol. Biol. Cell 16*, 396-404.

[152] Jadeja, D., Dogra, N., Arya, S., Singh, G., Singh, G., and Kaur, J. (2016) Characterization of LipN (Rv2970c) of *Mycobacterium tuberculosis* H37Rv and its Probable Role in Xenobiotic Degradation, *J. Cell. Biochem. 117*, 390-401.

[153] Singh, G., Arya, S., Narang, D., Jadeja, D., Singh, G., Gupta, U. D., Singh, K., and Kaur, J. (2014) Characterization of an acid inducible lipase Rv3203 from *Mycobacterium tuberculosis* H37Rv, *Mol. Biol. Rep. 41*, 285-296.

[154] Singh, P., Rao, R. N., Reddy, J. R., Prasad, R., Kotturu, S. K., Ghosh, S., and Mukhopadhyay, S. (2016) PE11, a PE/PPE family protein of *Mycobacterium tuberculosis* is involved in cell wall remodeling and virulence, *Sci. Rep. 6*, 21624.

[155] Xiong, Y., Chalmers, M. J., Gao, F. P., Cross, T. A., and Marshall, A. G. (2005) Identification of *Mycobacterium tuberculosis* H37Rv integral membrane proteins by one-dimensional gel electrophoresis and liquid chromatography electrospray ionization tandem mass spectrometry, *J. Proteome Res. 4*, 855-861.

[156] Sherman, D. R., Voskuil, M., Schnappinger, D., Liao, R., Harrell, M. I., and Schoolnik, G. K. (2001) Regulation of the *Mycobacterium tuberculosis* hypoxic response gene encoding alpha-crystallin, *Proc. Natl. Acad. Sci. USA 98*, 7534-7539.

[157] Rastogi, S., Agarwal, P., and Krishnan, M. Y. (2016) Use of an adipocyte model to study the transcriptional adaptation of *Mycobacterium tuberculosis* to store and degrade host fat, *Int. J. Mycobacteriol. 5*, 92-98.

[158] Richter, L., and Saviola, B. (2009) The lipF promoter of *Mycobacterium tuberculosis* is upregulated specifically by acidic pH but not by other stress conditions, *Microbiol. Res. 164*, 228-232.

[159] Fisher, M. A., Plikaytis, B. B., and Shinnick, T. M. (2002) Microarray analysis of the *Mycobacterium tuberculosis* transcriptional response to the acidic conditions found in phagosomes, *J. Bacteriol. 184*, 4025-4032.

[160] Stewart, G. R., Wernisch, L., Stabler, R., Mangan, J. A., Hinds, J., Laing, K. G., Young, D. B., and Butcher, P. D. (2002) Dissection of the heat-shock response in *Mycobacterium tuberculosis* using mutants and microarrays, *Microbiology 148*, 3129-3138.

[161] Kelkar, D. S., Kumar, D., Kumar, P., Balakrishnan, L., Muthusamy, B., Yadav, A. K., Shrivastava, P., Marimuthu, A., Anand, S., Sundaram, H., Kingsbury, R., Harsha, H. C., Nair, B., Prasad, T. S., Chauhan, D. S., Katoch, K., Katoch, V. M., Kumar, P., Chaerkady, R., Ramachandran, S., Dash, D., and Pandey, A. (2011) Proteogenomic analysis of *Mycobacterium tuberculosis* by high resolution mass spectrometry, *Mol. Cell. Proteomics 10*, M111.011627.

[162] Zheng, J., Liu, L., Wei, C., Leng, W., Yang, J., Li, W., Wang, J., and Jin, Q. (2012) A comprehensive proteomic analysis of *Mycobacterium bovis* bacillus

Calmette-Guerin using high resolution Fourier transform mass spectrometry, *J. Proteomics 77*, 357-371.

[163] Tallman, K. R., and Beatty, K. E. (2015) Far-red fluorogenic probes for esterase and lipase detection, *ChemBioChem 16*, 70-75.

[164] Xie, H., Mire, J., Kong, Y., Chang, M., Hassounah, H. A., Thornton, C. N., Sacchettini, J. C., Cirillo, J. D., and Rao, J. (2012) Rapid point-of-care detection of the tuberculosis pathogen using a BlaC-specific fluorogenic probe, *Nat. Chem. 4*, 802-809.

[165] Beatty, K. E., Williams, M., Carlson, B. L., Swarts, B. M., Warren, R. M., van Helden, P. D., and Bertozzi, C. R. (2013) Sulfatase-activated fluorophores for rapid discrimination of mycobacterial species and strains, *Proc. Natl. Acad. Sci. USA 110*, 12911-12916.

[166] Smith, E. L., Bertozzi, C. R., and Beatty, K. E. (2014) An expanded set of fluorogenic sulfatase activity probes, *ChemBioChem 15*, 1101-1105.

[167] Côtes, K., Bakala N'Goma, J. C., Dhouib, R., Douchet, I., Maurin, D., Carrière, F., and Canaan, S. (2008) Lipolytic enzymes in *Mycobacterium tuberculosis*, *Appl. Microbiol. Biotechnol. 78*, 741-749.

[168] Singh, G., Singh, G., Jadeja, D., and Kaur, J. (2010) Lipid hydrolizing enzymes in virulence: *Mycobacterium tuberculosis* as a model system, *Crit. Rev. Microbiol. 36*, 259-269.

[169] West, N. P., Cergol, K. M., Xue, M., Randall, E. J., Britton, W. J., and Payne, R. J. (2011) Inhibitors of an essential mycobacterial cell wall lipase (Rv3802c) as tuberculosis drug leads, *Chem. Commun. (Camb.) 47*, 5166-5168.

[170] Komatsu, T., Hanaoka, K., Adibekian, A., Yoshioka, K., Terai, T., Ueno, T., Kawaguchi, M., Cravatt, B. F., and Nagano, T. (2013) Diced electrophoresis gel assay for screening enzymes with specified activities, *J. Am. Chem. Soc. 135*, 6002-6005.

[171] Weissleder, R., and Ntziachristos, V. (2003) Shedding light onto live molecular targets, *Nat. Med. 9*, 123-128.

[172] Tian, L., Yang, Y., Wysocki, L. M., Arnold, A. C., Hu, A., Ravichandran, B., Sternson, S. M., Looger, L. L., and Lavis, L. D. (2012) Selective esterase–ester pair for targeting small molecules with cellular specificity, *Proc. Natl. Acad. Sci. USA 109*, 4756-4761.

[173] Lavis, L. D., Chao, T. Y., and Raines, R. T. (2006) Fluorogenic label for biomolecular imaging, *ACS Chem. Biol. 1*, 252-260.

[174] Zhang, Y., Chen, W., Feng, D., Shi, W., Li, X., and Ma, H. (2012) A spectroscopic off-on probe for simple and sensitive detection of carboxylesterase activity and its application to cell imaging, *Analyst 137*, 716-721.

[175] Kiyose, K., Aizawa, S., Sasaki, E., Kojima, H., Hanaoka, K., Terai, T., Urano, Y., and Nagano, T. (2009) Molecular design strategies for near-infrared ratiometric fluorescent probes based on the unique spectral properties of aminocyanines, *Chemistry 15*, 9191-9200.

[176] Corey, P. F., Trimmer, R. W., and Biddlecom, W. G. (1991) A New Chromogenic Beta-Galactosidase Substrate - 7-Beta-D-Galactopyranosyloxy-9,9-Dimethyl-9H-Acridin-2-One, *Angew. Chem. Int. Ed. USA 30*, 1646-1648.

[177] Tung, C. H., Zeng, Q., Shah, K., Kim, D. E., Schellingerhout, D., and Weissleder, R. (2004) In vivo imaging of beta-galactosidase activity using far red fluorescent switch, *Cancer Res. 64*, 1579-1583.

[178] Bueno, C., Villegas, M. L., Bertolotti, S. G., Previtali, C. M., Neumann, M. G., and Encinas, M. V. (2002) The excited-state interaction of resazurin and resorufin with amines in aqueous solutions. Photophysics and photochemical reactions, *Photochem. Photobiol. 76*, 385-390.

[179] Johnson, M. M., and Odell, J. A. (2014) Nontuberculous mycobacterial pulmonary infections, *J. Thorac. Dis. 6*, 210-220.

[180] Grognux, J., and Reymond, J. L. (2004) Classifying enzymes from selectivity fingerprints, *ChemBioChem 5*, 826-831.

[181] Fery-Forgues, S., and Lavabre, D. (1999) Are Fluorescence Quantum Yields So Tricky to Measure? A Demonstration Using Familiar Stationery Products, *J. Chem. Educ. 76*, 1260.

[182] Allison, R. D., and Purich, D. L. (1979) Practical considerations in the design of initial velocity enzyme rate assays, *Methods Enzymol. 63*, 3-22.

[183] Rasband, W. S. (1997) ImageJ, U.S. National Institute of Health, Bethesda.

[184] Tallman, K. R., Levine, S. R., and Beatty, K. E. (2016) Profiling Esterases in *Mycobacterium tuberculosis* Using Far-Red Fluorogenic Substrates, *ACS Chem. Biol. 11*, 1810-1815.

[185] Hotelier, T., Renault, L., Cousin, X., Negre, V., Marchot, P., and Chatonnet, A. (2004) ESTHER, the database of the alpha/beta-hydrolase fold superfamily of proteins, *Nucleic Acids Res. 32*, D145-147.

[186] Levine, S. R., and Beatty, K. E. (2016) Synthesis of a far-red fluorophore and its use as an esterase probe in living cells, *Chem. Commun. (Camb.) 52*, 1835-1838.

[187] ChemAxon. (2015) Calculator Plugins for Marvin were used for structure property prediction and calculation, http://chemaxon.com.

[188] Sambandamurthy, V. K., Derrick, S. C., Jalapathy, K. V., Chen, B., Russell, R. G., Morris, S. L., and Jacobs, W. R., Jr. (2005) Long-term protection against tuberculosis following vaccination with a severely attenuated double lysine and pantothenate auxotroph of *Mycobacterium tuberculosis*, *Infect. Immun. 73*, 1196-1203.

[189] Azema, J., Guidetti, B., Malet-Martino, M., Martino, R., and Roques, C. (2006) Efficient approach to acyloxymethyl esters of nalidixic acid and in vitro evaluation as intra-ocular prodrugs, *Bioorg. Med. Chem. 14*, 2569-2580.

[190] Warther, D., Bolze, F., Leonard, J., Gug, S., Specht, A., Puliti, D., Sun, X. H., Kessler, P., Lutz, Y., Vonesch, J. L., Winsor, B., Nicoud, J. F., and Goeldner, M. (2010) Live-cell one- and two-photon uncaging of a far-red emitting acridinone fluorophore, *J. Am. Chem. Soc. 132*, 2585-2590.

[191] Duo, T., Goddard-Borger, E. D., and Withers, S. G. (2014) Fluoro-glycosyl acridinones are ultra-sensitive active site titrating agents for retaining beta-glycosidases, *Chem. Commun. (Camb.) 50*, 9379-9382.

[192] Tufariello, J. M., Jacobs, W. R., Jr., and Chan, J. (2004) Individual *Mycobacterium tuberculosis* resuscitation-promoting factor homologues are dispensable for growth in vitro and in vivo, *Infect. Immun. 72*, 515-526.

[193] Keller, A., Nesvizhskii, A. I., Kolker, E., and Aebersold, R. (2002) Empirical statistical model to estimate the accuracy of peptide identifications made by MS/MS and database search, *Anal. Chem. 74*, 5383-5392.

[194] Nesvizhskii, A. I., Keller, A., Kolker, E., and Aebersold, R. (2003) A statistical model for identifying proteins by tandem mass spectrometry, *Anal. Chem. 75*, 4646-4658.

[195] Shi, L., Sohaskey, C. D., Kana, B. D., Dawes, S., North, R. J., Mizrahi, V., and Gennaro, M. L. (2005) Changes in energy metabolism of *Mycobacterium*

tuberculosis in mouse lung and under in vitro conditions affecting aerobic respiration, *Proc. Natl. Acad. Sci. USA 102*, 15629-15634.

[196] Daniel, J., Deb, C., Dubey, V. S., Sirakova, T. D., Abomoelak, B., Morbidoni, H. R., and Kolattukudy, P. E. (2004) Induction of a novel class of diacylglycerol acyltransferases and triacylglycerol accumulation in *Mycobacterium tuberculosis* as it goes into a dormancy-like state in culture, *J. Bacteriol. 186*, 5017-5030.

[197] Bachovchin, D. A., and Cravatt, B. F. (2012) The pharmacological landscape and therapeutic potential of serine hydrolases, *Nat. Rev. Drug Discov. 11*, 52-68.

[198] Xie, L., Wang, X., Zeng, J., Zhou, M., Duan, X., Li, Q., Zhang, Z., Luo, H., Pang, L., Li, W., Liao, G., Yu, X., Li, Y., Huang, H., and Xie, J. (2015) Proteome-wide lysine acetylation profiling of the human pathogen *Mycobacterium tuberculosis*, *Int. J. Biochem. Cell Biol. 59*, 193-202.

[199] Prisic, S., Dankwa, S., Schwartz, D., Chou, M. F., Locasale, J. W., Kang, C.-M., Bemis, G., Church, G. M., Steen, H., and Husson, R. N. (2010) Extensive phosphorylation with overlapping specificity by *Mycobacterium tuberculosis* serine/threonine protein kinases, *Proc. Natl. Acad. Sci. USA 107*, 7521-7526.

[200] Ravindran, M. S., Rao, S. P. S., Cheng, X., Shukla, A., Cazenave-Gassiot, A., Yao, S. Q., and Wenk, M. R. (2014) Targeting Lipid Esterases in Mycobacteria Grown Under Different Physiological Conditions Using Activity-based Profiling with Tetrahydrolipstatin (THL), *Mol. Cell Proteomics 13*, 435-448.

[201] Duckworth, B. P., Geders, T. W., Tiwari, D., Boshoff, H. I., Sibbald, P. A., Barry, C. E., 3rd, Schnappinger, D., Finzel, B. C., and Aldrich, C. C. (2011) Bisubstrate adenylation inhibitors of biotin protein ligase from *Mycobacterium tuberculosis*, *Chem. Biol. 18*, 1432-1441.

[202] Simon, G. (2015) Re: Abide Contact Submission, (Levine, S. R., Ed.).

[203] Rustad, T. R., Harrell, M. I., Liao, R., and Sherman, D. R. (2008) The enduring hypoxic response of *Mycobacterium tuberculosis*, *PLoS ONE 3*, e1502.

[204] Daugelat, S., Kowall, J., Mattow, J., Bumann, D., Winter, R., Hurwitz, R., and Kaufmann, S. H. E. (2003) The RD1 proteins of *Mycobacterium*

tuberculosis: expression in *Mycobacterium smegmatis* and biochemical characterization, *Microbes and Infection 5*, 1082-1095.

[205] Dieterich, D. C., Lee, J. J., Link, A. J., Graumann, J., Tirrell, D. A., and Schuman, E. M. (2007) Labeling, detection and identification of newly synthesized proteomes with bioorthogonal non-canonical amino-acid tagging, *Nat. Protoc. 2*, 532-540.

[206] Xu, G., Jia, H., Li, Y., Liu, X., Li, M., and Wang, Y. (2010) Hemolytic phospholipase Rv0183 of *Mycobacterium tuberculosis* induces inflammatory response and apoptosis in alveolar macrophage RAW264.7 cells, *Can. J. Microbiol. 56*, 916-924.